Simulation of the Atmospheric Circulation Using the NCAR Global Circulation Model With Present Day and Glacial Period Boundary Conditions

Jill Henderson Williams

NCAR Cooperative Thesis No. 31
INSTAAR Occasional Paper No. 10

University of Colorado and
Atmospheric Analysis and Prediction Division, NCAR

1974

The National Center for Atmospheric Research (NCAR) is operated by the nonprofit University Corporation for Atmospheric Research (UCAR) under the sponsorship of the National Science Foundation.

Simulation of the Atmospheric Circulation Using the NCAR Global Circulation Model With Present Day and Glacial Period Boundary Conditions

Jill Henderson Williams

A thesis submitted to the Faculty of the Graduate School of the University of Colorado in partial fulfillment of the requirements for the degree of Doctor of Philosophy, Department of Geography, based on research conducted in cooperation with the scientific staff of the Large-Scale Modeling and Analysis Group of the GARP Project under the Atmospheric Analysis and Prediction Division of the National Center for Atmospheric Research, Boulder, Colorado.

Ms. Williams received her B.Sc. degree from the University of East Anglia in 1971.

NCAR Cooperative Thesis No. 31
INSTAAR Occasional Paper No. 10

University of Colorado and

Atmospheric Analysis and Prediction Division, NCAR

1974

Williams, Jill Henderson (Ph.D., Geography)

Simulation of the Atmospheric Circulation Using the NCAR Global Circulation Model with Present Day and Glacial Period Boundary Conditions

Thesis directed by Professor Roger G. Barry

The National Center for Atmospheric Research (NCAR) global circulation model (GCM) has been used to investigate the influence of glacial period boundary conditions on the simulated atmospheric circulation. In the January and July control cases the atmospheric circulation was simulated with present day boundary conditions; in the January and July ice age cases boundary conditions were derived from paleoenvironmental evidence of conditions at the maximum of the last glacial period. Additional simulations were made in order to test the significance of the differences between control and ice age cases. It is considered that the major and consistent differences between the control and ice age cases represent the direction of change between present and glacial period maximum circulations.

Conclusions common to earlier studies, which are unsupported by the GCM results, include: winds stronger and storm tracks and winds forced south of ice in the northern hemisphere. Supporting earlier common conclusions the results did show: air temperatures in July

ice age case more like winter of today; Icelandic low shifted southward in January; pressure distribution more meridional; intensified Hadley cell; transient cyclone activity greater over Atlantic.

Study of the winds at 75°E, the 200 mb pressure distribution and temperatures indicates that the northern hemisphere summer monsoon is not simulated in the July ice age case, but it is found in the July control case. This influences the global energetics of the case.

The atmospheric moisture balance of the simulations is such that: the specific humidity of the atmosphere is reduced in the ice age cases compared with the control cases; the ice age case meridional and vertical transports by the mean circulation and eddies are weaker except in the tropics in the January ice age case, where transports by the mean circulation are stronger than in the control case.

The January ice age case has lower net heating than the control case in the northern hemisphere and slightly higher in the southern hemisphere. In the July ice age case the heating is much less than that in the control case in the northern hemisphere; in the southern hemisphere the heating is greater than that in the control case between 5°S and 35°S, but not greatly different elsewhere. Ice age case eddy transports of heat differ considerably from those in the control cases.

In the January cases, the differences in global mean zonal and eddy kinetic energy between the control and ice age cases are not great. In the July cases the global mean zonal kinetic energy is much greater in the ice age case, whereas the global mean eddy kinetic energy is much less in the ice age case than in the control case. The latter feature is due to the absence of the northern hemisphere summer monsoon in the July ice age case. Zonal internal energy is larger in the control cases than in the ice age cases.

Random error experiments show that for variables temperature and east-west wind at 1.5 km and low clouds the rms differences between the January control and ice age cases are above the noise level of the model. Pressure at sea level and north-south wind at 1.5 km differences are only just above, and precipitation differences are no greater than, the noise level.

ACKNOWLEDGEMENTS

I would like to thank the following people at the National Center for Atmospheric Research for their help in the preparation of this thesis:

Warren Washington and Akira Kasahara for reading and commenting on the thesis and helping me throughout all stages of the project.

Gloria Williamson for all the work involved in supervising the running of the model and statistics programs.

Harry Van Loon for reading and commenting on the thesis.

Takashi Sasamori and Stephen Schneider for reading and commenting on earlier drafts of certain chapters.

The NCAR computing facility for their support (NCAR is sponsored by the National Science Foundation).

I would also like to thank the following people from the University of Colorado for their support and help:

Roger Barry for much help and guidance through the development of the project.

Julius London for reading and commenting on the thesis.

Jack Ives and John Andrews for their support and interest.

I also acknowledge the support of a fellowship from the University of Colorado.

Lastly, I would like to thank Jo Ann Fankhauser for typing the thesis and Ann Lundberg of NCAR for all her help.

TABLE OF CONTENTS

CHAPTER PAGE

CHAPTER PAGE

CHAPTER PAGE

PAGE

LIST OF TABLES

FIGURE PAGE

LIST OF FIGURES

FIGURE PAGE

FIGURE PAGE

FIGURE PAGE

CHAPTER I

INTRODUCTION

In the early 19th century the concept of former glacial ages was first discussed. We now know that during the last 10 million years there have been repeated occurrences of the spreading of the great ice sheets into the middle latitudes of the northern hemisphere and subsequent shrinking of these ice sheets (Turekian, 1971). We still do not know exactly why these ice sheets have repeatedly advanced and retreated, nor do we have a firm idea of the prevailing atmospheric circulation and oceanic circulation when they advanced to their maximum extents.

During periods when ice sheets advanced to their maxima, the area occupied by glaciers was about three times as great as that occupied by glaciers today. It has been established that the last glacial maximum, at least at the southern margins of the ice sheets, occurred simultaneously in both hemispheres at about 18,000-22,000 years before present (BP). The total volume of glacier ice in the northern hemisphere was roughly twice that in the southern (Flint, 1971). Scandinavian ice reached 48°N and North American ice reached 37°N.

Obviously we do not have direct measurements of climatic indicators of a period, say 20,000 years ago. We have to infer these data from geologic, paleobiologic and isotopic measurements. For instance, the positions of former outer margins of glaciers give us some information about prevailing temperatures in the past; shifts in the ranges of terrestrial and marine organisms indicate corresponding changes in climatic controls such as precipitation and temperature; occurrence of ancient, fossilized dunes show former directions and perhaps indicate speed of the wind. But knowing the amounts of temperature, precipitation and wind at scattered locations does not tell us directly what the atmospheric circulation was like during some period in the past. Several studies have tried to piece together the evidence and come up with a picture of the atmospheric circulation at the maximum of a glacial period. Some of these studies will be described in Chapter II.

In this study we have used much of the evidence available concerning conditions at the maximum of the last glacial period (18,000-22,000 BP). The evidence includes the height and areal extent of the continental ice sheets and pack ice (derived from geological evidence, e.g. Andrews, 1970); the vegetation of non-glaciated areas (derived from biological evidence, principally palynology, e.g. Frenzel, 1968); temperatures of the ocean surface (derived from ocean core data, not based

on oxygen isotope data. Principal sources, Emiliani, 1971, and McIntyre, 1967). Details of the information used are described in Barry (1973) and Williams et al. (1974).

The aim of this study is to examine the influence of glacial period boundary conditions on the atmospheric circulation simulated by the National Center of Atmospheric Research (NCAR) global circulation model (GCM). Four principal experiments were made, January and July control cases had present day input boundary conditions (heights, albedos and ocean surface temperatures): January and July glacial period cases had input boundary conditions derived from geological and biological evidence of conditions at the maximum of the last glacial period. Additional experiments were made in order to test the significance of the differences between the control cases and the ice age cases and these will be described in Chapter IX.

The NCAR global atmospheric circulation model has been described in detail by Kasahara and Washington (1967, 1971) and Washington and Kasahara (1970). The model is global and employs spherical polar coordinates in the horizontal with a resolution of 5° in latitude and longitude. The longitudinal resolution is decreased near the poles to keep the geographical distances more uniform poleward of 60°. The vertical coordinate is height and the atmosphere is divided into six 3 km layers.

The prognostic variables are longitudinal and latitudinal components of momentum ρu and ρv, where u and v are the east-west and north-south components of the wind, pressure p, and water vapor content ρq, where q is specific humidity. The diagnostic variables are vertical velocity w, temperature T and density ρ. The main dynamical assumption is that the model atmosphere is hydrostatic.

The physical processes included in the model are: absorption of solar radiation in the atmosphere, cooling and heating due to infrared radiation, model-derived cloudiness at 3 and 9 km, heating due to the release of latent heat of condensation of water vapor, boundary layer transfers of momentum, sensible heat and water vapor, and horizontal and vertical diffusion of momentum, sensible heat and water vapor within the model atmosphere. Over non-ocean areas the surface temperature is computed from a surface energy balance of solar radiation, infrared radiation, sensible heat and evaporation and heat conduction into the ground. The diurnal variation of the sun is also included. One of the limitations of this version of the model is that a Bowen ratio of unity is assumed over all non-ocean areas, which means that the ratio of sensible heat flux to water vapor flux is not variable. The model as described here is not a complete climate model in the sense that the ocean temperatures are specified rather than computed. Given the ocean surface temperatures we can compute the

atmospheric global circulation within the limitations of the model.

While the results of the glacial period simulations can not be presented as the real atmospheric circulation at the last glacial maximum, it is considered that the major and consistent differences between the control and ice age cases represent the direction of change between present day and ice age maximum circulations.

The results presented are unless otherwise specified averages of the meteorological fields for day 51 to day 80 of the simulation. Williams et al. (1974) discuss preliminary results, mostly for the northern hemisphere; Williams and Barry (1973) discuss conditions in the vicinity of the Laurentide and Scandinavian ice sheets; Barry and Williams (1973) discuss southern hemisphere climatology and interhemispheric comparisons; Barry (1973) discusses input data and pressure and wind distributions; Kraus (1973) discusses the atmospheric circulation and wind stress over the oceans derived from the glacial period simulations. These papers will be briefly mentioned in Chapter III, in which climatological results of the simulations will be described.

It must be emphasized in this introduction to the study that all of the work has concentrated on the conditions at the maximum of the last glacial period (Wisconsin/Würm maximum) and not at the onset of the

last glacial. We have not investigated in this study anything about causes of glacial periods, nor can any consideration be given to the rapid disintegration of the ice sheets.

In Chapter II previous reconstructions of the atmospheric circulation at the maximum of the last glacial period are described. The input data used in this study and many of the climatological results are discussed in Chapter III. The momentum, moisture, heat and energy balances of the simulations are discussed in Chapters IV to VII respectively. Chapter VIII summarizes the latter four chapters and points out some of the model-dependent and data-dependent differences between the control case data and observed data. Tests to investigate the significance of the differences between cases are described in Chapter IX. The summary and conclusions of this study are presented in Chapter X.

CHAPTER II

PREVIOUS RECONSTRUCTIONS OF THE ATMOSPHERIC CIRCULATION AT THE MAXIMUM OF THE WÜRM/WISCONSIN GLACIAL PERIOD

(a) Introduction

As pointed out by Williams et al. (1973), paleoclimatic reconstructions until recently have been based on either simple analog principles, using "extreme" conditions in the meteorological record as a guide (Willett, 1950; Mather, 1954, for example), or on diagnostic relationships between circulation features and atmospheric parameters (e.g., Lamb et al., 1966; Lamb and Woodroffe, 1970). In this chapter, some of these paleoclimatic reconstructions will be described briefly, so that we can examine later whether the atmospheric circulation simulated by using glacial period boundary conditions in the NCAR GCM, bears any resemblance to the previously published ideas regarding glacial period atmospheric circulation.

In recent years development of numerical models of the atmospheric circulation has progressed, so that some of these models (of varying degrees of complexity) have been used to investigate the atmospheric circulation

with different boundary conditions. For example, MacCracken (1970), Shaw and Donn (1971) and Warshaw and Rapp (1973), have used models to investigate the response to removal of Artic Ocean ice. Before the present study was initiated, only one numerical model of the atmospheric circulation had been used to investigate the response to inclusion of glacial period boundary conditions (Alyea, 1972). Some results of the latter study will be compared with the results of the present one.

The numerical models mentioned above are not complete climate models since the ocean temperatures are specified rather than computed. If an ocean model could be successfully coupled to the atmosphere model then "climate" experiments could be performed (the boundary conditions, for instance, could be perturbed and the resulting climate examined). With an atmosphere model, experiments using different boundary conditions should properly be considered as sensitivity studies. As Warshaw and Rapp (1973) have pointed out, when models are used to examine results of experiments using different boundary conditions, the experiment estimates only the models ability to separate signal (purposeful changes in boundary conditions) from noise (random changes in boundary conditions); no claim can be made that the real atmosphere would respond in the same way as the model.

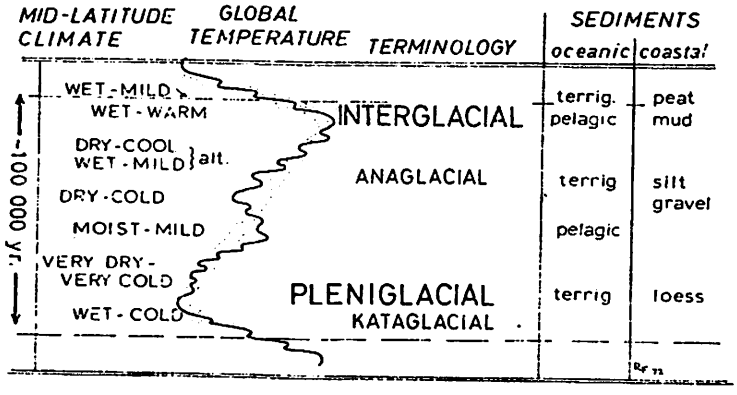

Figure 2.1. A single glacial cycle (from top to bottom) expressed in terms of relative global temperature (high to the right; low to the left), based on pelagic marine indicators. Examples are given of midlatitude climates (in maritime situations) and sedimentation. (From Fairbridge, 1972).

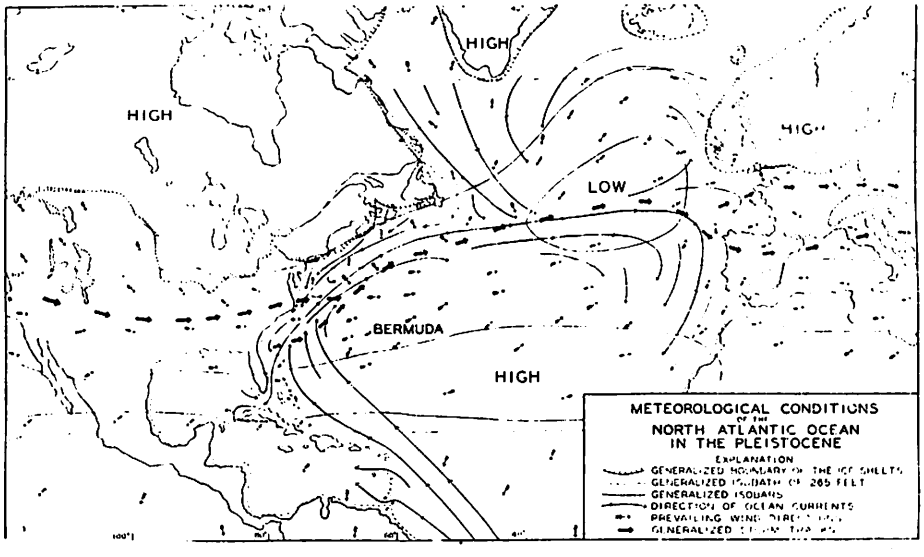

Figure 2.2. Meteorological conditions over the North Atlantic Ocean during a glacial period. From Bryan and Cady (1934).

A distinction must be made here between the atmospheric circulation at the maximum of the glacial period and that which existed at the onset of the glacial period and resulted in the build up of the continental ice sheets. The latter has been studied by Loewe (1971) and Brinkmann and Barry (1972), for example. In this study we are concerned with the circulation which prevailed when the ice sheets were at their maximum size. It is most probable that the atmospheric circulation at the maximum of the Wisconsin glaciation was quite different from that which provided the conditions for the build up of the ice sheets. For instance, it seems clear that the build up of ice sheets would need a considerable amount of moisture transport to the latitudes where the snow/ice first accumulated, while the maximum of the ice age would be characterized by a low atmospheric moisture content because of the lower temperatures. Figure 2.1 illustrates this point. Fairbridge (1972) has discussed the climatology of a glacial cycle and his study suggests that the onset of a glacial is characterized by alternating dry-cool and wet-mild climates in middle latitudes, while the glacial maximum (Pleniglacial) is characterized by very dry-very cold climates. In this study we are concerned with the pleniglacial conditions. In some earlier studies the distinction has not always been made, it has been assumed that the onset and full-glacial conditions were the same. In some of the work

described below, the latter assumption will be pointed out.

There have been many reconstructions of the glacial climate of specific parts of the globe (e.g., Fairbridge, 1964, for Africa; Damuth and Fairbridge, 1970, for South America; Galloway, 1965, for Australia; Coope et al., 1971, for the British Isles, etc.). Geologists and paleobiologists have been finding indicators which suggest the temperature, wind conditions, moisture conditions, etc., at particular locations at the maximum of the ice age. However, in this chapter only, those studies which have reconstructed global or hemispheric conditions will be discussed in general, i.e., we are interested in studies which have gone a little further than interpreting paleoenvironmental evidence at one or more localities in terms of some meteorological variable(s).

(b) Previous Reconstructions

Charlesworth (1957) discusses at length some very early theories concerning glacial period general circulation. In this chapter, the theories described, apart from one, are post-1945. That is, they were essentially proposed since modern developments in meteorology began, and since paleoenvironmental data began to accumulate sufficiently for reconstruction of prevailing conditions over different regions during the last glacial maximum.

In 1934, Bryan and Cady published a detailed discussion of the Pleistocene climate of Bermuda, in which they devoted nearly all of the discussion to the conditions at the glacial period maximum. Bryan and Cady based their analysis on the assumptions that the sea-level was lower and that the continental ice masses gave rise to air temperatures and pressures in summer and generally throughout the year similar to those now existing in winter. The authors discussed the resultant effects on the ocean currents and atmospheric circulation of the North Atlantic area. Figure 2.2 shows their reconstruction of meteorological conditions in the North Atlantic Ocean during glacial epochs.

Bryan and Cady concluded that in glacial periods, pressure gradients and winds were stronger. They believed that the subtropical belt of high pressure was reduced and shifted southward and that the Icelandic Low and storm tracks were also shifted in a southward direction. One of the most important conclusions of the study, which led to many of the conclusions regarding the glacial period atmospheric circulation was that the Gulf Stream was shifted eastward and southward. Bryan and Cady based their conclusions on an analysis of the glacial period boundary conditions, their resulting picture fitted very well with the geologic evidence for the climate of Bermuda in past epochs.

Willett (1949) in a discussion of long-period fluctuations of the general circulation states the belief that fluctuations of climate on a geological and on a secular time scale are all characterized by one basic change of the atmospheric circulation pattern. The basic change he refers to is a contraction or expansion of the "circumpolar zonal weather pattern" accompanied by decrease and increase respectively of cyclonic activity in the low pressure belts. Willett suggests that during glacial maxima a low index pattern occurs, the polar cells expand and storminess in north temperate latitudes is greatly increased. He believes that the ice sheets force the storm tracks and westerlies southward. These conclusions are based on a knowledge of recent climatic variations.

Hare (1953) superimposes a map drawn by Willett (1950) depicting the "probable" pressure distribution over Europe at the glacial maximum and a map drawn by Frenzel and Troll (1952) showing the "probable" natural vegetation of Europe at the climax of the last glacial period. The aim of Hare's study is not to question the validity of the maps but to see whether they are mutually consistent. Interestingly, Hare shows that the circulation depicted by Willett could not give a climate dry enough in southern Russia for the survival of the open steppe, depicted there by Frenzel and Troll. As Hare points out, we have no way of knowing which view is right.

This example points out that there are problems in the reconstruction of past environments.

A description of the probable general atmospheric circulation during a glacial period, very similar to that of Willett (1949) was given by Viete (1949). Viete says that the range of polar air over the northern hemisphere was increased during glacial periods, the centers of action and storm tracks were shifted southwards and the strength of the general circulation increased since the meridional temperature gradient strengthened. Viete makes a definite distinction between the circulation at the onset and that at the maximum of the glacial period. Many of the glacial maximum features are described as of a secondary nature, caused by the advance of the ice sheets.

Another discussion of glacial period climate based on recent atmospheric circulation patterns is that of Rex (1950b). Rex, in an earlier study (1950a) has discussed the effects of blocking action upon regional climate. He found that both in winter and summer, European blocking action produces climatic conditions which, in the mean, are unfavorable for Scandinavian glaciation. The climate associated with a zonal flow pattern aloft appeared, in the mean, to favor the growth of Scandinavian glaciers. Therefore, Rex proposes that during development of glaciation a predominantly zonal type of circulation would prevail over the area.

During a later stage, near the time of most rapid advance of ice margins, Rex suggests that blocking activity would increase until active growth of the ice mass ceases. Rex then says that forward movement of the ice mass would continue under gravitational flow, until, at the maximum extension a predominantly blocked type circulation would prevail. Thus Rex is proposing that at the maximum of the glacial period, the extent of the ice mass and the prevailing atmospheric circulation are out of phase, with the ice sheet not responding to the unfavorable conditions brought about by blocking activity. Viete (1949) suggests that the onset is characterized by a low index situation with the maximum characterized by a high index situation, Rex is suggesting that the opposite is the case.

Mather (1954), having studied large scale pressure, temperature and precipitation changes which had occurred over the northern hemisphere during the previous forty years, applies his knowledge to a reconstruction of glacial period climates. Mather's study suggests that the hemisphere as a whole might not have experienced the same change of meteorological conditions, so he extrapolates this observation in order to suggest that in the glacial periods each local region might have experienced its own climatic variation. Secondly, Mather finds that land and ocean areas were affected differently by recent climatic variations. Thirdly he finds that during

the warm 1931-1940 epoch (which he thinks could be correlated with an interglacial period), the storms and fronts were somewhat north of their normal positions. Mather emphasizes his belief that glacial and interglacial climates should be thought of as periods of climatic fluctuation of a slightly larger order and longer extent than recent ones but possessing many of the characteristics of the latter. Another study, which looks at small recent climatic variations in order to describe possible glacial climates is described by Kraus (1960). Briefly, Kraus believes that glacial periods were probably characterized by: a more active conversion of thermal into mechanical energy; an intensified Hadley-type circulation in the tropics, which caused heavier rainfall in the equatorial trough; an associated increase in wind strength, which produced heavier evaporation over the oceans; stronger upper westerlies, probably closer to the equator; probably deep meridional currents and poleward-moving depressions, which caused a vigorous exchange of heat and moisture between different latitudes. Kraus concludes that glacial periods were probably accompanied by pluvials in lower latitudes, a conclusion which he believed was consistent with recent global patterns of climatic changes.

A more simple idea on the changes of climate at the maximum of the last glacial period was presented by Budel (1959). Budel believes that at the Würm/Wisconsin

maximum the present climatic zones were displaced from pole to equator. The displacement in higher latitudes, according to Budel, was much greater than in lower latitudes. Budel states that because of this displacement, outside of the tropics the climate was drier than today but the strong cooling of the polar masses brought a displacement of polar fronts into lower latitudes and an intensification of the meridional circulation. Budel proposes that glacial period cooling caused an increase in precipitation in the tropics.

Lamb (1961) presents a tentative reconstruction of a glacial period climate. He suggests that the circulation during a glacial period would be intensified, both in the westerlies and the trades and that the zonal circulation was generally displaced towards lower latitudes. In winter in the higher latitudes over the ice, Lamb suggests that the circulation was probably weaker than now. The intensified upper westerlies were believed to cause greater mobility in the subtropical anticlyclones and Lamb suggests that the intense general circulation would mean that persistent anomalies were rare at all latitudes except over the ice. It is felt that there was probably less change of the character of the general circulation from winter to summer than there is now.

The maps given by Lamb suggest that in the glacial period in January, the Icelandic Low was less extensive

and shifted southward, that there was low pressure in the Mediterranean area, and that the Aleutian low was deeper. The subtropical anticyclones in the January ice age case are equatorward of those of the present day. Over the ice covered areas of the northern hemisphere in the glacial period, Lamb depicts a large area of high pressure. On the July maps, there is again high pressure over the ice in the glacial period map, the glacial Icelandic low pressure is deep and extensive, the lows over Asia are deeper and more extensive than those of the present day.

Lamb, Lewis and Woodroffe (1966) devised a method for calculating probable prevailing surface pressure and wind patterns in past epochs. This technique was applied to several stages of the last glacial period and the results of this study were reported by Lamb and Woodroffe (1971) and Lamb (1971). Firstly the winter and summer surface temperatures prevailing at a certain climatic stage are determined from paleobotanical and oceanographic research. From these surface temperatures, upper air temperatures and 1000-500 mb thickness distribution over the northern hemisphere are estimated. From these, regions of recurrent cyclonic and anticyclonic development are calculated and then probable prevailing surface pressure and wind patterns are derived.

In Figures 2.3a-d the distribution of probable monthly mean 1000-500 mb thickness over the northern hemisphere and the computed distribution of surface cyclonic

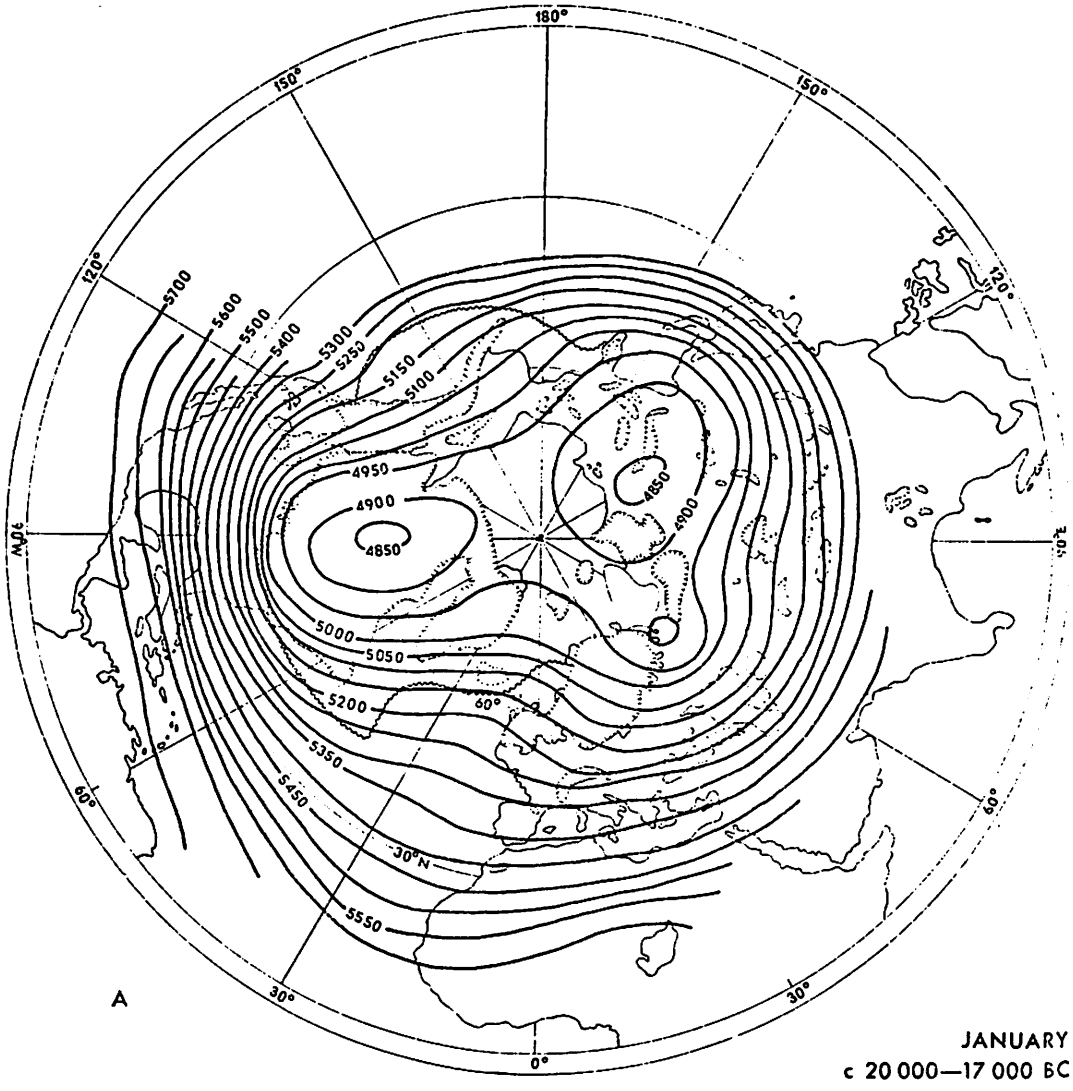

Figure 2.3a. Average 1000-500 mb thickness (meters), derived from evidence of surface temperatures, for January glacial period. From Lamb and Woodroffe (1971).

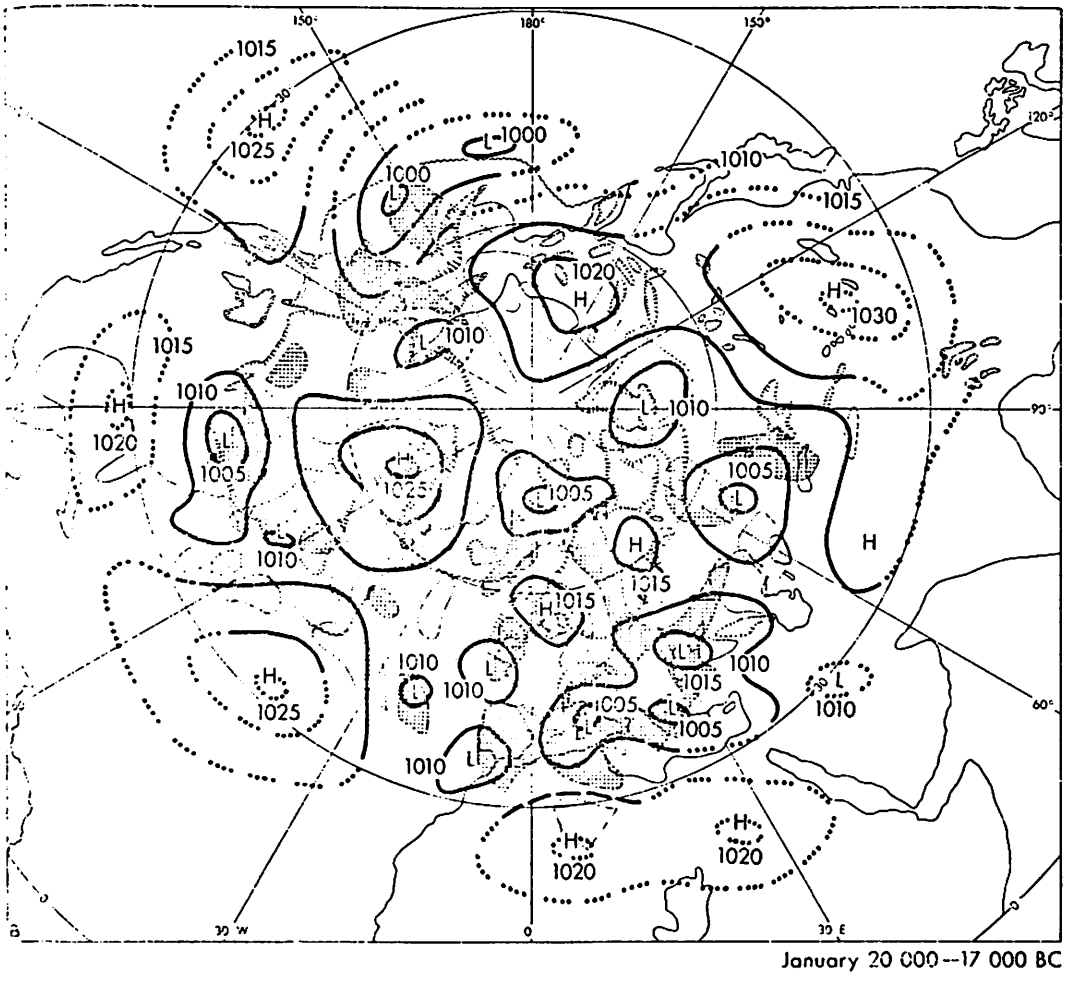

Figure 2.3b. Maximum glaciation, January, suggested MSL isobars with computed areas favoring cyclonic and anti-cyclonic development. From Lamb and Woodroffe (1971).

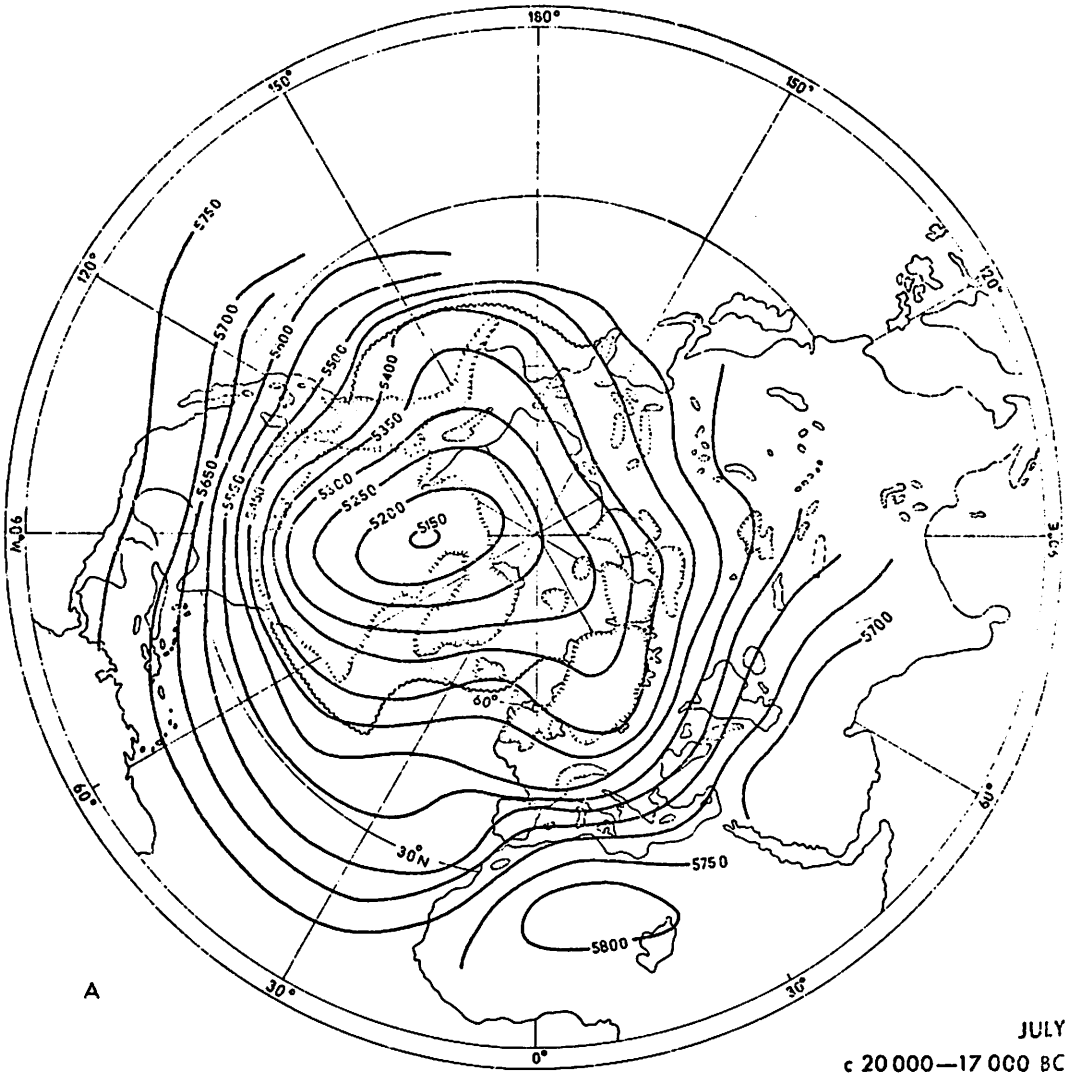

Figure 2.3c. Average 1000-500 mb thickness (meters), derived from evidence of surface temperatures, for July glacial period. From Lamb and Woodroffe (1971).

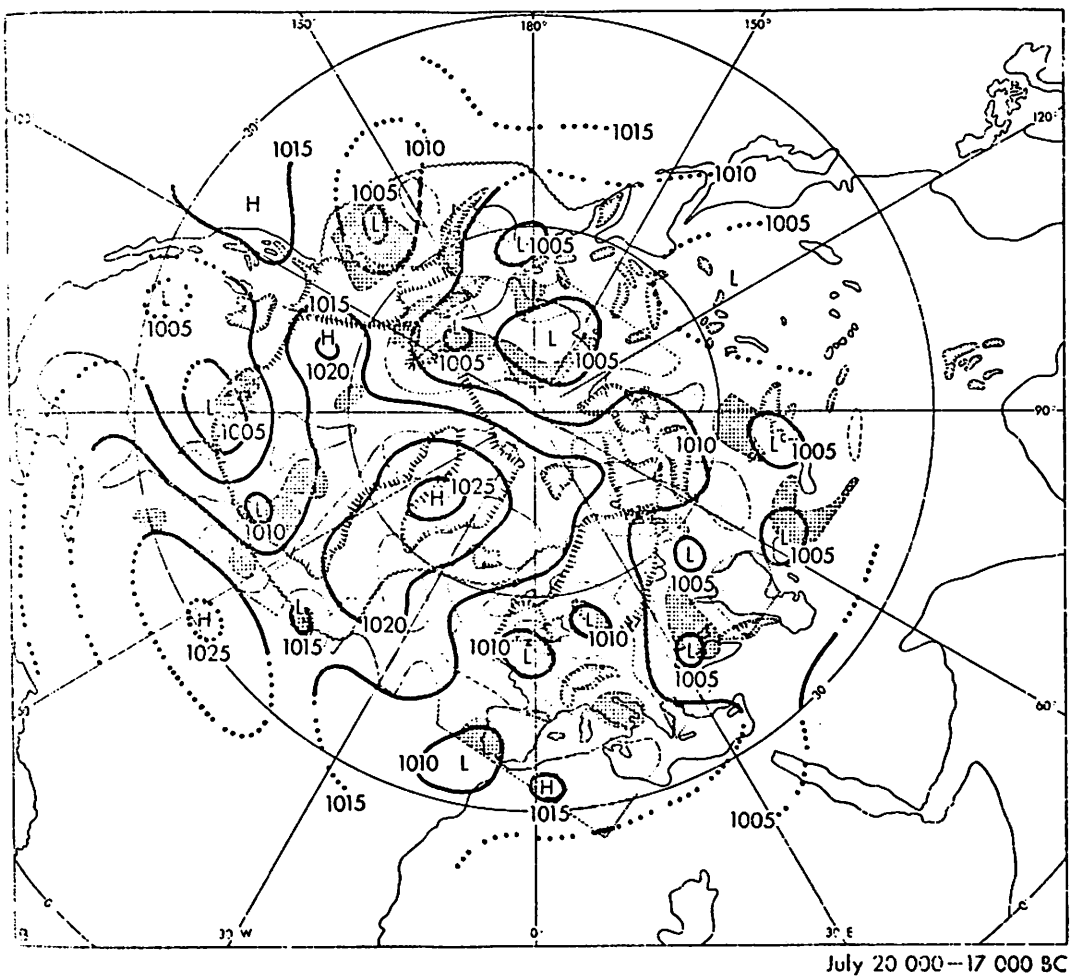

Figure 2.3d. Maximum glaciation, July, suggested MSL isobars with computed areas favoring cyclonic and anti-cyclonic development. From Lamb and Woodroffe (1971).

and anticyclonic development and mean surface isobars are shown for January and July at the glacial period maximum. These maps are from Lamb and Woodroffe (1971).

The conclusions reached by Lamb and Woodroffe, from consideration of the above maps, regarding the atmospheric circulation at the maximum of the last glacial period are:

1) The center of the circumpolar vortex and the surrounding pressure zones were displaced. The surface polar anticyclone generally occupied the region around Baffin Island and west to north-west Greenland.

2) The maps show great meridionality of the mean surface wind and pressure distributions, particularly in the Atlantic sector, with the polar anticyclone extending far south into the mid-Atlantic and blocking most of the west to east (or SW to NE) progression of cyclones.

3) Little seasonal change of vigor, or of latitude, of the mean circulation features. Some weakening and a more northern position of the cyclonicity in summer over Europe.

4) A cyclonic regime over western Siberia, both in summer and winter.

5) Reversal of the circulation over the inner-Arctic, probably in the ocean as well as in the atmosphere. Cyclonic rotation seems likely to have predominated over the polar region between north Greenland and the coast of Alaska. The main heat transport and the locus of

southerly surface winds entering the Arctic seems to have been from the Pacific over Alaska, not from the Atlantic and Europe as today.

As mentioned in the introduction, in only one earlier study has a model of the atmospheric circulation been used to simulate the possible climate of a glacial period and the study is that of Alyea (1972). Alyea developed a two-level quasi-geostrophic model for the northern hemisphere atmospheric circulation. The model was integrated forward in time for sixty days under two separate experimental conditions; one representing probable glacial maximum conditions the other representing a present day mean climate for July. The boundary conditions for the glacial period integration were established using geological sources.

The results of Alyea's simulations are very interesting. The glacial simulation reached a substantially higher kinetic energy level than the present day simulation. Alyea attributed this result to the stronger north-south temperature gradients generated along the southern edges of the large continental ice sheets and pack-ice. Nearly all of the difference between the kinetic energy of the July control and ice age cases of Alyea's study was due to the eddies.

The distributions of 500 mb (vertical mean) zonal wind profiles showed that in the glacial simulation the wind was very different from that of the present day

simulation in the belt from 40-70°N. Alyea proposed that the continental glaciers diverted zonal momentum southward, converging near 40°N approximately along their southern boundaries. The Hadley cell was somewhat stronger in the glacial period simulation.

Diabatic heating quantities are relatively comparable except in the latitude belt containing areas of glaciation and pack ice in the glacial period simulation. In the latter area, the presence of relatively cold underlying ice in the glacial period model inhibits upward transports of sensible and latent heat. Between 50°N and 70°N the total diabatic heating in the glacial simulation is substantially reduced compared to the present day simulation.

The climate results obtained from the two simulations show that in the glacial simulation the winds tended to skirt the edges of the ice. Alyea also thought that the results from the glacial simulation indicated the probability of a slight high pressure ridge over Central Canada due to the topography of the underlying ice. The circumpolar vortex center was therefore shifted to a position just south of Greenland. The most striking difference between the model climates, according to Alyea, was found in Europe. In the glacial simulation there is a large trough south of the Scandinavian ice sheet coupled with a sharp ridge to the east. No such features were observed in the present day

simulation results. The transient activity in the present day simulation is considerably less than that found in the glacial simulation across the northern Atlantic and in the regions of south-central to eastern Europe. A large number of cyclone waves under the influence of the strong steering currents over the North Atlantic were driven upon the Scandinavian ice sheet laden with moisture picked up from the ocean. Supported by orographic influences and stalled by the huge blocking high over Central Russia, Alyea believes that the Scandinavian ice could be maintained. The same blocking high pressure ridge, coupled with the severe continentality of Siberian Asia, served to deny the requisite moisture for glaciation in Siberia.

Alyea found that maintenance of the North American ice sheet was not so easily explained from the results of the model. Since there was a small pressure ridge over the North American ice sheet, which Alyea thought would diffuse the small number of cyclones which might reach the ice sheet, he felt that the simulation of July maximum glacial conditions did not supply enough moisture to maintain the North American ice sheet.

(c) Discussion

In this brief review we have seen that in the last few decades, several different descriptions of the possible atmospheric circulation at the maximum of the last

glacial period have been given. Most of the theories proposed by meteorologists have been explained on the basis of the patterns of recent secular variations of climate. That is, people have found out which meteorological conditions are favorable for snowy winters and cool summers and suggested that glacial period climates were prolonged periods of such circulation patterns. The use of glacial period boundary conditions in order to determine the climate at the maximum of the last glacial period, has been made recently by Lamb and Woodroffe (1970) and Alyea (1972). Before these two studies, others had used the knowledge of such things as the extent of the snow/ice or the temperature of the Atlantic as limits to their models but only recently have all of the known boundary conditions been applied to the problem. Lamb and Woodroffe's model was able to account for the thermal boundary conditions but was unable to account for the orographic effects. Alyea's model and the NCAR GCM do not have ocean models coupled to them so are unable to account for air-sea interaction effects which must have played some role in determining the glacial period climate. So we see that there are still some limitations on our reconstructions of paleoclimates.

Some of the problems involved in devising models of past climates are described in Beaty (1971). As Beaty points out, initially one man's model is as good as

another's, as long as it does not conflict too violently with known and inferred thermal and hydrodynamical "laws" of the atmosphere; but the validity of any model based on nonmeteorological data must ultimately depend on correct interpretation of the available evidence. It is clear, from the many examples which Beaty gives, that one of the greatest problems is agreeing on the meaning of the evidence. Beaty summarizes by saying that in view of great uncertainties about causes and effects of variations in atmospheric behaviour, considerable differences in interpretation of biological evidence of climatic change and no general agreement on past and present ranges of plant and animal species deemed critical to many climatic reconstructions, it is highly probable that simplistic climatic models (e.g., wetter and colder then, warmer and drier now) are of little or no practical value to anyone trying to arrive at an understanding of the causes and consequences of environmental change.

In the following chapter, some of the results from using the NCAR GCM with glacial period boundary conditions will be discussed. The discussion will in places involve comparison of the results with some of the models described in this chapter.

CHAPTER III

BOUNDARY CONDITIONS AND SOME CLIMATOLOGICAL RESULTS OF THE FOUR SIMULATIONS

(a) Introduction

Four different sets of boundary conditions have been used in the NCAR GCM in order to investigate the response of the simulated atmospheric circulation to large changes in boundary conditions. Two of the simulations have boundary conditions representing those of the present day January and July respectively, while the other two have conditions representing those of glacial period maximum January and July. The results of the latter two experiments do not necessarily describe the atmospheric circulation at the maximum of the last glacial period (about 20,000 years before present), but the major differences between the present day and glacial period simulations should give at least a first idea of the direction of the changes in atmospheric circulation between the present day and the last glacial period. Since this is the first time that a global model of the atmospheric circulation has been used to simulate the circulation with glacial period boundary conditions, the results will be interesting as a first estimate of the

impact of large changes in orography, albedo and sea surface temperature on the atmospheric circulation. Since the NCAR GCM includes many of the physical processes that we know are important and since all the equations involved in the motion and thermodynamics of the atmosphere are applied together, the results should give at least as good an estimate of the glacial period maximum circulation as earlier, more empirical studies. Inasmuch as this is a sensitivity study to examine how large changes in boundary conditions affect the simulated atmospheric circulation we must be careful not to place too much emphasis on the differences between the control cases and observed data. On the other hand, the question of whether the ice age cases results are realistic can only be answered on the basis of whether the GCM can simulate present day climate realistically in the first place.

(b) Boundary Conditions

As mentioned above, the boundary condition data consist of the orography and albedo at each grid point over land or ice and sea surface temperature at each ocean grid point. For the control cases the data were the same as those used by Kasahara and Washington (1971) except that some of the albedo data were adjusted to take account of recent measurements. The sources of these adjustments are listed in Williams et al. (1974).

For the ice age cases, data were taken from geological and paleobiological sources. Orography had to be changed to take account of the ice caps and increased pack ice extent; albedos were changed because of changes in vegetation and snow/ice extent; ocean surface temperatures were reduced in accordance with the limited ocean core evidence. The sources for all the boundary condition data for the glacial period cases are listed by Williams et al. (1974). Figures 3.1 and 3.2 taken from the same paper show the input data for the January ice age case.

(c) Climatological Results

In this section, results of this study which have already been published will be summarized. The results to be discussed are in each case averages of the meteorological fields for day 51 to day 80.

Williams et al. (1974) report results regarding pressure, wind, cloudiness and precipitation distributions and an examination of "synoptic features." The diagrams from the paper are reproduced in Appendix B. For the MSL pressure simulation, comparisons are made with observed data of Crutcher and Meserve (1970). It is pointed out that the model results may more nearly resemble a particular month than the long term mean condition. Differences between control and observed data are greater in the January case than in July. In the ice

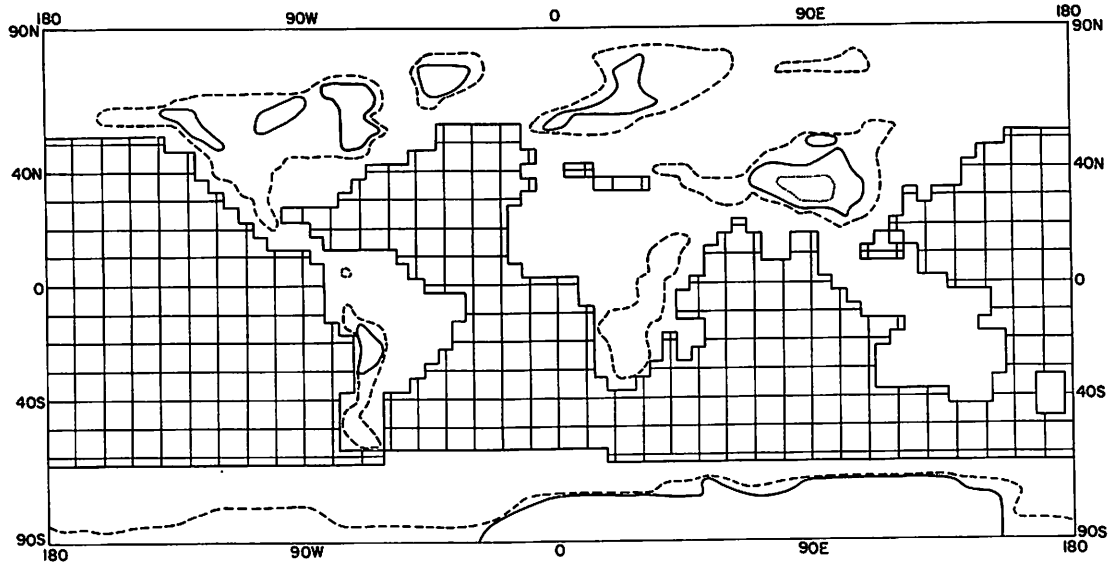

Figure 3.1. Outline of continents, ocean grid and orography used in January and July ice age cases. Contours shown are: dashed line, 1 km; solid line, 2 km; dotted line, 4 km.

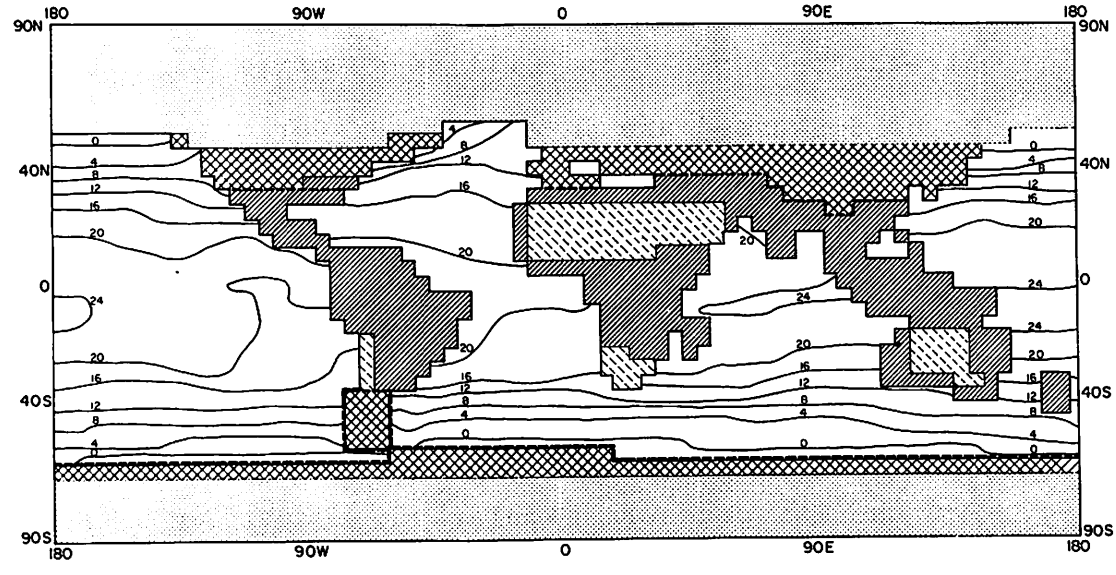

Figure 3.2. Albedos and sea surface temperatures used in January ice age case. Isotherms in °C. Dashed line is snowline. Albedos shown are: dotted, 61-100%; cross-hatched, 41-60%; broken-hatched, 21-40%; solid-hatched, 1-20%.

age cases there is a 10-degree southward displacement of the Icelandic and Aleutian lows in January while the Siberian high remains unchanged from the control case. Other small changes in the January case pressure distributions were noted. In July the most striking feature is the development of high pressure over most of Asia in the ice age case. The Aleutian low is more like the observed winter pattern of the present.

Synoptic activity was examined by preparing maps (see Appendix B) of the frequency of cyclone and anticyclone centers on days 51-80 of each of the four cases. For the January control case, major omissions compared with the observed data are the cyclone activity over the Mediterranean and mid-western North America. For July, the map of disturbance activity is considerably less satisfactory than the mean patterns. The January ice age map clearly shows the influence of major ice sheets and increased pack ice in displacing the zones of cyclonic activity southward. Analyses so far have not enabled us to distinguish between orographic and thermal effects of the ice sheets. In the July ice age case there is a major storm track across the North Atlantic and a continuation of this, or a further major track, from eastern Europe into Asia. In contrast with the January ice age case there is virtually no cyclonic activity in the vicinity of the Laurentide ice sheet. In the South Atlantic and South Pacific the distributions suggest blocking patterns

and there is apparently less synoptic activity in the southern westerlies.

The computed zonal mean cloudiness at 3 km is discussed by Williams et al. (1973) and illustrated in Figure 8.1. In the July ice age case there is considerably more cloud cover poleward of 25°N and in the January ice age case a similar increase in the subtropics but a decrease from 50-70°N.

Study of the geographical distribution of precipitation shows that many of the differences between the control case and observed zonal averages are caused by local areas of anomalously high or low precipitation in the simulation. Ice age case zonal averages of precipitation suggest for the southern hemisphere a negligible change in overall summer conditions and only a slight decrease in middle latitudes in winter. In the northern hemisphere, precipitation is decreased slightly in winter with the most pronounced effects between 0-10°N and 55-70°N. The July ice age case shows a dramatic reduction north of 10°N, by 50 per cent at 20°N and 75 per cent north of 60°N compared with the control case.

Williams and Barry (1973) discuss conditions in the vicinity of the northern continental ice sheets (see diagrams in Appendix B). In particular the distributions of ground temperature, zonal wind and precipitation are examined. Comparison of the control case ground temperatures with observed data indicates that in both January

and July the control case data compare favorably with observed data. The ice age case ground temperatures are much lower than those in the control cases. There is a stronger equator-to-pole temperature gradient over the North American continent in the ice age simulations. The July ice age case ground temperature distribution in the northern hemisphere strongly resembles that of the January control case and the present day summer continent-ocean thermal contrast is reversed so that the continents are colder than the oceans.

The zonal wind structure at 75°W (over the Laurentide ice sheet) and at 30°E (over the Scandinavian ice sheet) is discussed by Williams and Barry (1973). No major discrepancies between observed and control case zonal wind structure are found. At 75°W in the January ice age case the jet stream is weaker, the upper tropical westerlies are missing and the polar easterlies are less extensive compared with the control case. In the July ice age case the jet stream is stronger, upper tropical easterlies are again missing and lower tropical easterlies are less extensive. At 30°E in the January ice age case the jet stream has the same strength as that in the control case. In the July ice age case at 30°E there is no pronounced jet stream but rather a belt of westerlies of 20 m sec^{-1} extending from 50°N to the equator above 10.5 km. The July tropical easterly jet, situated between 35°N and 10°S in the control case, is not found

in the ice age case nor are surface westerlies in the tropics. Therefore, the response to the changed boundary conditions was not identical in the vicinity of the two ice sheets. There is no evidence to support the suggestion (Lamb and Woodroffe, 1971) that the jet stream was forced south to skirt the ice sheets. The ice age case jet stream is not consistently stronger or weaker than the control case jet stream, its strength and latitude vary with longitude and season. Elimination of the tropical easterly jet over Africa in the July ice age case suggests a weakening of the northern hemisphere summer monsoon, this will be discussed in a later section.

It is clear that there is a reduction of precipitation in the vicinity of the ice sheets in the ice age simulation, especially in July. This reduction is probably due to the very cold temperatures over the continents.

Barry and Williams (1973) discuss some southern hemisphere results and interhemispheric comparisons. Discrepancies in the pressure distributions and disturbance activity in the southern hemisphere between the control cases and observations are pointed out. One of the major discrepancies is the inadequate representation of the subpolar low pressure belt. This discrepancy is probably due to inadequate vertical and horizontal numerical treatment of Antartica and to very shallow low

pressure systems which are not well resolved. In the January ice age case the continental lows are displaced 5 to 10 degrees equatorward, there is a deeper Equatorial Trough at 15°S in the western Pacific and the subtropical anticyclones in the Indian Ocean Atlantic are weaker. In the July ice age case, there is a more meridional pattern in the middle latitudes and a broader, but weakened, Equatorial Trough in the Pacific sector. Maps of synoptic activity indicate fewer disturbances in January and a less continuous circumpolar pattern. In the July ice age case there is evidence of blocking patterns and cyclone "tracks" appear on both sides of the anticyclone cell at 45°S in the Pacific. Cyclonic activity is also increased in the Equatorial Trough over the Western Pacific and central Africa, and off southwestern Australia.

Precipitation amounts in the southern hemisphere, as in the rest of the world are overestimated by the model (this overestimation is discussed in Chapter 8), but distributions are fairly realistic in the control cases. In the July ice age case the dry zones are similar to the control case ones but the amounts of rainfall over the continents are reduced by about 50 per cent for Africa, Australia and South America and by about 30 per cent over Indonesia. The January ice age case shows complex changes.

Whereas the change in computed ground temperature is of the order of 30°C over the North American Arctic and Greenland[1] the computed reduction is about 5°C in the July cases and 6-8°C in the January cases in the southern hemisphere. In the northern hemisphere the cyclone tracks are considerably displaced by the ice sheets though jet streams are not affected consistently, but in the southern hemisphere the changes are smaller and quite complex.

(d) The Computed Glacial Period Circulation and Its Implications for the Ocean Circulation

Kraus (1973) has suggested that although the mean meridional temperature gradient at the bottom of the atmosphere was larger during ice ages than now, the temperature gradients were reduced, compared with those of the present day, in the upper troposphere. Basing his hypothesis on the relationship between sea surface temperature and the equivalent potential temperature of the atmosphere, Kraus shows that one may expect a threefold

---

[1] It has been pointed out that the parameterization of diffuse radiation in the GCM is not wholly realistic (Washington, personal communication, 1974). This discrepancy causes surface temperature to be underestimated when there is a high percentage cloudiness. This will result in particularly low ground temperatures in the July ice age case northern hemisphere, in which zonally averaged cloudiness was increased at nearly all latitudes compared with the control case.

amplification of tropical sea surface temperature changes in the upper troposphere and that above cold water this amplification is smaller. Therefore, he suggests that the upper equatorial troposphere was substantially colder during a glacial period while there was little change of the temperature at the same level at higher latitudes and consequently that the mean meridional temperature gradient in the upper troposphere was probably weaker during an ice age than today.

On the basis of the thermal wind relation, Kraus extends his agrument to suggest that wind shear (and therefore baroclinicity) was lower during an ice age than it is now. Using data derived from the glacial period and control cases of this study, Kraus describes the model derived evidence of reduced baroclinic instability of the ice age northern hemisphere winter. Using GCM-generated wind data, Kraus computed the curl of the wind stress over the North Atlantic and found that, with reservations regarding the realism of the model, the wind driven mid-latitude oceanic mass transport in the North Atlantic was considerably weaker in the ice age cases than control cases. This implies a reduced northward flux of warm water. Finally Kraus looks at the sea surface temperatures and clouds and suggests that since the sea was colder during an ice age, the infrared and latent heat losses should have been smaller. Since ocean heat transport was reduced, Kraus concludes that there must

have been more cloud cover at that time to satisfy heat balance requirements by reducing incoming radiation. He finds evidence in the GCM data for a reduction in cloudiness in the tropics during ice age cases.

(e) Temperatures in the Atmosphere in the Four Simulations

In order to evaluate Kraus's hypothesis at least as far as the GCM data are concerned, temperatures and temperature gradients will be examined in each of the four cases. Figures 3.3a and 3.3b show how the temperature changed from the control cases to the ice age cases for January and July respectively. It is immediately obvious that the model did not respond to the large changes in boundary conditions the same way in both months. In the January cases (Figure 3.3a) we see that in the lower troposphere (below say 6 km) the largest changes occurred in the polar areas, particularly in the northern hemisphere. In the upper atmosphere however we see that the January ice age case was colder than the control case at all latitudes but that the temperatures were reduced more in the tropics (by 10°C) than in middle latitudes (by 5°C).

In the July cases (Figure 3.3b) the temperature changes have a different pattern. The changes from the control case to the ice age case are greater (up to 40°C) and not roughly symmetric about the equator, as they are

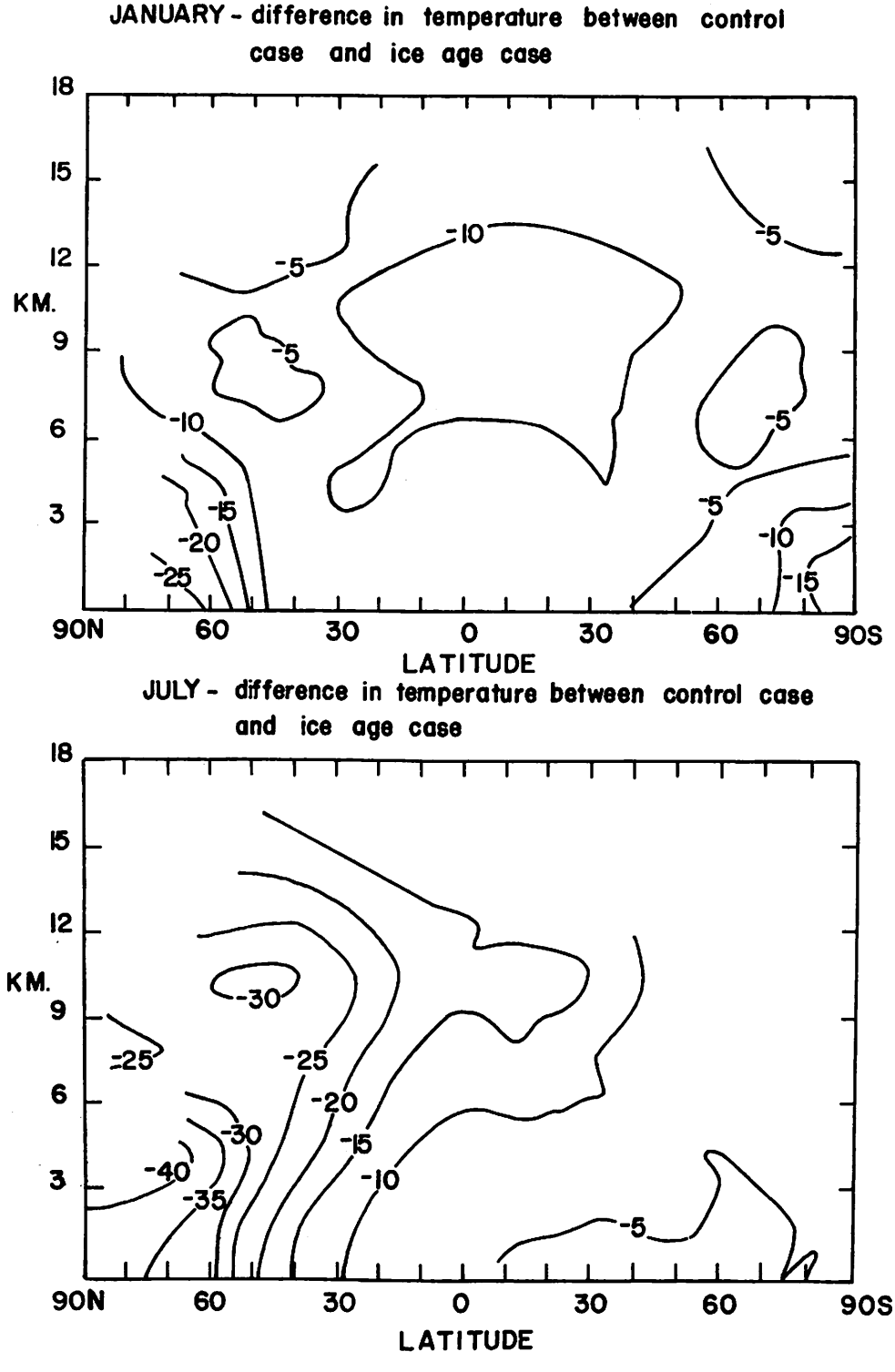

Figure 3.3. Latitude-height distribution of zonally averaged temperature change from the control case to the ice age case (a) for January cases, (b) for July cases. Units: °C.

in the January cases. The largest changes occur in the northern hemisphere at around 3 km poleward of 60°N. From these latitudes the reduction of temperature decreases and in the southern hemisphere the reduction of temperature was only 5°C in the layer below 3 km. In the July ice age case the temperature was much lower than that in the control case in the northern hemisphere middle and high latitudes lower troposphere. Figure 3.3b suggests that the July ice age case temperatures become like those of the January control case because of the inclusion of ice age boundary conditions.

Table 3.1 shows temperature gradients between different latitudes for the four cases. One set of gradients is taken at the 1.5 km level (c. 850 mb), the other set is taken at the 10.5 km level (c. 200 mb). The regions in which the temperature gradient is reduced from the control case to the ice age case are outlined. It is very clear that at 1.5 km for both January and July cases the temperature gradients increased from the control case to the ice age case at nearly all latitudes, which supports Kraus's hypothesis. For the northern hemisphere the gradient increases about 50 per cent in the January cases and about 250 per cent in the July cases at 1.5 km. In the southern hemisphere the increase is about 27 per cent in the January cases and only about 4 per cent in the July cases. The largest increase at 1.5 km in hemispheric temperature gradient is therefore

TABLE 3.1

TEMPERATURE GRADIENTS BETWEEN DIFFERENT LATITUDES FOR THE FOUR CASES

Latitudes	January Control	January Ice Age	July Control	July Ice Age
Temp. at 1.5 km				
0-90N	41.2	62.2	12.0	44.6
0-30N	12.9	14.4	0.7	6.1
30-60N	19.4	35.6	5.8	25.6
60-90N	8.9	12.2	5.9	12.9
0-90S	46.0	58.3	60.3	62.8
0-30S	4.2	4.8	10.8	10.6
30-60S	18.2	17.5	17.8	16.6
60-90S	23.6	36.0	31.7	35.6
Temp. at 10.5 km				
0-90N	35.3	28.6	17.6**	17.3**
0-30N	9.0	5.7	-4.0*	6.7
30-60N	21.6	16.3	8.3	12.2
60-90N	4.7	6.6	9.3	5.2
0-90S	31.6	24.5	37.6	28.7
0-30S	4.4	4.5	8.7	6.6
30-60S	19.1	13.1	22.2	16.0
60-90S	8.1	6.9	6.7	6.1

* Temperature increases from 0°N to 35°N.
** T from 30-90°N.

in the July ice age case in the northern hemisphere. At 10.5 km, on the other hand, temperature gradients are reduced in nearly all regions in both January and July. In the July ice age case the reduction of the temperature gradient is not great and only occurs between 60°N and 90°N where the reduction is about 22 per cent.

The results presented in Table 3.1 therefore support the hypothesis of reduction of temperature gradients in the upper atmosphere in the glacial periods for the January ice age case and for the southern hemisphere in the July ice age case. Support from the northern hemisphere in the July ice age case is more tentative.

(f) Further Discussion of the Kraus Hypothesis

Since it has been found that the model results support Kraus's theory for the January ice age case as far as atmospheric temperatures are concerned, other factors mentioned by Kraus should be looked for in the model results.

It was suggested that the infrared and latent heat fluxes would be reduced in the ice age in tropical latitudes because of the cooler ocean surface. As far as the net infrared radiation lost by the troposphere is concerned the hypothesis is supported by the model. In Chapter VI it is shown that in both January and July ice age cases the net infrared radiation flux is reduced. However, the latent heat flux is not reduced in both

January and July ice age cases in the tropics. Again, this heating term is discussed in Chapter VI and it is shown that in the July ice age case the latent heating rate is reduced in the tropics, by up to about 0.5°C day^{-1}. In the January ice age case the condensation heating is greater than that in the control case by as much as c. 0.3°C day^{-1} in the upward branch of the Hadley cell.

Horizontal heat transport by the eddies ($\overline{T'v'}$), which Kraus suggested would be reduced in the ice age case, is examined at the 3 km and 12 km levels in Chapter VI. In the northern hemisphere at the 3 km level in January and July the horizontal heat transport by the eddies is reduced in the ice age cases north of about 40-50°N. At the 12 km level the reduction is only large in the July cases. In Chapter VII the eddy kinetic energy of the atmosphere is discussed and this partial indicator of the baroclinicity of the atmosphere suggests that on a global average the baroclinicity decreased strongly in the July ice age case but slightly increased in the January ice age case compared with the control case data. Clouds in the tropics, which are also discussed by Kraus (1973) are discussed in a later section of this chapter.

We therefore see that Kraus's ideas about the ice age circulation are not all supported by the simulations

and that it is not consistently the July or January cases which oppose them.

(g) Latitude-Height Distributions of Zonally Averaged Winds

(i) u Component of Wind

In Figures 3.4 and 3.5 the zonally averaged u component of the wind is illustrated for the January and July cases and observed data. For the January cases (Figure 3.4) it is evident that the control case data and observed data compare favorably. The jet streams in the control case are about 5 m sec^{-1} stronger than those observed, but since the observed data (from Newell et al., 1972) are an average from December-February, small discrepancies in speed are probably not significant. The jet streams in control cases occur at too great an altitude and this is apparently a result of the upper boundary conditions in the model. The 12-layer version of the NCAR GCM, described by Kasahara et al. (1973), which has the upper boundary at 36 km instead of 18 km, produces jet streams at a lower altitude. The isotachs are closed below 18 km which is not the case with those illustrated in Figures 3.4 and 3.5. The only other discrepancy is that the model does not produce the observed weak upper tropical easterlies in the zonal average, although easterlies are present in small regions on geographical plots.

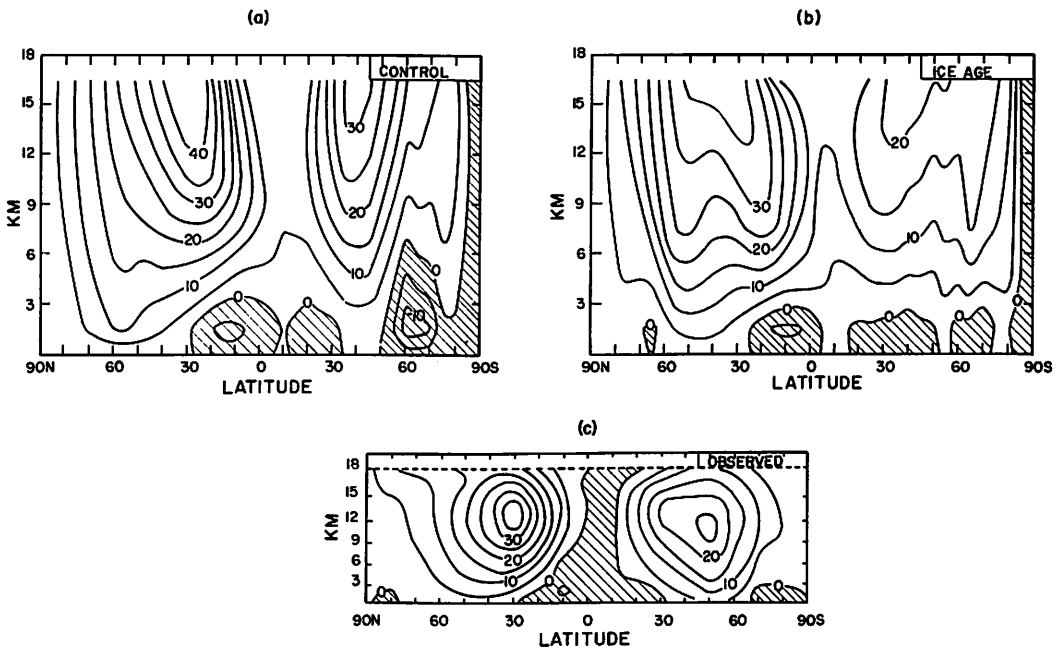

Figure 3.4. Latitude-height distribution of zonally averaged u component of the wind for (a) January control case, (b) January ice age case, (c) January observed data from Newell et al. (1972). Units: m sec^{-1}.

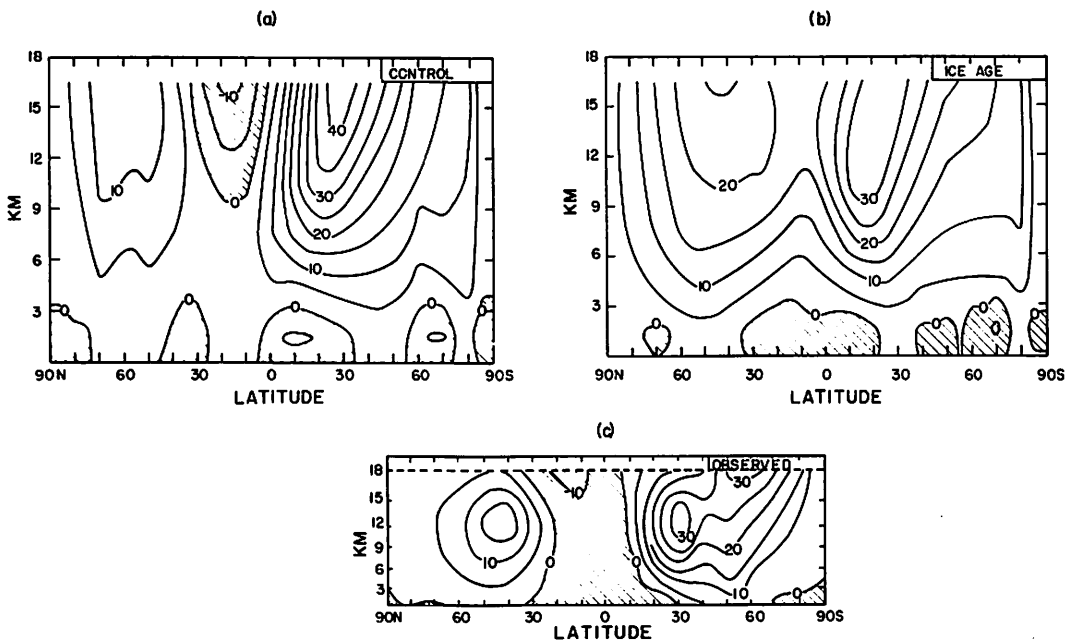

Figure 3.5. Latitude-height distribution of zonally averaged u component of the wind for (a) July control case, (b) July ice age case, (c) July observed data from Newell et al. (1972). Units: m sec^{-1}.

The January ice age case u component of the wind (Figure 3.4b) is certainly different from that in the control case. The northern hemisphere jet is weaker (by 5 m sec^{-1}) but more importantly shows indications of a double maximum and has its maximum 5 degrees equatorward of the control case position. The southern hemisphere jet is 10 m sec^{-1} weaker in the ice age case.

In the July control case the northern jet is 15 degrees poleward of its observed position but the strength of the jet is comparable with that observed (which is averaged from June through August). The upper tropical easterlies are simulated and the southern hemisphere jet, which is 10 m sec^{-1} stronger in the model than observed, soes not have the two definite maxima indicated in the observed data. The most important difference between the July control case and July ice age case zonal winds is in the tropics where the upper easterlies are eliminated in the ice age case. Both jets are about 10 m sec^{-1} weaker in the ice age case and occur about 3 km lower in the atmosphere.

(ii) v Component of the Wind

Figures 3.6 and 3.7 show the zonally averaged meridional component of the wind for January and July cases. The control cases will be compared with the observed data given by Newell et al. (1972), which are not illustrated here.

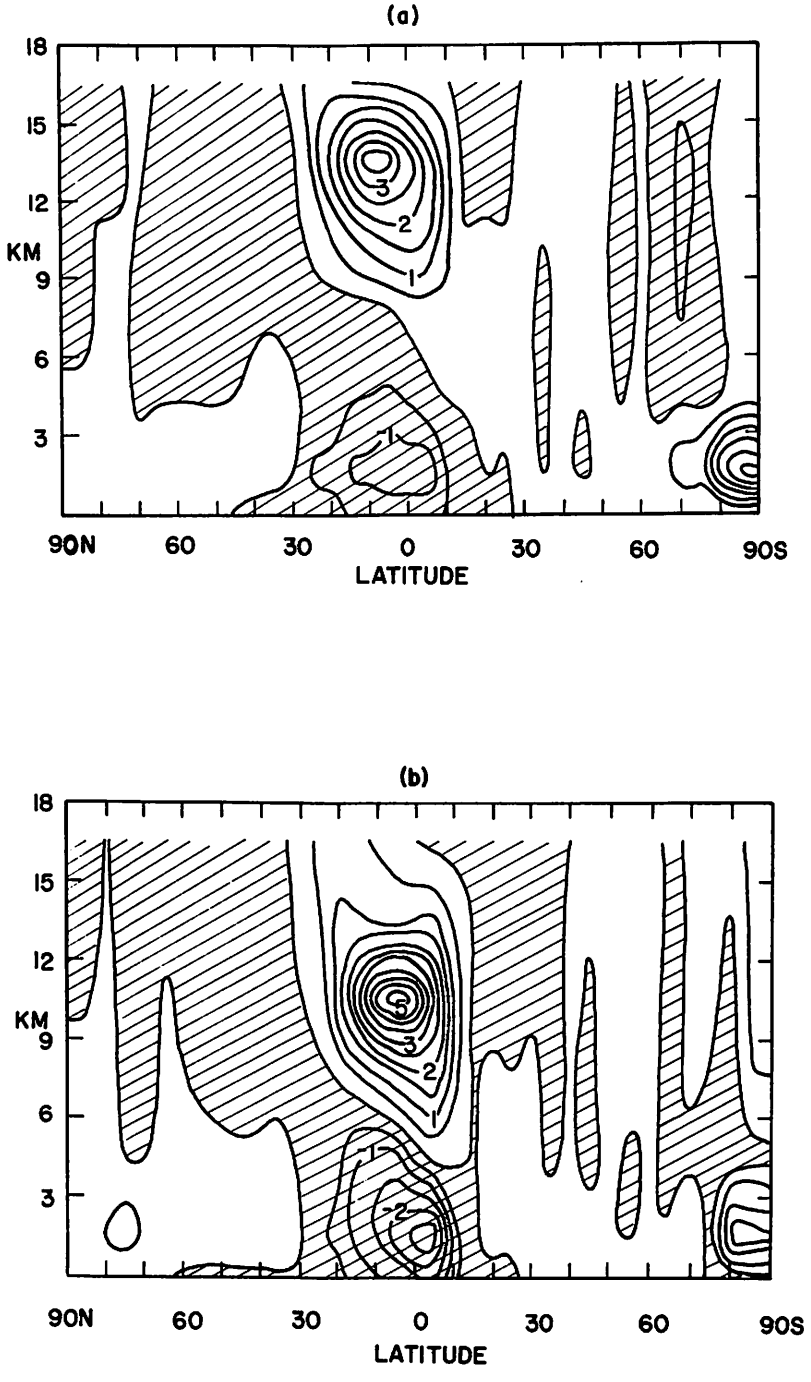

Figure 3.6. Latitude-height distribution of zonally averaged v component of the wind for (a) January control case (b) January ice age case. Units: m sec^{-1}.

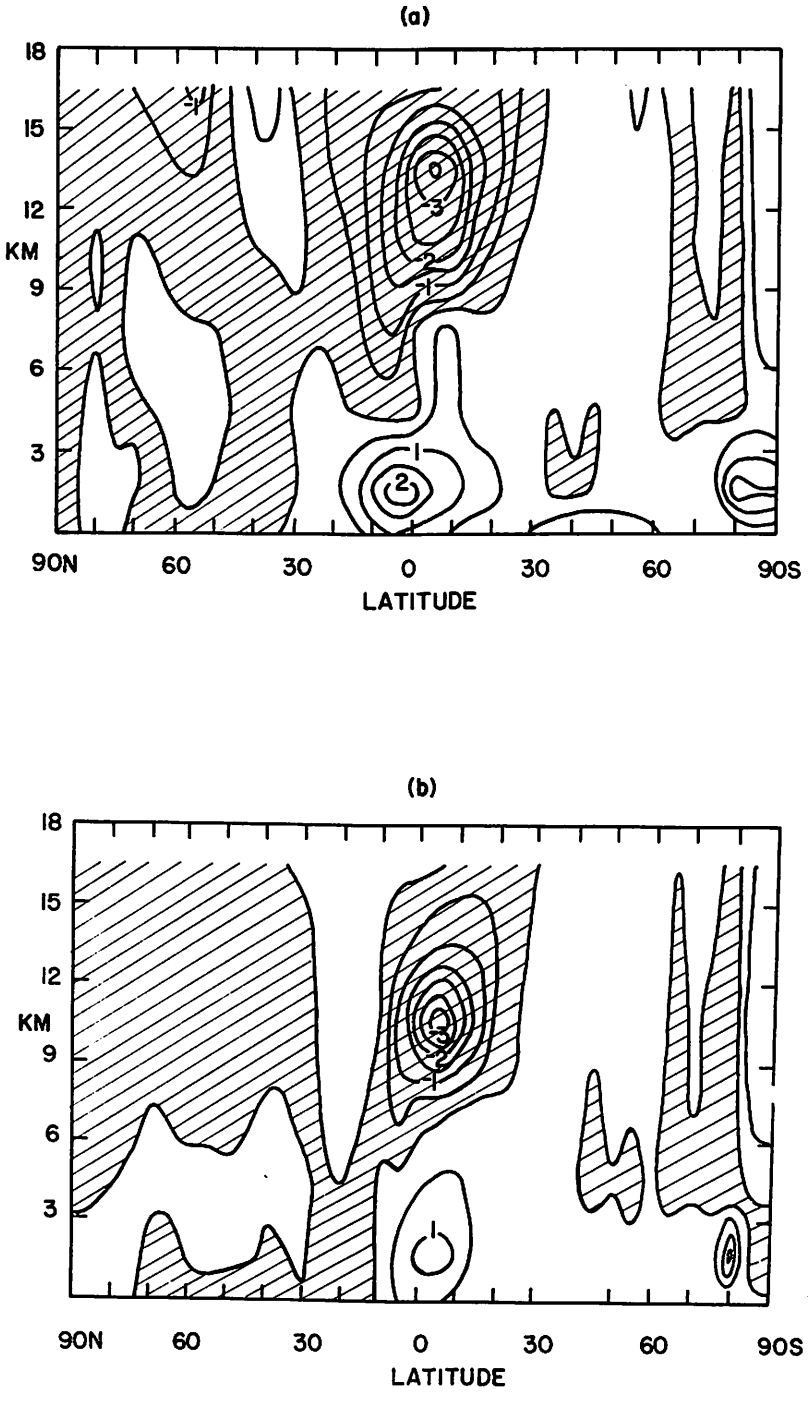

Figure 3.7. Latitude-height distribution of zonally averaged v component of the wind for (a) July control case (b) July ice age case. Units: m sec^{-1}.

In the January cases we see that the maximum meridional velocity occurs in the vicinity of the Hadley cell. Between 10°S and 30°N there is a region of maximum northward transport in the January control case. This maximum is in the same position as that observed by Newell et al., but it is 1 m sec^{-1} stronger. In the lower tropical atmosphere there is a secondary maximum, this time of southward transport. This maximum is again situated correctly, but it is about 0.5 m sec^{-1} weaker than that observed. Again it should be pointed out that the observed data are averaged over a three month period so small differences between the observed and control case data can be expected.

The meridional component of the wind in the January ice age case is quite different from that in the control case. The northward maximum at 10°S to 30°N is stronger by about 38 per cent in the January ice age case and the lower southward maximum is also stronger, in this case by about 100 per cent. So we see that in the January ice age case the north-south velocities in the Hadley cell are much stronger than those of the control case.

In the July cases (Figure 3.7) the meridional component of the wind is again simulated well by the GCM. The July control case has a maximum southward transport in the upper troposphere, located within the same latitude belt as that observed but is about 0.9 m sec^{-1}

greater than the observed maximum. The secondary maximum in the lower tropical atmosphere is about 0.4 m sec^{-1} greater than the observed maximum.

The July ice age case differs from the July control case in the tropics. The meridional velocity is slightly weaker in the ice age case than the control case in the upper troposphere. The northward maximum in the lower tropics is 45 per cent weaker in the July ice age case.

Therefore the north-south winds in the Hadley cell are all strengthened in the January ice age case and weakened in the July ice age case.

(iii) w Component of the Wind (Figures 3.8 and 3.9)

As with the meridional component of the wind, the vertical component is largest in the vicinity of the Hadley cell. It is clear that in each season the Hadley cell of the winter hemisphere is strongest. In the January control case there is a maximum of upward velocity at about 10°S and 9 km. The January control case data can be compared with observed distributions of w. However, the values of w are small (zonal averages less than 1 cm sec^{-1}) and the data is inhomogeneous. Therefore there are large variations in the observed values of w. For instance Tucker (1959) found a maximum value of 9 mm sec^{-1} in the descending branch of the Hadley cell in winter, whereas Vincent's (1969) diagram,

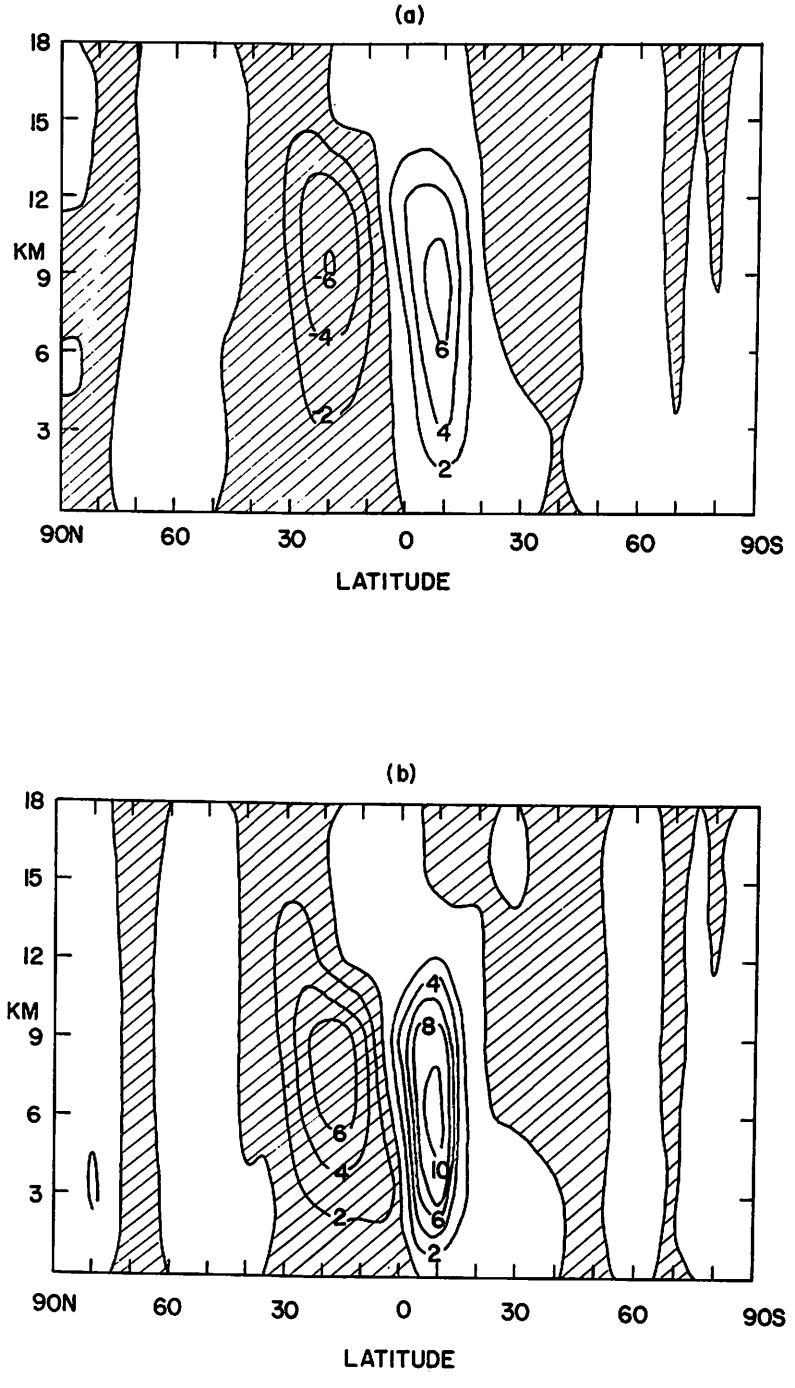

Figure 3.8. Latitude-height distribution of zonally averaged w component of the wind for (a) January control case (b) January ice age case. Units: mm sec^{-1}.

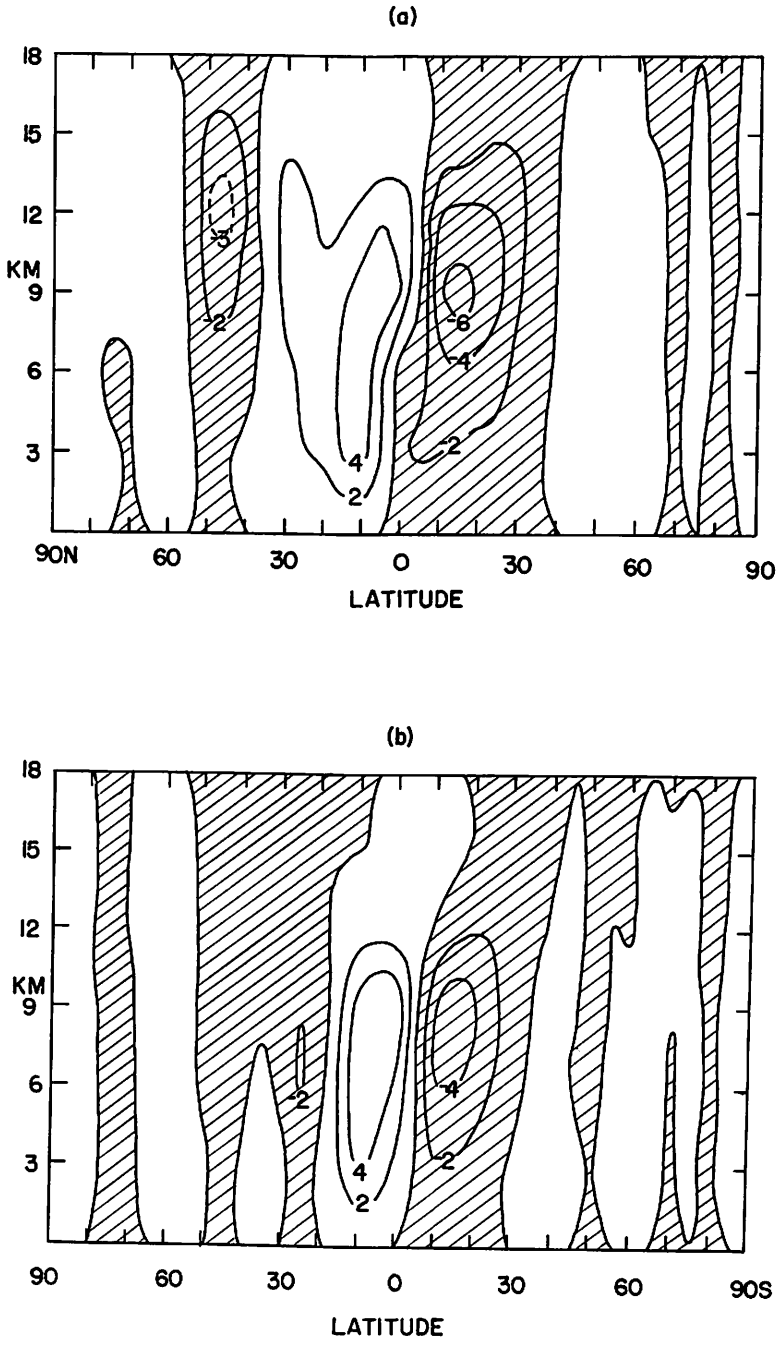

Figure 3.9. Latitude-height distribution of zonally averaged w component of the wind for (a) July control case (b) July ice age case. Units: mm sec^{-1}.

illustrated in Kasahara and Washington (1971), shows a value of 4 mm sec^{-1} in the same region and the same season. The January control case value of 6 mm sec^{-1} falls within the two observed values, so we know that it is of the right order. In view of the problems involved in the evaluation of the mean meridional circulation, which are outlined by Tucker (1959), an exact comparison of observed and computed data is probably not too meaningful at this stage.

In the January ice age case (Figure 3.8b) the vertical velocities in the Hadley cell, as is the case with the meridional velocities, increased. The maximum vertical velocity (upward) in the Hadley cell is at about 10°S, 6 km (i.e., lower than that in the control case) and about 57 per cent stronger than the control case maximum. The downward velocity maximum is located in the same position as that in the control case but is about 25 per cent stronger. Thus the overturning of the Hadley circulation is stronger in the January ice age case than the control case.

In the July cases (Figure 3.9), the maximum upward velocity occurs about 5°N and 3-12 km in the July control case and the maximum downward velocity occurs at about 15°S and 9 km. Comparison of the July control case data of w with observed data of Tucker (1959), shows that the region of upward motion in the northern hemisphere is well simulated. The downward velocity maximum in the

northern hemisphere is much larger in the observed data (-8 mm sec^{-1}) than the control case (-3 mm sec^{-1}).

In the July ice age case the maximum upward velocity is in approximately the same position as that in the control case (though the latitudinal extent of upward velocities is decreased by about 20 degrees latitude) and it is about 13 per cent stronger than the control case value. Since the northern hemisphere summer monsoon is eliminated in the July ice age case, one would expect the upward velocity at 5°N to be decreased. In fact it shows an increase and this can be explained by considering Figure A-1 in Appendix B. It is seen that the vertical velocity at 3 km in the July cases is downward over India in the ice age case and upward in the control case. Over the oceans between 0° and 30°N in the July control case there is considerable downward motion but this is reduced in the ice age case because the oceans are warmer than the continents. So the maintenance of the rising branch of the Hadley circulation in the July ice age case is because rising motion increased over the ocean areas and overcompensated for the decreased upward velocity over the monsoon lands. The maximum downward velocity is at about 15°S and 9 km in the July control case. In the ice age case the downward velocity maximum is at 9 km between 15°S and 20°S and is 24 per cent smaller than the control case value. The overturning does not increase in all branches of the

Hadley cell in the July ice age case compared with the control case.

Pittock (1973) has recently found evidence of interactions between the location of the subtropical high pressure belt over the east coast of Australia and variations in the strength and driving force of the Hadley circulation. As Pittock points out, the driving force of the Hadley circulation is related to evaporation rates and temperature at the tropical sea surface. He suggests that factors relating to the driving force of the Hadley circulation should be investigated. The information could lead to a greater understanding of the nature of global climatic change. We have seen that in the January ice age case the Hadley circulation is stronger than that in the control case. Reasons for the increase are unclear, but this emphasizes the need for more study on the role of changes in the Hadley circulation in climatic change.

(h) An Analysis of the Thermal and Orographic Influences on Mid-Tropospheric Pressure Distributions in the Four Simulations and Observed Data

Williams (1973a) investigated the thermal and orographic influences on the 6 km (c., 500 mb) pressure distributions. In this section the study will be briefly described.

The thermal and dynamic influences on the quasi-stationary mean motions of the atmosphere have been discussed in earlier literature from several different points of view. Some studies have proposed that orography is the prime cause of the quasi-stationary deviations from pure zonal flow (e.g., Charney and Eliassen, 1949; Bolin, 1950). Others (e.g., Smagorinsky, 1953; Döös, 1969) looked at the influence of large scale heat sources and sinks on the motions of the atmosphere. But the relative importance of the dynamical and thermal effects is hard to evaluate. Murakami (1967) suggested that the relative importance of the two effects is dependent upon latitude. Kasahara and Washington (1968, 1971) investigated the question by using the NCAR GCM. They find that the inclusion of orography improves the simulation of January climatology but it appears that the thermal effect is a major factor in determining the zonal tropospheric statistics for a January simulation.

To study the thermal and orographic-dynamical influences on the atmosphere simulated by the GCM, data for 45°N, 60°N, 45°S and 60°S were used. Pressure at 6 km was chosen for the investigation.

At each of the four latitudes selected the zonal average of pressure at 6 km was noted and for each line of latitude the difference from the zonal average at different longitudes was plotted. The orography along the four lines of latitude was plotted. In order to

discuss the thermal influences on the atmosphere, sections along lines of latitude showing differences from the zonal average of ground temperatures (30-day mean) were included. Ground temperature does not by any means provide the complete picture of the thermal influence on the atmosphere. What is really needed is a picture of the heat sources and sinks of planetary dimensions. The heat sources and sinks could be evaluated from model output and this aspect of the study will be pursued in the future.

The results of the study indicate that the thermal influences play a major role in determining the large scale atmospheric flow at 60°N and 60°S, while orography possibly exerts some dynamical influence over the Rocky Mountains and Andes. At 45°N and 45°S the atmospheric flow seems to be primarily influenced by the thermal effects of land-sea distribution and orography. In general, thermal forcing of the GCM boundary conditions seems most important but the relative importance depends upon the latitude. The inclusion of ice sheets (additional topographic barriers) in the boundary conditions did not create such large changes as one might have expected. Perhaps the changes would be more evident at higher elevations in the model atmosphere, where the thermal forcing from the earth's surface is not as great. The question of whether the ice age-control case differences in climatology are primarily a result of orographic

or thermal (sea surface temperature) changes will be investigated in future experiments. It is anticipated that the influences will vary with latitude since the changes of boundary conditions are not uniform.

(i) An Investigation of Zonal Variations of the Wind Field Using Data from the Four Simulations

The structure of the wind field shown by a meridional cross section is considerably influenced by the longitude of the section. For example, the upper westerlies flow in a wave pattern and there are differences between wind structures near troughs and ridges. Meridional cross sections of the zonal wind, u, at different lines of longitude have been examined by Williams (1973b). Special attention was given to the location and maximum speed of jet streams in the four GCM simulations. Generally, no systematic differences between the observed and control case data are found, although there are systematic variations between the control case southern hemisphere jet and that observed. In 10 of 14 cases, the two observed jets are replaced by one simulated jet. In the model it seems that the polar front jet and subtropical jet merge into one in the zonal average.

There are no strikingly systematic variations between the control case and ice age case mid-latitude wind fields at different longitudes. The ice age case

jet streams show considerable variation from the positions and speeds in the control cases. At 140°W, 130°W and 30°E in July the northern hemisphere jet is missing in the ice age case. At 75°W and 30°W in January and 130°W and 140°W in July the southern hemisphere jet is very weak or missing. The winds in the upper tropics do show some systematic variations between the control cases and ice age cases. At all but two of the lines of longitude the easterly winds in the upper tropics, seen in the control case, are not found in the ice age case cross sections.

Meridional cross sections along 75°E and 140°E show the wind structure over part of the Himalayas and to the lee of the Himalayas respectively. In Figure 3.10 the meridional sections along 75°E are illustrated for the four cases. In the July ice age case the main difference is the complete elimination of the tropical easterly jet. The latter feature suggests that the monsoon structure observed in the control case at 75°E is not simulated when ice age boundary conditions are introduced into the GCM. The suggestion that the monsoons were weaker or non-existent during the ice ages has been proposed on the basis of geological evidence by Joshi (1969). At 140°E there is again evidence that the summer monsoon structure is disturbed by the introduction of ice age boundary conditions into the NCAR GCM.

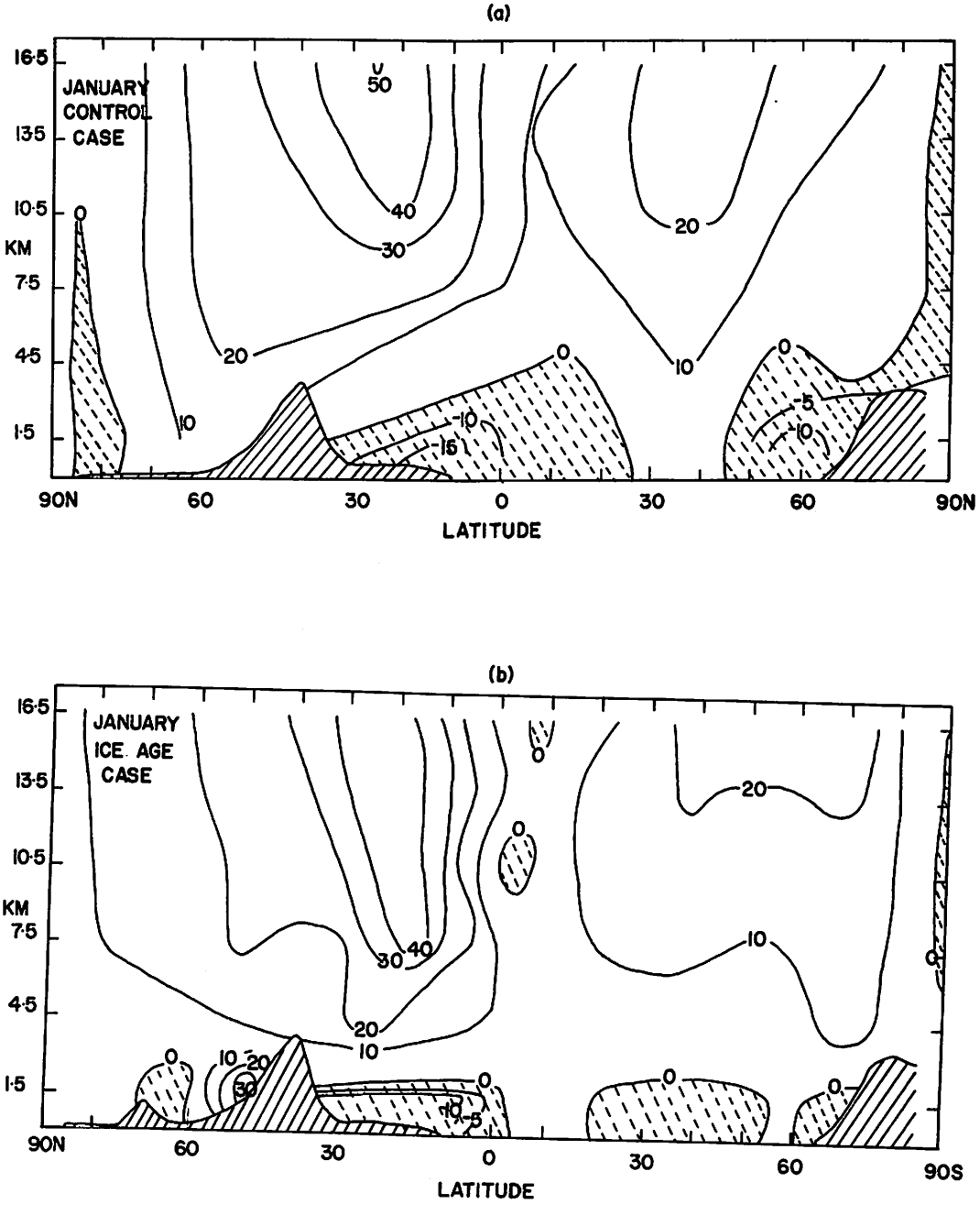

Figure 3.10. Meridional cross section of u component of the wind at 75°E for (a) January control case, (b) January ice age case, (c) July control case, (d) July ice age case. Units: m sec^{-1}.

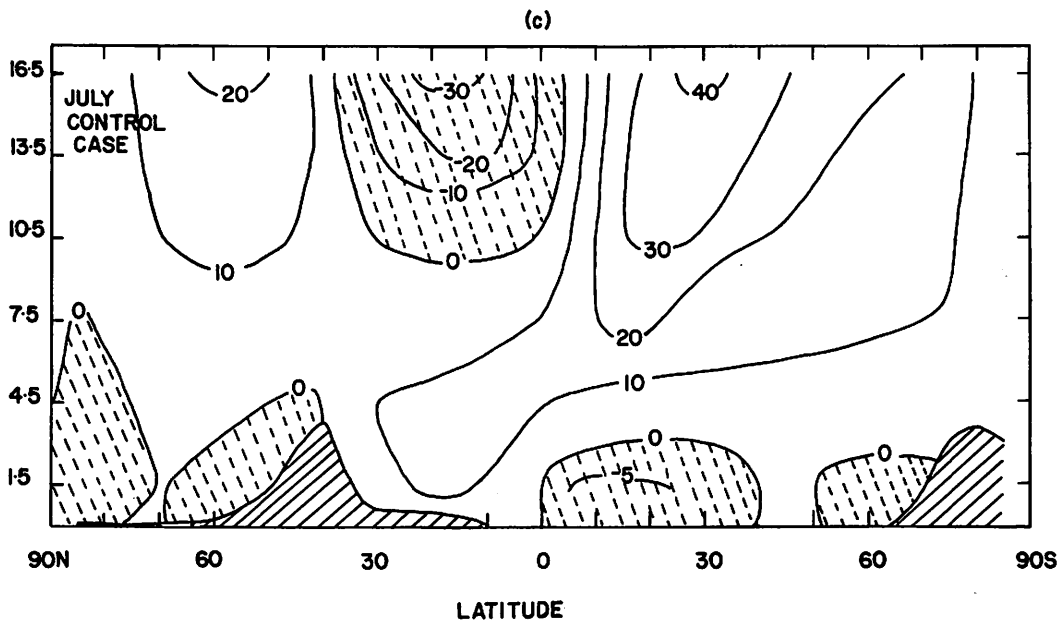
(c)
JULY
CONTROL
CASE
20
30
40
20
10
0
10
30
20
10
0
0
0
0
-5
16·5
13·5
10·5
7·5
4·5
1·5
90N
60
30
0
30
60
90S
LATITUDE

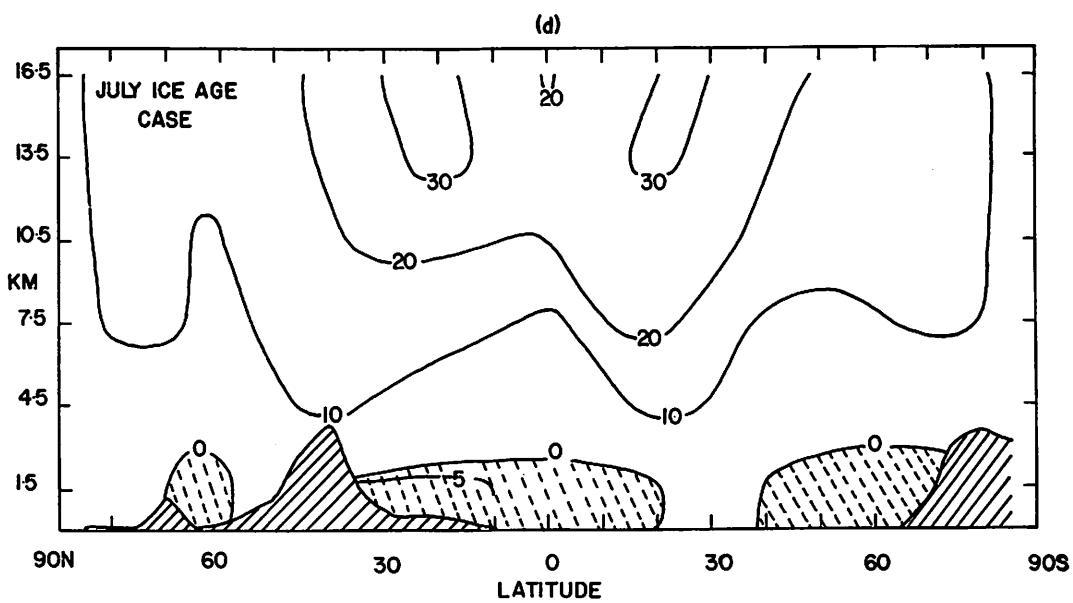
(d)
JULY ICE AGE
CASE
20
30
30
20
20
10
10
0
0
0
-5
16·5
13·5
10·5
KM
7·5
4·5
1·5
90N
60
30
0
30
60
90S
LATITUDE

(j) Upper Troposphere Tropical Circulation

Krishnamurti (1971a) and Krishnamurti et al. (1971a) have listed the primary entities of the large scale circulations over the northern summer hemisphere as (1) Tibetan High, (2) African High, (3) Mexican High, (4) Mid-Atlantic Trough, (5) Mid-Pacific Trough, (6) Easterly jet of southern Asia. These features are observed in daily and in seasonal means of the pressure and wind distributions at 200 mb. In Figures 3.11a and 3.11b the pressure distribution at 12 km (c. 200 mb) is illustrated for the July control case and ice age case respectively. We see that in the July control case, the Mexican, African and Tibetan Highs are simulated, as are troughs over the Pacific and Atlantic oceans. In Figure 3.10c we see that the tropical easterly jet is also simulated in the July control case. In the July ice age case the pressure distribution at 12 km is very different from that in the control case. Whereas in the control case there are east-west variations of pressure and pronounced circulation features, the pressure distribution in the July ice age case shows a steady increase from low pressure at the poles to high pressure at the equator with no pronounced circulation features. We have already noted that the tropical easterly jet is not simulated in the July ice age case.

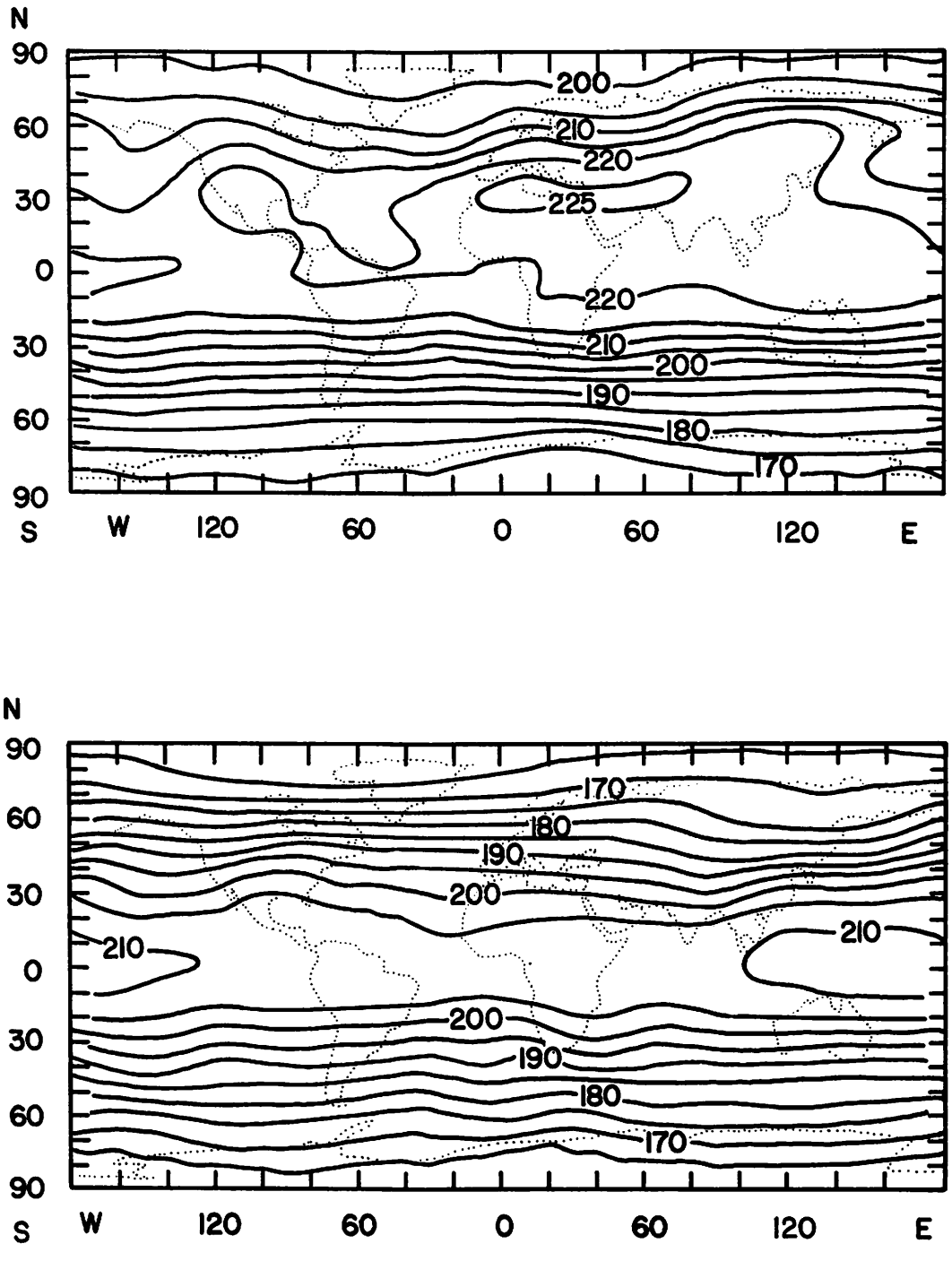

Figure 3.11. 30-day mean distribution of pressure (mb) at 12 km for (a) July control case (b) July ice age case.

All of the circulation features are related to the monsoon circulation of the northern hemisphere summer. As Wallace (1972) has pointed out, the monsoon flow is forced by the differential heating between sea and land masses. The release of latent heat in ascending air is very important in the generation of monsoons, as shown in general circulation model experiments by Manabe and Smagorinsky (1967) and Manabe et al. (1970a).

Krishnamurti (1971b) shows that an important part of the monsoon circulation consists of the tropical east-west circulations. The air over the Tibetan Plateau is warm and rises, the air over the Pacific and Atlantic Oceans is cool and sinks, giving an east-west circulation. Krishnamurti (1971b) found that these thermally direct east-west circulations have comparable intensity in the northern summer to that of the Hadley circulation. This thermally direct circulation plays an important role in the generation of kinetic energy. Computations by Krishnamurti et al. (1973b) show that the conversion of eddy kinetic energy to zonal kinetic energy in the tropics is positive in the northern hemisphere summer and negative in the northern hemisphere winter. It is clear that the monsoon plays an important role in global atmospheric energetics.

Figure 3.12 illustrates the temperature at 12 km for 30°N. In the July control case there are large zonal variations and the high temperature over the

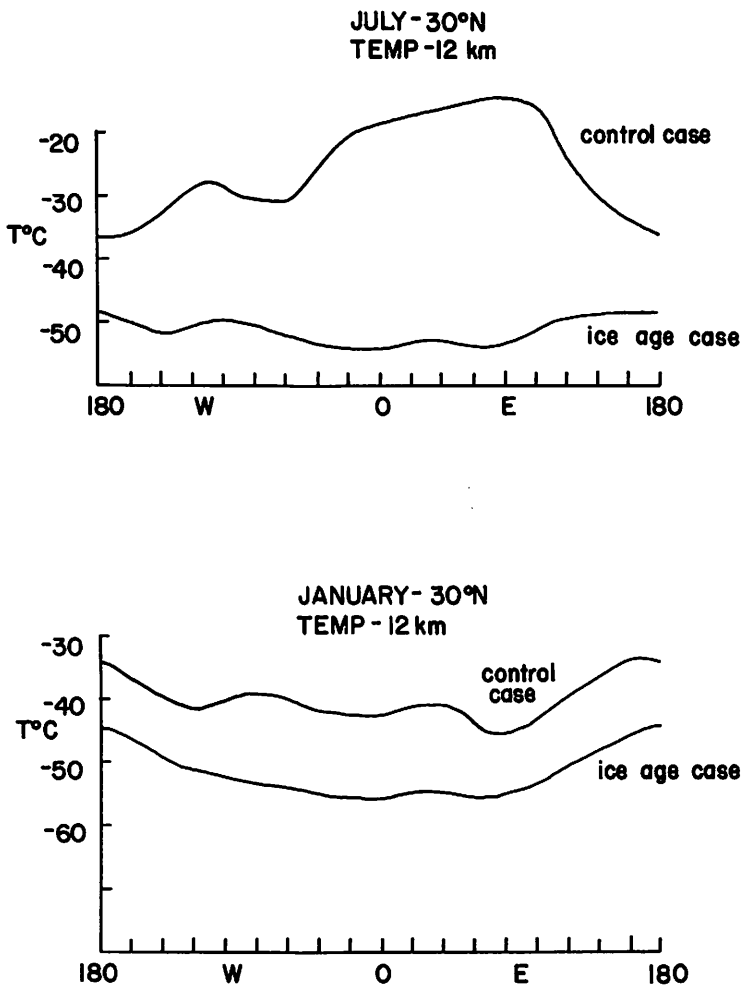

Figure 3.12. Temperature (30-day mean) along latitude 30°N at 12 km for the four simulations. Units: °C.

Tibetan Plateau is obvious. These temperature differences correspond to a monsoon circulation. In the July ice age case the values of T at 12 km along 30°N do not show large variations zonally and the absence of these variations signifies a reduced generation of eddy kinetic energy (which depends on the term W'T', see Chapter VII).

Since there are large differences in the upper troposphere tropical circulation between the July control case and ice age case we would expect large differences in the energetics of the two cases, i.e., the control case should have more eddy kinetic energy than the ice age case and less zonal kinetic energy. The ice age case should have energies resembling those of the January control case. In Chapter VIII it is shown that this is the case. Since the monsoon circulation is forced by land-ocean heating contrasts, the non-appearance of the monsoon in the July ice age case must be a result of the reduction of the temperature gradient along say 30°N. Williams and Barry (1973) have pointed out that the inclusion of ice age boundary conditions in the GCM caused the July ice age case ground temperature distribution to resemble strongly that of the January control case in the northern hemisphere. The present-day land-ocean thermal contrast was reversed so that the continents were colder than the oceans in the July ice age case.

Since the northern hemisphere summer monsoon plays an important role in global atmospheric energy and momentum balances, its absence is of significance. Krishnamurti et al. (1973a) discuss the relative success or failure of various models of the general circulation in simulating the northern summer 200 mb conditions. Among the models discussed is that of Alyea (1972), which failed to simulate the Tibetan High, mid-oceanic troughs, etc. Krishnamurti et al. looked at the physics of Alyea's model in order to find possible reasons for the major differences between observations and computations. They suggest that the intensity of the heating in Alyea's model was too weak in the subtropics and thus could not maintain a blocking thermal high over the Asian highlands. Since Alyea's model only covers the northern hemisphere there were apparently also problems with specification of the boundary conditions at the equator.

Since Alyea did not succeed in simulating the monsoon in either his July "present day" case or his July "ice age" case, it is to be expected that the energetics of his two cases and the two July cases of this study will differ. It would appear from the arguments presented above that the results of the present study are more realistic.

(k) Comparison of Results of this Study with Conclusions of Earlier Studies

In this section the major conclusions reached in earlier paleoclimatic studies (as described in Chapter II) will be compared with the results of the present study.

Bryan and Cady's (1934) main conclusions regarding the glacial period maximum circulation can be summarized as: (1) air temperatures and pressures in summer comparable with those in present winter, (2) winds stronger, (3) subtropical high pressure reduced and shifted southward, (4) Icelandic low and storm tracks shifted southward. We have already seen in this chapter that atmospheric temperatures in the July ice age case became like those of the January control case because of the inclusion of ice age boundary conditions. 30-day mean MSL pressure maps of the northern hemisphere are illustrated in Williams et al. (1974) and they show that the pressure distribution in the July ice case is not very similar to that of the January control case. Pressure gradients are weaker than those in the January and July control cases. Figures 3.4 and 3.5 show the zonally averaged u component of the wind and we see that a simple statement like "the winds were stronger" is unrealistic. For instance, Williams (1973b) finds that the jet streams were influenced differently at different longitudes in the ice age cases. Williams and Barry

(1973) find that in the vicinity of the Laurentide ice sheet the January ice age case northern hemisphere jet stream is weaker, while over the Scandinavian ice sheet the jet stream was about the same strength. The subtropical high pressure over the North Atlantic is weaker in the January ice age case than control case and is shifted about 20 degrees southward. The results of the present study which support the conclusions of Bryan and Cady (1934) pertain to: atmospheric temperatures in the July ice age, reduction of the subtropical high pressure shifting southward of Icelandic low. Changes of storm tracks are discussed by Williams et al. (1974) and later in this section.

Willett (1949) suggested that the following features characterized the glacial period maximum atmospheric circulation: (1) low index circulation, (2) storminess in northern temperate latitudes increased, (3) ice sheet forced storm tracks southward. Evaluation of low index versus high index is difficult, but it is clear (Williams et al., 1974, Figures 3 and 7) that the pressure distribution in the January ice age case is more meridional than in the control case, especially between 50°N and 70°N. Storminess did increase in the middle latitudes (and especially over the North Atlantic) in both ice age cases. Also, in both ice age cases cyclones occurred south of the Scandinavian ice sheet, skirting the edge. Not many cyclones were found in the

vicinity of the Laurentide ice sheet in the ice age cases especially in July. The ice sheets did not however force the westerlies southward.

The results of the simulations support Mather's (1954) conclusion that each local region experienced its own climatic variation. This is realistic since it is known that different regional climates are controlled by different parameters.

Viete (1949) also suggested that the storm tracks were shifted southward. It has not been determined by experiments whether the change in the distribution of cyclones was due to the orographic or thermal influences of the ice sheets. This will be investigated and reported on in the near future. Viete further concluded that the meridional temperature gradient was strengthened at the glacial period maximum. As discussed earlier in this chapter, the change of the temperature gradient depends on the level of the atmosphere under investigation. In the surface 3 km the temperature gradient increased from the control case to the ice age case. At 12 km the meridional temperature gradient generally decreased from the control cases to the ice age case.

Kraus (1960) suggested that the following features characterized the glacial period maximum circulation: (1) intensified Hadley circulation in the tropics, (2) heavier rainfall in the equatorial trough, (3) increased wind strength, stronger upper westerlies closer to the

equator, (4) poleward moving depressions. In the January ice age case, the Hadley circulation is stronger than that in the control case. In the July ice age case not all branches of the Hadley circulation are stronger. Examination of zonal averages of precipitation (not illustrated) shows that precipitation increased in the equatorial trough in the January ice age case (130 cm/90 days) compared with the control case (110 cm/90 days). In the July ice age case precipitation in the equatorial trough is c. 85 cm/90 days while that in the control case is c. 110 cm/90 days. In nearly all other latitudes zonally averaged precipitation decreased from the control cases to the ice age cases. As pointed out earlier, changes in wind strength and location of the upper westerlies are not uniform. Kraus's conclusion about poleward-moving depressions is somewhat supported (Williams et al., 1974) since, especially in the July ice age case, there are prominent SW-NE tracks over the North Atlantic and Europe. The simulation results therefore support some of the conclusions regarding glacial maximum climates of Kraus (1960). Specifically the Hadley cell in the January ice age case is strengthened, rainfall is heavier in the equatorial trough in the January ice age case, depressions moved poleward in favored places.

Conclusions reached by Lamb (1961) regarding the glacial maximum circulation were: (1) circulation

intensified except in winter over ice, (2) intensified upper westerlies, greater mobility in subtropical anticyclones, (3) less change from winter to summer than now, (4) January Icelandic low less extensive and shifted southward, (5) January low pressure in the Mediterranean area, Aleutian low deeper, (6) high pressure over ice in January and July, (7) July, Icelandic low deep and extensive, lows over Asia deeper and more extensive than now.

In the January and July ice age cases the subtropical anticyclones were less extensive (Williams et al., 1974, see Appendix B) and less mobile than in the control cases. The July ice age case does resemble more a winter pattern than July conditions of the present day. The Icelandic low in the January ice age case is shifted southward. There is high pressure in the Mediterranean area in the January ice age case, contrary to Lamb's conclusion but the Aleutian low is deeper in the January ice age case as Lamb proposed. Pressure maps do indicate high pressure over the ice caps but some of this is spurious because of the method of sea-level pressure reduction over orography (Williams et al., 1974; Kasahara and Washington, 1971, p. 659). The July ice age case does not have a deep and extensive Icelandic low nor deep lows over Asia. Only four of Lamb's conclusions are definitely supported by the model results.

The results of Lamb and Woodroffe (1970) can be summarized: (1) center of circumpolar vortex and

surrounding pressure zones displaced, (2) meridionality of mean surface wind and pressure especially in the Atlantic sector, (3) polar anticyclone far south into mid-Atlantic blocking most of west-east progress of cyclones, (4) little seasonal change of vigor or latitude of mean circulation features, (5) some weakening of and more northerly position of cyclonicity in July, (6) cyclonic regime over western Siberia in summer and winter, (7) reversal of circulation over Arctic, (8) displaced upper westerlies south of ice.

A comparison of the results of this study with those of Lamb and Woodroffe (1970) was made by Williams et al. (1974). Meridional cross sections of the zonal wind at 75°W indicated that the core of the westerlies was at about 50°N in the January ice age case, not shifted to the south. The broad pattern of the circumpolar vortex, as evidenced by 6 km pressure maps (not included), agrees well with Lamb and Woodroffe's inferred 1000--500 mb thickness field. But cyclones frequently travel northeastwards across the Atlantic in the January and July ice age cases with the polar anticyclone not extending south of 60°N in the mean picture. In contrast to Lamb and Woodroffe, we find that there are marked seasonal changes of vigor and latitude of the main circulation features. In agreement with their results we found a cyclonic regime over western Siberia in January and July ice age cases,

but we found no significant seasonal shift of cyclonic activity over Europe.

Lastly, the results of this study are compared with those of Alyea (1972). The results of Alyea's simulation of July ice age conditions can be summarized as: (1) higher kinetic energy level because of stronger north-south temperature gradients, (2) wind very different between 40°N and 70°N, (3) continental glaciers diverted zonal momentum southward, (4) Hadley cell stronger, (5) circulation tends to skirt edges of ice, (6) between 50°N and 70°N diabatic heating substantially reduced, (7) large trough south of Scandinavian ice sheet and large ridge to the east, (8) transient cyclonic activity greater especially over Atlantic, (9) maintenance of North American ice sheet not readily explained.

The above features can be compared with the results of the July ice age case of the present study. We do not find a higher kinetic energy level in the July ice age case and this is a result probably of the reduced temperature gradients in the upper atmosphere and the absence of monsoon circulation. There is no evidence that the ice sheets diverted winds (and therefore momentum) to the south. Not all branches of the Hadley circulation are stronger in the July ice age case compared with the control case. The sea-level pressure map for the July ice age case (Williams et al, 1974) shows

an area of lower pressure south of the Scandinavian ice sheet and a ridge to the east, but the pattern is not as pronounced as that described by Alyea. Total diabatic heating is substantially reduced in the northern hemisphere of the July ice age case (see Chapter VI). In agreement with Alyea's results, the July ice age case has a large amount of transient activity especially over the North Atlantic, and very few cyclones during the 30-day averaging period over the North American ice sheet.

(1) Geographic Plots of Differences Between Control and Ice Age Cases

(i) Pressure at Sea Level

The geographic distribution of differences in sea-level pressure between the January control case and January ice age case is plotted in Figure 3.13a. Positive areas are where the pressure is higher in the ice age case, negative areas (shaded) are where the pressure is weaker in the ice age case than in the control case. It is clear that in the January ice age case the largest changes from the control case PSL distribution occur in the northern hemisphere polar regions. Over the North Canadian Arctic, Greenland and the European Arctic the pressure is 50 mb greater in the January ice age case than the control case. South of 50°N there are no regions of increased pressure of the magnitude of those

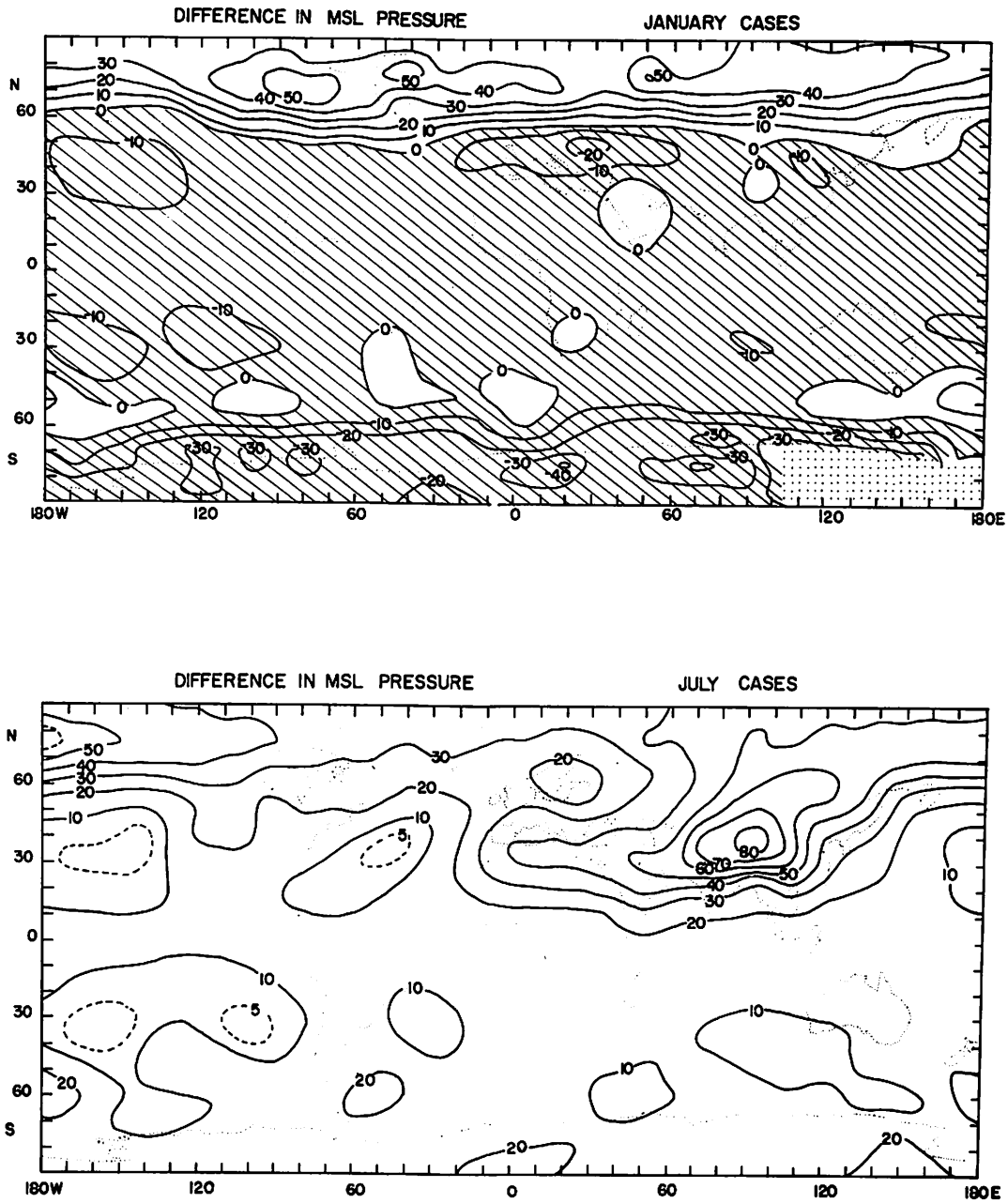

Figure 3.13. Geographical distribution of differences in sea-level pressure between (a) the January control case and January ice age case and (b) July control case and July ice age case. Positive areas occur where pressure is higher in the ice age case. Negative areas shaded. Units: mb. Sea-level pressure is reduced from surface pressure values.

north of 50°N. It is noticeable that the sea-level pressure changes are very small in the mid-latitudes and tropics. In a few areas, especially between 10°S and 30°S, there are local regions of increased pressure but the increases are less than 10 mb. Over the Antarctic continent sea-level pressure decreased by up to 40 mb. Therefore Figure 3.13a can be summarized by saying that major PSL differences occur in the polar latitudes of both hemispheres (increases in northern hemisphere and decreases in southern hemisphere, in the ice age case), while in middle latitudes and the tropics pressure changes are generally small (slightly decreased pressure in the ice age case).

The differences of PSL between the July cases are quite different from those described above. Figure 3.13b illustrates the differences, again positive values are increases in the ice age case. It is immediately obvious that sea-level pressure increased everywhere in the July ice age case (unlike the January ice age case in which pressure decreased in most places south of 50°N). The largest increase of PSL in the July ice age case occurs over the Tibetan Plateau, where the pressure increase is 80 mb. This large increase is because of the method used for sea-level pressure reduction (see Kasahara and Washington, 1971, p. 660, Footnote 2) over steep mountains. Over the southern hemisphere pressure increased by 10 or 20 mb in some

oceanic regions but elsewhere increases are less than 10 mb. Over Asia and northern Africa pressure increased 20-80 mb, this reflects the elimination of the northern hemisphere monsoon in the July ice age case. The monsoon low pressure (at the surface) of the July control case is replaced by high pressure in the ice age case causing the observed pressure difference.

(ii) Ground Temperature

Figure 3.14a illustrates the difference in ground temperature between the January control and ice age cases. The temperature decreased everywhere. The largest decreases occur over the North American (-30°C) and Scandinavian (-40°C) ice sheets and adjoining regions. Between 50°N and 70°S the largest decreases (-10°C) occur over India, Arabia and the Tibetan Plateau area. Over Antarctica however the decreases are slightly larger (-20°C to -30°C between 140°E and 140°W).

In the July cases the differences in ground temperature (Figure 3.14b) are again greatest in the vicinity of the North American and Scandinavian ice sheets, but there is one further area of large decrease (-40°C) and that is over northeastern Asia. This region does not experience such a large local decrease in the January ice age case. The large change seems to be the result of an abnormally high ground temperature in the July control case (31°C) rather than a very low

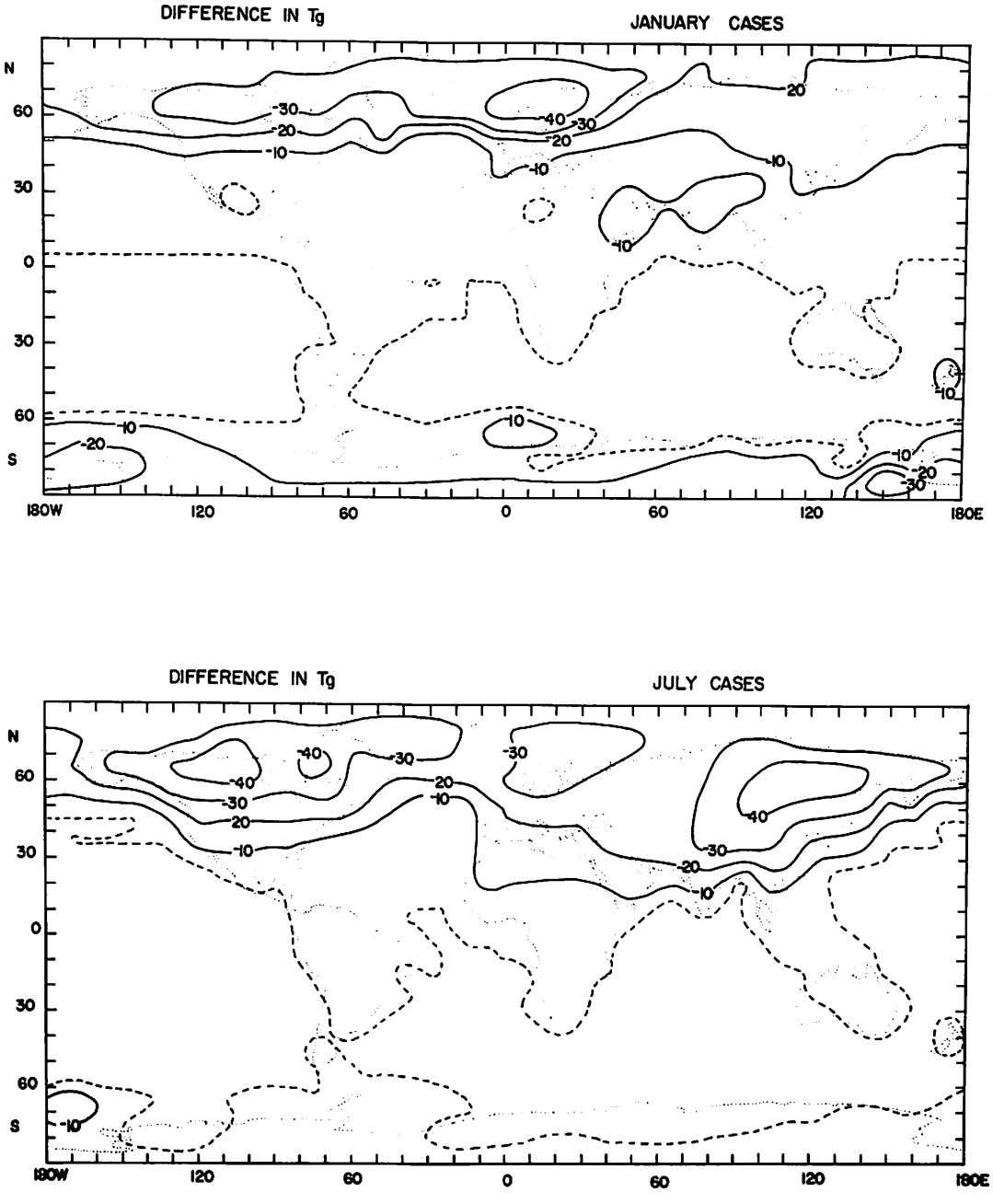

Figure 3.14. Geographical distribution of differences in temperature between (a) the January control case and January ice age case and (b) the July control case and July ice age case. Positive areas occur where the ice age case temperatures are higher. Units: °C.

temperature in the July ice age case (about -10°C over most of the region in question). In the tropics and southern hemisphere the changes in ground temperature are extremely small (generally less than 5°C) and only reach 10°C in one small region near 180°W.

Major temperature changes from the control cases to the January and July ice age cases occur in the northern hemisphere middle and high latitudes. Maximum decreases are about 40°C and occur in the vicinity of the ice sheets and in the July ice age case over north-eastern Asia.

(iii) Low Clouds

Differences in the distribution and amounts of low cloud (at 3 km) between the January control and ice age cases are illustrated in Figure 3.15a. Negative areas (ice age case values less than control case values) are shaded. The differences are more complex than those for pressure at sea level and ground temperature. Over the ice sheets cloudiness has decreased by up to 3-tenths in the ice age case. Over Alaska and Siberia the decrease is about 2-tenths. At about 30°N over the Pacific and Atlantic Oceans cloudiness has increased 2-to 3-tenths. On the equator cloudiness increases in the July ice age case over the western Pacific, western Atlantic and Indian Ocean.

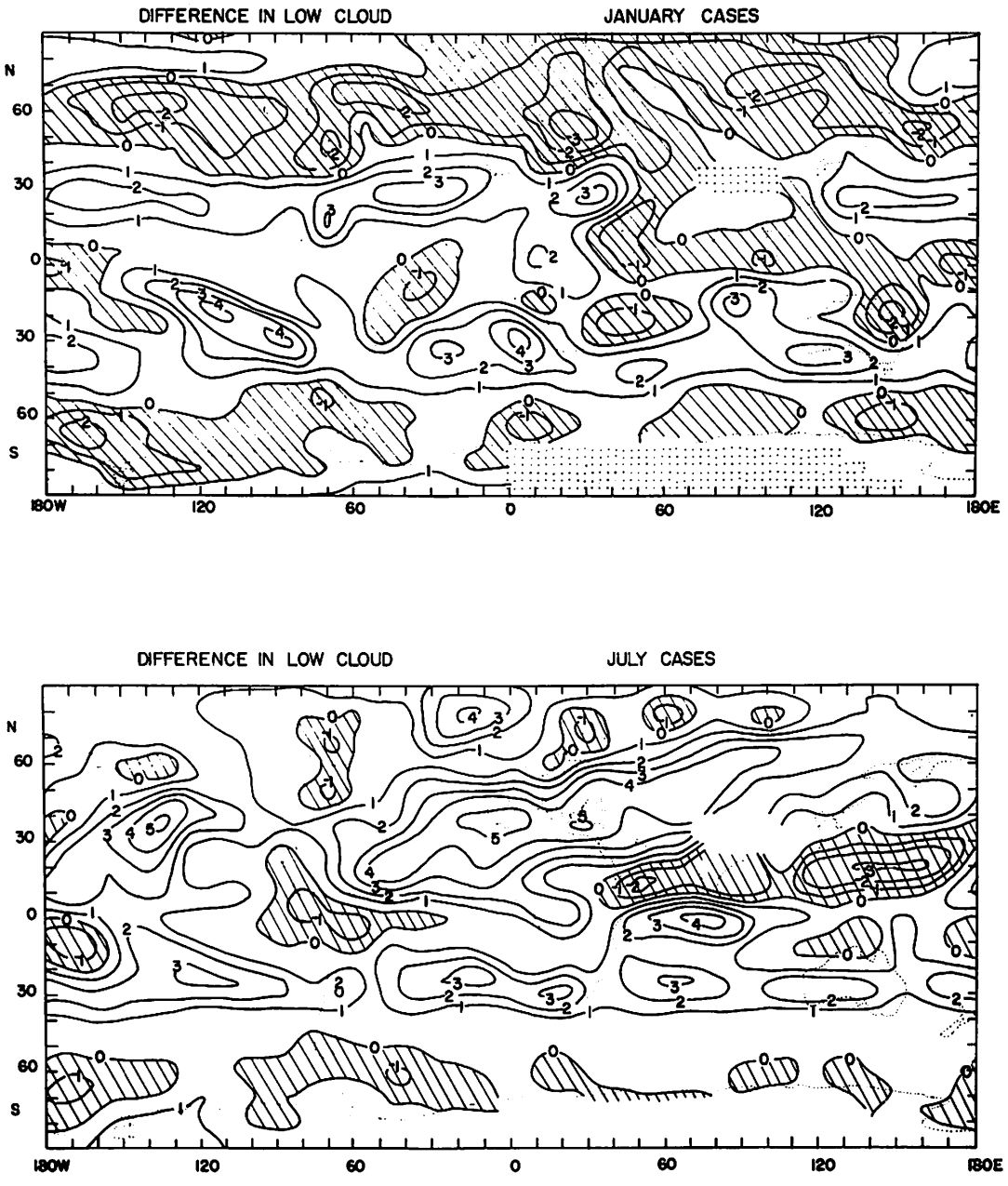

Figure 3.15. Geographical distribution of differences in low cloud between (a) the January control case and January ice age case and (b) the July control case and July ice age case. Positive areas occur where the ice age case values are higher. Negative areas shaded. Units: tenths.

The largest increases in cloudiness (4-tenths) occur over the eastern Pacific in a northeast to southwest band from the equator to 35°S and over the Atlantic west of South Africa. In general Kraus's theory that cloudiness increased over the tropical oceans during an ice age is supported, except for the Indian Ocean and western portions of the Pacific and Atlantic Oceans near the Equator. Cloudiness generally decreased over the middle and high latitudes of the southern hemisphere.

In the July ice age case (Figure 3.15b) cloudiness increased in more regions than it did in the January cases. The low cloud did decrease over the northern hemisphere ice sheets (by about 1-tenth). The largest increases in low cloud in the July ice age case occur over the eastern Pacific (off the California coast) and over the Mediterranean. In these two regions the increase is 5-tenths. Apart from one small area in the western Pacific cloudiness is increased over the tropical oceans in the July ice age case by as much as 3- or 4-tenths. The cloudiness is also increased in the southern hemisphere except for a zone along the Antarctic coast where the cloudiness decreased by up to 1-tenth.

(iv) Precipitation

The differences between precipitation distributions in the January control and ice age cases are shown in Figure 3.16a. Since the differences are very variable

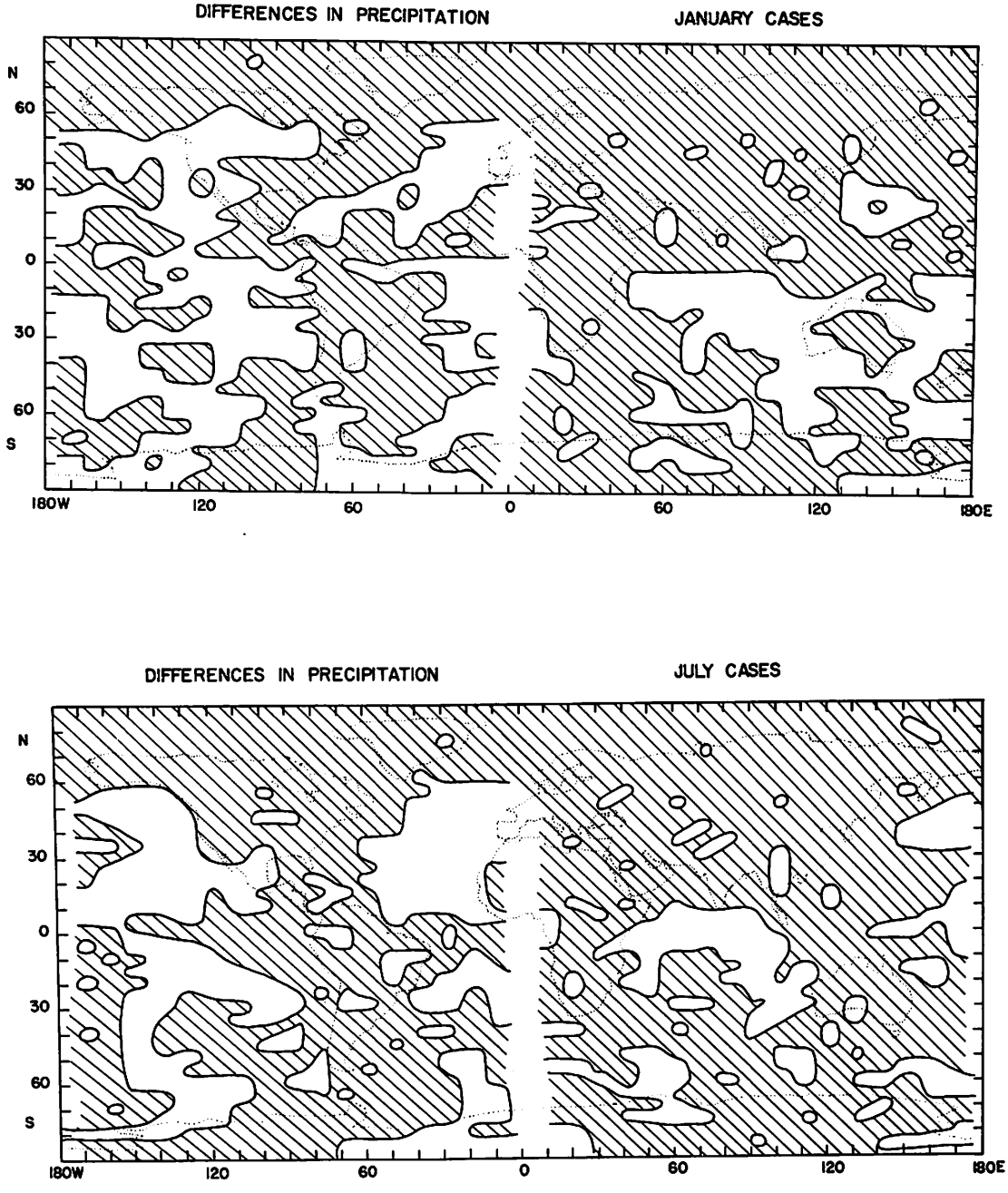

Figure 3.16. Geographical distribution of differences in precipitation between (a) the January control case and January ice age case and (b) the July control case and July ice age case. Positive areas occur where the ice age case values are higher. Negative areas are shaded.

from grid point to grid point only the distribution of positive versus negative values is plotted. Positive values indicate that the January ice age case precipitation is greater than that in the control case; negative values (shaded) indicate precipitation is less in the January ice age case. The blank area along the Greenwich meridian is due to the unavailability of data for this band. Over all of the continents except North America precipitation is less in the January ice age case. Over the oceans there are areas of increased and decreased precipitation, but it is clear that there are more precipitation increases over the oceans than the land. The primary reason for this feature is probably that while the oceans experienced a decrease of temperature of the order of 5°C, the continents became much colder in the January ice age case (see earlier section). The extreme cold of the continents probably led to a reduced moisture flux from the surface, while air flowing out over the warmer oceans would pick up moisture. The lack of moisture in the air over the continents and relative abundance in the air above oceans would lead to the distribution of precipitation observed and illustrated in Figure 3.16a.

For the July cases the differences are shown in Figure 3.16b. It is clear that precipitation decrease in the July ice age case occurred more than precipitation increase. In both January and July maps the

increased ice age precipitation resulting from the cyclone track (southwest to northeast) over the North Atlantic is obvious. In the July ice age case precipitation decreased over the continents as it did in the January ice age case. The only extensive areas of precipitation increase are over the Pacific, North Atlantic and Indian Oceans. Precipitation is decreased in January and July ice age cases over the Galapagos Islands (0°N, 90°W) as suggested by Newell (1973), but the cause of the increase is not that the ITCZ is forced south of the Equator in the ice age cases.

In general it seems that precipitation in the ice age cases is less than in the control cases over the continents and greater than that in the control cases over the oceans. The actual distributions are not quite as simple as this.

(m) Conclusions/Summary

1. The NCAR GCM has been used to simulate the atmospheric circulation with glacial period boundary conditions and the results have been compared with those from simulations with present day boundary conditions. The major differences between the present day and glacial period simulations should give a first estimate of the direction of the changes in atmospheric circulation between the present day and the maximum of the last glacial period.

2. Climatological results have been summarized by Williams et al. (1974), Williams and Barry (1973) and Barry and Williams (1973).

3. Kraus (1973) has suggested, on some theoretical grounds with support of some of the results of this study, that the meridional temperature gradient in the upper troposphere was probably weaker during an ice age than today. At 1.5 km in the model atmosphere the temperature gradient s increased from the control cases to the ice age cases at nearly all latitudes. At 10.5 km in the model atmosphere temperature gradients are decreased in nearly all regions in the January and July ice age cases.

4. Examination of the zonally averaged u component of the wind indicates that the ice age case distribution is certainly different from that in the control case. The northern hemisphere jet in January is weaker, but more importantly has a double maximum, and has its maximum 5 degrees equatorward of the control case position. The most important difference between the July control case and ice age case zonal winds is in the tropics, where the upper easterlies are eliminated in the ice age case. Both jets are about 10 m sec^{-1} weaker in the ice age case and occur about 3 km lower in the atmosphere.

5. The north-south components of the wind in the Hadley cell are strengthened in the January ice age

case and only in the upper atmosphere in the July ice age case.

6. Vertical velocities in the Hadley cell region increased in the January ice age case but only in the upward branch of the Hadley cell in the July ice age case.

7. Williams (1973a) investigated thermal and orographic influences on the 6 km (c. 500 mb) pressure distribution in the GCM. It was found that thermal influences play a major role in determining the large scale atmospheric flow in the GCM. The inclusion of ice sheets did not create such large changes as one might have expected.

8. Williams (1973b) examined cross sections of the zonal wind at different lines of longitude. These are no strikingly systematic variations between the control case and ice age case mid-latitude wind fields at different longitudes. Ice age case jet streams show quite a lot of variation from the positions and speeds in the control cases. In the July ice age case the main difference is the complete elimination of the tropical easterly jet over Asia and Africa. This suggests that the monsoon structure observed in the control case is not simulated when ice age boundary conditions are introduced into the GCM.

9. In the July control case the primary entities of the large scale circulations over the northern summer hemisphere are well simulated. In the July ice age case the

pressure distribution at 12 km is very different from that in the control case, no pronounced circulation features are noted. Since there are large differences in the upper troposphere tropical circulation between the July control case and ice age case (probably caused by the changed thermal character of the continents in the July ice age case) we would expect large differences in the energetics of the two cases. The east-west circulations associated with the northern summer monsoon are not simulated in the July ice age case, and since these circulations generate eddy kinetic energy the latter is reduced compared with the control case.

10. A comparison of the results of this study with the conclusions of earlier studies has been made. The comparisons made are summarized in Table 3.2. Some earlier ideas are supported, some are not. Conclusions common to earlier studies which are unsupported by the GCM results include: winds stronger and storm tracks and winds forced south of ice. However, in support of earlier common conclusions this study did show: air temperatures in July ice age case more like winter of present day; Icelandic low shifted southward in January; pressure distributions more meridional in ice age case; intensified Hadley cell in tropics; and transient cyclone activity greater over Atlantic.

11. Geographical distributions of differences between control and ice age cases are examined for four variables.

TABLE 3.2

COMPARISON OF THE RESULTS OF THIS STUDY WITH THOSE OF EARLIER RECONSTRUCTIONS

Study	Conclusions	Comparison with GCM Results
Bryan and Cady (1934)	(1) Air temperatures and pressures in summer comparable with those in present winter.	(1) Temperatures in July ice age case similar to present winter. Pressures not similar.
	(2) Winds stronger.	(2) Changes differ with longitude, season, etc.
	(3) Subtropical high pressure reduced and shifted southward.	(3) Subtropical high over North Atlantic weaker in ice age cases.
	(4) Icelandic low and storm tracks shifted southward.	(4) Icelandic low shifted 20 degrees southward in January ice age case. Storm tracks not consistently southward.
Willett (1949)	(5) Low index circulation.	(5) Pressure distribution more meridional in January ice age case.
	(6) Storminess in temperate latitudes increased.	(6) Increased especially over North Atlantic in both ice age cases.
	(7) Ice sheet forced storm tracks southward.	(7) Storm tracks south of Scandinavian ice sheet but not frequent south of Laurentide ice sheet.
Viete (1949)	(8) Ice sheet forced storm tracks southward.	(8) See comment 7.
	(9) Meridional temperature gradient strengthened.	(9) Strengthened at 3 km in troposphere but weakened at 12 km level.

TABLE 3.2 (Continued)

COMPARISON OF THE RESULTS OF THIS STUDY WITH THOSE OF EARLIER RECONSTRUCTIONS

Study	Conclusions	Comparison with GCM Results
Mather (1954)	(10) Local regions experienced own climatic variations	(10) Supported by ice age cases results.
Kraus (1960)	(11) Intensified Hadley cell in tropics.	(11) In January ice age case all branches of Hadley cell stronger. In July ice age case only vertical branches stronger.
	(12) Heavier rainfall in equatorial trough.	(12) Heavier in equatorial trough in January ice age case but not in July ice age case.
	(13) Increased wind strength, upper westerlies stronger and closer to the Equator.	(13) See comment 2.
	(14) Poleward moving depressions.	(14) Southwest-northeast tracks over Atlantic and Europe in both ice age cases.
Lamb (1961)	(15) Circulation intensified except in winter over ice.	(15)
	(16) Intensified upper westerlies, greater mobility in subtropical anticyclones.	(16) See comment 2 concerning winds. Subtropical anticyclones less mobile in ice age case than control cases.
	(17) Less change from winter to summer than now.	(17) See comment 1.

TABLE 3.2 (Continued)

COMPARISON OF THE RESULTS OF THIS STUDY WITH THOSE OF EARLIER RECONSTRUCTIONS

Study	Conclusions	Comparison with GCM Results
	(18) January Icelandic low less extensive and shifted southward.	(18) See comment 4.
	(19) January low pressure in Mediterranean area and Aleutian low deeper.	(19) High pressure in Mediterranean area in January ice age case. Aleutian low deeper in January ice age case.
	(20) High pressure over ice in January and July.	(20) High pressure over ice in both ice age cases but some is spurious.
	(21) July Icelandic low deep and extensive. Lows over Asia deeper and more extensive than now.	(21) July ice age case Icelandic low not deep. No deep lows over Asia.
Lamb and Woodroffe (1971)	(22) Center of circumpolar vortex and surrounding pressure zones displaced.	(22) Circumpolar vortex in ice age cases agree with Lamb and Woodroffe results.
	(23) Meridionality of mean surface wind and pressure especially in Atlantic sector.	(23) Pressure distributions more meridional in January ice age case.
	(24) Polar anticyclone far south into mid-Atlantic blocking most of east-west progression of cyclones.	(24) Cyclones frequently travel northeastward across Atlantic in both ice age cases. Polar anticyclone north of 60°N.

TABLE 3.2 (Continued)

COMPARISON OF THE RESULTS OF THIS STUDY WITH THOSE OF EARLIER RECONSTRUCTIONS

Study	Conclusions	Comparison with GCM Results
	(25) Little change of seasonal vigor or latitude of mean circulation features.	(25) Marked seasonal change of vigor and latitude of main circulation features.
	(26) Some weakening of and more northerly position of cyclonicity in July.	(26) No significant shift of cyclone activity over Europe.
	(27) Cyclonic regime over Western Siberia in summer and winter.	(27) Cyclonic regime over Western Siberia in both ice age cases.
	(28) Displaced upper westerlies south of ice.	(28) See comment 2.
Alyea (1972)	(29) Higher kinetic energy level: stronger north-south temperature gradients.	(29) No higher kinetic energy level in July ice age case (see text).
	(30) Wind significantly changed between 40°N and 70°N.	(30) No evidence that ice sheet diverted winds and therefore momentum south. See comment 2.
	(31) Continental glaciers diverted zonal momentum southward.	(31) See comment 30.
	(32) Hadley cell stronger.	(32) See comment 11.

TABLE 3.2 (Continued)

COMPARISON OF THE RESULTS OF THIS STUDY WITH THOSE OF EARLIER RECONSTRUCTIONS

Study	Conclusions	Comparison with GCM Results
	(33) Circulation tends to skirt edges of ice.	(33) See comment 30.
	(34) Between 50°N and 70°N diabatic heating substantially reduced.	(34) Total diabatic heating substantially reduced in the northern hemisphere of the July ice age case.
	(35) Large trough south of Scandinavian ice sheet and ridge to east.	(35) Qualitative agreement.
	(36) Transient cyclone activity greater especially over the Atlantic.	(36) July ice age case, large amount transient activity over Atlantic.
	(37) Maintenance of North American ice sheet not readily explained.	(37) Very few cyclones during 30-day averaging period over North American ice sheet in July ice age case.

The major sea level pressure differences in the January cases occur in the polar latitudes of both hemispheres (increases in the northern hemisphere and decreases in the southern hemisphere in the ice age case), while in mid-latitudes and the tropics pressure changes are generally small. Sea-level pressure increased everywhere in the July ice age case. The largest increase occurs over the Tibetan Plateau. In the southern hemisphere changes were small.

In the January and July ice age cases temperature at the ground decreased everywhere. In both ice age cases the largest decreases occur over the North American and Scandinavian ice sheets. In the July ice age case there is one further large increase and that is over northeastern Asia.

Differences in low cloudiness are more complex than those above. In both January and July ice age cases the cloudiness decreased over the ice sheets. In the January ice age case Kraus's theory that cloudiness increased over the tropical oceans during an ice age is supported, except over the Indian Ocean and parts of the Atlantic and Pacific near the Equator. In the July ice age case cloudiness increased in more regions than it did in the January ice age case. Again cloudiness decreased over the northern hemisphere ice sheets. The largest increases in low cloud in the July ice age case occur over the eastern Pacific and Mediterranean. Apart from

one small area in the western Pacific cloudiness is increased over the tropical oceans in the July ice age case by as much as 3- or 4-tenths.

CHAPTER IV

ANGULAR MOMENTUM BALANCE OF THE FOUR SIMULATIONS

(a) Introduction

There exist certain requirements which impose restrictions on the large scale motions of the atmosphere and impress characteristics on them. A dynamical system such as the atmosphere (or part of it) cannot change its angular momentum about a given axis except through the addition or subtraction of angular momentum from or by external agencies. In the case of the atmosphere the only significant interaction is with the earth's surface. In this chapter the effects on the atmospheric angular momentum balance of changing the surface conditions will be investigated. Both the changes in surface boundary conditions and changes in the surface wind (speed and direction) should have noticeable effects.

Basically, the global wind system consists of surface easterlies in low latitudes and surface westerlies in higher latitudes. Small regions of surface easterlies in high latitudes can be mainly disregarded in a discussion of the global angular momentum balance (Palmén and Newton, 1969, p. 8). The belt of tropical easterlies acts as a source of westerly momentum for

the atmosphere and the belts of westerlies act as sinks. Since the total angular momentum of the whole atmosphere must remain unchanged over a long period of time, the upward flux in low latitudes must equal the downward flux in middle and high latitudes. Angular momentum must be transferred poleward from source to sink regions by atmospheric processes.

When considering atmospheric fluxes of angular momentum, two processes are important: meridional mass circulations and eddy fluxes (Jeffreys, 1926). Many studies (for example: Starr, 1954; Starr and White, 1951; Palmén, 1951) stress the fact that eddy processes carry the bulk of momentum poleward in the troposphere. The relative importance of the mean meridional circulation decreases rapidly in extratropical latitudes (see for example, Riehl, 1962). Palmén and Alaka (1952) find that the ratio between mean meridional transport and eddy transport is 44 per cent at 20°N, 23 per cent at 25°N, and 11 per cent at 30°N. Even in the Hadley cell, eddy transport processes are dominant.

For detailed discussions of the angular momentum balance, including the mathematical framework and results of computations, reference may be made to Lorenz (1967), Reiter (1969) and Newton (1972). The kinds of circulation systems that accomplish the exchanges are described in Palmén and Newton (1969).

(b) Theoretical Considerations

The absolute angular momentum, per unit mass, about the earth's axis is given by the formula

$$m = ua \cos \phi + a^2 \Omega \cos^2 \phi \qquad (4.1)$$

The first term on the right hand side is the relative angular momentum, here call û-angular momentum, associated with motion relative to the earth. The second term is the angular momentum due to the earth's rotation, called the Ω-angular momentum.

Washington and Kasakhara (1970) derive the angular momentum equation used in the NCAR GCM and the partition of the angular momentum into zonal and eddy parts; modifications of these equations, because of the incorporation of orography into the GCM, are described by Kasahara and Washington (1971).

The fluxes of angular momentum due to mean meridional circulation and eddy motions are given by (Kasahara and Washington, 1971)

$$\overline{\rho\sigma}\,\hat{v}\hat{m} = \overline{\rho\sigma}\,\hat{v}\hat{u}a \cos \phi + \overline{\rho\sigma}\,\hat{v}\, a^2 \Omega \cos^2 \phi \qquad (4.2)$$

$$\overline{\rho}\,\hat{m}\,\overline{w} = \overline{\rho}\,\overline{w}\,\hat{u}a \cos \phi + \overline{\rho}\,\overline{w}\, a^2 \Omega \cos^2 \phi \qquad (4.3)$$

$$\overline{\rho\sigma v'm'} = \overline{\rho\sigma u'v'}\, a \cos \phi \qquad (4.4)$$

$$\overline{\rho m'w''} = \overline{\rho w''u'}\, a \cos \phi \qquad (4.5)$$

where:

$\overline{\rho\sigma}\ \hat{v}\hat{m}$ - meridional flux of angular momentum due to the mean meridional circulation motion.

$\overline{\rho\sigma}\ \hat{v}\hat{u}\ a \cos\phi$ - meridional transport of $\hat{u}$-angular momentum by the mean circulation.

$\overline{\rho\sigma}\ \hat{v}\ a^2\ \Omega \cos^2\phi$ - meridional transport of Ω-angular momentum by the mean circulation.

$\overline{\rho}\ \hat{m}\ \overline{w}$ - vertical flux of angular momentum due to the mean meridional circulation.

$\overline{\rho}\ \overline{w}\ \hat{u}\ a \cos\phi$ - vertical transport of $\hat{u}$-angular momentum by the mean circulation.

$\overline{\rho}\ \overline{w}\ a^2\ \Omega \cos^2\phi$ - vertical transport of Ω-angular momentum by the mean circulation.

$\overline{\rho\sigma v'm'}$ - meridional flux of angular momentum due to eddy motions.

$\overline{\rho\sigma u'v'}\ a \cos\phi$ - meridional transport of eddy angular momentum.

$\overline{\rho m'w''}$ - vertical flux of angular momentum due to eddy motions.

$\overline{\rho w''u'}$ a cos ϕ - vertical transport of eddy angular momentum.

The absolute angular momentum about the earth's axis, per unit mass, can be altered only by a torque (Lorenz, 1967, p. 15). The surface torques are those due to friction and to pressure differences across terrain features.

The zonal torque due to the longitudinal surface pressure difference across mountains is defined by Kasahara and Washington (1971) as

$$\eta_m = - \overline{p_s \frac{\partial H}{\partial \lambda}} = \overline{H \frac{\partial p_s}{\partial \lambda}} \qquad (4.6)$$

Since H is positive, η_m is positive (or negative) if the surface pressure on eastern sides of the mountains is higher (or lower) than on the western sides.

The zonal torque due to the longitudinal component of the frictional force per unit area, η_s, is defined by Kasahara and Washington as

$$\eta_s = - \overline{\tau}_{\lambda,s} \text{ a cos } \phi \qquad (4.7)$$

Similar to the mountain torque, the atmosphere gains or loses its angular momentum depending on whether η_s is positive or negative.

Results of the computations of the momentum transports and surface torques for the control cases

will be discussed and compared with observed data in the following sections.

(c) Meridional Transport of û-momentum by the Mean Circulation

Figure 4.1 shows the latitude-height distributions of meridional transport of û-angular momentum by the mean circulation (averaged with respect to time for days 51-80) for the four simulations. In the January control case (Figure 4.1a) there is a strong northward transport of û-angular momentum in the upper branch of the Hadley cell, with a maximum flux at 10°N. The transport of angular momentum by the meridional circulation is large only in tropical latitudes, which compares favorably with the investigations of Palmén and Alaka (1952) and Palmén (1964).

The northward transport of û-angular momentum in the upper branch of the Hadley cell is twice as strong in the January ice age case (28×10^{10} g sec^{-2}) (Figure 4.1b) than it is in the control case (14×10^{10} g sec^{-2}) and it occurs lower in the troposphere. In the ice age case, as in the control case, the only large transports of û-angular momentum by the mean meridional circulation occur in the low latitudes.

In the July control case (Figure 4.1c) the transport by the Hadley circulation is southward and the maximum flow (12×10^{10} g sec^{-2}) occurs in the upper

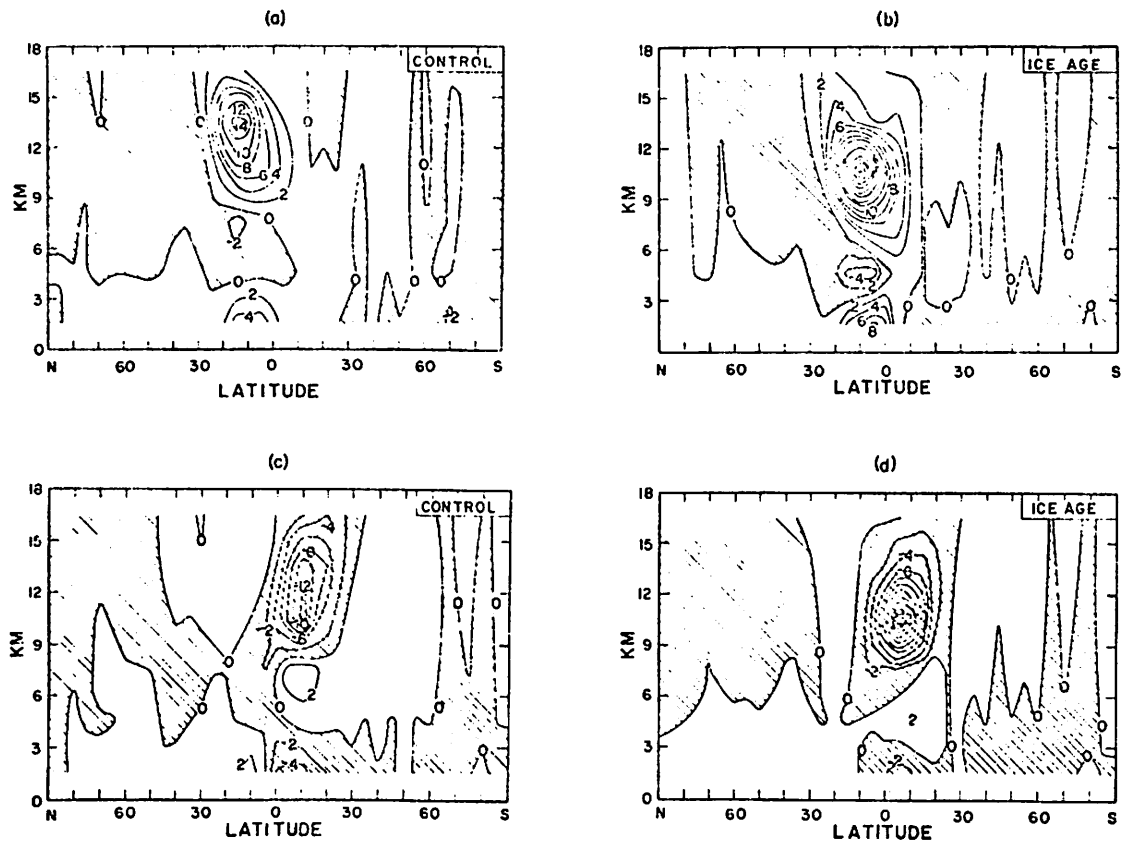

Figure 4.1. Latitude-height distribution of 30-day mean zonally averaged meridional transport of û-angular momentum by the mean circulation for (a) January control case, (b) January ice age case, (c) July control case, (d) July ice age case. Units: 10^{10} g sec^{-2}.

troposphere at about 10°S. The maximum is slightly weaker than in the January control case. As in the January cases, the main difference between the July control and ice age cases is that the transport of û-angular momentum in the tropics by the mean circulation is much stronger in the ice age case (22×10^{10} g sec^{-2}) (Figure 4.1d) and occurs slightly lower in the troposphere.

Therefore, in both ice age cases there is a much stronger meridional transport of û-angular momentum by the mean circulation. Palmén and Alaka (1952) discuss the consequences of strengthening the angular momentum transport by the mean meridional circulation. They point out that the flux of angular momentum due to the meridional circulation results in convergence of momentum in the upper layer and divergence in the lower layer, whereas the horizontal eddy transport has the opposite effect. They argue that at a period when the meridional circulation is stronger than usual, the horizontal and vertical eddy fluxes are not vigorous enough to drain all the momentum surplus in the upper troposphere. Continuous accumulation of angular momentum then means strengthening of the upper subtropical jet. This in turn will increase the eddy fluxes of momentum and act to restore the balance.

In the January and July ice age cases, we see a strengthening of the meridional transport of û-angular

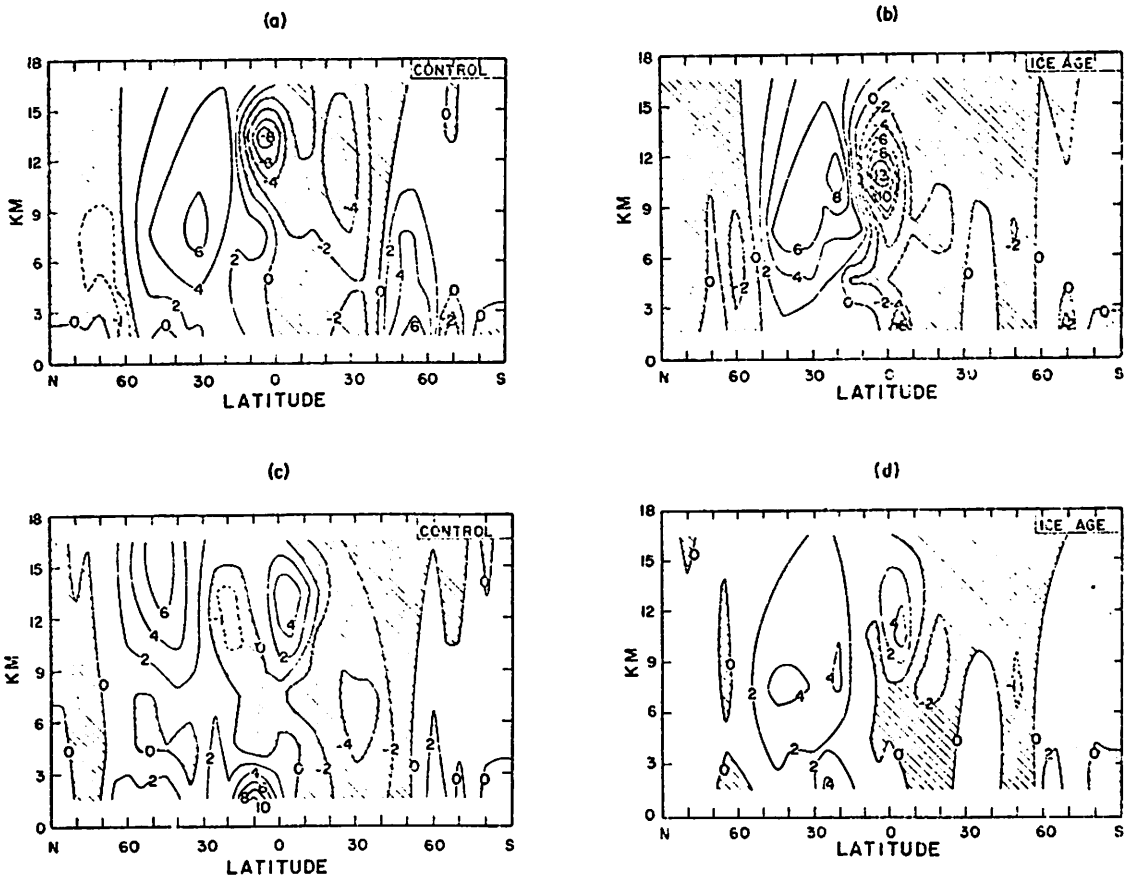

Figure 4.2. Latitude-height distribution of 30-day mean zonally averaged meridional transport of eddy angular momentum for (a) January control case, (b) January ice age case, (c) July control case, (d) July ice age case. Units: 10^{10} g sec^{-2}.

momentum so there should be a strengthened subtropical jet stream unless the eddy flux of angular momentum has been increased sufficiently to result in a net drain of angular momentum in the upper layer. This question will be discussed in the next section.

(d) Meridional Transport of Eddy Angular Momentum

Figure 4.2 shows the latitude-height distributions of 30-day mean zonally averaged meridional transports of eddy angular momentum ($\overline{\rho\sigma u'v'}$ a cos ϕ) for the four simulations. In the January control case (Figure 4.2a) and July control case (Figure 4.2c) it is clear that the transport of angular momentum in middle and high latitudes is mainly associated with eddies. This observation is equivalent to those made for atmospheric transports by earlier studies such as Starr and White (1951). Comparison of Figures 4.1 and 4.2 shows that in lower latitudes both eddy motions and the mean meridional circulation play a significant role in the budget of û-angular momentum. This observation has also been made for the atmosphere, see for example, Kidson et al. (1969), Tucker (1965), and for the NCAR GCM (Kasahara and Washington, 1971).

In the January ice age case (Figure 4.2b) the meridional transport of eddy angular momentum is quite different from that in the control case (Figure 4.2a); the poleward transport at about 30°N is about 30 per cent

greater and the maximum has been shifted southward and vertically higher; the southward transport of eddy angular momentum occurring near the equator and into the middle latitudes of the southern hemisphere in the control case, is about 30 per cent stronger in the tropics in the ice age case and about 50 per cent weaker in the middle latitudes.

The northward transport of eddy angular momentum in the northern hemisphere middle latitudes of the July control case (Figure 4.2c) is considerably weaker and lower in the atmosphere in the ice age case (Figure 4.2d). The poleward transport in the southern hemisphere is also weaker (about 50 per cent), while the tropical transport is virtually the same in both cases.

(e) Vertical Integral of the û-angular Momentum Transport by the Mean Circulation as a Function of Latitude

In order to compare the computed magnitude of the û-angular momentum transport ($\overline{\rho\sigma}\ \hat{v}\ \hat{u}\ a \cos\phi$), discussed in section c, with observed data, vertical integrals of $\overline{\rho\sigma}\ \hat{v}\ \hat{u}\ a \cos\phi$ as functions of latitude are shown in Figure 4.3 and 4.4, for January and July respectively. Comparing the January control case data with computations of the observed vertically integrated meridional transport of û-angular momentum by the mean circulation (Figure 4.3); it is clear that although the latitude locations of the maxima are similar for the observed and

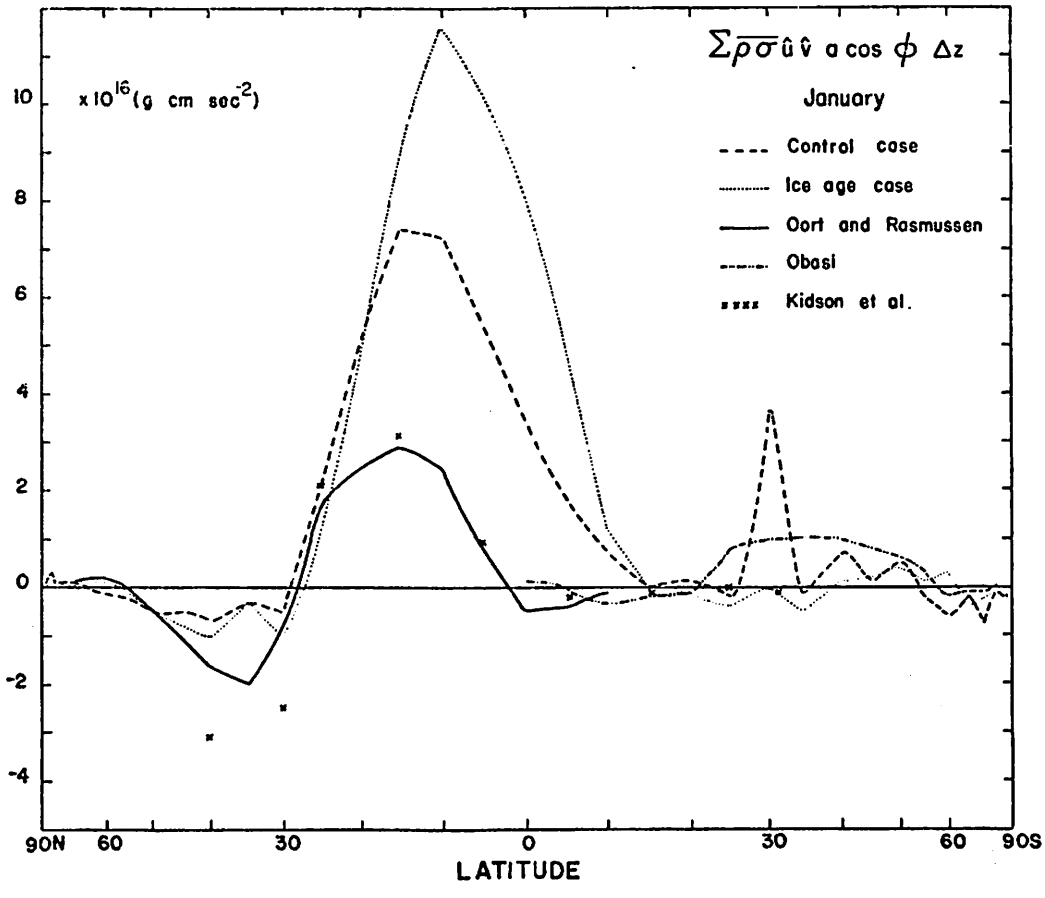

Figure 4.3. Vertical integral of $\overline{\rho\sigma}\ \hat{u}\ \hat{v}\ a\cos\phi$ as a function of latitude for January cases. Observed data from Oort and Rasmusson (1971) (January), Obasi (1963) (October-March, inclusive), Kidson et al. (1969) (December-February). Units: 10^{16} g cm sec^{-2}.

computed data, the magnitudes of the maxima differ. In the tropics the transport is almost a factor of two larger in the control case, whereas in the northern hemisphere middle latitudes the transport is larger in the observed data than in the control case. In high latitudes and the southern hemisphere, the observed and computed data are very similar apart from a sharp peak in the control case data at about 30°S. The only major difference between the ice age and control case vertically integrated meridional transport of û-angular momentum is in the northern hemisphere tropics, where the transport in the ice age case is about 30 per cent greater than that in the control case. Since this is the one area in which there are large differences between the control case and observed data (maximum difference, 60 per cent of control case value), it is difficult to assess the difference between the control and ice age case data.

Again in July (Figure 4.4) the computed control case meridional transport of û-angular momentum by the mean circulation in the tropics is much larger than that derived from the observed data (at 10°S difference between control case and observed data is about 75 per cent of the control case value). The middle and high latitude transports are similar in the control case and observed data. The ice age case and control case data

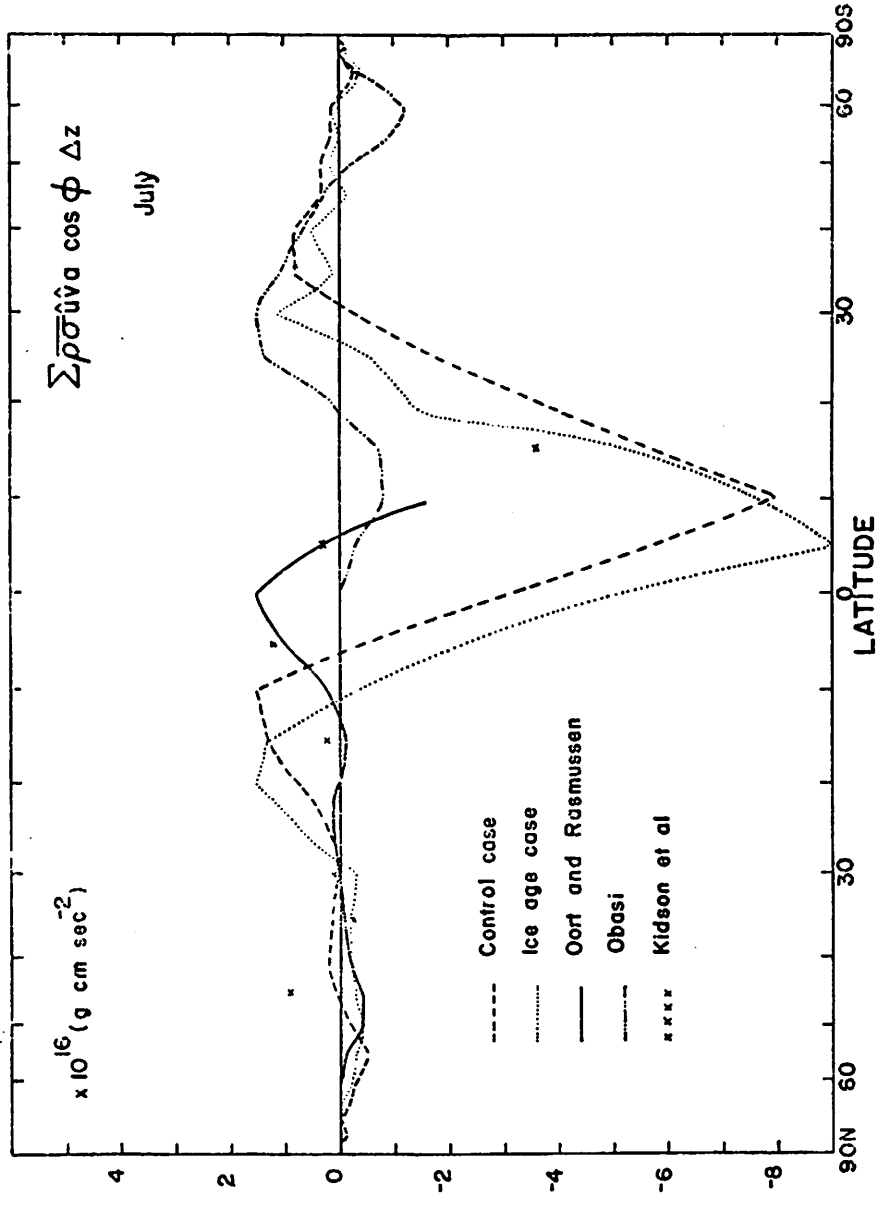

Figure 4.4. Vertical integral of $\rho\sigma\ \hat{u}\ \hat{v}\ a\cos\phi$ as a function of latitude for July cases. Observed data from Oort and Rasmusson (1971) (July), Obasi (1963) (April-September, inclusive), Kidson *et al.* (1969) (June-August). Units: 10^{16} g cm sec^{-2}.

are not greatly different, that is, the transport of û-angular momentum by the mean circulation when vertically integrated, is virtually the same in the ice age case and control case.

In both January and July ice age and control cases the maximum meridional transport of û-angular momentum by the mean circulation occurs in the tropics, i.e., is associated with the Hadley circulation. The vertically integrated transport by the Hadley circulation was greater in the January ice age case than in the control but was similar in the July ice age and control cases.

(f) Vertical Integral of the Eddy Angular Momentum Transport as a Function of Latitude

In Figure 4.5, the vertical integral of the eddy angular momentum transport ($\Sigma\ \overline{\rho\sigma u'v'}\ a \cos\phi\ \Delta Z$) in January for observed and computed data can be compared. The control case data and observed data are fairly similar; the maxima in the northern and southern hemisphere middle latitudes are slightly smaller (in the northern hemisphere in January the maximum in the control case is about 20 per cent less than that given by Oort and Rasmusson), and shifted equatorward in the control case.

In the northern hemisphere, the meridional transport of eddy angular momentum is very similar in the January control and ice age cases. At the equator there is a 50 per cent greater southward transport in the ice

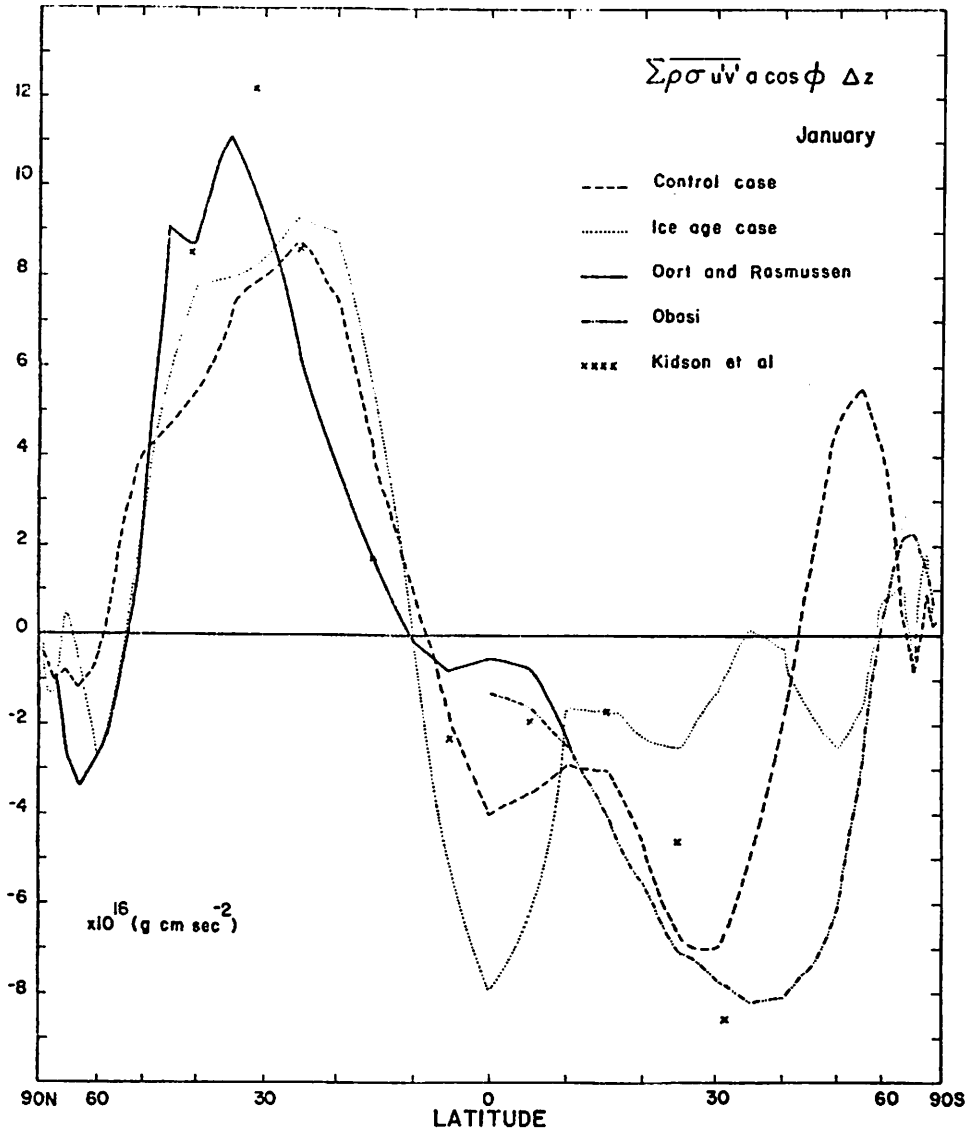

Figure 4.5. Vertical integral of $\overline{\rho\sigma u'v'}$ a cos ϕ as a function of latitude for January cases. Observed data from Oort and Rasmusson (1971) (January), Obasi (1963) (October-March, inclusive), Kidson et al. (1969) (December-February). Units: 10^{16} g cm sec^{-2}.

age case than in the control case. In the southern hemisphere meridional transport of eddy angular momentum is much lower in the ice age case than in the control case, at 30°S the ice age case value is about one-ninth of the control case value.

In July (Figure 4.6) the control case and observed data again compare reasonably. The maximum in the northern hemisphere mid-latitudes is 75 per cent greater in the control case than in the observed data and occurs 10 degrees further north. In the tropics the transport in the control case is 160 per cent greater than the observed value at the equator. In the southern hemisphere mid-latitudes the control case data is about 30 per cent less than that observed.

The main difference between the July ice age case and July control case meridional transports of eddy angular momentum is in the southern hemisphere mid-latitudes, where the ice age case transport is much smaller (at 30°S the ice age case value is zero while the control case value is about 6×10^{16} g cm sec^{-2}). In the northern hemisphere the ice age case transport is again smaller in middle latitudes than that in the control case and the maximum is nearer the equator.

In both January and July, the control case and observed vertically integrated transports of eddy angular momentum are similar. The ice age case transports are

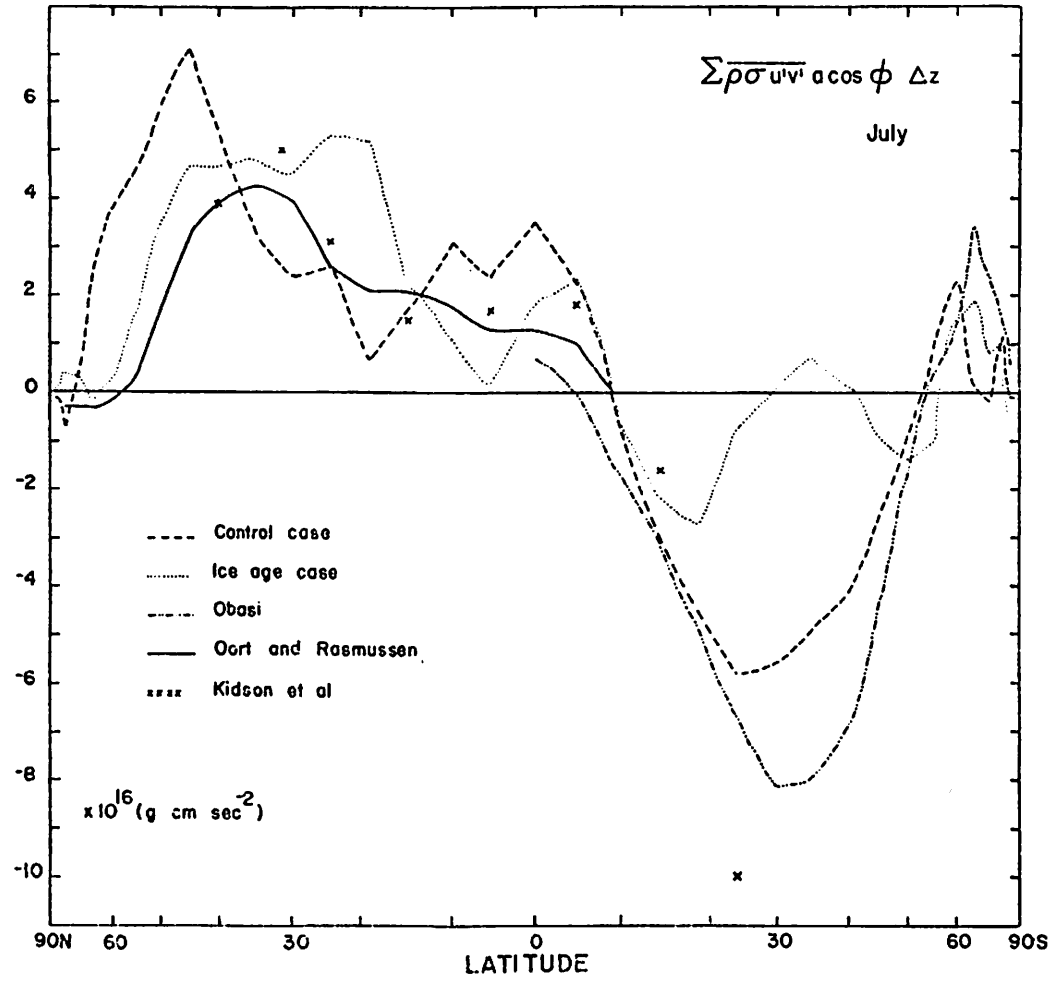

Figure 4.6. Vertical integral of $\overline{\rho\sigma u'v'}$ a cos ϕ as a function of latitude for July cases. Observed data from Oort and Rasmusson (1971) (July), Obasi (1963) (April-September, inclusive), Kidson et al. (1969) (June-August). Units: 10^{16} g cm sec^{-2}.

smaller than those of the control cases in nearly all latitudes in July and in the southern hemisphere in January.

(g) Mountain Pressure Torque

Figures 4.7a and 4.7b show the latitudinal distribution of the mountain torque ($H \frac{\partial p_s}{\partial \lambda}$) for January and July respectively. The observed and computed data are readily compared. Kasahara and Washington (1971) found that considering the year-to-year variations in the monthly averages, the agreement between the model calculations and the observed data is reasonably good except in higher latitudes. In Figure 4.7a, showing the mountain torque for January, the control case data differ from the observed data mainly in the higher latitudes. At about 20°N and 20°S, the control case data have maxima which are not found in the observed data.

The distribution of the mountain torque in the January ice age case does not differ greatly from that in the control case except in the belt north of 30°N. The large changes between 30°N and 80°N must be the result of the inclusion of the two major ice sheets in the ice age case. Between 30°N and 85°N the mountain torque is negative, i.e., the atmosphere is losing angular momentum in the control case in this belt; in the ice age case the torque is even more negative, so

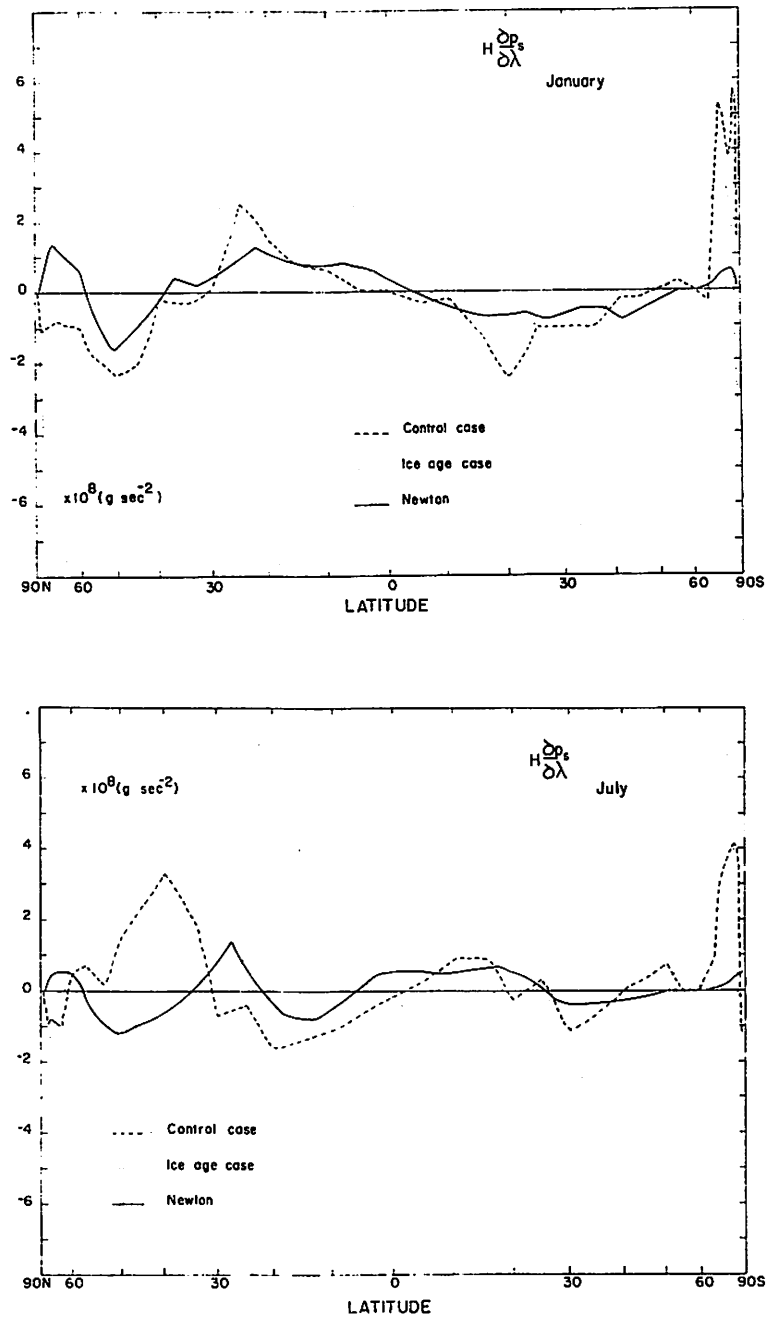

Figure 4.7. Latitudinal distributions of mountain pressure torque for (a) January cases, (b) July cases. Observed data from Newton (1971). Units: 10^8 g sec^{-2}.

the ice sheets are causing greater transfer of momentum from the atmosphere to the earth.

Figure 4.7b, showing the mountain torque in July, shows that agreement between control case and observed data is less in this month than in January, and is especially poor in the northern hemisphere. Between 30°N and 90°N the observed data show a minimum, centered at about 50°N, while the control case has a maximum centered at about 40°N. Some reasons for differences between the observed data and control case data are discussed in Chapter VIII. The maximum between 25°N and 5°N in the observed data is larger in magnitude and latitudinal extent in the control case. South of 60°S, the observed and computed mountain torques differ markedly. Because of the differences found between the control case data and observed data, it is difficult to assess the differences between the control case and ice age case. As in January, the ice age case and control case data are similar in the southern hemisphere. The torque is very different in the two cases between 0° and 60°N.

(h) Surface Stress Torque

The latitudinal distributions of surface stress torque, $-\overline{\tau}_{\lambda s}$ a cos ϕ, are illustrated in Figures 4.8a and 4.8b, for January and July respectively. Kasahara and Washington found that although the computed distribution agrees fairly well with the observed distribution in

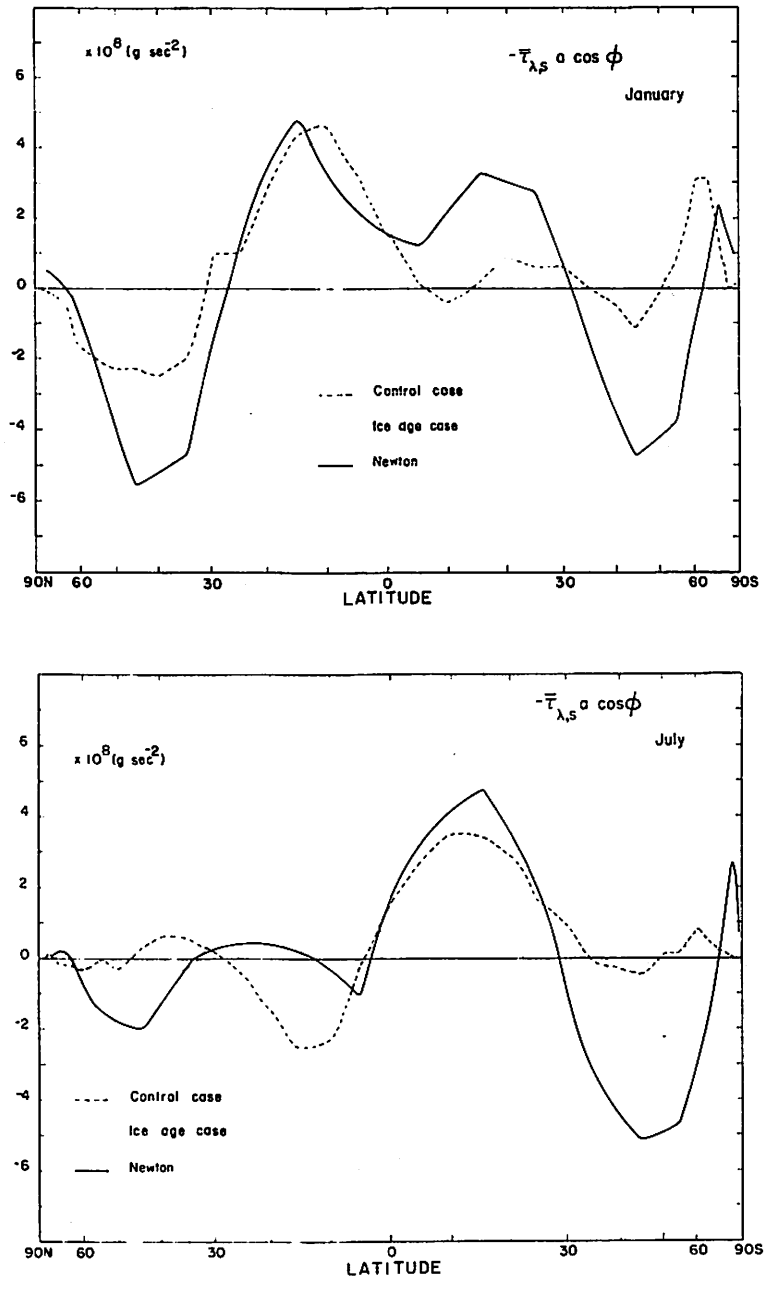

Figure 4.8. Latitudinal distribution of surface stress torque for (a) January cases and (b) July cases. Observed data from Newton (1972). Units: 10^8 g sec^{-2}.

the tropics, the computed values were too small in middle latitudes. Kasahara and Washington compared the computed values with the observed data of Hellerman (1967). For the present study, surface torque values are from Newton (1972), who combined data from six sources in order to provide the best estimate of surface stress torque distribution.

In both January and July the control case data and observed data are most similar in the tropical zone of the winter hemisphere. The surface stress torque is underestimated in both months in the latitudes of the surface westerlies. Palmén and Newton (1969, p. 8) suggest that use of the same surface drag coefficient in all latitudes may result in an underestimate of the stresses in the westerlies, where the winds are generally stronger and the ocean surface rougher. In the GCM the drag coefficient is constant for all latitudes and surface types (C_D = 0.003, Oliger et al., 1970, p. 17) and this fact could be one reason for the computed surface stress torque being lower than that observed. This point is discussed in Chapter VIII.

In the ice age cases, the surface stress torque in middle latitudes is again small, not very different from that in the control case. In January there is hardly any difference between the ice age case and control case surface stress torque distribution. In July the ice age case is especially different in the

northern hemisphere. These differences are due to the changes in the east-west wind velocity between the July control and ice age cases. Over the monsoon lands in the control case there are westerly surface winds but in the July ice age case, in the absence of the monsoon, the surface winds are easterly. This change in direction reverses the sign of the surface stress torque between 0° and 30°N.

(i) Conclusions/Summary

1. In the January and July control and ice age cases, the only large transports of $\hat{u}$-angular momentum by the mean meridional circulation occur in the low latitudes. In both ice age cases there is a much stronger meridional transport of $\hat{u}$-angular momentum by the mean circulation and the maximum transport occurs lower in the troposphere.
2. In the January and July control cases it is clear that the transport of angular momentum in middle and high latitudes is mainly associated with eddies.
3. In the January ice age case, the meridional transport of eddy angular momentum is different from that in the control case; the poleward transport at 30°N is greater, shifted southward and vertically higher. The southward transport near the equator and in the southern hemisphere middle latitudes is stronger in the tropics and weaker in the middle latitudes.

4. The northward transport of eddy angular momentum in the northern hemisphere middle latitudes of the July control case is considerably weaker and lower in the atmosphere in the ice age case. The poleward transport in the southern hemisphere is also weaker.

5. The distribution of the mountain torque in the January ice age case does not differ greatly from that in the control case except in the belt north of 30°N. In the July ice age case the mountain pressure torque differs most from that in the control case in the northern hemisphere.

6. In the January cases there is hardly any difference between the ice age case and control case surface stress torque distribution. The July ice age case distribution is especially different from that in the control case in the northern hemisphere because of changes in surface wind direction between the control and ice age cases.

CHAPTER V

MOISTURE BALANCE OF THE FOUR SIMULATIONS

(a) Introduction

The earliest theories devised to explain the origin of till and erratics were based on the idea of transport by water; it was thought that the deposits were the result of the biblical Noah's flood. In the middle of the 19th Century, Glacial Theory was conceived and developed (see Flint, 1971, for a review of the history). From the first geological evidence, it was easy to conclude that during the last ice age, an increase in precipitation produced the great ice fields, while in warmer latitudes there was increased rainfall. Evidence for "Pluvial" ages corresponding to the great Ice Ages seemed overwhelming. New evidence on various aspects of Late Pleistocene climates suggests that the assumption of pluvial-glacial synchrony should be reexamined.

Fairbridge (1964, 1970) has found much evidence for his theory of "ice age aridity," in which he suggests that the coldest parts (maxima) of the ice ages were characterized by worldwide aridity. Geological and palynological evidence has been found increasingly in

the last few years to support this concept; for example, Galloway (1970) (North America), Damuth and Fairbridge (1970) (South America), Frenzel (1968) (Northern Eurasia), Grove (1968) (Africa), Galloway (1965) (Australia), Bonatti (1966) (Mediterranean) and Bonatti and Gartner (1973) (Caribbean).

Flohn (1969) discusses the question of ice age aridity. He calculates that evaporation and precipitation amounts were reduced 20 to 30 per cent from their present day values at the maxima of the ice ages. Flohn attributes this aridity to reduction of the areal extent of the oceans (he calculated that exposure of continental shelf areas due to ice age sea level lowering and covering of certain seas with ice led to a decrease of the coverage of the earth's surface by ocean from 71 to about 68 per cent) and to lowered temperatures, which reduced the amount of evaporation from the oceans.

Most evidence supports the idea of a global arid phase at the height of the last glacial period, although some workers still equate "pluvial" with "glacial" (e.g., Morrison, 1965). As Flohn (1969) points out, there were probably a few areas where the displacement of cyclone tracks overcompensated for the reduced water content of the atmosphere giving more ice age precipitation than at present. Galloway (1970) has suggested that some lake levels in the United States rose at the maximum of the ice age due to "minevaporal" conditions, in which

evaporation was greatly reduced owing to the lowering of temperature allowing water to accumulate.

In this chapter the atmospheric moisture balance of the four simulations will be discussed. While, as pointed out before, we cannot say that the conditions simulated in the two ice age cases are those which occurred at 20,000 BP, the major and consistent changes between the control and ice age cases are probably indicative of the direction, if not the magnitude, of differences between present day and ice age circulations. The major differences between the moisture balances of the control and ice age cases will be examined to see whether they suggest glacial period maximum aridity or pluvial conditions.

Before going into details of the simulations, the water balance of the atmosphere will be briefly discussed. Detailed descriptions of the global water balance are found in, for example, Lorenz (1967), Newton (1972), Malkus (1962), Reiter (1969) and Palmén (1967).

If one considers the total mass of water contained in a region of the atmosphere north of a certain latitude, this amount may be temporarily increased by evaporation from the earth's surface or decreased by precipitation. It may also be increased by inflow of moist air across the southern boundary and decreased by a similar outflow. The amount of evaporation north of a given latitude need not balance the amount of

precipitation over a long time period--if they do not balance, then enough water must be transported into or out of the region to balance the deficit or excess of evaporation. As in the case of the angular momentum balance (Chapter IV), water may be transported by the mean meridional circulation or by the eddies.

Sutcliffe (1956) describes very well the water balance problem. He shows the uncertainty in our knowledge of precipitation and evaporation distributions. Brooks and Hunt (1930) made the original determinations of precipitation for land areas and their values are generally accepted by later writers. Ocean data have usually been derived on the basis of values of precipitation at coastal stations. This type of estimate is now known to be unrealistic, e.g., Tucker (1961) and Laevastu et al. (1969). Recent studies have determined that the precipitation distribution at ocean weather stations differs from earlier estimates. Tucker (1961) finds that over most of the North Atlantic precipitation is less than that at coastal stations. Reed and Elliott (1973) find that there is much less precipitation over the North Pacific than previously estimated. Available estimates of average precipitation and evaporation differ over a range of 20 per cent. As Newton (1972) points out, precipitation is inadequately sampled over oceanic areas and evaporation measurements are based on many different formulae, not on direct measurements. Laevastu, Clarke and

Wolff (1969) review our present state of knowledge of evaporation and precipitation at sea and the transport of moisture, they show that computations of evaporation on monthly, seasonal and annual bases carried out by various authors show some similarities but also considerable differences, which in most cases can be traced to differences in methods of computations and basic data used.

Thus our knowledge of precipitation and evaporation data is not good and is based on limited observed data and/or unreliable computations. Comparisons of the GCM control case output with observed data will be problematical because of the uncertainty of the latter. Moreover a recent study of the water vapor flux and its divergence by Adem (1968) has shown that there are large year-to-year differences in the quantity "evaporation minus precipitation." These differences may be as large as the mean values of this quantity.

Within a profile of zonally averaged water vapor flux, three zones are distinguishable (Reiter, 1969, p. 136): from 0°N to 10°N (equatorial trough) precipitation exceeds evaporation. In the zone from 10°N to 35°N (subtropical anticyclones) evaporation exceeds precipitation. North of 35°N precipitation is greater than evaporation. It follows that the net motions of the atmosphere must be such as to transport water from the subtropics to lower and higher latitudes.

(b) Theoretical Considerations

In simple terms the amount of water vapor in a given volume can be changed by meridional or vertical fluxes of water vapor across the boundaries of the volume, evaporation and precipitation (condensation) in the volume.

Washington and Kasahara (1970) show how the zonally averaged equation of the moisture per unit volume is derived for the NCAR GCM. This equation is modified, because of inclusion of orography in the GCM, by Kasahara and Washington (1971) to the equation used in the version of the GCM employed in this study:

$$\frac{\partial}{\partial t}(\overline{\rho\sigma}\,\hat{q}) + \frac{1}{a\cos\phi}\frac{\partial}{\partial\phi}[(\overline{\rho\sigma}\,\hat{v}\,\hat{q} + \overline{\rho\sigma v'q'})\cos\phi] + \frac{\partial'}{\partial z}[\overline{\rho}\,\hat{q}\,\overline{w} + \overline{\rho q''w''}] = \overline{\sigma M} + \overline{\sigma\rho E}. \qquad (5.1)$$

The terms on the left side of Equation (5.1) represent: the rate of change with time of water vapor per unit volume, the rate of change with latitude of the meridional flux of water vapor, the rate of change with height of the vertical flux of water vapor. Those on the right side represent the rate of condensation of water vapor per unit volume, plus the rate of change of water vapor content per unit mass due to vertical and horizontal diffusion of water vapor.

The second term in Equation (5.1) is split into two parts, the first term in the square brackets represents the meridional flux of water vapor due to the mean meridional circulation, the second term represents the meridional flux due to eddies. Similarly in the third term in Equation (5.1), the first term within the square brackets represents the vertical flux of water vapor due to the mean meridional circulation and the second term represents the vertical flux due to the eddies.

If Equation (5.1) is averaged over a long time period, then the first term should vanish (i.e., the long term average water vapor per unit volume is constant). If the resulting equation is integrated with respect to height (z) from the surface to the top of the atmosphere then the third term in Equation (5.1) vanishes, because of the boundary conditions on w.

Therefore,

$$\frac{1}{a \cos \phi} \frac{\partial}{\partial \phi} \int_H^{z_T} [(\overline{\rho\sigma}\ \hat{v}\ \hat{q} + \overline{\rho\sigma v'q'})\ \cos \phi]^{dz}$$

$$= \int_H^{z_T} (\overline{M} + \overline{\rho E})\ dz, \qquad (5.2)$$

for a steady state.

$\int_H^{z_T} (\overline{M} + \overline{\rho E})_{dz}$ is the difference between evaporation and precipitation. In the GCM it has been noted (Barry and Williams, 1973) that the assumption of a

Bowen ratio of unity leads to an overestimation of precipitation, especially in desert areas. This should be borne in mind when examining the moisture balance results.

(c) Specific Humidity Distribution

Figure 5.1 shows the latitude height distributions of the zonally averaged specific humidity field, $\bar{q}$, for the January and July control and ice age cases. Specific humidity is defined as the ratio of the mass of water vapor to the mass of moist air containing the vapor.

Comparison of Figures 5.1a and 5.1b shows that there is less water vapor in the atmosphere in the January ice age case than there is in the control case (in the equatorial lower atmosphere, where specific humidity is at a maximum, the specific humidity is decreased from 14 g kg^{-1} in the January control case to 10 g kg^{-1} in the ice age case), water vapor does not occur as high in the atmosphere in the ice age case (> 9 km in the control case, < 9 km in the ice age case) and does not occur in significant amounts north of 50°N and south of 70°S. In the July control and ice age cases (Figures 5.1c and 5.1d) the picture is very much the same, the equatorial maximum is reduced from 14 g kg^{-1} to 10 g kg^{-1}, the vertical extent is reduced from > 9 km to nearly 6 km and the latitudinal extent of water vapor is decreased especially in the northern hemisphere.

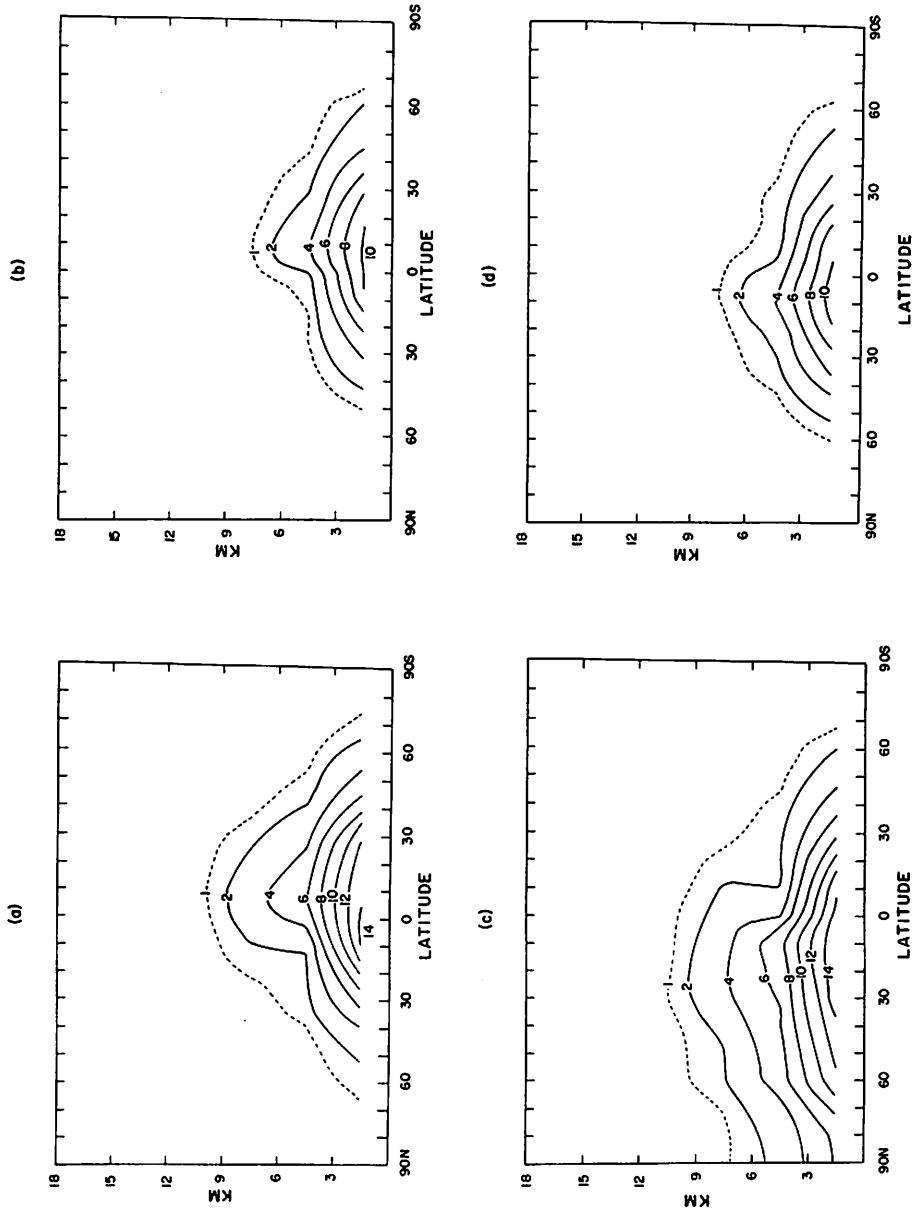

Figure 5.1. Latitude-height distributions of zonally averaged 30-day mean specific humidity for (a) January control case, (b) January ice age case, (c) July control case, (d) July ice age case. Units: g kg^{-1}.

This evidence strongly supports the concept of glacial period maximum aridity. The control case data compare very favorably with the observed data of Peixoto (1958) and Peixoto and Crisi (1965).

(d) Meridional and Vertical Transports of Water Vapor by the Mean Meridional Circulation

Figure 5.2a shows the latitude height distribution of the 30-day mean of zonally averaged meridional transport of water vapor by the mean circulation for the January control case. It is clear that the transport occurs in the lower atmosphere below 6 km, and within tropical latitudes. The transport by the mean circulation is southward and reaches a maximum at about 0° and 1.5 km. Clearly the only significant transport of water vapor by the mean circulation occurs in the vicinity of the Hadley circulation.

In the January ice age case (Figure 5.2b) the southward transport of water vapor by the Hadley circulation is 50 per cent greater than the control case amount and the maximum occurs at 5°S, that is, farther south than in the control case.

Figure 5.2c shows the same transport for the July control case. In July the Hadley cell transports water vapor northward across the equator and this northward flux is 70 per cent greater than the southward flux in the January control case. Transports in extratropical

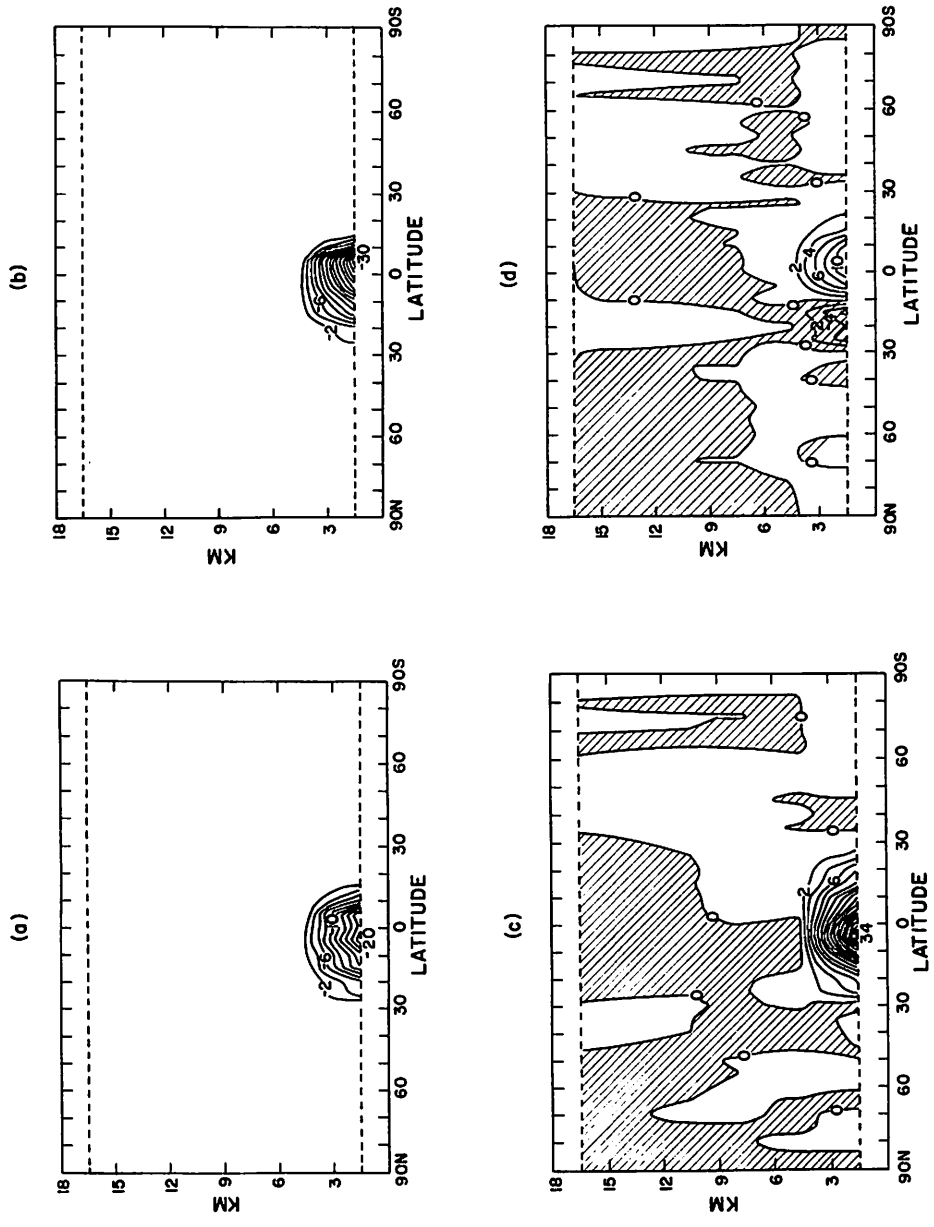

Figure 5.2. Latitude-height distribution of 30-day mean zonally averaged meridional transport of water vapor by the mean circulation for (a) January control case, (b) January ice age case, (c) July control case, (d) July ice age case. Units: 10^{-4} g cm^{-2} sec^{-1}.

latitudes are very much weaker than those in the Hadley cell. In the July ice age case, the northward transport of water vapor by the Hadley cell is considerably weaker than that in the control case (ice age case value 70 per cent less than control case value) and ends at 10°N compared with 30°N in the control case. In the ice age case there is a zone of southward transport of significant magnitude between 10°N and 30°N. Thus there is an area of strong convergence of water vapor at about 10°N.

The vertical transports of water vapor by the mean circulation in the four cases are not illustrated but will be discussed briefly. As with the meridional transports, the largest transports by the mean circulation occur in the vicinity of the Hadley circulation. In the January control case there is an area of strong upward transport (maximum value 4×10^{-6} g cm^{-2} sec^{-1}) between 5°N and 30°S, with the maximum at 10°S, this is the area of the rising branch of the Hadley circulation. In the January ice age case, the upward transport by the Hadley circulation is stronger (maximum 6×10^{-6} g cm^{-2} sec^{-1}) and in approximately the same location. Therefore in the January ice age case the southward and upward transports of water vapor by the Hadley circulation are greater than in the control case.

In the July ice age case the upward and downward transports of water vapor by the Hadley circulation are weaker. The upward transport at 10°N is weaker in the

ice age case (maximum about 3 x 10^{-6} g cm^{-2} sec^{-1}) than in the control case (maximum 5 x 10^{-6} g cm^{-2} sec^{-1})--an observation which is strange in view of the considerable horizontal meridional convergence of water vapor observed at 10°N in the July ice age case; the E-P curve (Figure 5.9) has a negative maximum at 10°N suggesting that the greater flux was balanced by precipitation in this region.

(e) Meridional and Vertical Transports of Water Vapor by the Eddies

Figure 5.3 shows the latitude-height distributions of 30-day mean zonally averaged meridional transports of water vapor by the eddies. It is clear that, similar to the discussion of transports of angular momentum in Chapter IV, whereas the Hadley circulation is responsible for transports in lower latitudes, the eddies are most important in middle latitudes.

Consideration of Figure 5.3 shows that, as for transports by the mean circulation, the significant meridional transports of water vapor by the eddies occur in the lower atmosphere. In Figure 5.3a (January control case) we see that the eddies transport water vapor northward in the northern hemisphere middle latitudes and southward in the southern hemisphere middle latitudes. In the January ice age case (Figure 5.3b) the eddy transports are weaker (25-30 per cent less than control case

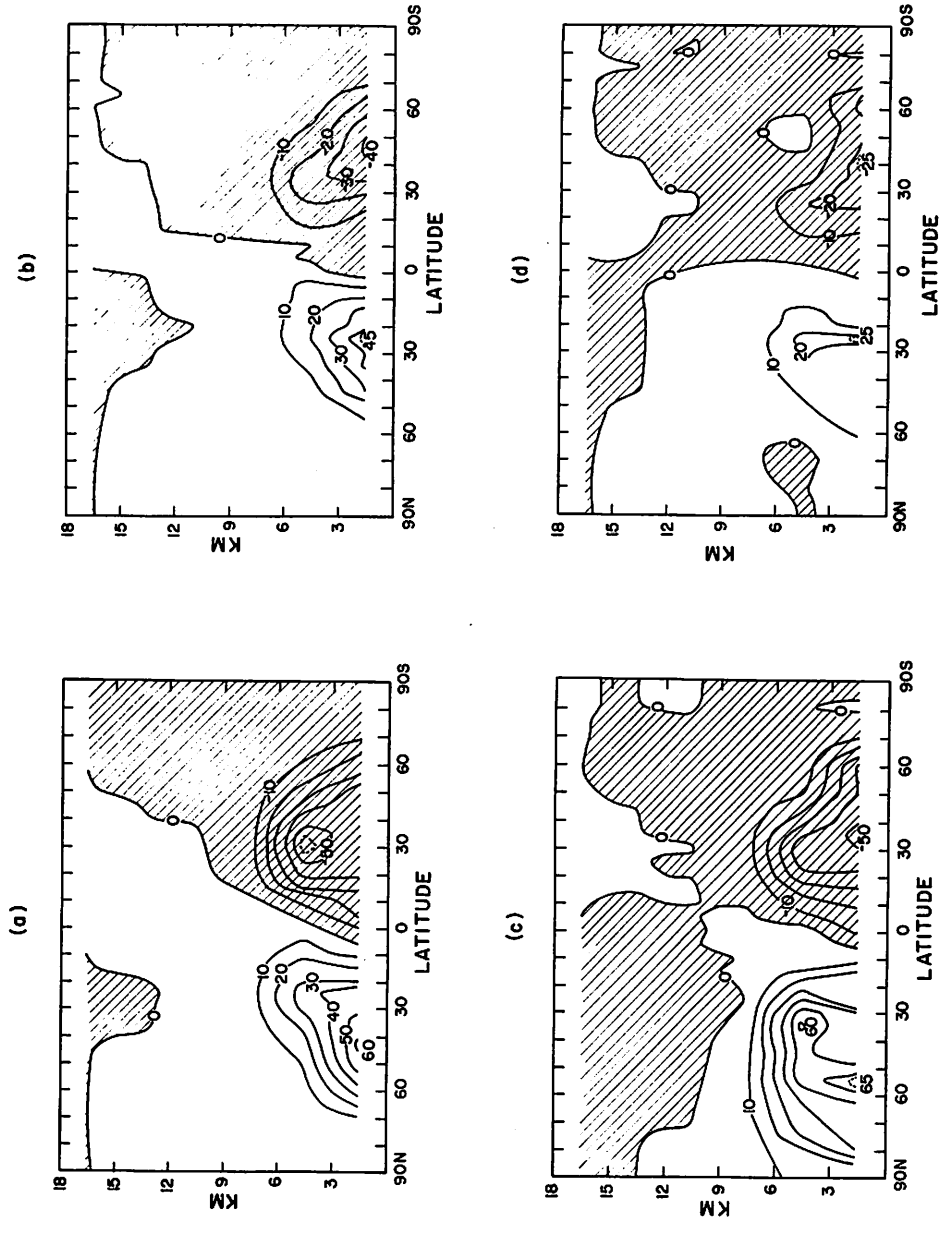

Figure 5.3. Latitude-height distributions of 30-day mean zonally averaged meridional transport of water vapor by eddy motions. (a) January control case, (b) January ice age case, (c) July control case, (d) July ice age case. Units: 10^{-5} g cm^{-2} sec^{-1}.

values) and do not extend as far poleward. In the July cases (Figures 5.3c and 5.3d) the direction of transport is the same as in the January cases and again the poleward transport of water vapor is reduced in the ice age case (by 50-60 per cent of the control case values), with a greater reduction than observed in the January cases.

The vertical transports of water vapor by the eddy motions (not illustrated) are stronger in the control cases than in the ice age cases. The eddies cause an upward transport of water vapor in the middle and low latitudes in all four cases. For the vertical, as seen above for the meridional, transports, the weakening of the transport was most pronounced in July.

(f) Vertically Integrated Meridional Transports of Water Vapor by the Mean Circulation

Figures 5.4 and 5.5 show the latitudinal distribution of $\Sigma\ \overline{\rho\sigma}\ \hat{v}\ \hat{q}\ \Delta\ Z$ for January and July respectively. The control case data are compared with the observed data of Oort and Rasmusson (1971).

In Figure 5.4 it can be seen that the vertically integrated transports of the control case and observed data agree well except in equatorial regions where the control case has more southward transport of water vapor than is observed (observed value 35 per cent less than control case value). The only large difference between the January control case and ice age case is also in the

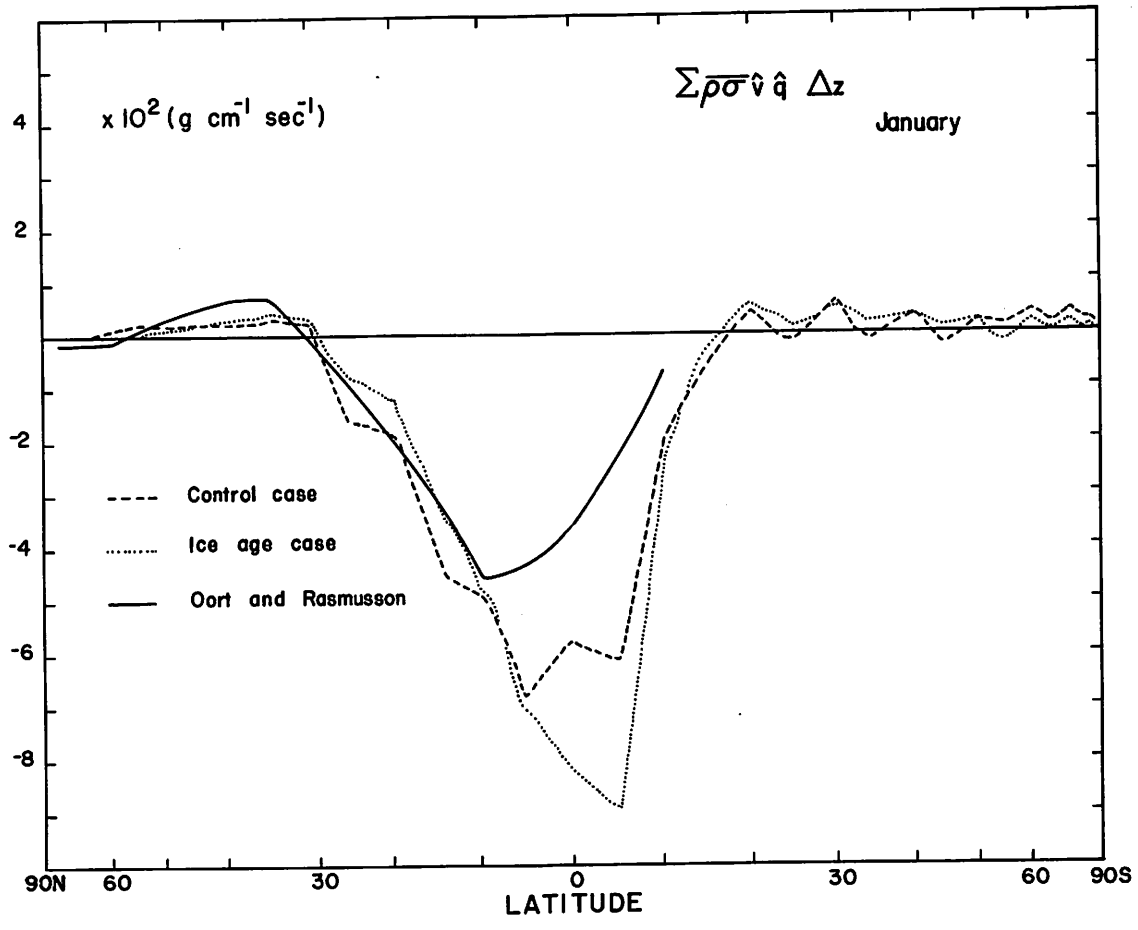

Figure 5.4. Vertical integrals of $\overline{\rho\sigma}\ \hat{v}\ \hat{q}$ as a function of latitude for January cases. Observed data are taken from Oort and Rasmusson (1971). Units: 10^2 g cm^{-1} sec^{-2}.

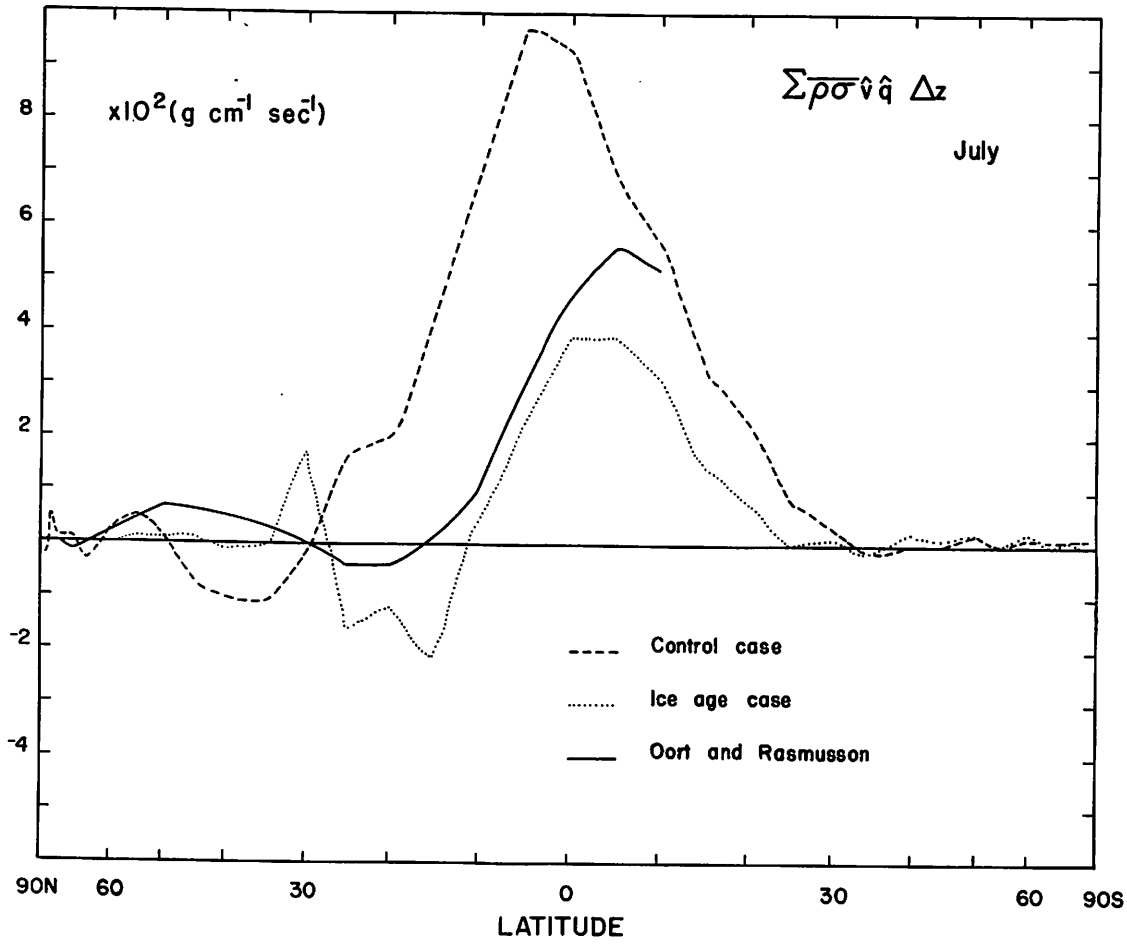

Figure 5.5. Vertical integrals of $\overline{\rho\sigma}\ \hat{v}\ \hat{q}$ as a function of latitude for July cases. Observed data are taken from Oort and Rasmusson (1971). Units: 10^2 g cm^{-1} sec^{-2}.

tropics where the southward transport of water vapor between 10°N and 10°S is even greater than that in the control case (ice age case value is about 40 per cent greater than control case value).

For the July data (Figure 5.5) we see that there is less agreement between the observed and control case data. Between 35°N and 10°S (where the observed data ends), the control case has a much larger northward transport of water vapor than is observed (maximum difference is about 50 per cent of control case value). Between 35°N and 50°N the observed and control case transports are in opposite directions. In the July ice age case, the only significant transport (horizontal) of water vapor occurs in the vicinity of the Hadley cell. Between 30°N and 10°N the southward transport noted in Figure 5.2d is clearly shown. Between 10°N and 20°S the transport is northward and much weaker than in the control case (ice age case value 60 per cent less than control case value).

Examination of Figures 5.4 and 5.5 leads to the conclusion that the Hadley cell in the model is producing too much meridional transport of water vapor (northward in July and southward in January). In the January cases, the transport in the tropics is greater in the ice age case than in the control case. In the July cases, the transport is greater in the control case.

(g) Vertically Integrated Meridional Transport of Water Vapor by the Eddies

Figures 5.6 and 5.7 show the latitudinal distributions of $\Sigma\ \overline{\rho\sigma v'q'}\ \Delta\ Z$ for January and July respectively. The control case data are compared with the observed data of Oort and Rasmusson (1971).

For January (Figure 5.6) the observed data and control case data compare very favorably (observed data available only for 70°N to 10°S). In general the meridional transport of water vapor by the eddies is smaller in the January ice age case than in the control case.

The July control case (Figure 5.7) middle latitude eddies produce more meridional transport (northward) of water vapor than is observed (maximum difference about 63 per cent of the control case value at about 55°N). As in the January cases, the ice age case vertically integrated transport is smaller than that of the control case at most latitudes.

(h) Latitudinal Distributions of the Difference Between Evaporation and Precipitation

It was pointed out in the introduction that our knowledge of the distributions of precipitation and evaporation is not good. E-P can be calculated from a knowledge of P and of E or from the divergence of the atmospheric water vapor flux. Newell *et al.* (1970) combined the values derived by the first approach by

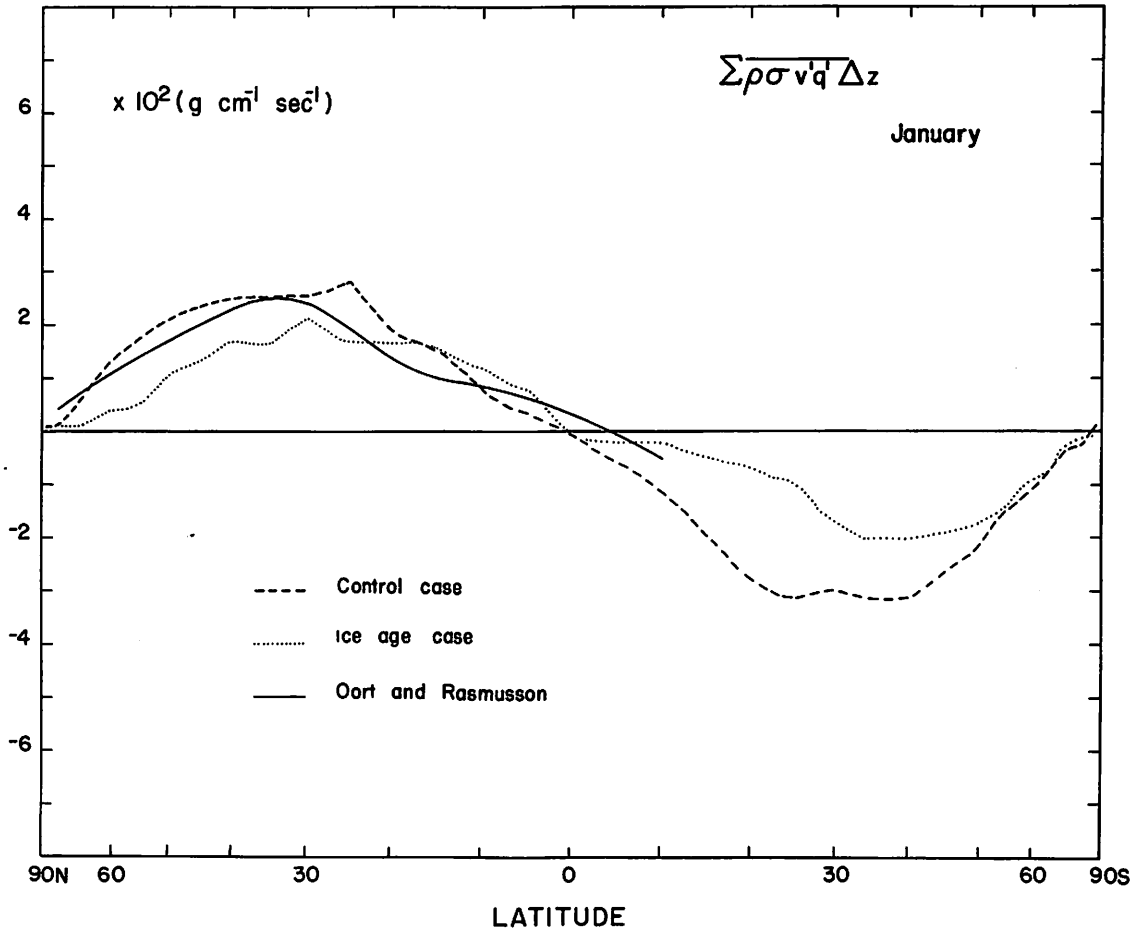

Figure 5.6. Vertical integrals of $\overline{\rho\sigma v'q'}$ as a function of latitude for January cases. Observed data are taken from Oort and Rasmusson (1971). Units: 10^2 g cm^{-1} sec^{-2}.

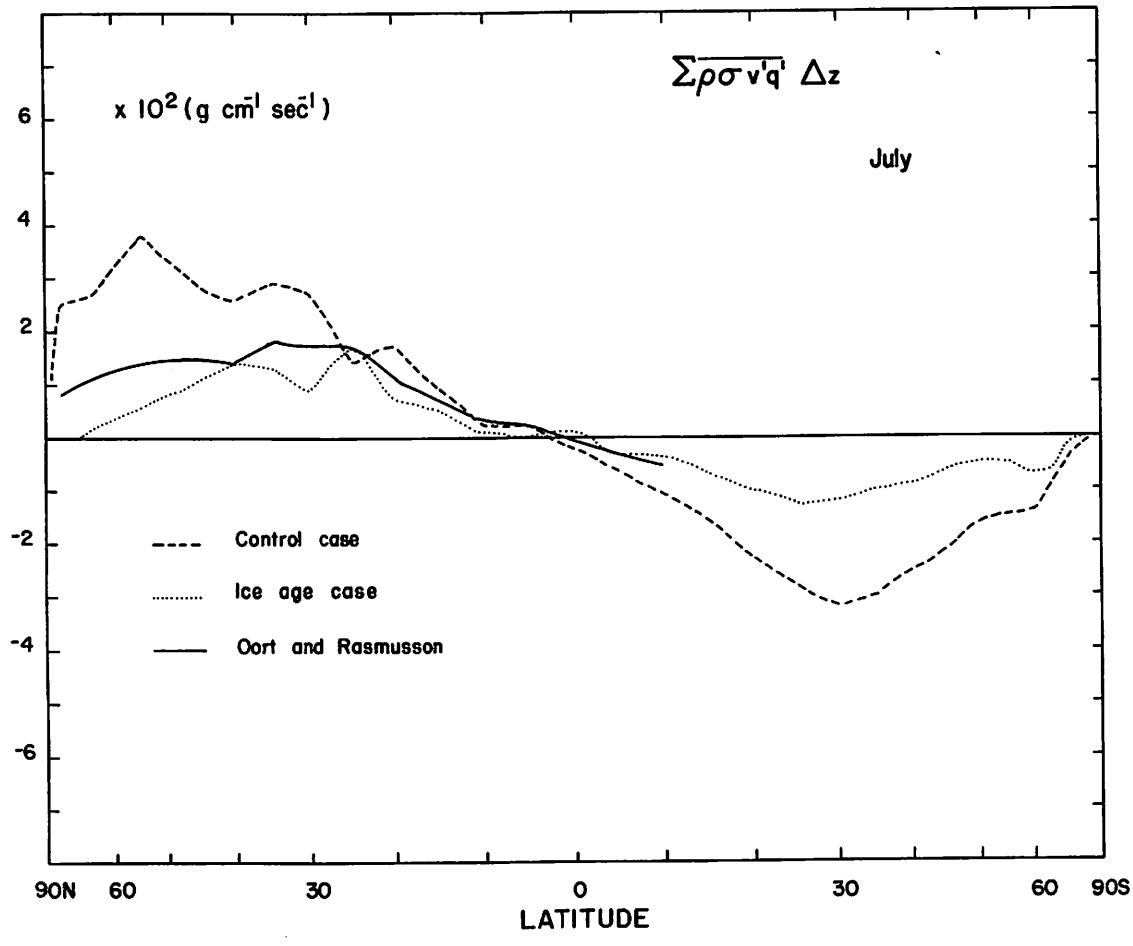

Figure 5.7. Vertical integrals of $\overline{\rho v'q'}$ as a function of latitude for July cases. Observed data are taken from Oort and Rasmusson (1971). Units: 10^2 g cm^{-1} sec^{-2}.

Gabites (1950) and Rasool and Prabhakara (1966) and by the second approach by Rasmusson (1972). Notable discrepancies between the three sources occurred at high latitudes in the southern hemisphere.

The data compiled by Newell et al. have been compared with control case distributions derived from direct calculations of $\overline{M}$ and $\overline{\rho E}$ (see section on theoretical considerations). Figure 5.8a shows the latitudinal distributions of the difference between evaporation and precipitation for the January control case and ice age case and for observed data (December-February). Kasahara and Washington (1971) find that the computed values from the model calculations are in good agreement with the observed data except near 10°S, where the model calculations give somewhat larger negative values. Consideration of Figure 5.8a shows that the latter statement also applies to this study. The maxima and minima of the control case and observed data occur in approximately the same positions (latitudinally) but, especially in the tropics and southern hemisphere, the magnitudes differ (at 10°S, the observed value of E-P is about -50 g cm^{-2} year^{-1}, while the computed value is about -150 g cm^{-2} year^{-1}). In view of the differences between the control and observed data, it is difficult to comment on the differences between the control case and ice age case data. The only large difference between the latter

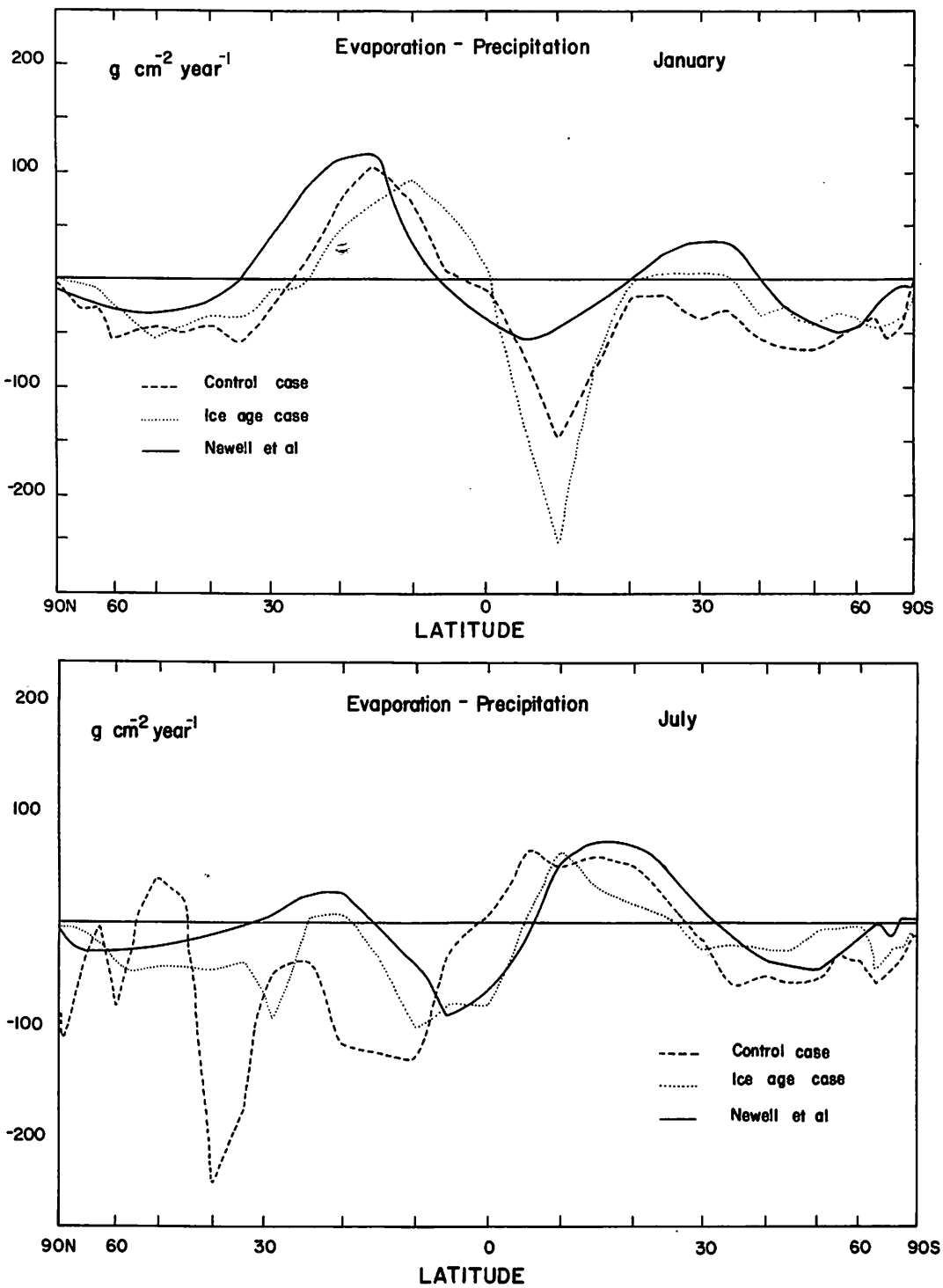

Figure 5.8. Latitudinal distributions of the difference between evaporation and precipitation for (a) January and (b) July cases. Observed data are taken from Newell et al. (1970). Units g cm^{-2} $year^{-1}$.

is at about 10°S where the ice age calculations give much larger negative values.

In Figure 5.8b similar distributions are plotted for the July cases. In this month the observed and control case data are quite similar in the southern hemisphere but there are great differences between the two distributions in the northern hemisphere. The July control case curve shows great fluctuations in the northern hemisphere and these are not seen in the observed data. As far as the July distributions of evaporation minus precipitation are concerned there are large differences between the observed and control case data, which makes interpretation of the smaller differences between the control case and ice age data impossible.

(i) Summary and Conclusions

Recent geological and biological evidence has suggested that earlier theories of "glacial-pluvial synchrony" should be rejected in favor of the theory of "glacial period maximum aridity." Evidence indicates that several areas experienced cold, dry conditions at the maximum of the past glacial period, although some areas are still believed to have been wetter than present. Flohn (1969) calculates that precipitation/evaporation amounts were reduced 20-30 per cent from their present values at the glacial period maximum.

Flohn (1953) outlines a model of the distribution of E-P during a glacial period. He given no magnitudes but the shape of his northern hemisphere curve for a glacial period E-P is very similar to that of the January ice age case except north of 45°N.

In considering the output from the four GCM simulations, we expect that the major differences between the moisture balances of the control and ice age cases are indicative of the direction if not the magnitude of the changes between present day and ice age circulations.

In both January and July cases, the amount and vertical and latitudinal extents of water vapor in the atmosphere are less in the ice age case than they are in the control case. The simulated specific humidity distributions support the concept of ice age aridity. Williams et al. (1973) discuss changes in zonally averaged, 3 km cloudiness. In general cloudiness increased from the control cases to the ice age cases. This suggests that although the specific himidity decreased the relative humidity increased (because of reduced temperatures) in the ice age cases. This feature is also noted by Kraus (1973).

The meridional transport of water vapor by the mean circulation occurs in the lower atmosphere and within tropical latitudes. In the January ice age case the southward transport of water vapor by the Hadley

circulation is greater than that in the control case, the maximum occurs further south. In the July ice age case the northward transport by the Hadley circulation is weaker than that in the control case and there is a zone of southward transport of significant magnitude between 10°N and 30°N not found in the control case. In the January cases the vertical transport of water vapor in the Hadley circulation is stronger in the ice age case. In July the vertical transports are weaker in the ice age case.

Therefore the Hadley circulation transports more water vapor vertically and meridionally in the January ice age case than in the control case and less in the July ice age case than in the control case. This conclusion is supported by consideration of the vertically integrated meridional transports.

Eddies act to transport water vapor poleward and upward in the middle latitudes in all cases. In both ice age cases, the meridional transports and vertical transports of water vapor by the eddies were weaker than in the control cases, the reduction was greater in July.

Our knowledge of the distributions of precipitation and evaporation is uncertain, and there is evidence of great interannual variability. The compilation of data by Newell et al. has been taken as a best estimate of our current knowledge and compared with the control case data. The January control case latitudinal

distribution of evaporation minus precipitation has peaks in approximately the same places as do the observed data but magnitudes are different. The July control case distribution does not compare favorably with the observed data. It is difficult to make comparisons between the control and ice age case distributions since there are such large differences between the observed and control case data. Some of the latter differences may, however, be attributed to the quality of the observed data.

Therefore, the water balance of the atmosphere in the four simulations is such that: the specific humidity of the atmosphere is reduced in the ice age cases compared with the control cases. The ice age case meridional and vertical transports by mean circulation and eddies are weaker except in the tropics in January, where transports by the mean circulation are stronger than in the control case.

CHAPTER VI

HEAT BALANCE OF THE FOUR SIMULATIONS

(a) Introduction

Solar radiation is the principal energy source of the earth-atmosphere system. As described by Sasamori et al. (1972), the heating of the earth is not uniform because of differences in solar elevation at different latitudes. Geographic variation of the earth's albedo produces further modifications to the heating distribution. Since temperature gradients are set up by this non-uniform heating there is a potential source of energy to drive circulations. Heat is transported from warmer regions to cooler regions. In general there is atmospheric and oceanic transport of heat from the equatorial regions (where net radiation is positive) to polar regions (where net radiation is negative), but there are some east-west transports too in response to land/ocean thermal contrasts. The earth-atmosphere system becomes adjusted to a balance between heating by solar radiation and cooling by infrared radiation.

During the Würm/Wisconsin glacial period the magnitude of the various terms of the heat balance of the earth's atmosphere must have been different from

that observed at present. The solar heating would have been changed because of changes in the earth-orbital parameters and planetary albedo for instance. Outgoing long wave radiation amounts would change if the temperature of the radiating surface changed. The heat exchange between the earth and atmosphere, which is due to vertical sensible and latent heating, can be changed by altering the character of the underlying surface. Therefore it can be expected that the atmospheric heat balance simulated by the GCM will differ in the control cases and the ice age cases.

Before discussing the details of the latter differences, the general principles of the atmospheric heat balance will be discussed.

Most of the atmosphere is characterized by a strong radiative deficit, which must be compensated by a net transfer of energy from the earth's surface, where there is a surplus of radiative heating. This drives the system to an equilibrium value, in which the atmosphere does not experience a continual decrease of temperature. Sensible heat and latent heat are transferred from the earth (i.e., land, sea or ice surface) to the atmosphere by turbulent heat fluxes to the atmosphere; both forms are then carried upward by air motions of several scales. Latent heat is realized when condensation occurs as the air becomes greater than supersaturated. Meridional transports also

occur and they are basically a result of the latitudinal distribution of net radiation.

As Palmén and Newton (1969) describe, insolation varies strongly because of differences in solar elevation, whereas outgoing radiation does not vary so much either latitudinally or seasonally. On an annual basis there is a surplus of net (solar minus terrestrial) radiative heating equatorward of latitude 37° and a corresponding deficit at higher latitudes. Therefore there is a poleward flux of energy from the tropics to the poles which reaches a maximum at about latitude 37°. This transport, as in the case of the angular momentum and moisture discussed previously, is carried out by the mean meridional circulation and the eddy motions and the oceans.

The atmospheric heat balance of the northern hemisphere has been studied by London (1957), Davis (1963) and Katayama (1967) for example, and the results of these studies have been referred to in the present study. Similarly the heat balance of the southern hemisphere has been discussed by Sasamori et al. (1972). Newell et al. (1970) and Davis (1971) discuss the global heat budget and Palmén and Newton (1969) and Lorenz (1967) describe the general principles of the atmosphere heat balance and the vertical and meridional fluxes of energy. Recently meteorological satellites have measured reflected solar radiation and outgoing terrestrial

radiation from the earth-atmosphere system (e.g., Vonder Haar and Suomi, 1969, 1971).

The planetary albedo, which is an important factor in the calculation of the earth-atmosphere heat budget, is not used explicitly in the model but calculations have been made of this variable for the four GCM cases and the results are discussed in Appendix C.

(b) Theoretical Considerations

The rate of heating/cooling in the model is expressed by

$$Q = Q_{dv} + Q_{dh} + Q_{al} + Q_{as} + Q_c, \qquad (6.1)$$

(Kasahara and Washington, 1971).

Q - total heating rate

Q_{dv} - vertical diffusion of sensible heat

Q_{dh} - horizontal diffusion of sensible heat

Q_{al} - long wave cooling of the atmosphere (Q_{al} is negative for cooling)

Q_{as} - absorption of solar radiation by water vapor

Q_c - release of latent heat of condensation of water vapor.

Sometimes it is convenient to express a heating rate in terms of the vertical difference in flux. By using the same subscripts for fluxes as used to represent the heating rates, we can express,

$$Q_{as} = -\frac{1}{\rho}\frac{\partial F_{as}}{\partial z} \tag{6.2}$$

$$Q_{al} = -\frac{1}{\rho}\frac{\partial F_{al}}{\partial z} \tag{6.3}$$

By integrating equation (6.2) through the depth of the atmosphere and using the zonal mean operator (denoted by a bar, see Appendix A),

$$\overline{\Delta F_{as}} \equiv \int_{H}^{z_T} \overline{\rho Q_{as}}\, dz, \tag{6.4}$$

the last equation has been utilized to plot zonal averages of the heat fluxes in order to compare their magnitudes and identify differences between simulations.

It should be emphasized at this point that the heat balance terms described in this chapter are 30-day mean values. In view of some of the inaccuracies in the model computation of these terms (see Chapter VIII) these heating rates should not be extrapolated for extended time intervals in order to examine the origin or disintegration of the ice sheets.

(c) Solar Radiation Absorbed in the Troposphere by Water Vapor

Figure 6.1a shows the January zonal mean distribution of $\overline{\Delta F_{as}}$, the solar radiation absorbed in the

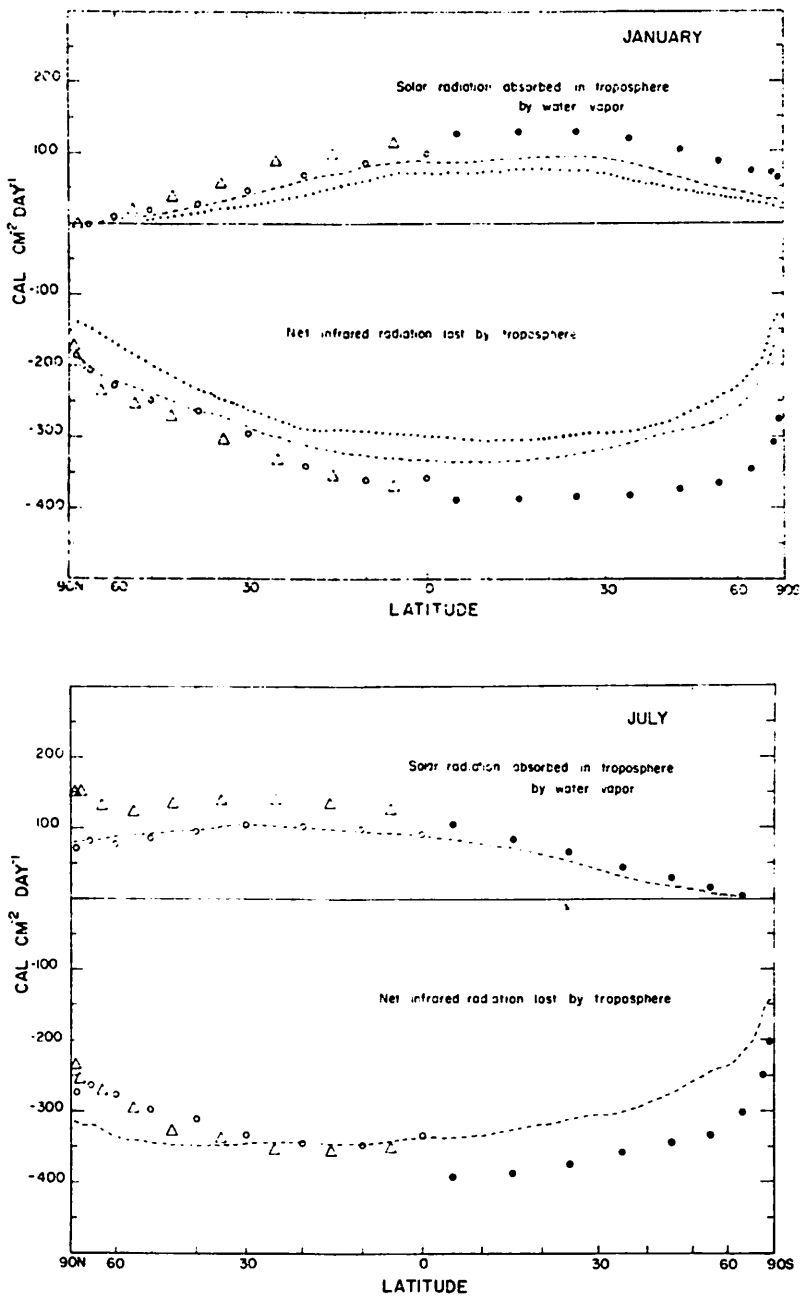

Figure 6.1. Solar radiation absorbed in the troposphere by water vapor (upper curves) and net infrared radiation lost by the troposphere (lower curves) in (a) the January cases and (b) the July cases. Dashed line represents control case, dotted line represents ice age case. Observed data from London (1957) (triangles), Sasamori et al. (1972) (black dots), and Katayama (1967) (open circles).

troposphere by water vapor in the upper section of the diagram. Data from Katayama (1967), London (1957) and Sasamori et al. (1972) have been compared with the computed data. In the northern hemisphere the control case data (dashed line) are virtually identical with the values found by Katayama. The control case values are lower than those published by London for the northern hemisphere by about 40 per cent at 25°N and less than 40 per cent elsewhere. For the southern hemisphere the control case data are again less than published values, in this case the values are about 40 cal cm^{-2} day^{-1} lower in the control case at all latitudes. Kasahara and Washington (1971) also found that the computed absorption of solar radiation in the troposphere by water vapor was generally the same as that given by Katayama and less than that given by Sasamori et al. and London.

In the July control case zonal mean distribution of the solar radiation absorbed in the troposphere by water vapor (Figure 6.1b) the values are again virtually identical to those given by Katayama (1967) for the northern hemisphere. Also, the control case distribution has lower values than those of London for the northern hemisphere and Sasamori et al. for the southern hemisphere. However, in July the differences between the control case values and those of Sasamori et al.

are not large ($\sim$ 20 cal cm^{-2} day^{-1}), whereas the differences between the control case values and those of London are between 35 and 70 cal cm^{-2} day^{-1}.

As Katayama has pointed out, the amount of solar radiation absorbed in the troposphere by water vapor depends not only on the amount of incident solar radiation, the altitude of the sun and the water vapor amount, but also on the amount and type of clouds. The relationship between $\overline{\Delta F_{as}}$ and cloudiness is rather complicated. The equations used to calculate the solar heating Q_{as} are described in Kasahara and Washington (1971) and in detail in Oliger et al. (1970). Since the model only computes cloudiness at 3 and 9 km on the basis of empirically derived formulae (see Smagorinsky, 1960, for examples of such formulae), it is very possible that the differences between the observed and computed values of solar radiation absorbed in the troposphere by water vapor largely result from the assumptions regarding cloud cover of both data sets. However Sasamori et al. point out that the absorption by water vapor and clouds is slightly larger in their calculations than those of London (1957) because of differences in the calculations. London, Katayama and Kasahara and Washington all use the technique given by Mügge and Müller (1932) for computation of absorption of solar radiation by water vapor. As Washington (1971) emphasizes, the formulation for absorption of solar radiation

used in the GCM, does not take cloud absorption into account. The only effect of cloudiness is to reduce the amount of direct solar radiation available below the cloud for further absorption. The effect of this assumption is discussed briefly in Chapter VIII.

In the ice age cases for both January and July, the solar radiation absorbed in the troposphere by water vapor is less than that found in the control cases. In the January cases there is a reduction of about 10 to 20 cal cm^{-2} day^{-1} from the control case to the ice age case at nearly all latitudes, the differences become smaller in polar latitudes (where absorption is least anyway). In the July cases the reduction of solar radiation absorption is not as uniform as in the January cases. The difference between the ice age case and control case values (see Figure 6.2) is negligible south of about 40°S, is about 10 to 20 cal cm^{-2} day^{-1} between 40°S and 20°N and is greater at the north pole (about 60 cal cm^{-2} day^{-1}). Since the zonal means of solar radiation in the northern hemisphere computed in the July control case are virtually identical to those calculated by Katayama, the large difference between the control case and ice age case values looks significant.

The most obvious reason for the reduction in the amount of solar radiation absorbed by water vapor from the control case to the ice age case is that the amount

of water vapor in the atmosphere was reduced in the ice age case (see Chapter V on the moisture balance). Changes in the distribution of cloudiness will also cause changes in absorption.

The largest change in absorption between control case and ice age case occurs in the July cases north of 30°N. Figure 5.1 in the moisture balance chapter shows that this is also the region where the largest change in specific humidity occurred from the July control case to the ice age case. North of 60°N, specific humidity is reduced from 1 to 12 g kg^{-1} to 0 to 1 g kg^{-1}.

(d) Net Infrared Radiation Lost by the Troposphere

Infrared heating/cooling, Q_{al}, represents the other radiational term of Q. Q_{al} is generally negative in the troposphere, i.e., long wave cooling is usually occurring. Q_{al} is strongly affected by the mean temperature of the troposphere and the cloud cover. As with the absorption of solar radiation, the effect of clouds is not simple (see, for example, Katayama, 1967, p. 13). The contribution of cloud cover to Q_{al} varies completely with the variation of cloud type and especially cloud height.

In Figure 6.1a, the lower curves show the computed and observed net infrared radiation lost by the troposphere in the January cases. As for absorbed radiation,

the control case data for the northern hemisphere are very similar to those of Katayama, except that the control case and observed infrared data differ equatorward of 30°N. At 10°N the difference between the control case and Katayama's data is only 35 cal cm^{-2} day^{-1}, which is about 10 per cent of the control case value. The difference between the control case and ice age case values at 10°N is also 35 cal cm^{-2} day^{-1}. The data on net infrared radiation lost by the troposphere taken from London (1957) are not very different from those of Katayama. The values given by Sasamori et al. are greater than those in the control case. At 75°S the net infrared cooling is about 135 cal cm^{-2} day^{-1} greater in the data of Sasamori et al. than it is in the control case; this is the largest difference between the observed and computed data. Kasahara and Washington (1971) also found that the GCM control case produced less infrared cooling by the troposphere than is given by the data of Sasamori et al.

The differences between observed and computed values of net infrared radiation lost by the troposphere must be due to either differences in the temperature, water vapor or cloudiness of the troposphere .

In the July cases (Figure 6.1b), the control case zonal mean distribution of net radiation lost by the troposphere is more similar to the observed distributions

in the northern hemisphere and is less than the values published for the southern hemisphere. The values for the northern hemisphere given by Katayama and London show approximately the same distribution. The control case data are similar to the observed data between 0° and 25°N, then the curves diverge and the control case data are greater (more cooling) than those given by London and Katayama.

In the ice age cases, the net infrared radiation lost by the troposphere is less than that computed for the control cases for both January and July cases. In the January cases, the difference between the control and ice age case values is between about 10 and 50 cal cm^{-2} day^{-1} and the largest differences occur in the northern hemisphere. In the July cases the largest differences again occur in the northern hemisphere, with a difference of about 150 cal cm^{-2} day^{-1} (or about 80 per cent of the ice age case value) at 85°N. The reduction in the amounts of net radiation lost from the control cases to the ice age cases, which is largest in the northern hemisphere, is the result of (a) a reduction of tropospheric temperature and (b) a change in the cloudiness distribution, in the ice age cases. In the July cases the largest reduction in temperature occurs in the lower troposphere (below 6 km) and north of 60°N, where the difference in temperature between the control

case and the ice age case is 30-40°C (see Figure 3.3b in Chapter III which shows latitude-height distribution of the difference in temperature between July control case and ice age case).

Schneider (1972) has discussed the effect of variations in cloudiness on the radiation balance of a vertical column through the earth-atmosphere system. He found that the effects depend on the season and the geographical location of the column and also on the nature of the variation. The role of clouds in the net infrared radiational cooling of the troposphere is to increase the cooling rate near the cloud top and decrease the cooling rate or even cause slight heating near the cloud base (London, 1953, 1957). In higher latitudes, London found that cooling was increased by the strengthened greenhouse effect produced by clouds in a relatively stable atmosphere. In GCM output, Washington (1971) finds that in higher latitudes, where cloudiness is high, there is a small heating rate under the cloud of about 0.2°C day^{-1} and above the clouds, a cooling rate of 3-4°C day^{-1}. In the tropics he finds that the cooling rates are highly variable and show a strong dependence on cloudiness. This relationship between Q_{al} at 1.5 km and 4.5 km and cloudiness at 3 km is found in each of the four simulations of this study. In the July cases the amount of low cloud is increased in the ice age case by about 33 per cent of the control

case amount between 30°N and 85°N but in the January case the low cloud amount is less in the ice age case than in the control case (about five per cent reduction). It is difficult therefore to attribute the changes in net infrared radiation to cloudiness changes, since opposite changes in cloud amount are accompanied by similar changes in the long wave cooling in the northern hemisphere. Nevertheless, cloudiness changes must have influenced the amounts of net infrared radiation.

(e) Latitudinal Distributions of Zonal Means of Heating Rates Integrated Through the Model Atmosphere

In Figures 6.2, 6.3, 6.4, 6.5 the heating rates calculated for the four simulations are illustrated. Each figure shows six curves and these show the latitudinal distributions of $\overline{Q}/c_p$ the total heating rate, $\overline{Q}_c/c_p$ the latent heating rate, $\overline{Q}_{dv}/c_p$ vertical sensible heating, $\overline{Q}_{dh}/c_p$ horizontal diffusion of sensible heat, $\overline{Q}_{al}/c_p$ infrared cooling, $\overline{Q}_{as}/c_p$ solar heating. Values are plotted in °C day^{-1}.

The infrared cooling $\overline{Q}_{al}/c_p$ and the condensation heating are the principal sources of heating/cooling and the condensation heating can be seen in Figures 6.2-6.5 to be the main influence on the distribution of total heating. In this section, zonal averages of the heating rates integrated through the whole atmosphere

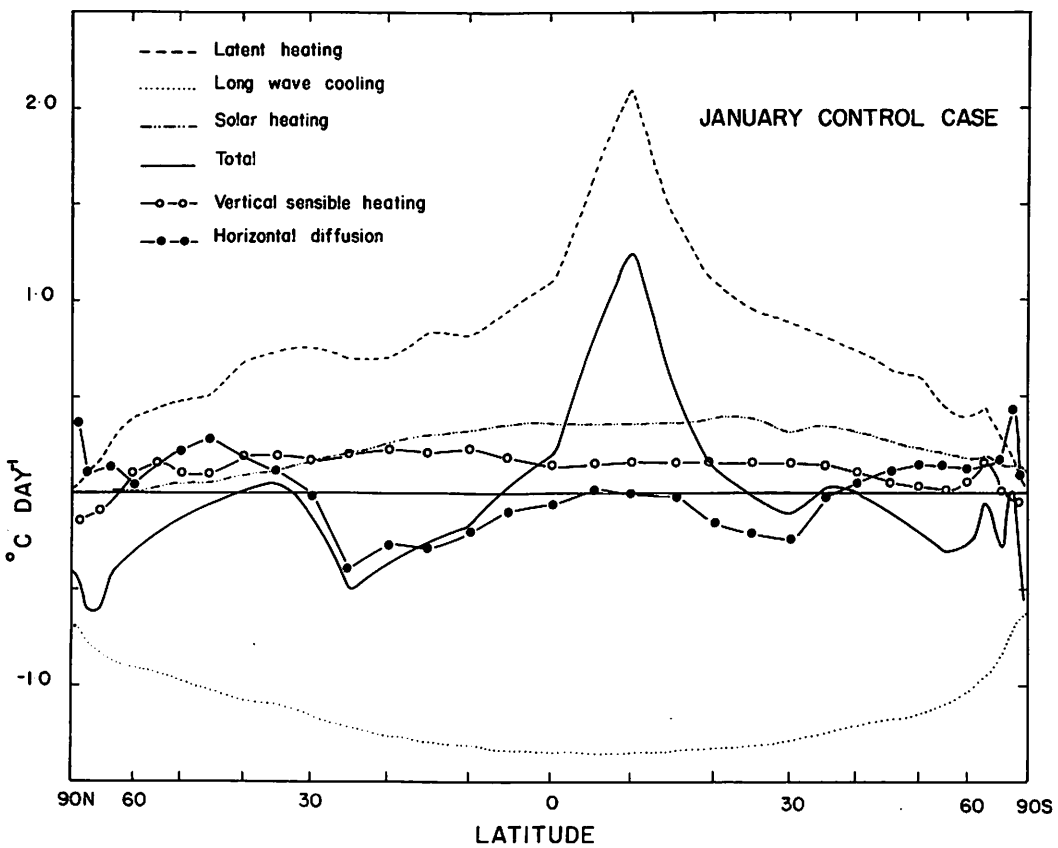

Figure 6.2. Latitudinal distributions of zonal averages of various heating rates (°C day^{-1}) averaged through the model atmosphere for the January control case.

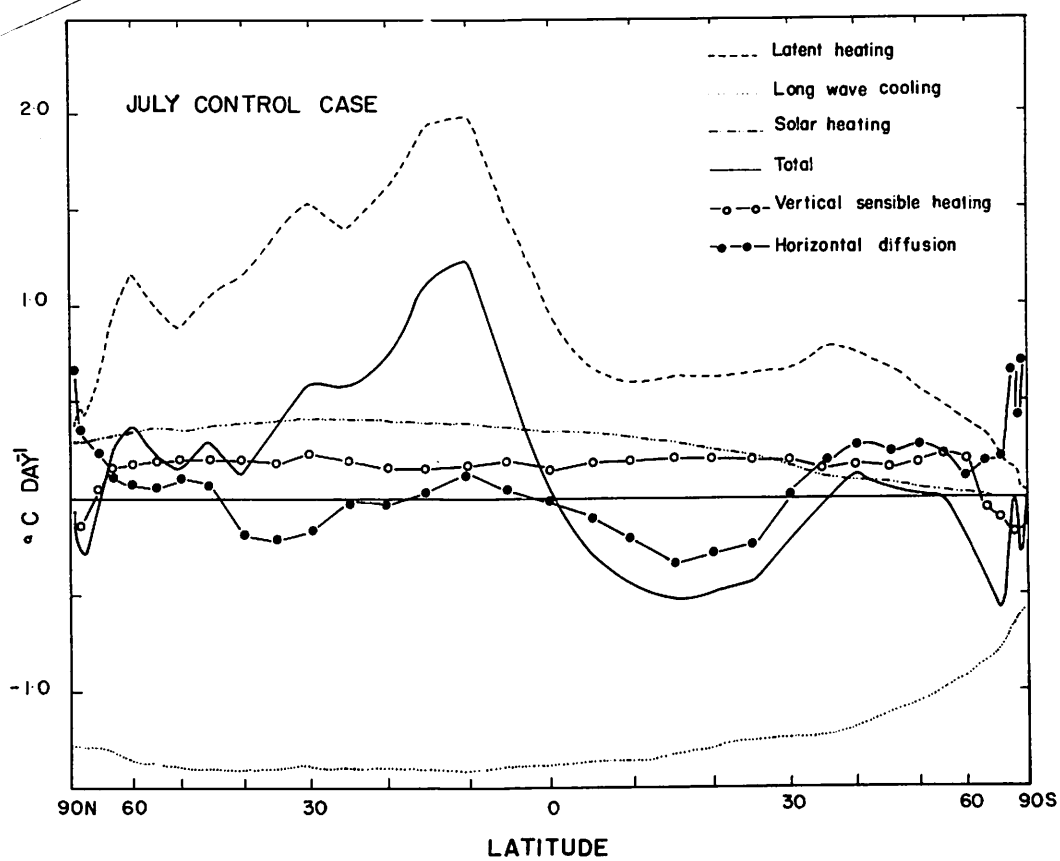

Figure 6.3. Latitudinal distributions of zonal averages of various heating rates (°C day^{-1}) averaged through the model atmosphere for the July control case.

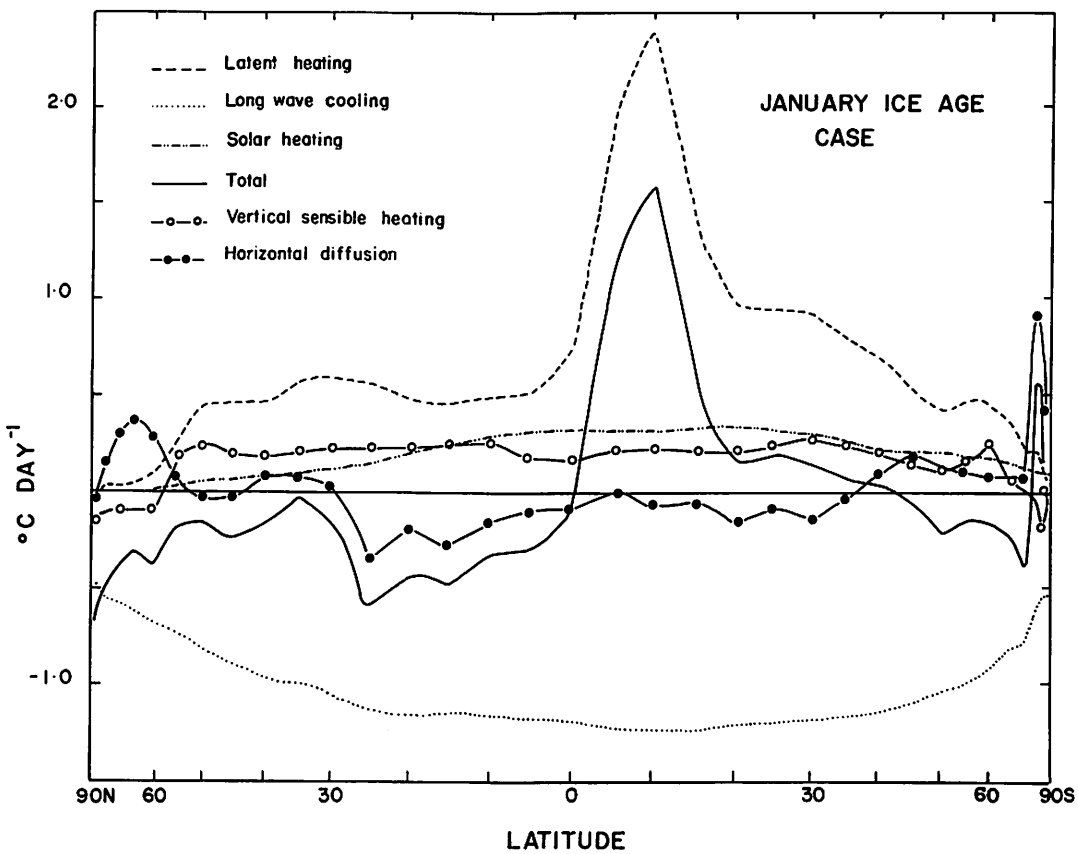

Figure 6.4. Latitudinal distributions of zonal averages of various heating rates (°C day^{-1}) averaged through the model atmosphere for the January ice age case.

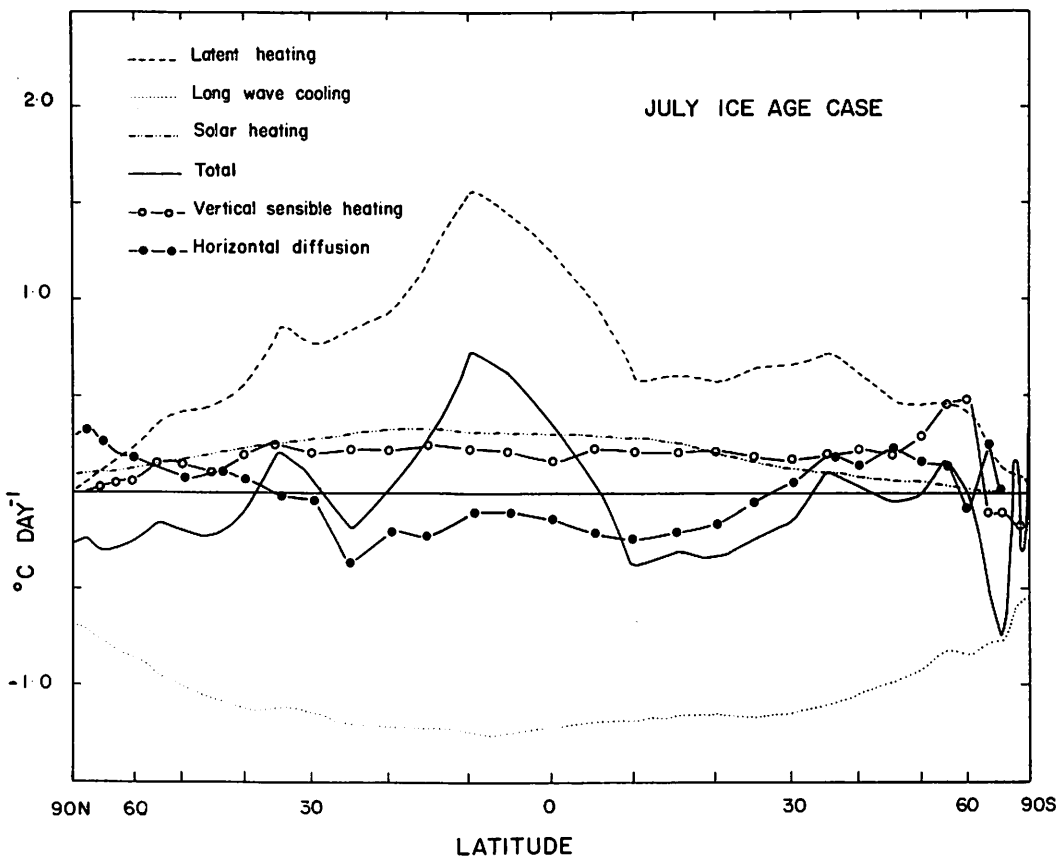

Figure 6.5. Latitudinal distributions of zonal averages of various heating rates (°C day^{-1}) averaged through the model atmosphere for the July ice age case.

will be discussed. In a later section the latitude-height distributions will be illustrated and described.

(i) Condensation Heating Rate

The maximum condensation heating occurs in the upward branch of the Hadley circulation. In the January control case the maximum occurs at 10°S and is 2.1°C day^{-1}. In the July control case the maximum occurs at 10°N and is $\sim$2.0°C day^{-1}, while in the ice age case the maximum at 10°N is about 1.5°C day^{-1}. Thus the release of latent heat of condensation of water vapor in the tropics is greater in the January ice age case than in the control case and less in July ice age case than in the control case.

The heating rate due to release of latent heat of condensation, Q_c, is given by (Oliger et al., 1970)

$$Q_c = \frac{LM}{\rho} \qquad (6.4)$$

L is the latent heat of condensation of water vapor. M is the rate of condensation of water vapor. Computation of M has been described by Washington and Kasahara (1970). Basically, if the value of q (specific humidity) exceeds that of 95 per cent of q_a (saturation specific humidity) the excess amount of water vapor is available for condensation. There is also a constraint that the motion must be upwards in the supersaturated air. Therefore the condensation heating depends on the specific

humidity and the saturation specific humidity of the air in question and on the condition of upward velocity. Increases or decreases in amounts of condensation heating could thus be attributed to any of several factors, e.g., saturation vapor pressure, horizontal or vertical divergence (or convergence) of water vapor, etc.

In the January cases, although the maximum of condensation heating in the upward branch of the Hadley cell is greater in the ice age case, the condensation heating is less than or equal to that in the control case at all other latitudes. In the northern hemisphere the condensation heating rate in the ice age case is less than that in the control case at all latitudes. In the southern hemisphere, south of 10°N the control case and ice age case condensation heating amounts are similar.

In the July cases the condensation heating is less in the ice age case than in the control case at all latitudes except between about 5°N and 5°S, where the ice age case condensation heating is 0-0.3°C day^{-1} greater in the control case.

Therefore, apart from the area around 10°S in the January cases and around 5°N to 5°S in the July cases, the amount of heating of the troposphere due to the release of latent heat of condensation is less in the ice age cases than in the control cases.

(ii) Vertical Sensible Heating Rate

The other mechanism for transferring heat from the earth, where there is an excess of radiative heating, to the atmosphere, where there is a deficit, is vertical sensible heating. It can be seen in Figures 6.2-6.5 that the amount of heating is not as large as that due to condensation heating, but it is more evenly distributed. At nearly all latitudes, the atmosphere is heated by vertical sensible heating, but in polar latitudes there is cooling. This is because the earth's surface is generally cooler than the overlying air in polar latitudes and so the transfer of sensible heat is from the atmosphere to the earth (see Sellers, 1965, p. 104).

The equations used for calculating Q_{dv}, the vertical diffusion of sensible heat, are described in detail in Washington and Kasahara (1970, equations 18-25) and Oliger et al. (1970, section 2.5).

In the January control case (Figure 6.2) the vertical diffusion of sensible heat is positive everywhere equatorward of about 65°N and 70°S. The distribution is fairly uniform, the heating rate is never more than 0.25°C day^{-1}

In the July control case (Figure 6.3) the vertical diffusion of sensible heat is again positive except in the polar latitudes. And again, the heating is nowhere greater than 0.25°C day^{-1}. Compared with the

vertical sensible heating in the January control case, the heating in the July case is less only between 5°N and 25°N (maximum difference 0.05°C day^{-1}) and poleward of 65°S (maximum difference 0.20°C day^{-1}). In the July control case there are no pronounced maxima in the distribution of vertical sensible heating, although there is still a slight peak at 55°S. Gabites (1950) found a "zone of heat source persisting in the southern hemisphere from October to July, varying from 35°S to 60°S" but does not discuss the origin of this heat source. In the January control case, the heat source is reflected in the curve showing total heating.

The distribution of vertical sensible heating in the January ice age case (Figure 6.4) differs more from that of the January control case in the southern hemisphere than in the northern hemisphere. From 0°S to 70°S the vertical sensible heating is greater in the January ice age case than it is in the control case, although the difference is at most 0.20°C day^{-1} and generally 0.05-0.10°C day^{-1}. According to Sellers (1965), "the sensible heat flux from land surfaces to the atmosphere is greatest when and where the soil is driest and the temperature difference between the surface and air is largest." The soil moisture is fixed at saturation in this version of the GCM, so the temperature difference between the surface and the air must be the cause of the increase in the vertical sensible heating.

Since the changes in surface boundary conditions involved a decrease in ocean surface temperature and inclusion of an ice cap (over South America) in the ice age cases, one would initially think that the surface-air temperature gradient would be reduced, because surface temperature was reduced. However, as discussed by Kraus (1973) and Schneider and Washington (1973) there is an amplification within the GCM of surface temperature changes with height. Kraus has suggested that the tendency to conserve equivalent potential temperature in the real atmosphere leads to approximately a threefold amplification of tropical sea surface temperature changes in the upper troposphere; above colder water this amplification becomes much smaller. Schneider and Washington found, using the GCM, that a decrease of global ocean surface temperature of 2°C gave a resultant decrease in global mean temperature computed at 3 km of 3.6°C.

Table 6.1 shows values of T_g (ground temperature) and T_3 (temperature at 3 km) averaged between 0°S and 85°S. The values represent 30-day means (days 51-80). As discussed above for the study of Schneider and Washington (1973), there is an amplification of surface temperature changes with height in the southern hemisphere. The difference in ground temperature between the two January cases is 6.51°C, the difference in the temperature at 3 km is 7.17°C.

Therefore in the southern hemisphere in the January cases, the gradient of temperature between the surface and atmosphere is increased in the ice age case, so that one would expect the vertical flux of sensible heat to increase.

In the northern hemisphere in the January cases, the vertical diffusion of sensible heat is virtually the same in the control case and ice age case between 0°S and 40°N. Between 40°N and 55°N the ice age case values are greater than the control case values (maximum difference, c. 0.1°C day^{-1}) and between 65°N and 85°N the ice age case values are again greater (maximum difference 0.2°C day^{-1}).

The vertical diffusion of sensible heat in the July ice age case in the southern hemisphere is virtually the same as that in the July control case between 0°S and 30°S. Between 30°S and 65°S the vertical sensible heating in the July ice age case is greater than that in the control case (maximum difference almost 0.30°C day^{-1}). As was shown above for the January cases, the amplification of surface temperature changes with height corresponds to the changes in vertical sensible heating.

Table 6.2 shows averages of surface temperatures and of temperatures at 3 km, the averages have been taken (a) over the whole southern hemisphere, (b) over

TABLE 6.1

GROUND TEMPERATURES (T_g) AND TEMPERATURES AT 3 km (T_3) AVERAGED FOR THE SOUTHERN HEMISPHERE (0°-85°S) USING 30-DAY MEAN VALUES FOR THE JANUARY CONTROL CASE AND ICE AGE CASE

	January Control	January Ice Age	Difference
T_g(°C)	7.38	0.87	-6.51
T_3(°C)	2.97	-4.20	-7.17

TABLE 6.2

GROUND TEMPERATURES (T_g) AND TEMPERATURES AT 3 km (T_3) AVERAGED FOR THE SOUTHERN HEMISPHERE AND BELTS OF THE SOUTHERN HEMISPHERE USING 30-DAY MEAN VALUES FOR THE JULY CONTROL CASE AND ICE AGE CASE

	July Control	July Ice Age	Difference
0-85°S			
T_g(°C)	0.5	-4.3	-4.8
T_3(°C)	-2.2	-7.3	-5.1
0-30°S			
T_g(°C)	21.9	15.6	-6.3
T_3(°C)	15.2	10.1	-5.1
30-65°S			
T_g(°C)	4.5	1.1	-3.4
T_3(°C)	-0.7	-6.3	-5.6

the latitude belt 0-30°S and (c) over the latitude belt 30-65°S. Over the southern hemisphere as a whole and over the latitude belt 30-65°S, the decrease of surface temperature is amplified with height in the atmosphere. The change in surface temperature of the belt 30-65°S from the control case to the ice age case is -3.4°C, while the change in temperature at 3 km in the same belt is -5.6°C. In this same belt the vertical sensible heating is greater in the ice age case than in the control case. In the latitude belt 0-30°S, however, the change in surface temperature between the control case and the ice age case is -6.3°C and the change in temperature at 3 km is -5.1°C. There is no amplification with height of the temperature decrease in this latitude belt and likewise there is no increase in vertical sensible heating in the July ice age case in this belt.

In the northern hemisphere the vertical diffusion of sensible heat is greater in the July ice age case than in the control case between 0° and 40°N but the difference is 0.1°C day^{-1} at most. Between 40°N and 70°N, the ice age vertical sensible heating is less than that in the control case, again with a maximum difference of 0.10°C day^{-1}. Poleward of 70°N the ice age case vertical sensible heating is again greater (maximum difference, 0.15°C day^{-1}).

Therefore the distribution of vertical diffusion of sensible heat is different in the control cases and ice age cases. The four simulations have produced realistic distributions, since the only areas which experience negative (downward) vertical diffusion of sensible heat, are the polar areas. The differences between the control cases and the ice age cases can be explained in terms of the changes in gradient of temperature between the ground and atmosphere. This explanation has been illustrated for the southern hemisphere for both January and July cases.

(iii) Sensible Heating Due to Horizontal Diffusion

It is well known that there is a net radiative energy surplus in the tropics and subtropics (equatorward of 37°, see for example Palmén and Newton, 1969) and a net deficit of radiative energy in middle and high latitudes. Since neither the tropics are warming up nor the poles cooling down, it follows that there must be a poleward transport of energy. (As Lorenz, 1967, points out, the net heating cannot be regarded as the cause of the transport. If the atmospheric and oceanic circulations could not carry as much energy then the poles would get colder and the tropics would get warmer.) The required poleward energy transfer has been discussed by many studies, e.g., Sellers (1965), Lorenz (1967), Newell et al. (1970). In a later section the poleward transfer

of heat by eddies and the mean circulation will be discussed. In this section the horizontal diffusion of sensible heat (by sub-grid scale processes), $\overline{Q_{dh}}$, will be examined.

$\overline{Q_{dh}}$, the horizontal diffusion of sensible heat is calculated using the following equation:

$$\rho\, Q_{dh} = \frac{c_p}{a^2 \cos\phi}\left[\frac{1}{\cos\phi}\frac{\partial}{\partial\lambda}\left(\rho\, K_{TH}\frac{\partial\theta}{\partial\lambda}\right) + \frac{\partial}{\partial\phi}\left(\rho\, K_{TH}\cos\phi\,\frac{\partial\theta}{\partial\phi}\right)\right] \qquad (6.5)$$

(Oliger et al., 1970, p. 16).

K_{TH} is the horizontal diffusivity of sensible heat, other terms are defined in the Appendix. The first term on the right hand side represents an east-west diffusion of sensible heat; the second term represents a north-south diffusion of heat. The zonal averages of $\overline{Q_{dh}}/c_p$ are plotted in Figures 6.2-6.5. The first term on the right hand side of equation 6.5 becomes equal to zero when the zonal average of Q_{dh} is taken. Therefore $\overline{Q_{dh}}/c_p$ represents sensible heating due to meridional diffusion.

In the January control case, the meridional diffusion of sensible heat is negative (cooling) between 30°N and 35°S (there is a slight area of warming between 5°S and 10°S but this only amounts to about 0.02°C day^{-1}). Poleward of 30°N and 35°S the meridional diffusion of

sensible heat is positive. At 45°N the diffusion of sensible heat amounts to almost +0.3°C day^{-1} and at 50°S it amounts to +0.15°C day^{-1}. Near the poles the value of $\overline{Q_{dh}}/c_p$ suddenly increases, the large value of 0.40°C day^{-1} at 85°N is an example of this. The sudden change near the poles is probably not realistic and is believed to be due to the evaluation of $\partial\theta/\partial\phi$ near the poles.

In the July control case (Figure 6.3) the meridional diffusion of sensible heat is negative (cooling) between 15°N and 45°N and between 0° and 30°S. Between 0° and 15°N there is a small amount of heating (maximum, 0.10°C day^{-1}). Again there is an unrealistic peak at 85°N and 85°S in the value of $\overline{Q_{dh}}$.

In both January and July control cases, the contribution of horizontal diffusion of sensible heat to the total heating rate is very small, however its effects are noticeable in the middle latitudes where the positive values of $\overline{Q_{dh}}/c_p$, amounting to 0.25°C day^{-1} in places are reflected in the distribution of total heating.

The horizontal diffusion of sensible heat in the January ice age case is similar to that in the control case in the southern hemisphere and between 0° and 30°N. Between 30°N and 55°N the ice age curve deviates noticeably from that of the control case. At 45-50°N there is cooling due to horizontal diffusion of sensible heat in the January ice age case. At 45°N the difference between

the ice age case and control case values is 0.30°C day^{-1}. Between 55°N and 80°N the ice age case values are larger than those in the control case, with a maximum difference of 0.25°C day^{-1}. Therefore, in the middle and high latitudes of the northern hemisphere the meridional diffusion of sensible heat in the January ice age case is quite different from that in the control case, this must be due to the meridional temperature gradient ($\partial\theta/\partial\phi$).

The July ice age case horizontal diffusion of sensible heat has a distribution quite different from that in the July control case. Between about 30°N and 10°S, the values of $\overline{Q_{dh}}/c_p$ are lower in the ice age case and they are negative. Between 30°N and 80°N and between 10°S and 35°S, the horizontal diffusion of sensible heat is greater in the ice age case than in the control case. Polewards of 80°N and 35°S the ice age case values of $\overline{Q_{dh}}/c_p$ are again lower. Therefore in the tropics the horizontal diffusion of sensible heat is generally less in the ice age case than in the control case. In the middle latitudes, the control case values are lower. At 10°N the difference between values of $\overline{Q_{dh}}/c_p$ for the two cases is 0.2°C day^{-1} and apart from in the near polar areas the differences in the values of $\overline{Q_{dh}}/c_p$ did not exceed that figure.

The introduction of ice age boundary conditions into the GCM has caused noticeable (and some probably

significant) changes in the values of $\overline{Q_{dh}}/c_p$, the horizontal diffusion of sensible heat. However, as Kasahara and Washington (1971, p. 684) point out, the contribution of this heating rate to the total net heating rate is relatively small. The changes in the distribution and magnitude of $\overline{Q_{dh}}/c_p$ have not been large enough to produce significant changes in the total heating rate.

(iv) Absorption of Solar Radiation by Water Vapor and Net Long Wave Radiation Lost by the Troposphere

The distributions of the zonal averages of solar heating and long wave cooling in the four simulations have been discussed earlier in the chapter. In Figures 6.2-6.5 $\overline{Q_{as}}/c_p$ and $\overline{Q_{al}}/c_p$ are plotted in units of °C day^{-1}. In this section, the contributions of these two terms to the total heating will be discussed.

As has been noted before, the net long wave cooling of the troposphere is everywhere greater than the heating due to absorption of solar radiation in the troposphere. In the GCM, Q_{as} includes only the absorption of insolation by water vapor. Kasahara and Washington (1971, p. 683) state that since absorption of solar radiation by dust, cloud, ozone and other minor atmospheric constituents has not been considered in $\overline{Q_{as}}/c_p$, the actual value of insolation absorbed in the troposphere should be higher than $\overline{Q_{as}}/c_p$ by 60-70 per cent. Kasahara and Washington believe that this

uncertainty is small compared with the condensation heat flux $\overline{Q_c}/c_p$. (For example, in the January control case, the maximum value of $\overline{Q_{as}}/c_p$ is 0.40°C day^{-1}. A 70 per cent increase of this value would make it 0.68°C day^{-1}, while the value of $\overline{Q_c}/c_p$ at the same point is 0.95°C day^{-1} and the maximum value of $\overline{Q_c}/c_p$ is about 2.1°C day^{-1} in this simulation.)

In Figures 6.2-6.5 it can be seen that $\overline{Q_{al}}/c_p$ is by far the largest contribution to cooling. $\overline{Q_{as}}/c_p$ is smaller than $\overline{Q_c}/c_p$ but is often larger than the other contributors to the total heating. The contribution of $\overline{Q_{al}}/c_p$ is most noticeable in middle and high latitudes where it gives a cooling which is greater than the contributions of the heating terms.

(v) Total Heating

In the January control case, the maximum net heating of the troposphere occurs at 10°S, a direct reflection of the maximum of condensation heating at the same latitude. Between 5°N and 25°S there is net heating of the troposphere. There are minima of heating (net cooling) between 5°N and 35°N and between 25°S and 35°S. The minimum in the northern hemisphere amounts to -0.50°C day^{-1} at 25°N. At 35°N and 35°S there are slightly positive heating rates but polewards of 40°N and 40°S the total heating becomes negative and drops to a minimum

near the poles. The maximum net heating is about 1.25°C day^{-1} in the January control case. The secondary maxima in the middle latitudes are not greater than 0.05°C day^{-1} and result from an increase in the amount of vertical sensible heating in these latitudes.

In the July control case the maximum net heating of 1.25°C day^{-1} occurs at 10°N, again a reflection of the maximum condensation heating associated with the upward branch of the Hadley cell. Owing primarily to the large condensation heating rate, the net heating in the northern hemisphere is largely positive, with cooling only occurring poleward of 70°N. In the southern hemisphere there is net cooling between 0° and 35°S, which is a result mainly of the cooling in these latitudes due to the horizontal diffusion of sensible heat. Between 35°S and 55°S there is net heating, with a maximum of about 0.10°C day^{-1}, resulting from a maximum in the horizontal diffusion of heat and also a slight increase in these latitudes of the amount of condensation heating. Poleward of 55°S there is net cooling which reaches a minimum of nearly 0.6°C day^{-1}.

In the January ice age case, the maximum of net heating in the tropics is about 0.3°C day^{-1} greater than that in the control case. This is basically because the condensation heating in the upward branch of the Hadley cell (10°S) is greater in the January ice age case than it is in the control case.

In all of the northern hemisphere, except between 60°N and 75°N the total heating in the January ice age case is about 0.2°C day^{-1} less than that in the control case, although the curves follow the same pattern. In the southern hemisphere the net heating is greater or equal in the ice age case from 0°S to 60°S. Between 60°S and 70°S the control case net heating is about 0.15°C day^{-1} greater than that in the ice age case and poleward of 70°S the ice age case net heating is again the stronger.

Therefore the January ice age case has lower net heating than the control case in the northern hemisphere and slightly higher net heating in the southern hemisphere.

In the July ice age case the net heating in the upward branch of the Hadley cell is much less than that in the control case (difference between the two cases at 10°N is approximately 0.5°C day^{-1}, i.e., 40 per cent of the control case value). Poleward of 5°N the total heating in the ice age case is much less than that in the control case everywhere except near 75-80°N. At 25°N the difference between the net heating in the two cases is about 0.75°C day^{-1}, with net heating in the control case and net cooling in the ice age case. The main reason for the dramatic reduction of net heating in the ice age case is the similar decrease of condensation heating.

Between 5°N and 35°S the net total heating in the ice age case is greater than that in the control case by about 0.2°C day^{-1}. Beyond 35°S the net total heating rates are similar with the ice age case values ±0.15°C day^{-1} of the control case values, except for a slight peak in the ice age case curve at 55°S (value ∿ 0.15°C day^{-1}).

As far as total heating (or cooling) of the troposphere is concerned, the northern hemisphere amounts show the most difference between the ice age cases and the control cases. In both the January and July cases there is a reduction of total heating in the ice age case northern hemisphere. The southern hemisphere total heating is not so consistently different between the ice age cases and control cases. In the tropics, because of the changes in condensation heating, the total heating in the upward branch of the Hadley circulation is greater in the January ice age case than in the control case and less in the July ice age case than in the control case. The implications of such changes with reference to the Kraus hypothesis are discussed in Chapter III.

(f) Latitude-Height Distributions of 30-Day Means of Zonally Averaged Heating Rates for Four Simulations

The zonal average distributions of various heating rates averaged through the atmosphere were discussed in

section (v) and the differences between the ice age cases and control cases were pointed out. In this section we will briefly discuss the latitude-height plots of $\overline{Q}$, $\overline{Q_{as}}$, $\overline{Q_{al}}$, $\overline{Q_c}$, so that the levels of the zones of heating and cooling may be examined. The latitude-height plots are shown in Figures 6.6-6.9. $\overline{Q_{dh}}$ and $\overline{Q_{dv}}$, the horizontal and vertical diffusion of heat, are not illustrated in this section. Kasahara and Washington (1971) point out that the contributions of $\overline{Q_{dh}}$ and $\overline{Q_{dv}}$ to the net heating rate are small; the vertical sensible heating is concentrated only near the surface and is negligible in the free atmosphere. Sensible heat is redistributed in the vertical by convective adjustment (see for example Washington and Kasahara, 1970). The horizontal diffusion of sensible heat gives either heating or cooling in the mid-troposphere, but its magnitude is too small to be the major heat source.

(i) Condensation Heating Rate

In Figure 6.6a, it is clear that the maximum condensation heating rate occurs in the upward branch of the Hadley circulation, located at about 10°S in the January control case. The amount of condensation heating in the January ice age case is roughly the same in the upward branch of the Hadley cell but the vertical extent and horizontal extent of the condensation heating are

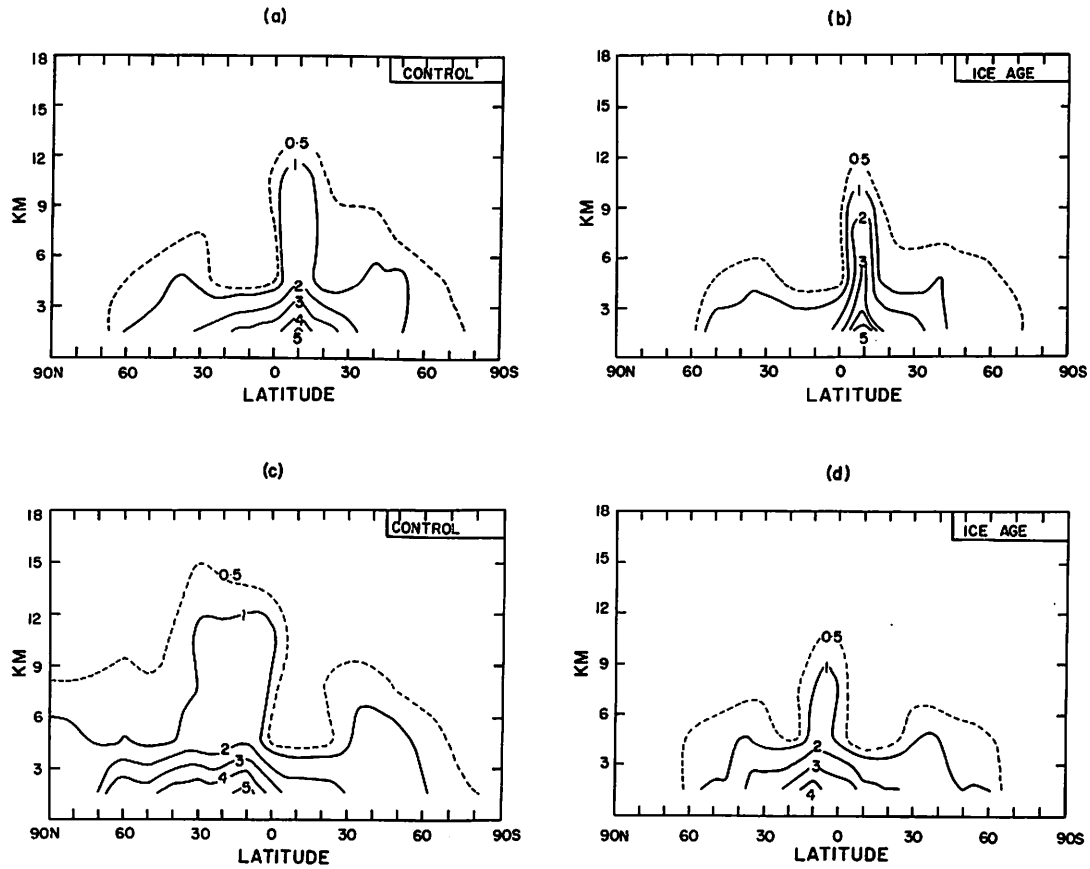

Figure 6.6. Latitude-height distributions of 30-day means of zonally averaged condensation heating rate (Q_c) for (a) January control case, (b) January ice age case, (d) July ice age case. Units: °C day^{-1}.

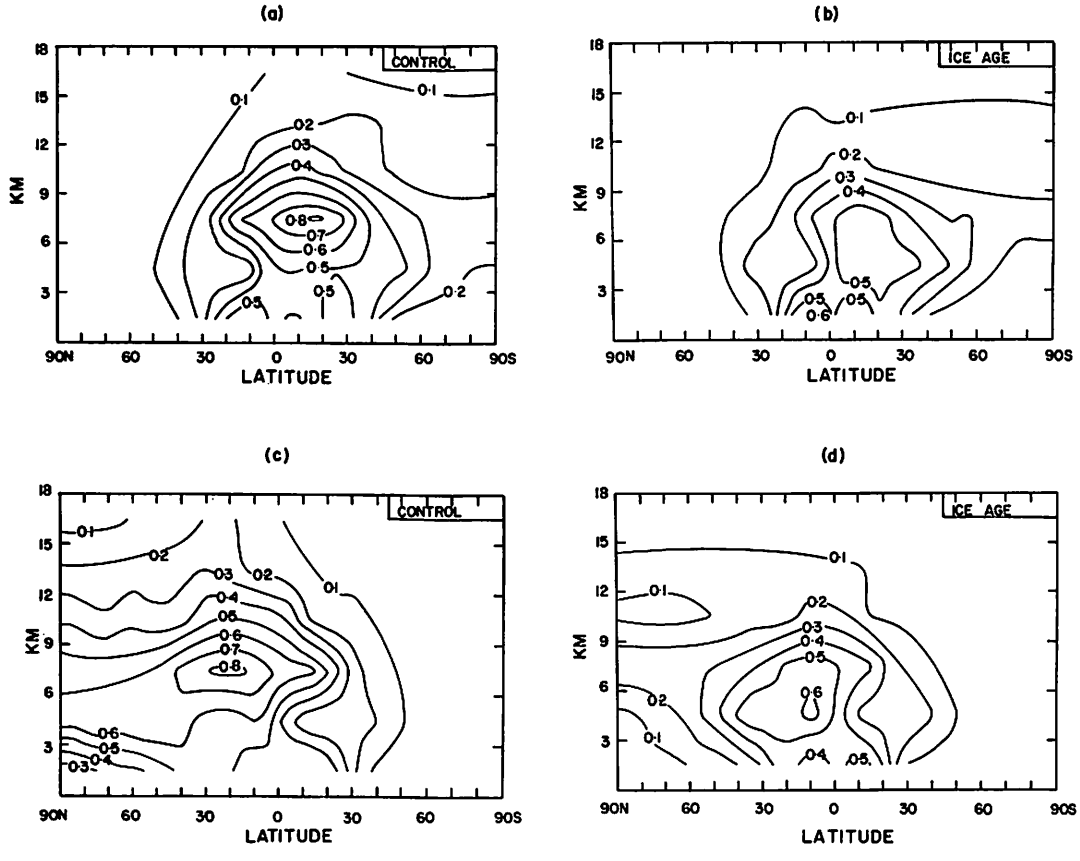

Figure 6.7. Latitude-height distributions of 30-day means of zonally averaged heating rate due to absorption of solar radiation in the troposphere by water vapor (Q_{as}) for (a) January control case, (b) January ice age case, (c) July control case, (d) July ice age case. Units: °C day^{-1}.

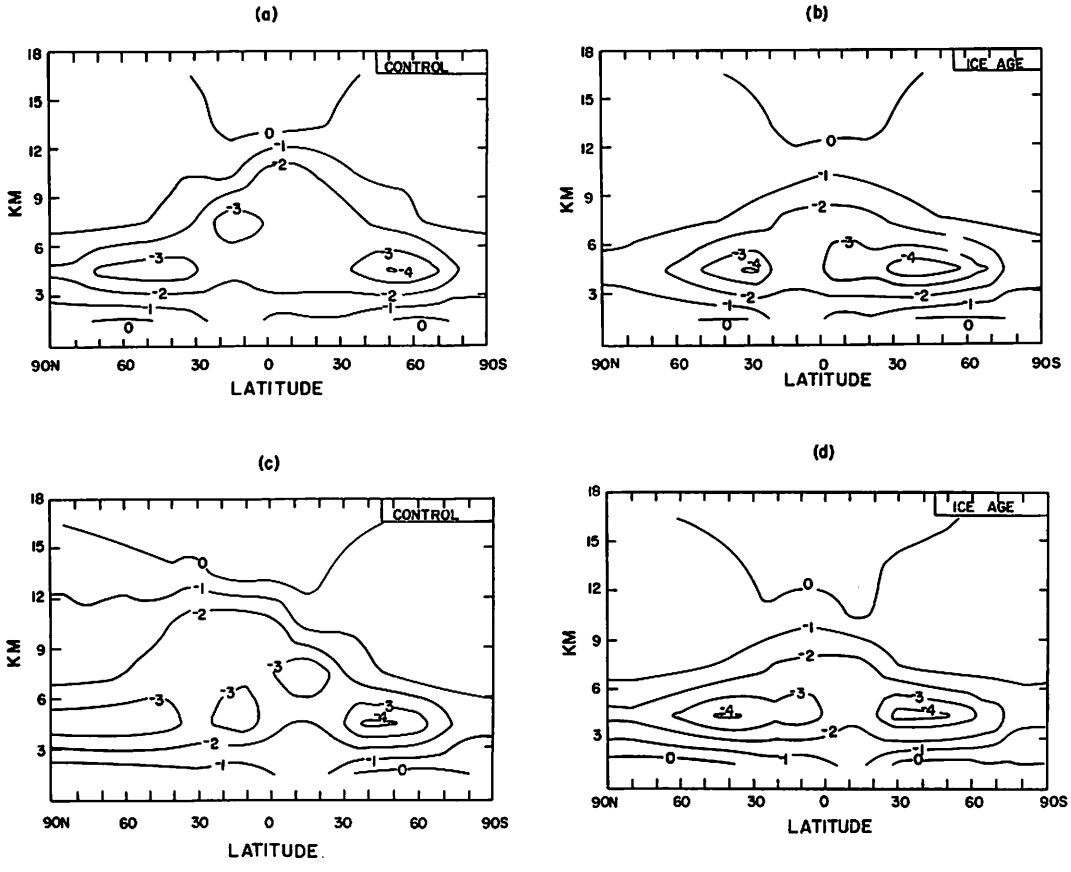

Figure 6.8. Latitude-height distribution of 30-day means of zonally averaged heating rate due to infrared radiation lost by the troposphere (Q_{al}) for (a) January control case, (b) January ice age case, (c) July control case, (d) July ice age case. Units: °C day^{-1}.

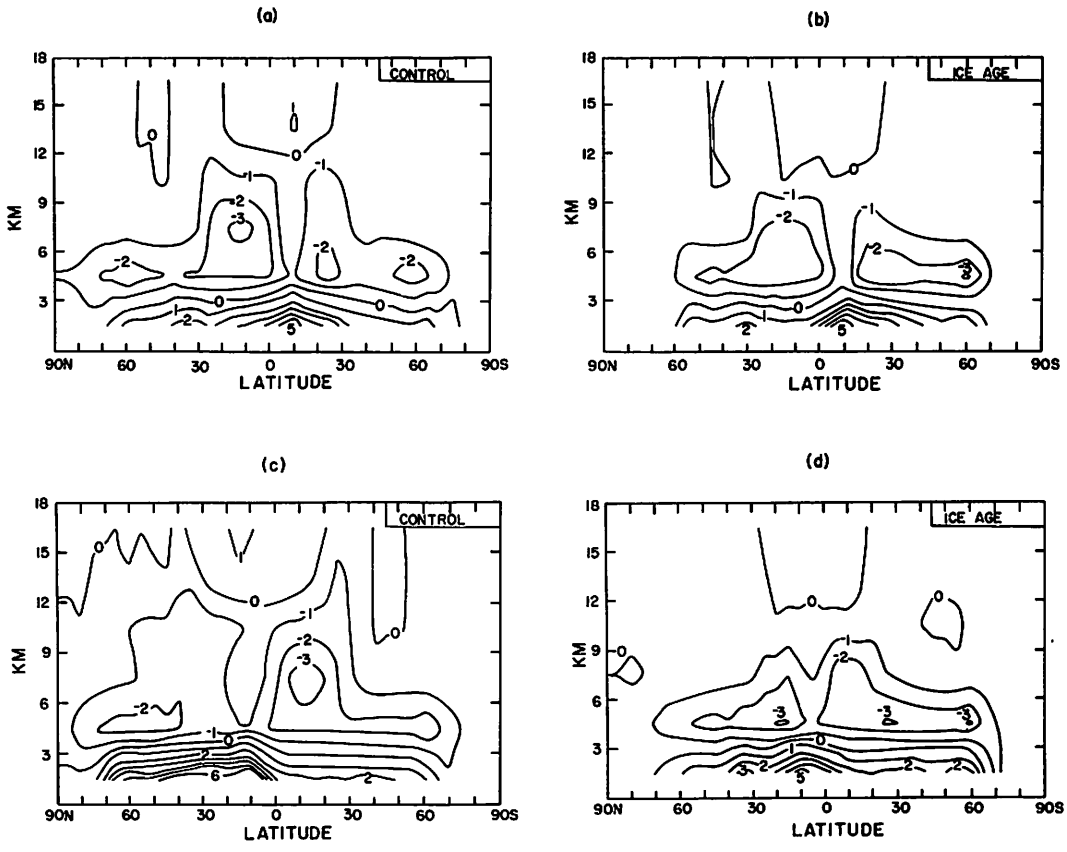

Figure 6.9. Latitude-height distribution of 30-day means zonally averaged total heating rate (Q) for (a) January control case, (b) January ice age case, (c) July control case, (d) July ice age case. Units: $^{\circ}C\ day^{-1}$.

reduced in the ice age case (Figure 6.6b). The heating at 10°S extends to 13.5 km in the January control case and only to about 12 km in the ice age case. In the control case, the condensation heating at 1.5 km extends from about 65°N to 75°S; in the ice age case it extends from 60°N to 70°S. The heating in the tropics is more restricted in the ice age case than in the control case.

In the July control case, the maximum heating again occurs in the upward branch of the Hadley cell, but the horizontal and vertical extent of the condensation heating is greater than in the January case. In the July ice age case (Figure 6.6d) the maximum condensation heating is 4°C day^{-1}, compared with 5°C day^{-1} in the control case. As in the January cases, the July ice age case vertical and horizontal extent of condensation heating is reduced from that in the control case. The reduction is especially noticeable in the northern hemisphere, where one can expect that the cooling induced by the ice sheets and lower ocean temperatures caused a decrease (or complete elimination) of condensation heating.

In considering the four parts of Figure 6.6, it is clear that the inclusion of ice age boundary conditions in the NCAR GCM influences the amount and distribution of condensation heating most in the July cases. The extent is reduced in both January and July cases while the amount is reduced in the July ice age case.

(ii) Heating Rate Due to the Absorption of Solar Radiation in the Troposphere by Water Vapor

The solar heating rates in Figure 6.7 for the two control cases have been compared with the recent computations based on observed data by Dopplick (1970). Dopplick shows latitude-height plots of zonal averages of solar heating for December-February and for June-August. However, the data of Dopplick includes absorption of solar radiation by carbon dioxide and ozone, so the plots are necessarily slightly different from those computed.

In the January control case the maximum heating occurs again in the vicinity of the upward branch of the Hadley circulation; this is reasonable in view of the concentration of water vapor in this area. The maximum heating according to Dopplick's data is latitudinally more extensive, but in the vicinity of 10°S and at between 6 and 9 km, the observed solar heating is 1°C day^{-1} for December-February and in the January control cast heating (due to absorption of solar radiation by water vapor only) is 0.8°C day^{-1}. The agreement is very good in view of the difference in time period and in absorbing gases and lack of cloud droplet absorption.

The July control case solar heating compares favorably with Dopplick's data; again, if the differences outlined above are taken into account the plots

are similar quantitatively and the distributions are also very similar. There is no absorption in the polar areas of the northern hemisphere in the January cases and the southern hemisphere in the July cases because of the polar night.

In the January ice age case, the maximum absorption of solar radiation by water vapor, although still in the vicinity of the upward branch of the Hadley cell, occurs at a lower elevation (about 3 km lower than in the control case) and is not as great (solar heating has a maximum of 0.8°C day^{-1} in January control case and 0.5°C day^{-1} in the ice age case). This reduction in elevation and amount must be due to the decrease of water vapor in the atmosphere in the ice age case. The plots of Figures 6.7a and 6.7b show roughly the same distribution of heating, the main difference between them is that the ice age case solar heating is lower.

In the July ice age case the maximum heating, in the vicinity of the upward branch of the Hadley circulation, is 0.6°C day^{-1}, while that in the control case is 0.8°C day^{-1}. The maximum is about 3 km lower in the ice age case. These differences must again be attributable to the reduction in the amount of water vapor in the ice age case. The vertical distribution of solar heating is also reduced in the ice age cases.

(iii) Net Long Wave Radiation Lost by the Troposphere

The latitude-height plots of $\overline{Q_{al}}/c_p$ have been compared with the computed/observed data of Dopplick for the net thermal heating/cooling for December-February and June-August. In the January control case, the amount of cooling is greater than that observed (maximum in control case is 3-4°C day^{-1}; maximum in Dopplick's data is 1-2.5°C day^{-1}). The maximum cooling also occurs 3-4 km lower in the control case than in the observed data. Kasahara and Washington (1971) found that the maximum cooling in the middle latitudes appeared at 4.5 km in model, whereas London (1957) showed the maximum between 2-3 km. They explain that the discrepancy is due to the low level cloudiness in the model being at 3 km--since the maximum long wave cooling occurs in the next layer above the clouds, the maximum cooling in the model will always be at 4.5 km.

Apart from discrepancies in the amount and level of maximum cooling, the distribution of net long wave radiation lost by the troposphere is reasonably comparable in the control cases and observed data.

The January ice age case distribution of $\overline{Q_{al}}/c_p$ is different from that of the January control case especially in the mid-troposphere. In the control case there is a maximum of cooling at about 8 km between 10°N and 20°N of 3°C day^{-1}. In the ice age case this maximum

occurs at 4.5 km between 10°S and 20°S with a value of 3°C day^{-1}. This change must be related to a change in the distribution of low clouds and/or a change in the atmospheric temperature in the low latitude mid-troposphere. The mid-latitude maxima at 4.5 km are about 0.5°C day^{-1} greater (more cooling) in the ice age case than in the control case.

In the July cases the main differences between the two occur in the mid-troposphere in middle and low latitudes. In the northern hemisphere the maximum cooling at 4.5 km occurs around 40°N in the ice age case and between 80°N and 50°N in the control case. The ice age case cooling is also about 1°C day^{-1} greater in the northern hemisphere. In the southern hemsiphere, the mid-latitude maximum cooling at 4.5 km is in roughly the same location is that in the control case, but the ice age cooling is stronger (about 1°C day^{-1}). The cooling of 3°C day^{-1} at about 7.5 km in the July control case is not seen in the ice age case.

In all four cases there is net heating in the upper troposphere in the tropics, this is due to the cold temperatures associated with the tropical tropopause (Dopplick, 1970, p. 45).

(iv) Total Net Heating of the Troposphere

The latitude-height plots of Q in Figure 6.9 show the total of $\overline{Q_{as}}$, $\overline{Q_{al}}$, $\overline{Q_{dv}}$, $\overline{Q_{dh}}$, $\overline{Q_c}$ in heating or cooling

the troposphere. In the lower troposphere the net heating is positive, a reflection of the heating due to the absorption of solar radiation, the horizontal and vertical diffusion of heat. In the mid-troposphere, centered at 4.5 km, there is net cooling due primarily to the radiation terms $\overline{Q_{al}}$ and $\overline{Q_{as}}$.

In the January cases (Figures 6.9 a and b, the distribution of net heating/cooling is less extensive latitudinally in the ice age case. The values are similar in the two cases at lower elevations. In the middle troposphere the differences in net long wave cooling between the two cases are reflected.

In the July cases, the distribution of heating/cooling maxima and minima is restricted in vertical and horizontal extent in the ice age case as compared with the control case. The same general comments apply as were made above for the January cases.

(g) Meridional Transport of Sensible Heat by Eddies

There are two major mechanisms for the poleward transport of heat in the atmosphere: transfer by large-scale eddies and by the mean meridional circulation. Oort and Rasmusson (1970, 1971) have compared the magnitudes of the energy fluxes by these two mechanisms. The data from Oort and Rasmusson (1971) have been used in this study for comparison with the computed data. Other studies which produced plots of the poleward transport

heat include Holopainen (1965), Lorenz (1967), Newell et al. (1970), Kidson et al. (1969) and Peixoto (1960). These studies have been referred to in the present study.

Washington and Kasahara (1970) found that the values of $\overline{V'T'}$, the poleward sensible heat transport by the eddies, computed by the two-layer version of the NCAR GCM were smaller than observed.

In this study the poleward transport of heat by the eddies has been examined at two levels, (a) 3 km, which is roughly 700 mb and (b) 12 km, which is roughly 200 mb. Oort and Rasmusson found that for transient eddies, there were two maxima of poleward heat transfer, one at about 850 mb and the other at 200 mb, near the tropopause. Both maxima are located in the latitude belt from 40°N to 60°N.

(i) January - 3 km

The poleward transport of heat by eddies at 3 km ($\sim$ 700 mb) in January is shown in Figure 6.10 for the two January simulations and observed data. The latter, from Oort and Rasmusson, extends only from 70°N to 10°S. Within these latitudes the observed and control case values are quite similar. The peak transport occurs at 50°N, where the transport is about 23 m sec^{-1} °C in the control case data and 26 m sec^{-1} °C in the observed data. In the southern hemisphere the peak transport is only about 9 m sec^{-1} °C in the control case. However one

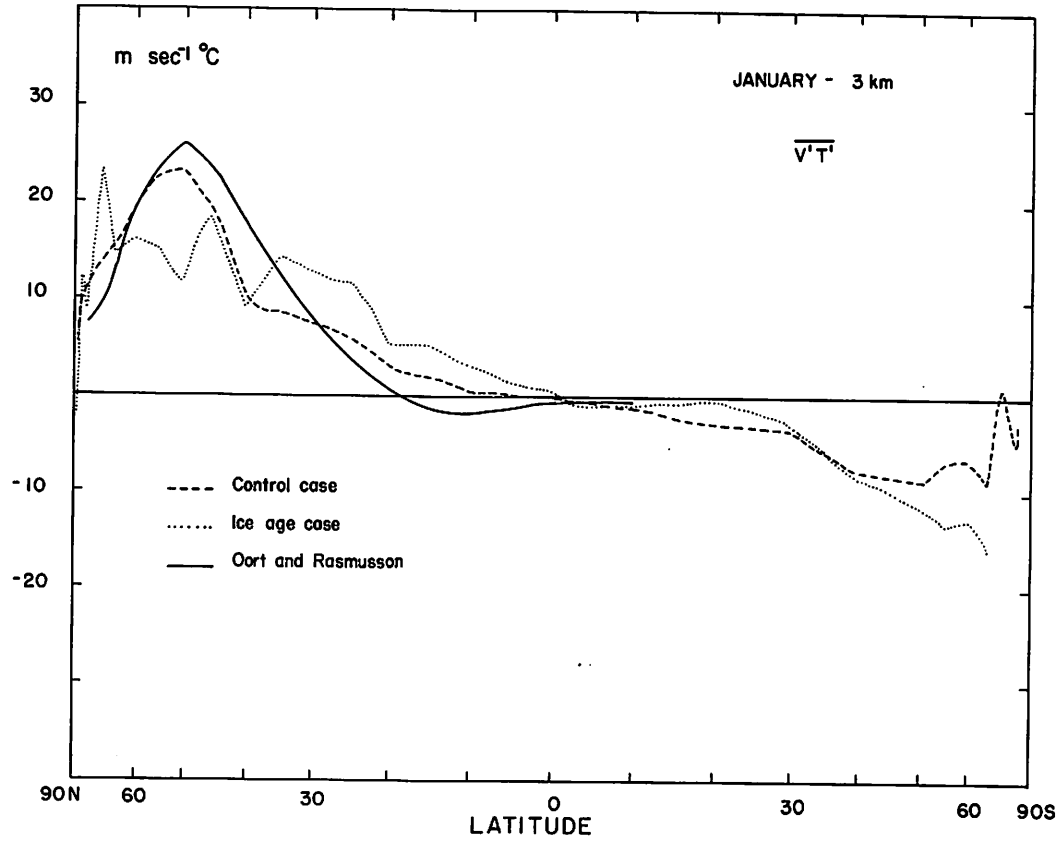

Figure 6.10. Latitudinal distributions of zonal averages of the northward transport of heat by eddies ($\overline{V'T'}$) in the January cases at 3 km. The observed data are taken from Oort and Rasmusson (1971).

would expect it to be weaker here since this is the southern hemisphere summer when the meridional temperature gradient is weaker.

The ice age case values of $\overline{V'T'}$ are quite different from those of the control case. Between 0°N and 40°N the poleward transport of heat by the eddies is greater in the ice age case than in the control case. Between 0°S and 35°S the transport is less than in the control case. Poleward of 35°S the eddy transport of heat is greater in the control case (suggesting that the two hemispheres are more similar in the January ice age case than they are in the January control case). Beyond 70°S, the curves have not been compared since the control case and ice age case values show large amplitude fluctuations which are obviously unrealistic. Between 40°N and 80°N the ice age case values of eddy transport of heat also oscillate. In general the values in this latitude belt are less than the control case values. Therefore the ice age boundary conditions have caused a reduction in the eddy transport of heat in the middle and high latitudes of the northern hemisphere and the transport is very variable in these latitudes.

(ii) January - 12 km

At 12 km, Figure 6.11, the observed and computed data are not alike as they are at 3 km. The peak in the northern hemisphere energy transport of 19.5 m sec^{-1} °C

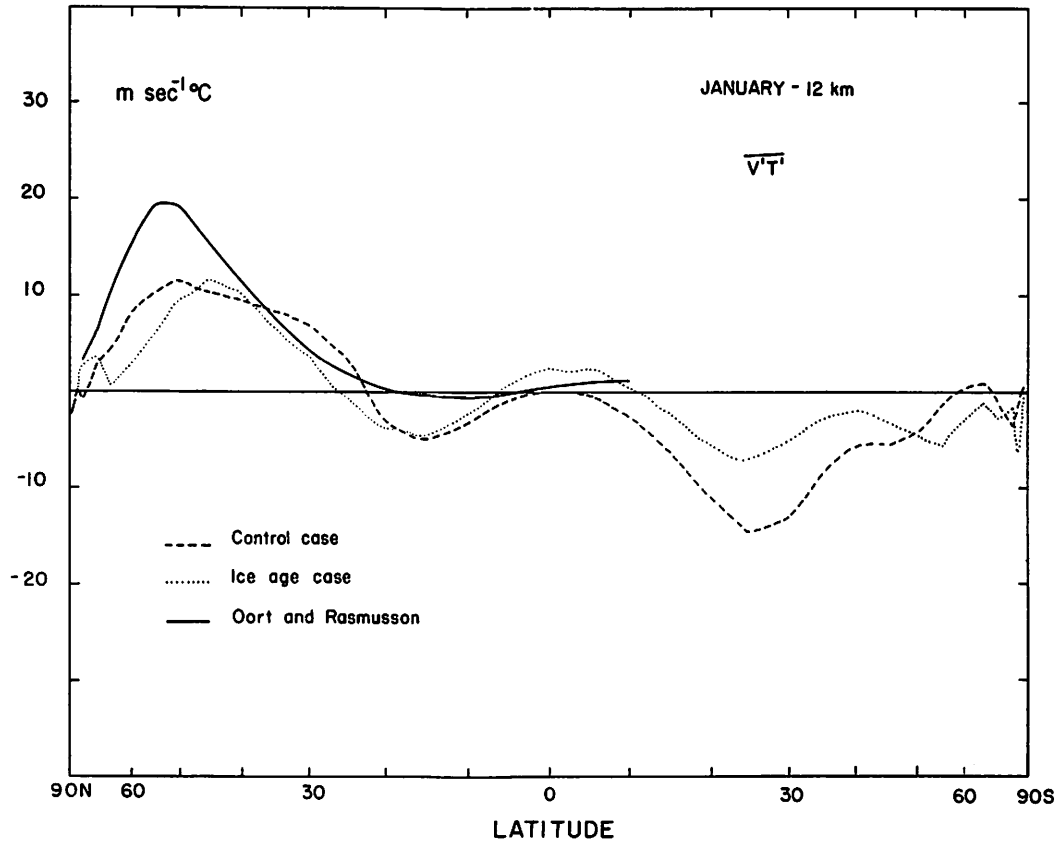

Figure 6.11. Latitudinal distribution of zonal averages of the northward transport of heat by eddies ($\overline{V'T'}$) in the January cases at 12 km. The observed data are taken from Oort and Rasmusson (1971).

in the observed data is at 50-55°N. The peak in the computed data which amounts to 11.5 m sec^{-1} °C occurs at 50°N. Between 0° and 20°N the GCM indicates more equatorward energy transport than the observed data.

In the northern hemisphere, the ice age case transports are not greatly different from those in the control case. The peak transport has about the same value but is shifted 5 degrees equatorward. In the southern hemisphere the poleward eddy transfer of heat is much less in the ice age case than in the control case between about 10°S and 50°S. Poleward of 50°S the ice age case transport is slightly greater than that in the control case at all but one latitude (75°S).

(iii) July - 3 km

In the July cases, Figure 6.12, the control case data for the northern hemisphere overestimate the observed data in the middle and high latitudes. Between 10°N and 40°N the control case curve has two maxima and a minimum which do not appear in the observed data. Between 10°N and 10°S the transport is extremely small and the observed, control case and ice age case data are all very close.

In the July ice age case the poleward energy transport is reduced considerably in the southern hemisphere. The peak transport in the control case is at 60°S and has a value of 20 m sec^{-1} °C. The peak transport

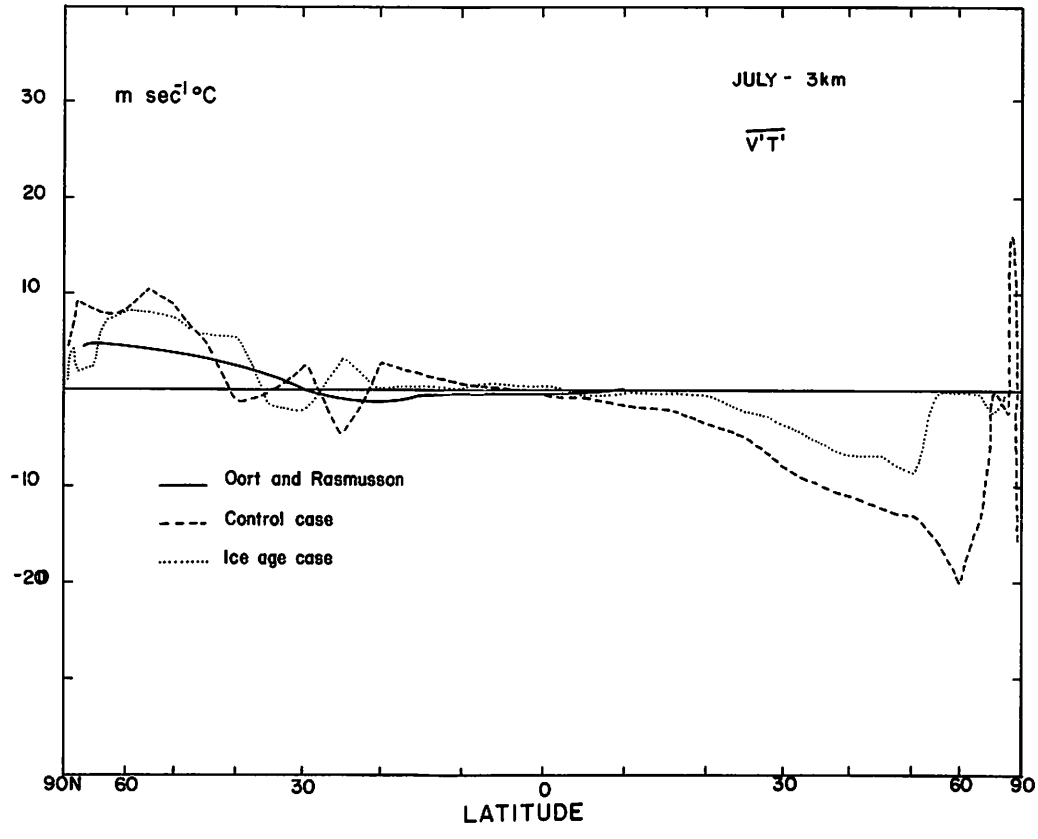

Figure 6.12. Latitudinal distribution of zonal averages of the northward transport of heat by eddies ($\overline{V'T'}$) in the July cases at 3 km. The observed data are taken from Oort and Rasmusson (1971).

in the ice age case is at 50°S and amounts to 8.5 m sec^{-1} °C, which is less than half of the control case value.

In the northern hemisphere, between 20°N and 35°N there is a small minimum and small maximum in the poleward transport of energy by eddies in the ice age case. These peaks are virtually equal and opposite to peaks in the control case data. The maximum poleward transport of energy is about 2 m sec^{-1} °C less in the ice age case than it is in the control case, which is possibly insignificant in view of the 6 m sec^{-1} °C difference between the control case and observed data at this point.

(iv) July - 12 km

The control case data and observed data differ in the northern hemisphere, Figure 6.13, with the computed values about twice as large as those observed in middle and high latitudes. At 10°N the observed and computed values are close and between 10°S and 10°N the observed values are about 2 m sec^{-1} °C greater than those computed.

Between 35°N and 85°N and between 5°S and 80°S the July ice age case poleward transport of sensible heat by eddies is clearly less than that in the control case. At 55°N, where the maximum transport occurs at this level in the July control case, the control case transport is 19.5 m sec^{-1} °C and the ice age case transport is only 9 m sec^{-1} °C. The ice age case values are

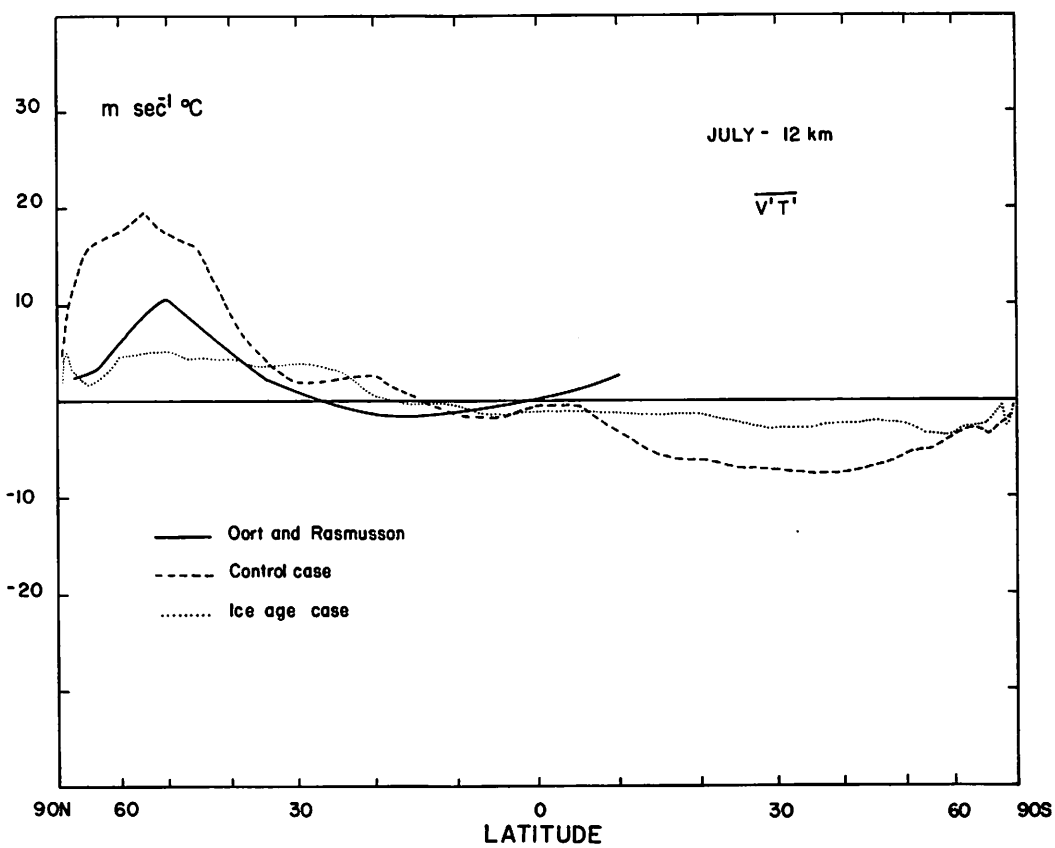

Figure 6.13. Latitudinal distributions of zonal averages of the northward transport of heat by eddies ($\overline{V'T'}$) in the July cases at 12 km. The observed data are taken from Oort and Rasmusson (1971).

greater than those of the control case between 25°N and 35°N (maximum difference 2 m sec^{-1} °C) and between 5°N and 15°N (maximum difference 1 m sec^{-1} °C).

Overall, the January control case underestimates the observed eddy transport of heat and the July control case overestimates the transport. It must be pointed out that we have not distinguished between standing and transient waves so we cannot say how the transports are taking place. The ice age case transports differ considerably from those in the control cases. In the July cases at 3 km and at 12 km, the ice age case transport maxima in both hemispheres are less than the maxima in the control case. In the January cases, the ice age case peak transport is only greater than that in the control case at 3 km in the southern hemisphere. In tropical and subtropical latitudes in both January and July cases at 3 km and 12 km the ice age case eddy transport of heat is often greater than the control case transport. However, the transport in these latitudes is usually not large, especially between 15°N and 15°S, so the differences in transport are possibly not significant.

(h) Summary and Conclusions

In this section we will review the differences found in the atmospheric heat balance between the control cases and the ice age cases. The atmospheric heat

balance, as described in the introduction, is determined by the difference between incoming solar radiation and outgoing long wave radiation, heat exchange between the earth and the atmosphere and transport of energy by eddies and the mean circulation.

For both January and July, the solar radiation absorbed in the troposphere by water vapor is less in the ice age cases than that found in the control cases, the largest reduction occurs in the northern hemisphere in the July cases. The most obvious reason for the reduction in the value of $\overline{Q_{as}}$ is that the amount of water vapor in the atmosphere was reduced in the ice age case.

The net infrared radiation lost by the troposphere is less than that computed for the control cases for both January and July ice age cases as a result of a reduction of tropospheric temperature and water vapor and a change in cloudiness distribution in the ice age cases.

The release of latent heat of condensation of water vapor in the upward branch of the Hadley cell is greater in the January ice age case than in the control case, but the condensation heating is less than or equal to that in the control case at all other latitudes. In the July cases, the condensation heating is less in the ice age case than in the control case at all latitudes except between about 5°N and 5°S, where the ice age case heating is 0-0.3°C day^{-1} greater in the control case.

In the southern hemisphere in the January cases, the gradient of temperature between the surface and the atmosphere is increased in the ice age case and consequently the vertical diffusion of sensible heat ($\overline{Q_{dv}}/c_p$) is increased. In the July cases, the vertical sensible heating is greater in the ice age case than in the control case between 30°S and 65°S and this increase is again related to an increase in the ground-atmosphere temperature gradient. In the northern hemisphere in both January and July cases, the ice age case vertical diffusion of sensible heat by subgrid scale eddies differs, but not greatly, from the control case values.

The introduction of ice age boundary conditions into the GCM has caused noticeable (and some probably significant) changes in the values of $\overline{\Delta F_{dh}}$, the horizontal diffusion of sensible heat. In the middle and high latitudes of the northern hemisphere the meridional diffusion of sensible heat in the January ice age case is quite different from that in the control case, this must be due to the changes in the meridional temperature gradient. In the July cases, in the tropics the diffusion of sensible heat is generally less in the ice age case than in the control case; in the middle latitudes the control case values are lower.

The January ice age case has lower net heating than the control case in the northern hemisphere and slightly higher net heating in the southern hemisphere.

In the July ice age case the net heating is much less than that in the control case in the northern hemisphere. In the southern hemisphere the ice age case net heating is greater than that in the control case between 5°S and 35°S and not greatly different (± 0.15°C day^{-1}) from the control case values elsewhere. As far as total heating (or cooling) of the troposphere is concerned, the northern hemisphere amounts show the most difference between the ice age cases and the control cases.

The ice age case eddy transports of sensible heat differ considerably from those in the control cases. In the July cases at 3 km and 12 km, the ice age case transport maxima in both hemispheres are less than the maxima in the control case. In the January cases the ice age case peak poleward eddy heat transport is only greater than that in the control case at 3 km in the southern hemisphere. In tropical and subtropical latitudes in both January and July at 3 km and 12 km the ice age case eddy transports of heat are often greater than control case transports but the transport in these latitudes is usually not large.

CHAPTER VII

THE ENERGY BALANCE OF THE FOUR SIMULATIONS

(a) Introduction

Several authors have described the maintenance of the total amounts of kinetic, potential and internal energy in the atmosphere. Those referred to in this study include: Lorenz (1967), Newell *et al.* (1970), Palmén and Newton (1969), Dutton and Johnson (1967), Oort (1964), Van Mieghem (1973).

Because of the differential heating along meridians there is a continuous generation of zonal available potential energy (which is the energy available for conversion into kinetic energy). Large scale eddies in the middle latitudes determine a poleward transport of sensible heat and this transport causes some of the zonal available potential energy to be converted to eddy available potential energy (see Van Mieghem, 1973, pp. 226-227). Also in middle latitude belts warm air rises and cool air sinks in east-west overturnings which convert eddy available potential energy into eddy kinetic energy. The process involved in the transport of momentum by the eddies is responsible for a transfer of kinetic energy from the large scale eddies to the

zonal circulation, thus maintaining the energy of the zonal circulation against frictional dissipation (Van Mieghem, 1973). Fluxes of kinetic energy and total potential energy distribute these energy forms in the atmosphere across the boundaries of their source regions. The generation of available potential energy by heating, the conversion of available potential energy into kinetic energy by reversible adiabatic processes and the dissipation of kinetic energy by friction may be regarded as the three steps in the energy cycle of the atmospheric circulation (Lorenz, 1967, p. 103).

(b) The Energy Balance Equations of the GCM

The energy equations were first described by Kasahara and Washington (1967) and Washington and Kasahara (1970), but the equations had to be modified when orography was included in the model. The modified equations, used in the version of the GCM employed in this study, were described by Kasahara and Washington (1971). The four forms of energy defined in the model are given by:

$$\overline{K} = \frac{1}{2}\,\overline{\sigma\rho}\,(\hat{u}^2 + \hat{v}^2) \qquad \text{zonal kinetic energy} \qquad (7.1)$$

$$K' = \frac{1}{2}\,\overline{\sigma\rho(u'^2 + v'^2)} \qquad \text{eddy kinetic energy} \qquad (7.2)$$

$$\overline{P} = \overline{g\sigma\rho z} \qquad \text{zonal potential energy} \qquad (7.3)$$

$$\overline{I} = C_v\,\overline{\sigma\rho}\,\hat{T} \qquad \text{zonal internal energy} \qquad (7.4)$$

The energy equations, which describe the time rate of change of the above forms of energy are given in Kasahara and Washington (1971). The terms $\overline{K}$ and $\overline{P}$ were combined in the model equations to give $(\overline{K} + \overline{P})$, the zonal mechanical energy. This was done to avoid problems which arose if the equations for $\partial\overline{K}/\partial t$ and for $\partial\overline{P}/\partial t$ were separated (see Kasahara and Washington, 1967, pp. 396-397).

The three equations for conversions between forms of energy in the model are given by:

$$\begin{aligned} C(\overline{K} + \overline{P}, K') = & - \overline{\sigma\rho u'v'} \frac{\cos\phi}{a} \frac{\partial}{\partial\phi}\left(\frac{u}{\cos\phi}\right) \\ & - \overline{\sigma\rho v'^2} \frac{1}{a}\frac{\partial\hat{v}}{\partial\phi} + \frac{\tan\phi}{a}\hat{v}\,\overline{\sigma\rho u'^2} \\ & - \overline{\rho u'w''}\frac{\partial\hat{u}}{\partial z} - \overline{\rho v'w''}\frac{\partial\hat{v}}{\partial z} \end{aligned} \tag{7.5}$$

$$C(\overline{I}, \overline{K} + \overline{P}) \approx - \overline{\rho}\,\overline{w}\,\hat{T}\left(\frac{R}{\rho}\frac{\partial\overline{\rho}}{\partial z}\right) \tag{7.6}$$

$$C(\overline{I}, K') \approx - \overline{\rho}\,\overline{w''T'}\left(\frac{R}{\rho}\frac{\partial\overline{\rho}}{\partial z}\right) \tag{7.7}$$

The value of C(A,B) is positive if there is a transfer of energy from A to B.

(c) Time Variations of Global Mean Kinetic and Internal Energy

Figures 7.1 and 7.2 show the time variations of the global mean zonal kinetic energy $\overline{K}$ and eddy kinetic energy K' for the control and glacial period cases, for days 51 through 80.

In the January cases (Figure 7.1), we see that the global mean zonal kinetic energy is somewhat larger than the global mean eddy kinetic energy. $\overline{K}$ increases between days 51 and 80 in the ice age case but seems fairly constant in the control case. The increase in the January ice age case amounts to about 11 per cent of the initial value of $\overline{K}$. Between day 51 and day 80 the values of $\overline{K}$ for the two January cases are quite different (maximum difference, day 51, is 15 per cent of the control case value). The difference between the time variation of $\overline{K}$ for the two January cases is in general not large.

The global mean eddy kinetic energy is slightly larger in the January ice age case than the control case, but the differences are not very great (maximum difference, day 65, is 18 per cent of the ice age case value). After day 74 the global mean K' values decrease but the drop is not great.

In the July cases (Figure 7.2), it can be seen that the ice age case values differ substantially from the control case values. On day 66.5, the difference

between the control and ice age case values of $\overline{K}$ is 35 per cent of the ice age case value. When values of $\overline{K}$ are averaged for the 30 days then the difference between the time-averaged global means of $\overline{K}$ is about 28 per cent of the ice age case value, with the ice age case value of $\overline{K}$ always greater than the control case value. For the eddy kinetic energy, K', the global means again differ greatly. On day 68.5 the difference in the value of K' between the cases is 43 per cent of the control case value. The control case value of K' is larger than that of the ice age case every day; the difference between the time-averaged values of the zonal means is 32 per cent of the control case value.

In summary, in the January cases the differences in global mean zonal and eddy kinetic energy between the control and ice age cases are not great. In the July cases the global mean zonal kinetic energy is much greater in the ice age case, whereas the global mean eddy kinetic energy is much less in the ice age case than in the control case.

In contrast, Alyea (1972) found that for his July cases, the eddy kinetic energy was greater in the ice age case than in the control case and the zonal kinetic energy did not vary between the two cases. Alyea (1972, Figure 13, p. 68) shows the time variations of $\overline{K}$ and K' for the 60 days of each of his simulations. He finds that by day 15 there is no large time variation of the

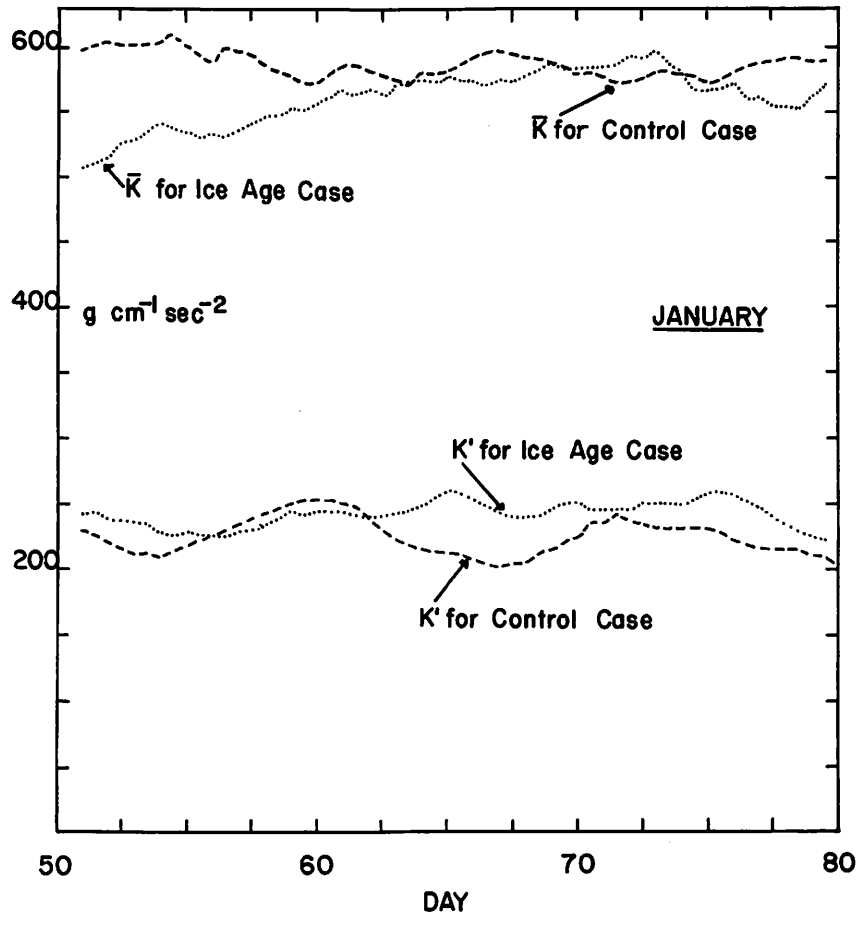

Figure 7.1. Time variation of global mean zonal kinetic energy and eddy kinetic energy for the January control case and January ice age case.

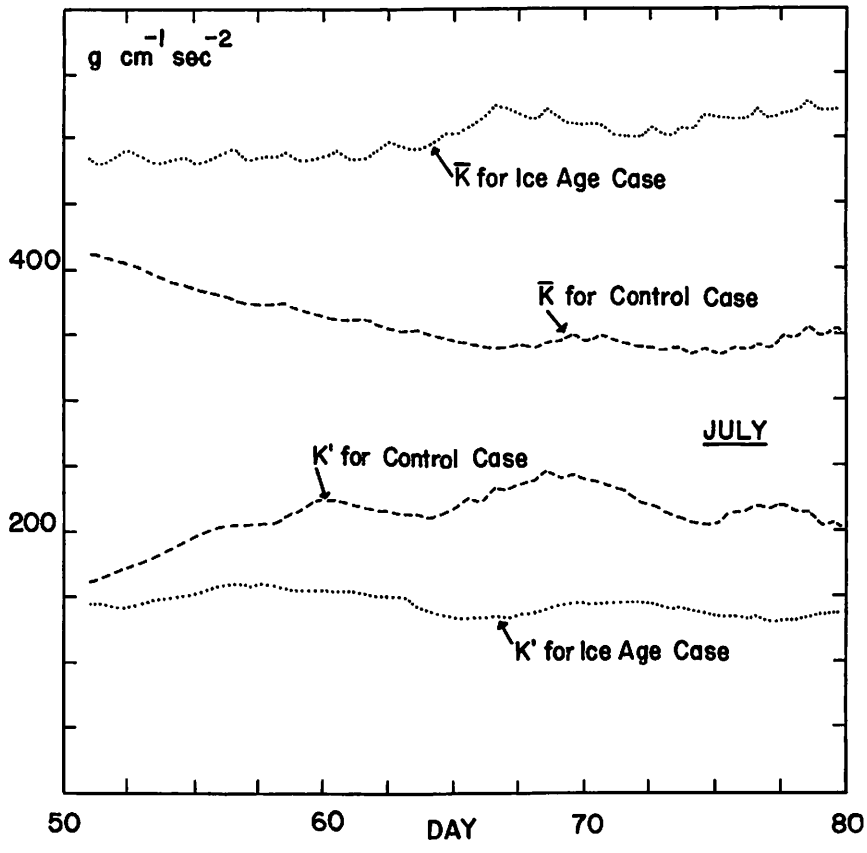

Figure 7.2. Time variation of global mean zonal kinetic energy and eddy kinetic energy for the July control case and July ice age case.

energy quantities (i.e., the models have reached a state of quasi-equilibrium). He attributes the larger value of K' in his ice age case to the stronger north-south temperature gradients generated along the southern edges of the ice. At day 48, the energy level of Alyea's ice age model begins to drop rapidly and he calls this change "the occurrence of a degenerate solution," which is a result, he believes, of the influence on the general circulation model of 60 days of July forcing.

We have therefore a considerable difference between the energy forms produced by two different general circulation models with ice age boundary conditions. The question is, whether the ice age boundary conditions should cause increased or decreased eddy kinetic energy in the model atmosphere. Although Alyea argues for increased baroclinicity in the ice age case on the basis of stronger temperature gradients; Kraus (1973, p. 4) shows that the mean meridional temperature gradient was probably weaker in an ice age than today. Kraus also suggests that it is probable, but less certain, that the colder tropical troposphere was associated with a reduced baroclinicity. In Chapter III it is shown that whereas the equator-to-pole temperature gradient generally increases in the lower troposphere in the ice age cases, the gradients decreased in the upper troposphere in accordance with Kraus's hypothesis. Newell (1973) proposed that the increased temperature gradient at 700 mb

in a glacial period would have caused increased baroclinicity. So, Newell's hypothesis is supported by Alyea's results and Kraus's hypothesis is supported by the results of this study. The basic question is whether temperature gradient changes in the upper or lower troposphere have more influence on baroclinic eddy activity and while Newell argues for the lower trosphere Kraus argues that the reduced temperature gradients in the upper troposphere caused reduced baroclinicity. We see in Figure 7.2 that eddy kinetic energy, which is a partial indicator of baroclinicity, is reduced (as far as a global average is concerned) in the July ice age case. In Chapter III it was shown that the temperature gradients were reduced in the upper troposphere (10.5 km, c. 200 mb) suggesting that Kraus's hypothesis is supported at least in the July cases.

A possible explanation for the different results from the two general circulation models is that, while the NCAR GCM was able to cope with processes described by Kraus, Alyea's two-level model was unable to do so--consequently the temperature gradients and baroclinicity in the upper troposphere were different in the two models. Alyea did not study January cases. In the January cases of this study, the boundary conditions did not cause such large changes in eddy kinetic energy as they did in the July cases.

However, as suggested in Chapter III, probably the primary difference between the July ice age cases of this study and that of Alyea, in terms of the energetics, is the difference in the simulation of the monsoon between the two models. The monsoon generates eddy kinetic energy (see Chapter III) because of the east-west circulations established in response to land/ocean thermal contrasts. In this study the northern hemisphere summer monsoon was simulated in the July control case but not in the July ice age case. Therefore the eddy kinetic energy is greater in the former than the latter. Alyea's model was unable to simulate the monsoon in either the July control or ice age case and consequently the eddy kinetic changes are different from those in this study. If Alyea's interpretation is correct (since he shows no figures of temperature gradient it is not verifiable here) then the increase of eddy kinetic energy in the July ice age case is due to increased temperature gradients (and it could now be added, inability to simulate the monsoon in the July control case).

A brief study of the time variation of the global mean zonal internal energy was made, no diagram is included here. It was seen that in three of the four cases there was an increase in $\overline{I}$ between days 51 and 80. The increases were not large and the increase expressed as a percentage of the value on day 51 was 1.7 per cent

for the January control case, 1.3 per cent for the January ice age case and 1.6 per cent for the July ice age case. In the July control case the value of $\overline{I}$ increased between days 51 and 67 and the increase as a percentage of the value on day 51 was 0.4 per cent.

(d) Conversion Between Zonal Internal Energy and Eddy Kinetic Energy

$C(\overline{I},K')$ shown in Figure 7.3 is a major term contributing to the production of eddy kinetic energy. In both the January and July cases, the values are nearly all positive, so that $\overline{I}$ is being converted to K' the majority of the time. The production of eddy kinetic energy is associated with baroclinic wave activity (Kasahara and Washington, 1971), so the largest maxima in $C(\overline{I},K')$ are seen in the middle latitudes.

In the January cases, (top half, Figure 7.3), the values for the control case and ice age case are not very different. The maximum value of $C(\overline{I},K')$ occurs in the middle latitudes of the northern hemisphere in both cases.

In the July cases (lower half, Figure 7.3) it can be seen that the differences between the ice age and control case are larger than they are in the January cases. In the tropical latitudes the two curves are the same but in the middle latitudes the value of $C(\overline{I},K')$ is less in the July ice age case. Therefore in the July ice age case there is less production of eddy kinetic energy by

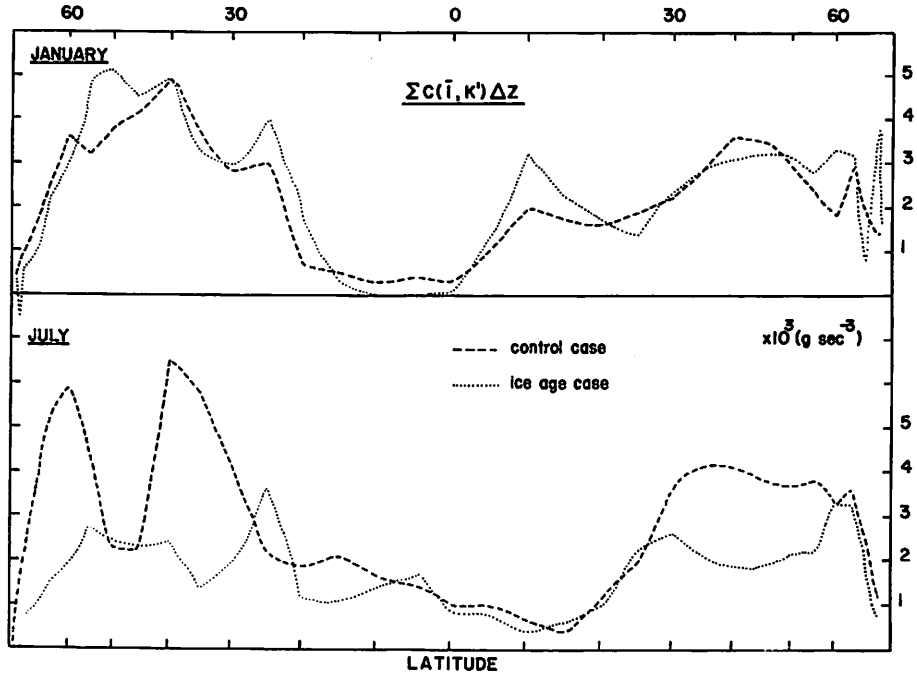

Figure 7.3. Vertical integrals of $C(\bar{I},K')$ (10^3 g sec^{-3}) for January (upper half) and July (lower half) control and ice age cases.

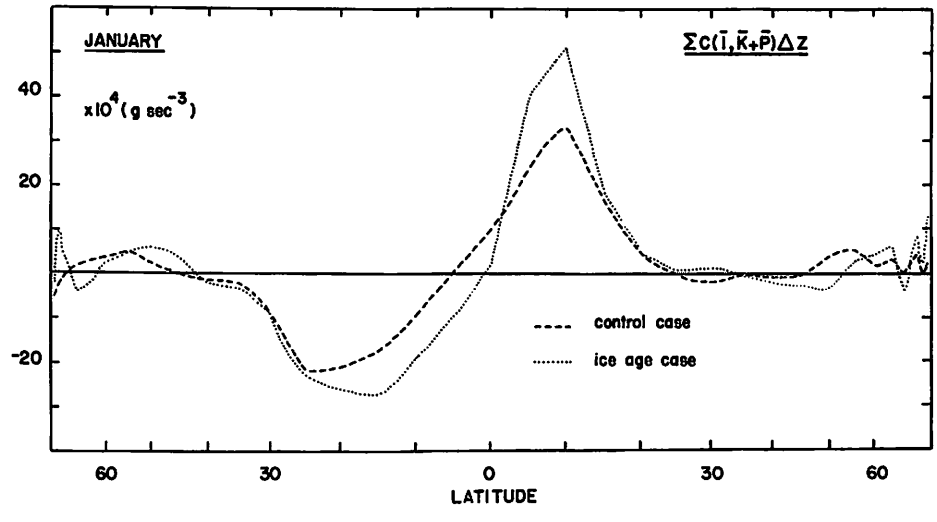

Figure 7.4. Vertical integrals of $C(\bar{I}, \bar{K} + \bar{P})$ (10^4 g sec^{-3}) for January control and ice age cases.

baroclinic wave activity. In equation (7.7) we see that $C(\overline{I},K')$ depends on a correlation between deviations from the mean of temperature and of vertical velocity, i.e., on the vertical eddy transport of sensible heat. The equation for $C(\overline{I},K')$ is virtually the same as that for C_E of Lorenz (1955) and Lorenz explains that the positive value of C_E is associated with a sinking of colder air and a rising of warmer air at the same latitude in eddies. In the July ice age case this process is reduced compared with the control case.

As described in Chapter III and earlier in this chapter, conversion to K' from other forms of energy in the northern hemisphere summer is primarily a function of the monsoon circulation. In the July ice age case the normal July land/ocean thermal contrast is reversed in the northern hemisphere and the east-west circulations are therefore reduced or eliminated. Since it is these east-west circulations which comprise sinking of colder air and rising of warmer air at the same latitudes and generate eddy kinetic energy, it is clear that their reduction (or the elimination of the monsoon circulation) in the July ice age case corresponds to the decrease of C(I,K') in the ice age case.

(e) Conversion from Zonal Internal Energy to Zonal Mechanical Energy, $C(\overline{I}, \overline{K} + \overline{P})$

The term $C(\overline{I}, \overline{K} + \overline{P})$ corresponds to C_z as defined by Lorenz (1955) (see Kasahara and Washington, 1967, p. 396). The equation for $C(\overline{I}, \overline{K} + \overline{P})$ differs from the equation for $C(\overline{I},K')$ only in that the former involves the vertical transport of sensible heat by the meridional circulation instead of the eddies. The sign of $C(\overline{I}, \overline{K} + \overline{P})$ is difficult to determine; its magnitude seems to be small because the meridional circulations have not been found to be strong. The value of C_z was estimated by Starr (1954) and he gave it a negative sign because the mid-latitude indirect cell occupies the zone of maximum temperature gradients.

In Figure 7.4 we see the vertically averaged values of $C(\overline{I}, \overline{K} + \overline{P})$ for the January cases. In the tropics between 0° and 25°S the Hadley cell converts $\overline{I}$ to $\overline{K} + \overline{P}$ (warm air rising, cold air sinking at different latitudes). In the northern hemisphere between 10°N and 40°N zonal mechanical energy is converted to zonal internal energy. In the southern hemisphere (= summer hemisphere) the values of $C(\overline{I}, \overline{K} + \overline{P})$ are very small poleward of 20°S. In the tropical latitudes (30°N to 30°S) in the January ice age case the value of the conversion is somewhat larger than the control case value (about 55 per cent larger at 10°S). Since it was

noted in Chapter III that the Hadley circulation is stronger in the January ice age case than the control case, the increased conversion rate in the Hadley circulation is not surprising.

In the northern and southern hemisphere middle latitudes the values of $C(\overline{I}, \overline{K} + \overline{P})$ do not differ largely and consistently between the January control case and January ice age case.

In the July cases (Figure 7.5) the larger values of $C(\overline{I}, \overline{K} + \overline{P})$ occur between 30°N and 0° (positive) and 0° and 40°S (negative). In the region between 30°N and 0° where conversion is from zonal internal to zonal mechanical energy (warm air rising, cold air sinking) the values in the July control case and ice age case are similar but the ice age case peak is shifted slightly equatorward. Between 0° and 40°S where the conversion is from zonal mechanical to zonal internal energy, the ice age case values are about 18 per cent smaller than those in the control case. The equatorward shifting of the positive maximum does mean that between 10°N and 40°N the conversion is less in the July ice age case than the control case. This implies less production of zonal kinetic energy in the July ice age case in these latitudes and this is verified in Figures 7.8c and 7.8d.

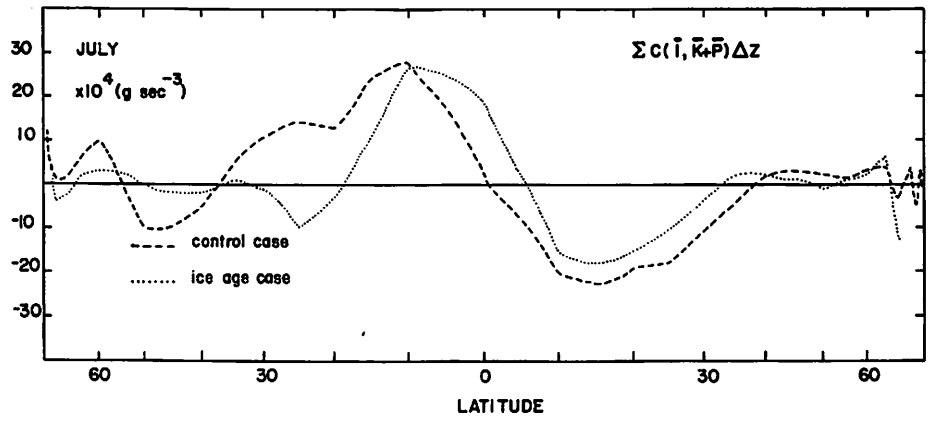

Figure 7.5. Vertical integrals of $C(\bar{I}, \bar{K} + \bar{P})$ (10^4 g sec^{-3}) for July control and ice age cases.

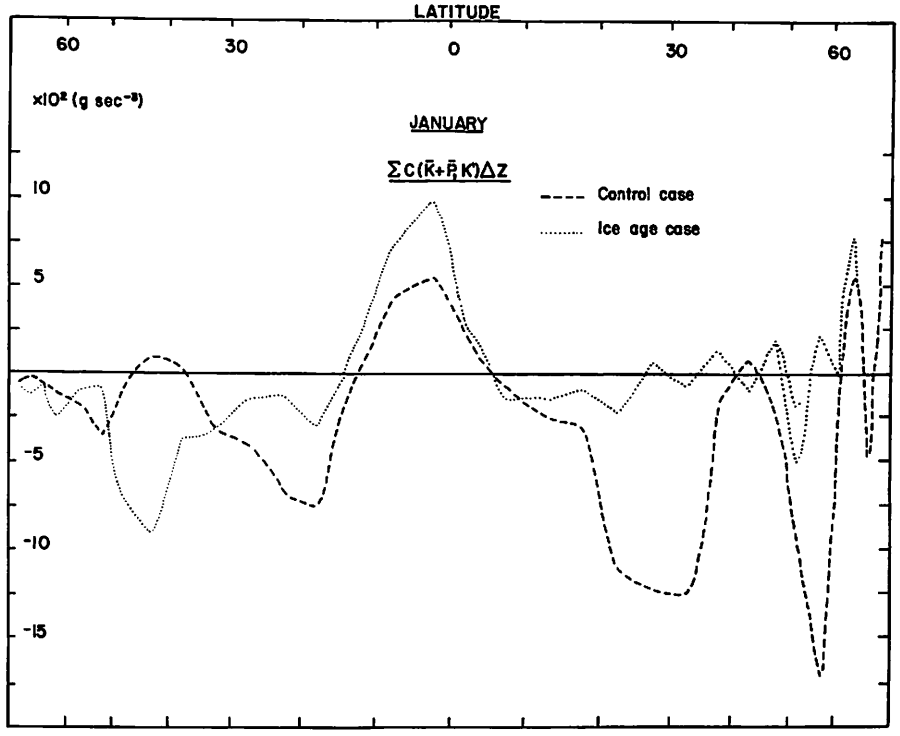

Figure 7.6. Vertical integrals of $C(\bar{K} + \bar{P}, K')$ (10^2 g sec^{-3}) for January control and ice age cases.

(f) Conversion from Zonal Mechanical Energy to Eddy Kinetic Energy

Figures 7.6 and 7.7 show the values of $C(\overline{K} + \overline{P}, K')$ for the January and July cases respectively. In the January cases the value of the conversion is negative at many latitudes, indicating that eddy kinetic energy is being converted to zonal mechanical energy to maintain the zonal flow against frictional dissipation. This conversion from K' to $\overline{K} + \overline{P}$ takes place in the middle latitudes; in the tropics the value of $C(\overline{K} + \overline{P}, K')$ is positive, indicating that zonal kinetic energy is converted into K' in these latitudes.

In the January cases, the largest difference between the control case and the ice age case (Figure 7.6) is in the southern hemisphere, where the ice age case value of $C(\overline{K} + \overline{P}, K')$ oscillates around the value zero while the control case values have a maximum of -12.5×10^2 g sec^{-3} at 32°S. In the northern hemisphere the ice age case values and control case values differ in the middle latitudes but not consistently. In the southern hemisphere the ice age case values are less than those of the control case except at 42.5°S.

In the July cases (Figure 7.7) the values of $C(\overline{K} + \overline{P}, K')$ are smaller than those for the January cases. While the values of the conversion are positive only in the tropics and a few other small areas in the July control case, the values of $C(\overline{K} + \overline{P}, K')$ are

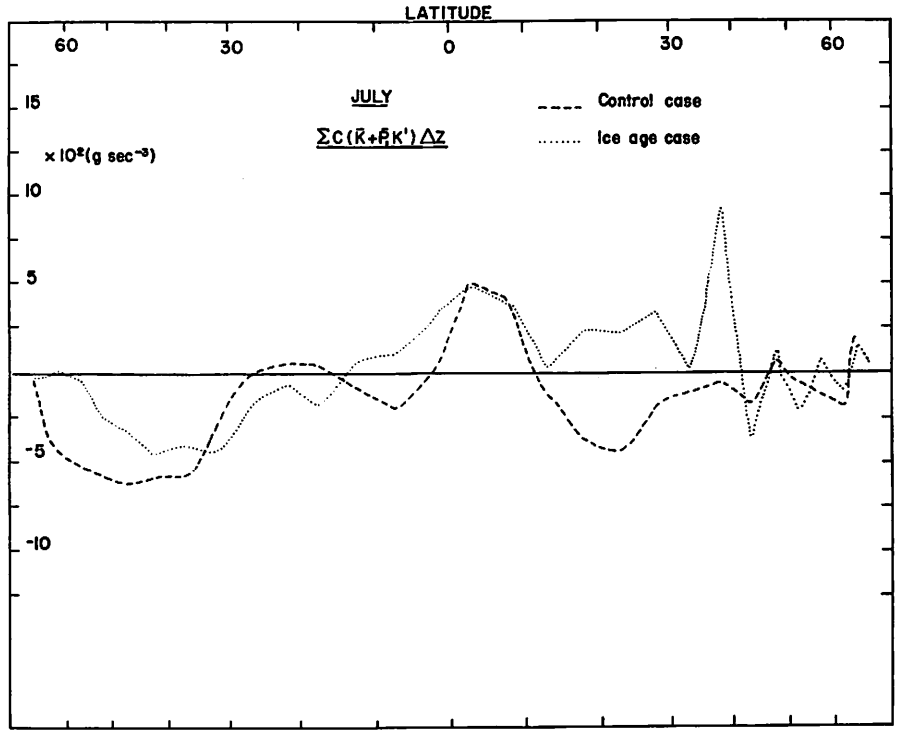

Figure 7.7. Vertical integrals of $C(\bar{K} + \bar{P}, K')$ (10^2 g sec^{-3}) for July control and ice age cases.

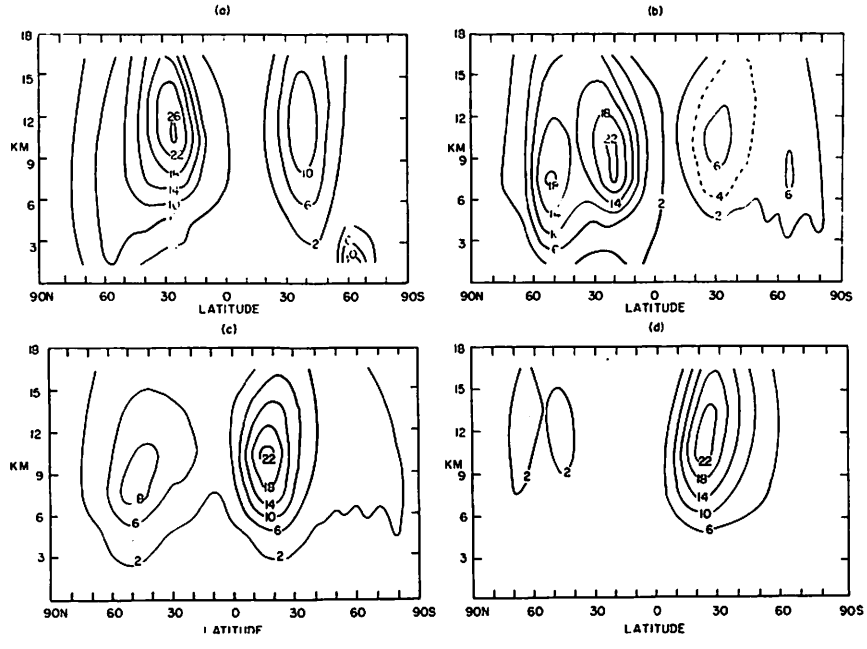

Figure 7.8. Latitude-height distributions of zonally averaged zonal kinetic energy (a) January control case, (b) January ice age case, (c) July control case, (d) July ice age case.

positive between 15°N and 40°S and in other areas in the southern hemisphere. North of 35°N the value of $C(\overline{K} + \overline{P}, K')$ is larger (negative) in the control case than in the ice age case (also negative). Between 15°N and 35°N the ice age case values are more negative, that is, there is more conversion from K' to $\overline{K} + \overline{P}$ in the ice age case. In the July ice age case tropics and most of the southern hemisphere the ice age case value of the conversion is positive ($\overline{K} + \overline{P}$ to K') and therefore greater than the control case value.

(g) The Distribution of Eddy and Zonal Kinetic Energy in the Model Atmosphere

Figure 7.8 shows the latitude-height distribution of zonally averaged zonal kinetic energy, $\overline{K}$, for the four cases. It is clear that the maxima of $\overline{K}$ occur in the jet streams of both hemispheres, with more energy associated with the winter hemisphere jet. In the January control case the maximum $\overline{K}$ is at 25°N and has a magnitude of approximately 27×10^2 g cm^{-1} sec^{-2}. In the January ice age case the maximum is split into two with one of 19×10^2 g cm^{-1} sec^{-2} at 50°N and one of 23×10^2 g cm^{-1} sec^{-2} at about 20°N. This split reflects the evidence for a split in the zonally-averaged u component of the wind (Figure 5, Williams, Barry and Washington, 1974). In the southern hemisphere the maximum value of $\overline{K}$ is reduced from about 13×10^2 g cm^{-1} sec^{-2} in the

control case to about 7 x 10^2 g cm^{-1} sec^{-2} in the ice age case. The maximum in the southern hemisphere is also split in the January ice age case.

In the July cases (Figures 7.8c and 7.8d) the $\overline{K}$ maximum in the northern hemisphere is weaker in the ice age case (9 x 10^2 g cm^{-1} sec^{-2}). The southern hemisphere $\overline{K}$ maximum is not very different in magnitude in the two July cases, it occurs at about 20°S in the control case and 20-30°S in the ice age case.

The value of $\overline{K}$ can be compared with the observed values given by Oort and Rasmusson (1971). Unfortunately the latter are plotted in units of m^2 sec^{-2}, that is, the density factor (see equation 7.1) has not been taken into account. However the location of the northern hemisphere $\overline{K}$ maxima can be compared. In the January control case the maximum $\overline{K}$ occurs between 25 and 30°N at 10.5-12 km. In the observed data the maximum is also between 25 and 30°N and occurs at about 200 mb. The control case maximum is slightly higher than observed, but it has been noted earlier that zonally-averaged wind maxima are higher in the control case, probably because of the upper boundary conditions of the GCM, and this could explain the $\overline{K}$ discrepancy. In the July control case the maximum $\overline{K}$ occurs between 40-60°N and 7-11 km. The observed maximum is at about 200 mb between 40 and 50°N. The distribution of $\overline{K}$ is not so well simulated in the

July control case, since the computed maximum is slightly poleward (5 to 10 degrees) and lower than that observed. The observed maximum $\overline{K}$ is reduced by about 71 per cent from January to July, the GCM maximum is reduced by about 68 per cent from the January control case to the July control case so we see that the seasonal difference of $\overline{K}$ is well simulated.

In Figure 7.9 are plotted the latitude-height distributions of the zonally-averaged values of K'. Kasahara and Washington (1971) found that although the maximum of K' in the northern hemisphere agreed well in terms of height and latitude with observed data, the magnitude of K' was about 60 per cent smaller than observed. Wellck et al. (1971) pointed out that the intensity of K' is very much dependent on the horizontal grid resolution of the model and showed that with a 2.5 mesh the eddy kinetic energy did increase. Miyakoda et al. (1969) also found that model-computed eddy kinetic energy was smaller than observed. They suggested that the deficiency was due to the effective von Karman constant governing "internal viscosity" employed. Manabe et al. (1970b) showed that resolution and dissipative effects were linked in causing changes in model-derived eddy kinetic energy. They found that, since the scale at which the nonlinear dissipation is most effective decreases with decreasing grid size, it is reasonable that dissipation of large scale motion by horizontal

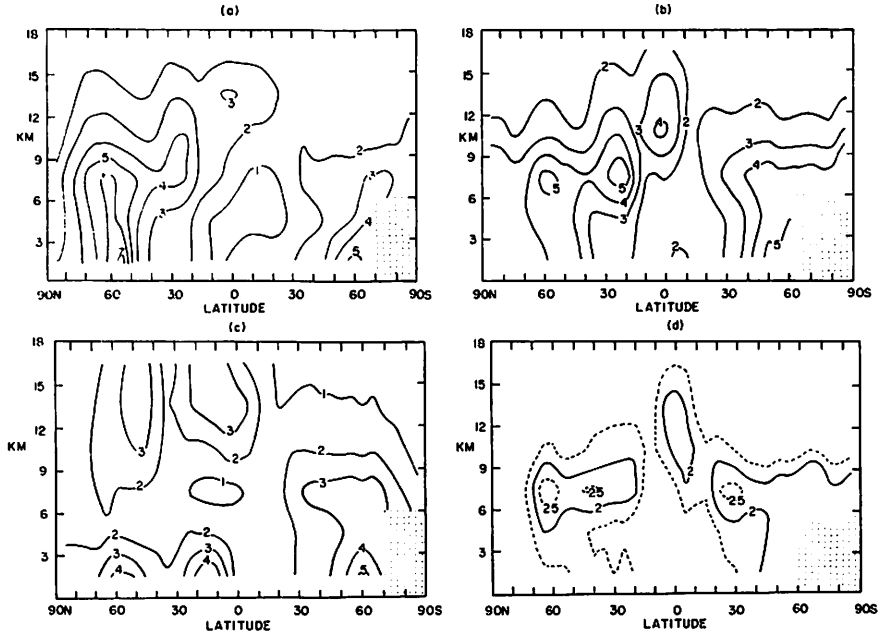

Figure 7.9. Latitude-height distribution of zonally-averaged eddy kinetic energy (a) January control case, (b) January ice age case, (c) July control case, (d) July ice age case.

mixing is larger for the low resolution than high resolution model. It was concluded that a further increase of horizontal resolution would result in more realistic eddy activity, because of the greater separation between the synoptic scale and the scale of dissipation by horizontal sub-grid scale mixing.

It is clear from consideration of Figure 7.9 that the distribution of K' is quite different in each of the four cases. In the January control case (Figure 7.9a) the maximum of 7×10^2 g cm^{-1} sec^{-2} occurs at 50-60°N in the lowest 3 km, whereas in the January ice age case (Figure 7.9b) the maxima in the northern hemisphere occur between 6 and 9 km with a magnitude of 5×10^2 g cm^{-1} sec^{-2}. One occurs at about 60°N, another at 20-30°N. When the time-averaged global mean of K' is considered, the value of K' in the January ice age case is about seven per cent greater than the value in the control case.

In the July control case (Figure 7.9c) the distribution shows four maxima in the northern hemisphere, two below 3 km and two above 9 km. The former have values of 4×10^2 g cm^{-1} sec^{-2}, the latter 3×10^2 g cm^{-1} sec^{-2}. The distribution in the southern hemisphere of the two control cases is similar. In the July ice age case the values of K' are much smaller than those of the control case. The time-averaged global mean of K' for the ice age case is about 32 per cent less than the value

for the July control case. In the July ice age case the maxima of K' (2.5×10^2 g cm^{-1} sec^{-2}) are between 6 and 9 km, as in the January ice age case, there are no maxima at low or high elevations as in the control cases. In the observed data for January (Kasahara and Washington, 1971, p. 694) the maximum of K' occurs between 6 and 9 km.

The values in the vicinity of Antarctica have been omitted because the distribution is unrealistic in this region. Problems with the energy components were noted by Kasahara and Washington (1971) and attributed to a possible unsatisfactory handling of mountain blocking near Antarctica.

(h) Dissipation of Kinetic Energy

Dissipation of total kinetic energy is given by the vector product $\overline{\mathbb{V}\cdot \mathbb{F}}$, dissipation of $\overline{K}$ is given by $\hat{\mathbb{V}}\cdot \mathbb{F}$ and of K' is given by $\overline{\mathbb{V}\cdot \mathbb{F}} - \hat{\mathbb{V}}\cdot \mathbb{F}$. As Dutton and Johnson (1967) point out, frictional dissipation can be expected in the boundary layer and near the cores of jet streams. Recent work by Holopainen (1963) and Kung (1966) indicates that considerable frictional dissipation does occur in the free atmosphere. Newell et al. (1970) describe the various methods employed by different authors to calculate frictional dissipation in the boundary layer and free atmosphere. As Lorenz (1967) points out, the final estimate of total dissipation has

yet to be made. Lorenz believes that the generally accepted values could be revised upward.

Unfortunately "observational" studies of the frictional dissipation have not been global in coverage nor long-term in extent. For example, Holopainen's (1963) study used an 18-day sample in January, 1954, for eight stations in the British Isles. Kung's (1969) study used 12 months of North American data. There is also the problem that although frictional dissipation is a small scale phenomenon the mthods of investigating it have largely centered about large scale considerations, this was pointed out by Newell et al. (1970). Lastly, there has been considerable disagreement between different studies. For example, Elsaessar (1969) finds some of Kung's work questionable since Kung, for instance, assumed a constant surface roughness for the oceans.

Since there are many problems and insufficiencies associated with the dissipation data, the distributions of $\overline{\mathbb{V}\cdot\mathbb{F}}$ and $\overline{\mathbb{V}\cdot\mathbb{F}} - \hat{\mathbb{V}}\cdot\mathbb{F}$ will not be compared with observations. Newell et al. (1970) tabulate the frictional dissipation estimates by various investigators, the values for total dissipation range from 4.1 watts m^{-2} estimated by Kung (1967) to 10.3 watts m^{-2} estimated by Holopainen (1967).

The latitude-height distribution of $\overline{\mathbb{V}\cdot\mathbb{F}}$ (not illustrated) shows that in all four cases there is a maximum of dissipation in the lowest 3 km. There is a

secondary maximum above 12 km in all cases. These features coincide with general observations. The global means of total dissipation for the four cases are: 3.95 watts m^{-2} for the January control case; 4.48 watts m^{-2} for the January ice age case; 4.07 watts m^{-2} for the July control case, 3.15 watts m^{-2} in the July ice age case. The values for the control cases are rather small compared with the range of observed values. The January ice age case dissipation is larger than that in the control case by about 13 per cent, the July control case dissipation is larger than that in the ice age case by about 29 per cent.

(i) Global Energy Balance

TABLE 7.1

GLOBAL AVERAGES OF VERTICALLY INTEGRATED ENERGIES (ergs cm^{-2})

	January Control	January Ice Age	July Control	July Ice age
K	10.6×10^{8}	10.1×10^{8}	6.5×10^{8}	9×10^{8}
P	58×10^{10}	57×10^{10}	57×10^{10}	58×10^{10}
I	17.4×10^{11}	16.8×10^{11}	17.3×10^{11}	16.8×10^{11}
K'	4.1×10^{8}	4.4×10^{8}	3.8×10^{8}	2.6×10^{8}

The values in Table 7.1 show some of the differences between the four cases which had been pointed out earlier. For zonal kinetic energy, the January control

case is about 5 per cent larger than the ice age case, the July control case is about 46 per cent larger than the ice age case. Zonal potential energy is not very different between the four cases. Zonal internal energy is larger in the two control cases (17.4×10^{11} ergs cm^{-2} in January, 17.3×10^{11} ergs cm^{-2} in July) than in the ice age cases (16.8×10^{11} ergs cm^{-2} in January and July). Since $\overline{I}$ depends on atmospheric temperature and this was reduced in the ice age cases, the reduction of $\overline{I}$ was to be expected. Eddy kinetic energy, K', was increased about 7 per cent from the January control case to the January ice age case, and decreased about 32 per cent from the July control case to the July ice age case.

In Figure 7.10 the components of the global energy balance are shown for each of the cases. The arrows show the direction of energy transfer between boxes or generation or dissipation. The magnitudes and directions of most of the conversions are very similar to those described by Kasahara and Washington (1971, p. 697) and their comments are in general applicable to Figure 7.10. Kasahara and Washington do point out that the global average of $C(\overline{I}, \overline{K} + \overline{P})$ is difficult to evaluate because very large positive and negative values compensate in the global average. Kasahara and Washington found a large value (7 watts m^{-2}) from the model calculations, however they found this value was too large when the

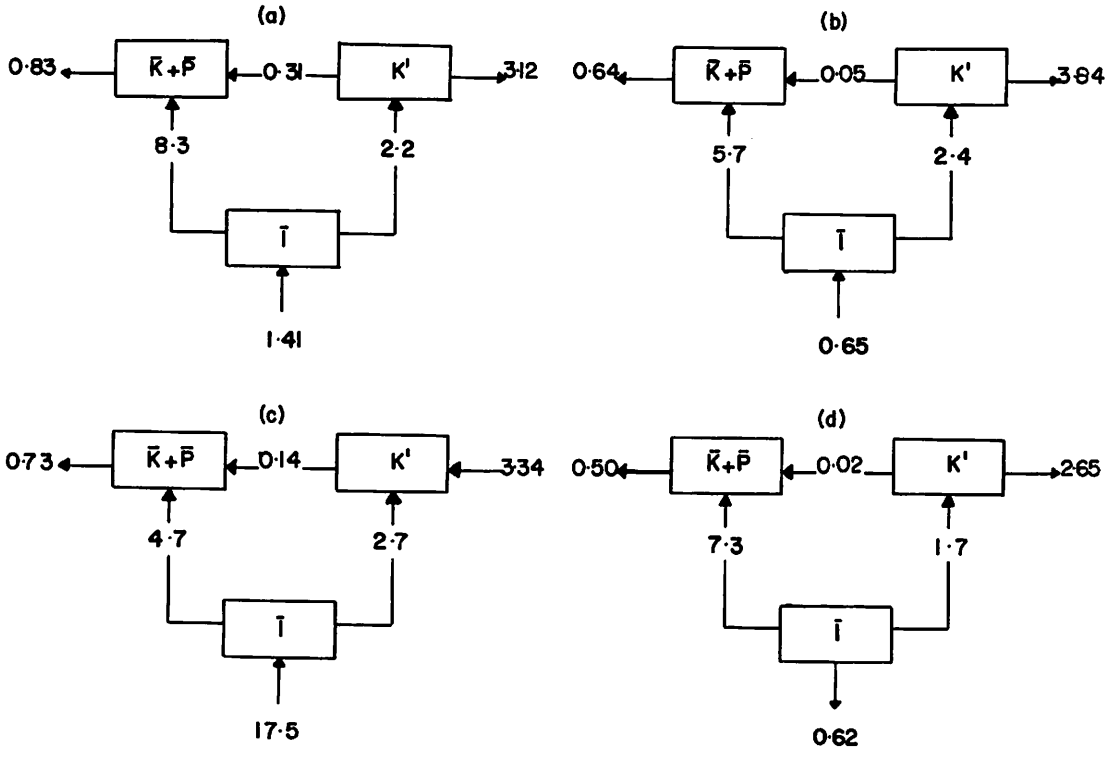

Figure 7.10. Global energy balance (a) January control case, (b) January ice age case, (c) July control case, (d) July ice age case.

energy balances of $\overline{K} + \overline{P}$ and $\overline{I}$ were considered and suggested a more reasonable value on the order of 1 watt m^{-2}.

Another occurrence of compensation of terms is in the evaluation of the generation of $\overline{I}$ or $\overline{\rho Q}$. Consideration of Figure 6.6 in the chapter on the heat balance, shows that the vertical integral of $\overline{\rho Q}$ is positive in low latitudes and negative in high latitudes. When a global average of $\overline{\rho Q}$ is taken we are again averaging large positive and large negative values. Moreover the resulting average is quite sensitive to small changes in the latitudinal averages of $\overline{\rho Q}$. The latter changes are also sensitive to changes in the components of $\overline{\rho Q}$. In Table 7.2 we see the global averages of components of $\overline{\rho Q}$ for the four cases.

As discussed in Chapter VI (on the heat balance) $\overline{\rho Q}$ is the result of a balance between the negative $\overline{\rho Q_{AE}}$ (long wave cooling) and positive $\overline{\rho Q_C}$ (latent heat released upon condensation). Small changes in these two components can lead to large variations in the global average value of $\overline{\rho Q}$. Equation (52) p. 684 of Kasahara and Washington (1971) shows that $\overline{\rho Q}$ is the generation term for zonal internal energy. In Figure 7.10, we see that in the July ice age case $\overline{\rho Q}$ is negative. This is a result of the above-described sensitivity of the global average of $\overline{\rho Q}$. Table 7.2 shows that whereas $\overline{\rho Q_{AE}}$ decreased 15 per cent from the July control case to the

TABLE 7.2

GLOBAL AVERAGES OF COMPONENTS OF $\overline{\rho Q}$

	$\overline{\rho Q_{DV}}$	$\overline{\rho Q_{as}}$	$\overline{\rho Q_{al}}$	$\overline{\rho Q_c}$	$\overline{\rho Q_{dh}}$
January Control Case	16.1	29.5	-142.7	101.1	-2.6
January Ice Age Case	21.2	23.9	-127.4	86.8	-4.0
July Control Case	20.2	33.7	-154.8	119.2	-.54
July Ice Age Case	22.9	23.8	-131.2	27.1	-3.3

ice age case, $\overline{\rho Q_c}$ decreased about 19 per cent from the July control case to the ice age case. This small difference meant that $\overline{\rho Q}$ became negative in the July ice age case. However to put this topic into perspective, the values for Q amount to at most, of the order of 10 watts m^{-2}, the solar constant is 350 watts m^{-2}.

CHAPTER VIII

SUMMARY OF DIFFERENCES BETWEEN CONTROL AND ICE AGE CASES AND BETWEEN CONTROL CASE AND OBSERVED DATA FOR MAJOR TERMS OF THE MOMENTUM, MOISTURE, HEAT AND ENERGY BALANCES DISCUSSED IN PRECEDING CHAPTERS

In this chapter some of the results of the preceding chapters will be reviewed in an attempt to point out the major differences between the ice age cases and control cases and observed data. Differences due to inaccuracies in the model will be discussed with reference to the NCAR GCM and other models and differences due to inaccuracies in the observed data will be discussed. In addition to describing these differences it is hoped that the chapter will bring together some of the results of various chapters. For example, the eddy transports of momentum, heat and moisture will be discussed together so that changes in eddy transports can be compared. The summary of "model-dependent" and "data-dependent" errors points out necessary areas of future research.

It should be emphasized at this point that this study is primarily a sensitivity study; we have simulated the atmospheric circulation with four different sets of boundary conditions using the NCAR GCM. Results

have been examined to see how the control cases compare with observed data and to see what the major differences are between the control cases and ice age cases. Inaccuracies in the model are due to (a) mathematical approximations, e.g., grid-size, finite-differencing scheme, (b) physical, e.g., parameterization of cloud physics. If the geographical distributions of certain parameters are examined we find that the control cases compare favorably with the observed data, although the magnitudes may not be exactly the same. Large discrepancies in some of the climatological parameters can be explained; for example, the precipitation distribution differences are a result of inadequate observational data and of the saturated soil moisture assumption used in the model employed in this study. There is evidence (from further GCM experiments) that many of the discrepancies can be corrected with an improved formulation of the physics of the model or with less sparse observed data.

The large differences between the control cases and ice age cases represent the response of the physics of the model to the large changes in boundary conditions. In Chapter IX the response of the model to small changes in initial conditions will be discussed and compared with the response to the vast changes in orography and sea-surface temperatures involved in the ice age cases. For the purposes of a sensitivity study it is this type of

comparison which is important. This is the first time that a global model of the atmospheric circulation has been used to investigate the influence of ice age boundary conditions on the atmospheric circulation and although the approach will no doubt be used again with more refined models, the results of this study are a first estimate of the likely direction of changes between the present day and ice age atmospheric circulations. In this chapter the causes of the differences between the control cases and ice age cases are examined. Some of the results would change if more refined calculations were included in the GCM and these refinements are also discussed.

(a) Meridional Transport of Momentum and Moisture by the Mean Circulation

In the NCAR GCM January control case simulations the Hadley cell produces too much meridional transport of moisture and û-momentum compared with observed data and in the middle latitudes the meridional transport by the mean circulation is greater in the observed data than control data. The increased value of the meridional transport in the Hadley circulation corresponds to increased values of u and v compared with observed data (see Chapter III). In the January ice age case the maximum meridional transports in the Hadley cell of moisture and momentum are greater than the control

case maxima. In the July ice age case the maximum momentum transport is greater than and occurs northward of the control case maximum. The maximum moisture transport is much smaller than the control case value. This latter occurrence reflects the large reduction in the moisture content of the atmosphere in the July ice age case.

(b) Eddy Transports of Momentum, Moisture and Heat

In general the January control case underestimates the observed eddy transport of sensible heat and the July control case overestimates it. The January control case also underestimates the observed eddy transport of momentum but the eddy transport of moisture is not significantly different from the observed. The July control case has more eddy transport of momentum in the northern hemisphere than observed and less than observed in the southern hemisphere and the moisture transport is overestimated in the northern hemisphere.

In the January ice age case, the maximum eddy transport of sensible heat is only greater than that in the control case at 3 km in the southern hemisphere. The January ice age case eddy transport of momentum is slightly (probably not significant) greater than the control case maximum in the northern hemisphere and in the middle latitudes of the southern hemisphere the ice age case value is much smaller than the control case value.

The January ice age case eddy transport of moisture is less than the control case transport in both hemispheres. That the eddy transports of sensible heat and moisture are reduced in the January ice age case is predictable in view of the reduced moisture and sensible heat content of the atmosphere as seen in Chapters III, V, VI. Changes in momentum transports are less predictable because of the more irregular changes in wind velocity. The eddy transports of moisture, sensible heat and momentum are reduced in the July ice age case.

Rasmusson (1972) has described many of the difficulties inherent in any attempt to define humidity conditions. Apparently the present lack of data precludes the possibility of definitive regional water balance investigations over much of the tropics and leads to some uncertainty in zonally-averaged quantities. Since the maximum value of meridional flux is usually found below 850 mb, according to Rasmusson, most often near 1000 mb in the region of strongest meridional flow, there is a necessity for a good 1000 mb analysis and this is not readily available. Data problems are also apparent in the description of the angular momentum budget. Newell et al. (1972) point out that maps of the eddy transport of momentum at the surface and up to at least 850 mb are difficult to analyze due to the patchy nature of the patterns. Also, the less detailed structure of the eddy flux patterns over the oceanic

areas is more than likely a consequence of the relatively sparse data in these regions as compared to continental areas.

(c) The Mountain Pressure Torque

In Chapter IV we described the distributions of the mountain torque ($H\ \partial p_s/\partial\lambda$) for January and July cases without interpretation. Since large changes in orography have been incorporated in the boundary conditions of the ice age cases, changes of the mountain torque are of interest. The July control case differs markedly from Newton's (1972) observed data although the January control case looks more reasonable. Jao (1972) has discussed the mountain torque in detail and other studies were mentioned in Chapter IV. However, the problems associated with the evaluation of the mountain torque have not been thoroughly discussed since White's (1949) pioneer study.

White states that one of the difficulties in measuring the mountain torque is the construction of accurate topographic profiles of sufficient simplicity to permit easy calculation of pressure differences across mountain ranges that would be representative. White concluded that isolated mountain peaks extending far above the level of a mountain chain could be of little consequence in the computing of the pressure difference across a range, he assumed that only mountain ranges of broad

latitudinal or longitudinal extent could be significant as barriers across which, on average, significant differences in pressure could occur. Since mountains rise irregularly it was necessary to simplify profiles considerably. White believed that his simplifications would lead to inaccuracies but felt that these would not be detrimental to the final result. Newton (1971a) also pointed out some problems with evaluation of the basic data. Since data are not available on the scale of individual mountains, Newton emphasizes that the computations only represent the mountain effect insofar as pressure gradients can be determined on a "synoptic scale." Brinkmann (1973) found that the mean torque produced by mountains on the atmosphere in 13 wind storms in Boulder was almost twice that for the entire globe at that latitude in winter. Neglect of such mesoscale contributions to the global mountain torque in both the "observed" data and models obviously needs to be remedied. Lilly (1972) points out that energy and momentum removed from the troposphere by breaking of large amplitude mountain lee waves may be significant in the evolution and maintenance of the large scale atmospheric circulation. Lilly describes experiments with the NCAR GCM to determine the sensitivity of the atmosphere to a force resembling wave drag and outlines a program for improving knowledge and understanding of this phenomenon and for incorporating its effects into numerical models.

Obviously there are problems in the calculation of the mountain torque from observed data, especially in finding a scale on which the data can be evaluated easily. The mountain pressure torque evaluated by the model depends on the determination of the mountains and on the surface pressure. For instance, the topography in the GCM is smoothed and probably differs (especially between 20-40°N, where the mountain ranges are complex) from that used by Newton (1971a). The mountain torque is computed in the NCAR GCM according to the longitudinal surface pressure differences across the mountains and to the height of the mountains (Kasahara and Washington, 1971, p. 675). Newton (1971a) on the other hand computed the torque using the pressure at different levels between $z = 0$ and $z = H$, the surface of an orographic feature.

In the January control case and particularly in the July control case the mountain torque is different from that observed north of 30°N and south of 60°S. We have already noted that the model has difficulty in dealing with the blocking in the vicinity of Antarctica and so the discrepancies south of 60°S are no doubt model-dependent. In the northern hemisphere, we have already suggested that the topographical smoothing in such a complex area is probably different in the model and Newton's data. The pressure distribution simulated by the GCM is not exactly the same as that observed

(Williams et al., 1973) and this too will lead to differences in the distribution of the torque. The largest differences between the ice age cases and the control cases occur north of 30°N. Elsewhere the small differences in the torque are probably due to differences in the pressure distribution. In the northern hemisphere the large changes in the torque distribution are probably due to a combination of changes in topography and pressure distribution. Since one extra topographic barrier the size of the Rocky Mountains has been included the increased values of $(H\ \partial p_s/\partial\lambda)$ are not surprising.

(d) The Surface Stress Torque

The latitudinal distributions of surface stress torque, $\tau_{\lambda s}$ a cos ϕ, are illustrated in Figures 4.9 and 4.10 for the January and July cases. In both the January and July control cases the data are most similar to those observed in the tropical zone of the winter hemisphere. The surface stress is underestimated in both months in the latitudes of the surface westerlies. In the ice age cases, the surface stress torque in the middle latitudes is again small, not very different from that in the control case. In January there is hardly any difference between the ice age case and control case values. In the July cases the ice age case is especially different in the northern hemisphere. The differences between the ice

age and control cases are mainly due to differences in the speed and direction of the surface winds.

In Chapter IV we suggested that some of the differences between the control case and observed surface stress values were due to the formulation of C_D in the NCAR GCM ($C_D = 0.003$). It appears that there are different ways of evaluating τ and that the value of C_D depends on several factors, including the underlying surface type and the stability of the atmosphere. The constant value of C_D in the model probably causes errors in the evaluation of the surface stress torque.

Delsol et al. (1971) experimented with a GCM to find out how the formulation of the boundary layer processes affects the results of gross scale atmospheric circulation experiments. They experimented with C_D constant everywhere with a value of 2×10^{-3} and then with $C_D = 4.3 \times 10^{-3}$ over land and $C_D = 1.1 \times 10^{-3}$ over ocean. These data were based on the studies of Kung (1963, 1968). The complexity of the problem was emphasized by Delsol et al. with a consideration of the influence of the change of C_D on the precipitation rate. An increase in C_D contributes to the filling of depressions and therefore to a reduction in precipitation. On the other hand, a large value of C_D intensifies upward currents as well as the pumping of water vapor at the top of the boundary layer and this could favor an increase in precipitation. Delsol et al. emphasize that

the processes are completely nonlinear and some completely counteract each other. They found that the larger surface drag suppresses the baroclinic instability more and that the use of values of C_D varying between land and sea produced a somewhat larger effect than more detailed specification of turbulent transfer processes in the constant flux layer. Noting Cressman's (1960) geographic distribution of C_D, Delsol *et al.* point out that the orography used in the GFDL model is very smooth, several hundred meters of "ruggedness" have been eliminated, and that this should be accounted for.

We see now how unrealistic a constant value of $C_D = 0.003$ is for the computation of surface stress. We noted that the control cases are underestimating the surface stress torque in the westerlies. If a larger value of C_D were used in the northern hemisphere mid-latitudes to take into account the drag of the mountain ranges then the value of $\tau_{\lambda s}$ would be increased.

However, even if a better formulation of C_D were used in the GCM the comparison with observed data would not be improved since most of the "observed" curves are inaccurate. The observed data used for comparison in Figures 4.9 and 4.10 are derived from Newton (1971b, 1972) and he has pointed out the inaccuracies in the data. In particular, he was obliged to assume that oceanic stresses represented the mean around the globe and he questioned the validity of some of the ocean stress data.

A few experiments have been made using different values of C_D in the NCAR GCM. Chervin (personal communication) experimented with the values of C_D, which he changed to 0.0015 in one experiment and 0.006 in another experiment. When C_D was doubled, the value of τ increased in both the westerly and easterly belts of maximum stress. For days 50-55 the increase of τ at 45°S was about 12 per cent of the control case value (where the control case has C_D of 0.003). At 50°N the increase was about 20 per cent of the control case value. We see therefore, that when C_D is increased in the middle latitudes to a value more like those of Cressman the value of τ is increased. When C_D was decreased to 0.0015, τ decreased by about 20 per cent of the control case value at 45°S and by about 25 per cent at 50°N. The large changes in the values of τ between experiments occurred at the maxima and minima in the latitudinal distribution curve. For the five-day average of days 60-65 the value of τ with $C_D = 0.006$ was about 110 per cent greater than the control case value at 55°N.

Schneider and Washington (personal communication) changed the value of C_{DW} (Oliger et al., 1970, p. 17) in the GCM from 0.7 to 1.0. This would firstly influence r, the moisture flux in the boundary layer, and subsequently other properties. Precipitation increased at most latitudes, presumably because of the increased upward moisture flux. Changes in cloudiness were random, but large

changes did occur in the high latitudes (poleward of 70°N, where the noise level is higher too). Ground temperatures also increased at nearly all latitudes.

In the ice age cases both the surface characteristics of flat land and the distribution of orography were changed. Values quoted by Cressman suggest that ice has a low drag coefficient (1.5×10^{-3}) so that the increased extent of pack ice and land ice should have been accounted for by a lower drag coefficient. However, in North America, Scandinavia and Patagonia in particular the form drag of the earth's surface was considerably increased because of the inclusion of 2.5 km "mountains." Unfortunately, the drag coefficient was kept constant at 0.003 in the ice age case as well as the control case and these changes in surface conditions are not reflected in the ice age case distribution of τ, illustrated in Figure 4.8. If the drag coefficient had been changed to reflect the boundary conditions in the ice age cases, it seems likely that in the middle latitudes of the northern hemisphere the surface stress would have increased because of the increased form drag.

(e) Evaporation Minus Precipitation

Figures 5.8 a and b show the latitudinal distribution of the zonally averaged difference between precipitation and evaporation. In the January cases, the maxima and minima of the control case and observed data occur in

approximately the same positions (latitudinally) but, especially in the tropics and southern hemisphere the magnitudes differ. In the July cases the observed and control case data are quite similar in the southern hemisphere but there are great differences between the two distributions in the northern hemisphere. Williams, Barry and Washington (1974) point out that the zonal means of 90-day precipitation show that, in comparison with Möller's (1951) estimates, the computed values from the control case are too large by a factor of 2-5. Study of the geographical distribution of precipitation shows that many of the differences between the observed and control case zonal averages are caused by local areas of anomalously high or low precipitation in the simulation.

As pointed out by Barry and Williams (1973) the absolute values of precipitation computed by the model are almost consistently too large (compared with observed data) and this seems to be primarily due to the assumption of a Bowen ratio equal to unity. An experiment with a July simulation and a Bowen ratio of 10 caused a reduction in the precipitation amounts. Precipitation was reduced particularly in the "desert" areas, e.g., Sahara, where amounts had been unrealistic earlier.

Problems with precipitation distributions have been noted by other authors in connection with other models. Delsol et al. (1971) found that when D_w, the availability of soil moisture, was equal to 0.5 over

land the model gave excessive precipitation for instance over the Sahara Desert, and a greatly deficient sensible heat flux. With a soil moisture formulation included in the model the moisture balance is improved. Washington (1974) describes the soil moisture calculation which has been included in a more recent version of the NCAR GCM. The version of the GCM used in this study cannot distinguish dry and wet portions of the land and thus overestimates evaporation and precipitation.

As pointed out in Chapter V, our knowledge of precipitation and evaporation distributions is based on limited observed data and/or unreliable computations. Available estimates of the global averages of P and E differ over a range of about 20 per cent. As Newton (1972) emphasizes, precipitation is inadequately sampled except over land areas and evaporation measurements are even more sparse and uncertain of interpretation. Rasmusson (1972) also outlines the inadequacies of the present observational network and its implications.

Thus we see that both the simulated and observed (E-P) data have problems and this makes the evaluation of the ice age case data difficult or in some cases impossible. The large differences between the control case and observed data in Figures 5.8 and 5.9 are probably "model-dependent" but the inaccuracies of the observed data must also be borne in mind.

(f) Heat Balance

The major differences between the control case, ice age case and observed data were described and summarized in Chapter VI. In this chapter the model-dependent and data-dependent problems will be discussed.

The relation between $\overline{Q_{as}}/c_p$, absorption of solar radiation by water vapor in the atmosphere, is rather complicated. Since the model only computes cloudiness at 3 and 9 km and computes on the basis of empirically derived formulae, there are bound to be differences between the observed and control case values of $\overline{Q_{as}}/c_p$. Actual absorption of solar radiation by clouds is not taken into account in the model. For January in the southern hemisphere, Sasamori et al. (1972) found that absorption of solar radiation by clouds was about 19 per cent of the total absorption of solar radiation, in July it was about 15 per cent. It is therefore not a negligible amount. Absorption by dust and ozone is not considered in the GCM either. Kasahara and Washington (1971) estimated that if absorption by clouds, dust and ozone were taken into account, $\overline{Q_{as}}/c_p$ would be higher by 60-70 per cent, but they felt that this uncertainty is small compared with the condensation heating flux, ΔF_c. The most obvious reason for the reduction in the amount of solar radiation absorbed by water vapor from the control case to the ice age case is that the amount of water vapor was reduced in the ice age case atmosphere.

The GCM control case produces less long wave cooling by the troposphere than is given by the data of Sasamori et al. (1972). This must be due to differences or inaccuracies in the temperature or moisture of the troposphere or the cloudiness distribution. Figure 8.1 shows the distribution of zonally-averaged cloudiness (model-generated clouds at 3 km plus those generated at 9 km) for the four cases. The observed data are from Van Loon (1972) and Telegadas and London (1954). We see that there are some large differences between the observed and computed distributions especially in the northern hemisphere in January and the southern hemisphere in July.

Since the computation of cloudiness in the GCM only involves clouds resulting from large scale uplifting, there are obviously several types of cloud (such as small scale convective clouds, local stratus, etc.) which are not well simulated by the model but are nevertheless observed. Since clouds play such an important role in the radiation balance of the earth-atmosphere system, an improvement in their calculation in the model would be profitable. The problem is, of course, that the cloud physics and processes involved in the development of the many different types of cloud are extremely difficult, if not impossible, to incorporate into a large-scale GCM.

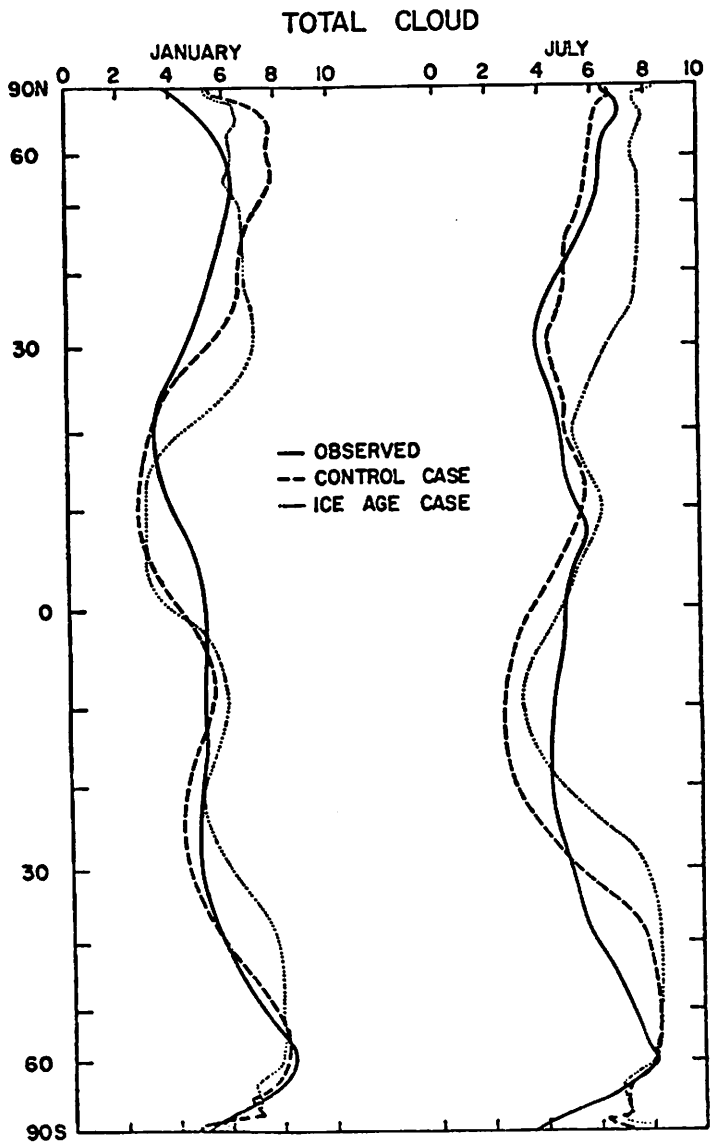

Figure 8.1. Latitudinal distributions of zonal averages of total cloud for all cases. Observed data from Van Loon (1972) for the southern hemisphere and Telegadas and London (1954) for the northern hemisphere.

Comparison of Figure 6.7a with Figure 7 of Newell et al. (1970) indicates that the condensation heating maximum in the upward branch of the Hadley cell is being overestimated in the GCM. This is not surprising since we have already noted that precipitation is overestimated in the control cases, reasons for this problem are discussed elsewhere. The general decrease in the maximum condensation heating from the control cases to the ice age cases is a reflection of the cooler, drier atmosphere in the ice age case. However, the condensation heating in the upward branch of the Hadley cell in the January ice age case is greater than that in the control case. This feature is not anticipated by Kraus's (1973) hypothesis (see Chapter III). We find that the vertical velocity between 0° and 20°S also increases in the January ice age case and this could be one reason for the increase in $\overline{Q_c}/c_p$ (velocity components for the four cases are illustrated in Figure 3.8). The increase in w is almost 60 per cent of the control case value. In the July ice age case, the value of w is decreased by 20 per cent from the control case value and the condensation heating is also reduced (by about 40 per cent of the control case value).

Data-dependent problems are also evident in the evaluation of the heat balance. Lack of data on such terms as $\overline{Q_{dh}}/c_p$, $\overline{Q_{dv}}/c_p$, $\overline{Q_c}/c_p$ is apparent and means that the control case distributions cannot be evaluated.

(g) Energy Balance

In the January cases, the differences in global mean zonal and eddy kinetic energy between the control and ice age cases are not great. In the July cases the global mean zonal kinetic energy is much greater in the ice age case, whereas the global mean eddy kinetic energy is much less in the ice age case than the control case. The reduction of K' and increase of $\overline{K}$ seems to be due to the presence or absence of the monsoon in the model. The monsoon is a source of K' and it occurs in the July control case but not in the ice age case (see Chapter III for more details). The difference in the eddy kinetic energy between the July cases is probably also due to the reduced temperature gradients ($\partial T/\partial \phi$) in the upper atmosphere in the ice age case (see Table 3.1) and to the monsoon differences. The discrepancy between observed and control case values of K' is due primarily to the horizontal resolution of the model (Wellck et al., 1971) and has been discussed in an earlier chapter.

The conversion between zonal internal and eddy kinetic energy $\Sigma\, C(\overline{I},K')\Delta Z$ is generally positive, so that $\overline{I}$ is being converted to K' most of the time. In the January cases, the values for the control case and ice age case are not very different. In the July cases the value of $\Sigma\, C(\overline{I},K')\Delta Z$ is less in the middle latitudes in the ice age case than in the control case. This reduction corresponds to the non-occurrence of the monsoon in

the ice age case. However, the conversion from zonal internal to zonal mechanical energy is increased when the monsoon does not occur. Lastly, the conversion term $\Sigma\ C(\overline{K} + \overline{P}, K')\Delta Z$ is greater in the southern hemisphere in the January control case than in the ice age case and in both January and July cases differences elsewhere are variable.

The global energy balance for each case shows that while $\overline{K}$ is about 5 per cent larger (probably not a significant difference) in the January ice age case as compared with the control case, it is smaller in the July ice age case than the control case. Zonal potential energy is not very different between the four cases. Zonal internal energy is larger in the control cases than the ice age cases since atmospheric temperature was also larger in the control cases. Eddy kinetic energy was increased by about 7 per cent from the January control case to the January ice age case and decreased about 32 per cent from the July control case to the ice age case (because of the monsoon and baroclinicity differences between the two cases).

(h) Problems due to Inaccuracies of the Model

In this section we will briefly discuss some of the features in the model which lead to discrepancies in the final results. In recent versions of the NCAR GCM some of these features have already been emended.

As pointed out in an earlier section of this chapter, the model used in this study did not include a complex treatment of physical processes near the earth's surface. Contrary to more recent versions of the model, this one did not include a snowcover calculation, the snowline was assumed to be geographically fixed. In more recent formulations the snowcover is allowed to accumulate or melt and albedo is modified depending on snow depth (Washington, 1974). The other important aspect of the moisture cycle which is not accounted for in the model used in this study is the soil moisture cycle. The model assumes that the land surfaces are saturated with moisture and that the Bowen ratio is equal to unity. This assumption causes the model to produce too much precipitation, especially in areas like the Sahara. Washington (1974) describes the treatment of soil moisture in more recent versions of the general circulation model. In particular it would be useful to run a simulation with ice age boundary conditions and a snowcover calculation. However Washington (personal communication, 1974) has pointed out that this type of experiment probably wouldn't come to an equilibrium for a perpetual January or July simulation. There would be a problem in determining the initial conditions for the runs.

Precipitation processes are probably too effective in the model since it is assumed that precipitation

occurs whenever the air becomes greater than saturated. But since we do not know the actual global precipitation distribution with a great deal of confidence, it is difficult to evaluate how important this problem is.

We pointed out earlier that the cloud formulation in the model, while not completely realistic, would be difficult to improve immediately. Obviously, at some time in the future, more than two layers of cloud will have to be computed and more than just large-scale cloudiness resulting from uplift and saturation will have to be considered. Also, more interaction between clouds and radiation processes will have to be included. Albedos of different cloud types should be considered so that the reflection of solar radiation is realistically simulated and absorption and transmission of solar radiation must be accounted for.

As pointed out in the introduction of the thesis, the model used in this study is not a complete climate model since ocean temperatures are specified rather than computed. The atmospheric circulation is simulated, with specified ocean surface temperatures and within the limitations of the model. For a complete discussion of the influence of glacial period boundary conditions on climate, an ocean model would have to be coupled to the atmosphere model. The coupling of the two types of model was attempted by Manabe and Bryan (1969) and they found several problems. Bearing in mind recent estimates

of the role of the oceans in transporting energy, by Vonder Haar and Oort (1973), it is clear that the oceans cannot be neglected in any study of climate. Also the neglect of air-sea interaction effects is probably significant, especially when discussing differences between the ice age and present circulations. But, the specification of ocean surface temperatures does at least constrain the model to produce a realistic atmospheric circulation. Holloway and Manabe (1971) point out that an error in planetary albedo may not result in an extremely unrealistic climate if the distribution of ocean surface temperatures is specified as a lower boundary condition. A difference of several per cent in planetary albedo could markedly alter the climate of a joint atmosphere-ocean model.

The effect of horizontal grid resolution on the model has been discussed earlier. Wellck et al. (1971) found that with increased resolution the model eddy kinetic energy was more like that observed. They concluded that the five-degree mesh model is acceptable for the study of the atmospheric circulation but that the intensity of transient eddy motions with wave number greater than say six, in middle latitudes is underestimated and the effect of the mean circulation in meridional transports of momentum, heat and water vapor is overestimated in the tropics. Holloway and Manabe (1971) find that a doubling of the resolution of the

finite-difference grid greatly improves the horizontal pressure distribution. The latter exhibited a poleward shift of pressure patterns, reduction of high polar pressures, intensification of sub-tropical highs and middle latitude low pressure belts in the higher resolution model.

Other problems have been discussed elsewhere in this chapter, e.g., the evaluation of the surface stress torques and formulation of C_D. The last problem to be discussed in this section is that of time-averaging of the GCM data. Leith (1973) has recently investigated how the accuracy of an estimate of a climatic mean depends on the length of the record used for computing averages. As he emphasizes, the study of climatic change with numerical models is concerned with detecting the influence on climate of external changes such as in sea-surface temperature; the problem is that the signal of interest, namely the change in climatic mean, is obscured by the noise of unpredictable fluctuations in finite time average estimates of the mean. Leith shows that we need a signal-to-noise ratio of at least 1.0 before we can draw significant conclusions about climatic change. He finds that a typical climate change experiment in which one could try to detect a shift in climatic mean of one-eighth of the standard deviation of day-to-day fluctuations would require a record length of at least one year. In this study however the changes

are probably greater than one-eighth of the standard deviation of day-to-day fluctuations. In Chapter IX we shall discuss the significance of the differences between the four simulations of this study.

(i) Data-Dependent Problems

Basically the data-dependent problems arise from the lack of good data. Meteorological stations are sparse in the southern hemisphere and over the oceans and for some parameters the length of record is very short. We have noted several times that precipitation distributions are not well-known. Reed and Elliot (1973) have recently found that precipitation over the North Pacific is much less annually than has been previously estimated. Their results and Tucker's converse findings for the North Atlantic show that rainfall over coastal and island stations cannot be regarded as representative of that over the open sea and consequently that the present mean rainfall maps over the oceans must be inaccurate. Other inadequacies have been noted in cloudiness data, boundary layer data and global energy balance data.

For evaluation of fluxes (especially moisture) in the atmosphere we need more and closer (spatially) observations. It appears that satellites will solve part of the data problem in the near future. But data unattainable by satellites will still be required, e.g., information on drag coefficients and pressure distributions.

CHAPTER IX

THE SIGNIFICANCE OF THE DIFFERENCES BETWEEN THE CONTROL AND ICE AGE EXPERIMENTS

(a) Introduction

As pointed out at the end of the last chapter, the problem of determining the significance of the differences between the control and ice age experiments results from the fact that in a numerical model there are unpredictable fluctuations in finite-time averages of the mean of climatic variables. The differences, say between the January control case and January ice age case, are a result of the response to both the changed boundary conditions and the random changes inherent to the model. As Leith (1973) has pointed out, the significance of any computed change will depend on the ratio of actual signal to the unpredictable noise. During the last few years, different attempts have been made to compute the significance of differences between numerical "climate change" experiments.

Houghton *et al.* (1974) have investigated the response of the NCAR GCM to a sea temperature change in the North Atlantic. They needed to determine whether their results from the GCM with changed sea-surface

temperatures in the North Atlantic differed significantly from the control case results (i.e., whether they exceeded the noise level of the model). However as they point out, the noise level of the model is not well-known since there has been a limited number of random perturbation experiments. Houghton et al. approach the problem by assuming that the natural variation of the real atmosphere is equal to or greater than the noise level of the model simulations. If the changes between a case with altered boundary conditions and a control case are greater than the natural variations of the real atmosphere then the changes are taken to be significant (i.e., a result of the boundary conditions). This method is certainly useful but does rely on the assumption of equal variation in the model and real atmosphere, which is questionable especially in view of some of the assumed boundary conditions of the model.

Warshaw and Rapp (1973) use the Mintz-Arakawa model to simulate the atmospheric circulation with and without ice over the Arctic Ocean. In order to test whether the ice-in and ice-out cases are significantly different, four experiments are made in which small random errors are added to the initial free air temperatures of the first two experiments. Warshaw and Rapp are therefore looking at the results of six experiments to see whether the differences between an ice-in and an ice-out case are greater than the differences between

say an ice-in and a slightly perturbed ice-in case. They list several reasons why the change in boundary conditions could fail to produce a significant change in some climatic variables. These are: (1) random perturbations in initial conditions produce inordinately large changes in final climatic variables, totally obscuring the actual effect of different boundary conditions; (2) boundary condition change is not large enough to produce an effect in the allotted simulation time; (3) the change in boundary condition is not physically significant, i.e., it was either a wrong choice for influencing the simulated climate or the model did not properly represent the physics. These three points should be noted with respect to the present study. Warshaw and Rapp test the hypotheses that the boundary condition change had no effect; and, that the additive noise had no effect; using the analysis of variance procedure. However, this technique assumes that the variables are independent. It is clear that variables are temporally correlated (e.g., Leith, 1973) and spatially correlated (e.g., Gandin, 1965) so the assumption of independence is not justified and this suggests that an alternate approach is required. It would be possible to filter out spatially and temporally correlated variables and perform an analysis of variance on the remainder. But if, for instance, we take Leith's (1973) assumption that the characteristic time between effectively independent sample values is about seven

days, then out of 30 simulated days we would have only four independent samples in the time domain and such a small sample would be of limited use in further statistical tests.

Warshaw (1973) has described a computer program specifically to test the significance of differences between climate simulations. Techniques of non-parametric multivariate analysis are used to remove space and time correlations but there are still restrictions on the application of the method.

Washington (1972) describes a set of experiments with the NCAR GCM to investigate possible climatic changes by man's generation of thermal energy. Again, the problem is to determine whether changes in atmospheric circulation are due to the addition of thermal energy or to noise in the model. Washington describes two experiments; in one, called the random error experiment, a small random initial error was added. The other, called a control experiment, contained no initial error. Washington finds that the differences in numerical experiments with and without thermal energy input produce changes of the same order as the natural fluctuations of the model, as derived from the random error experiments. Hence the results were inapplicable to the investigation of such small magnitude changes.

It was decided that the significance of differences between control and ice age cases in this study

should be investigated by examining random perturbation and non-random perturbation experiments. Essentially the random perturbation experiments will give some estimate of the noise level of the GCM.

(b) Random Perturbation Experiments

The results of five experiments will be discussed here. These experiments are:

Case 1: A simulation of January of the present day (a January control case). This is the January control case described by Kasahara and Washington (1971) and Williamson (1973) and not the one discussed in the rest of this study.

Case 2: A perturbed January control case. A time integration starting with slightly different initial conditions than case 1. This case has been discussed by Williamson and Kasahara (1961) and Williamson (1973).

Case 3: January ice age case. The simulation discussed elsewhere in this study.

Case 4: Perturbed January ice age case. A time integration starting with slightly different initial conditions than case 3.

Case 5: January control case. The simulation discussed elsewhere in this study.

The difference between two GCM experiments is expressed by the root mean square (RMS) difference, which is defined for a scalar quantity, x, by,

$$\text{rms}(x) = \left[\sum_i (x_i - x_i^*)^2 \cos \phi_i \Big/ \sum_i \cos \phi_i\right]^{1/2}$$

where ϕ is geographical latitude and the sum is taken over a set of grid points, i. The starred and unstarred variables distinguish two experiments. When the sum is taken over all grid points at one level (= 2052) in the vertical we refer to the rms difference. Rms errors of temperature, surface pressure, wind, low cloud and precipitation will be discussed in this chapter, in which case x represents T, p_s, u, v, low cloud and precip-s.

Random error experiments with the NCAR GCM have been described by Williamson and Kasahara (1971), Williamson (1973), Williamson and Washington (1973), for instance. These experiments were designed to look at the origin of errors and their growth characteristics in the GCM primarily, although Williamson and Washington look at both short term and long term climate simulations. It should be noted that, in general, the difference between two experiments (usually a control case and a perturbed control case) grows very rapidly during the first day of simulation, but after day 1 the difference grows less rapidly until the states of the two experiments are related to each other as random fields, after which the rms differences are fairly constant with time. Since this study will be concerned with days 51 to 80 of

each simulation, the rms differences between cases should be fairly constant with time.

The perturbed January control case (case 2) (Williamson and Kasahara, 1971; Williamson, 1973) was computed by adding a 1 m sec^{-1} initial random error in u to the control case (case 1). The perturbed January ice age case (case 4) was computed by adding an initial random error to the temperature field of case 3.

(c) Results of Random Perturbation Experiments

In Figure 9.1 the values of rms differences between cases are plotted as a function of time for variable T1, i.e., temperature at 1.5 km in the GCM. The solid line represents the rms differences between the January control case (5) and ice age case (3). The values are all just above 10°C, which means that from day 51 to day 80 the rms difference in temperature for grid points at 3 km between the January control and ice age cases is 10°C. The dotted line represents the rms differences between another January control case (1) and a perturbed version (2) of that control case (values are only available from days 51 to 70). For these two cases the rms differences are 3-4°C, i.e., about half of the rms difference between the control and ice age case. The dashed line shows the rms difference between the January ice age case (3) and perturbed January ice age case (4). For these cases the differences are 4-6°C, again about

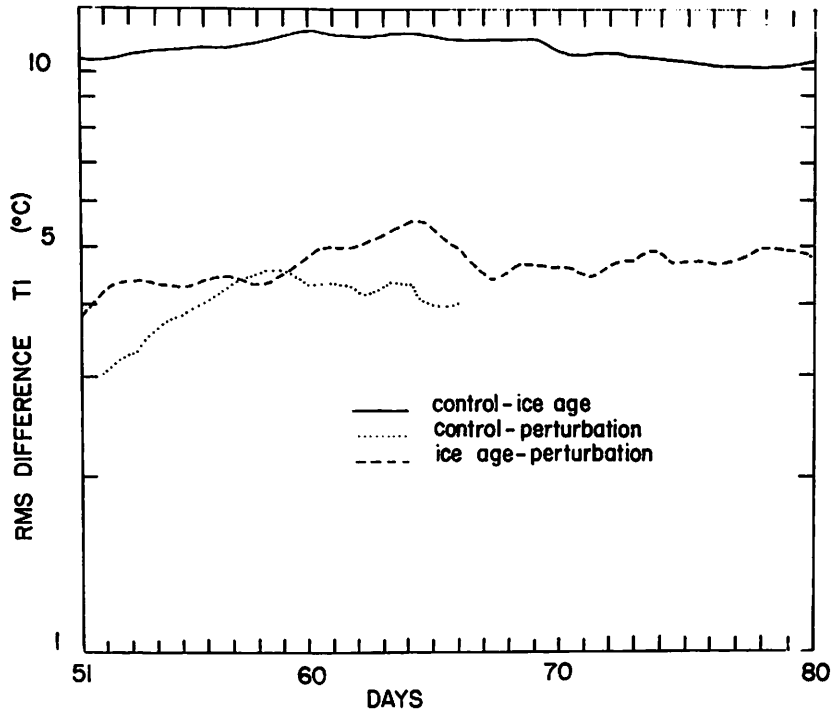

Figure 9.1. Rms differences between cases for temperature at 1.5 km. Solid line - differences between January control case (5) and January ice age case (3). Dashed line - differences between January ice age case (3) and perturbed January ice age case (4). Dotted line - differences between January control case (1) and perturbed January control case (2).

half of the control and ice age case rms differences. The large change in boundary conditions between the January control and ice age case has produced a much larger change in temperature at 3 km than have random initial perturbations.

Figure 9.2 shows the rms differences for the variable U1 (west-east component of the wind at 1.5 km). The solid line represents the rms differences between the January control case (5) and January ice age case (3) of this study and it has a value of about 7-8 m sec^{-1}. The rms differences between the ice age case (3) and perturbed ice age case (4), represented by the dashed line are between 5-6 m sec^{-1}. The control case (1) and perturbed control case (2) rms differences are more variable, starting out at about 4 m sec^{-1} at day 51 and leveling off at between 6 and 7 m sec^{-1} by day 70. The rms differences of U1 suggest that the differences between the control case and ice age case are above the noise level of the GCM, but not as far above as they were in the case of T1.

Figure 9.3 shows that the differences between the control case and ice age case for the variable V1 (north-south component of the wind at 1.5 km) are hardly above the noise level of the GCM. The control case (5)-ice age case (3) rms differences in V1 are 7-8 m sec^{-1} (solid line), while the control (1)-perturbation (2) rms

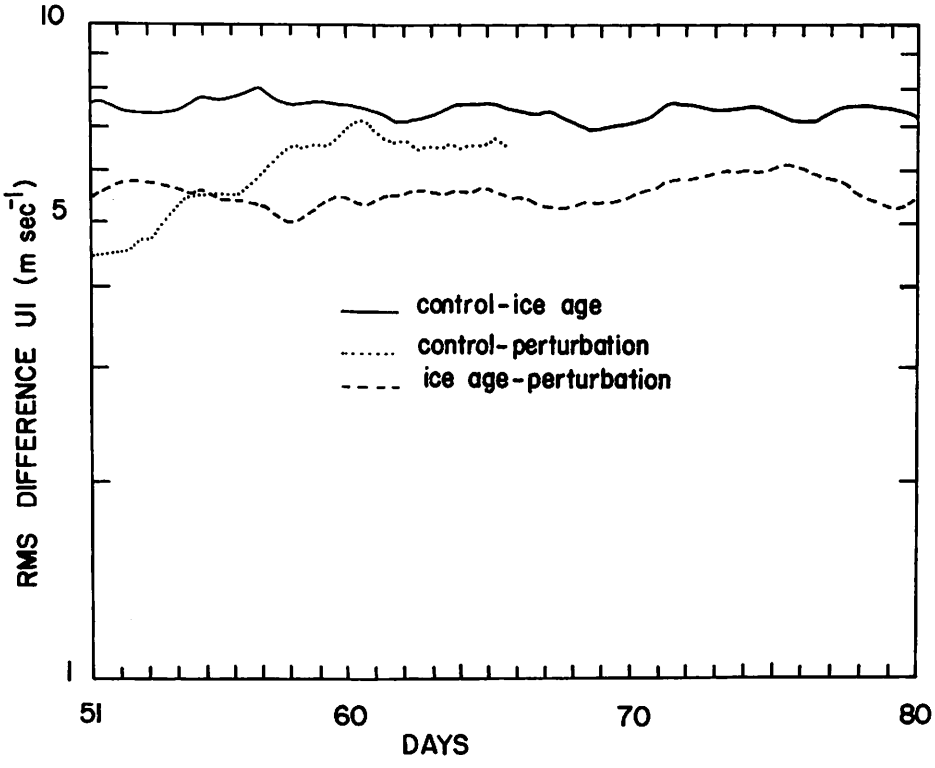

Figure 9.2. Rms differences between cases for west-east component of wind at 1.5 km. Solid line - differences between January control case (5) and January ice age case (3). Dashed line - differences between January ice age case (3) and perturbed January ice age case (4). Dotted line - differences between January control case (1) and perturbed January control case (2).

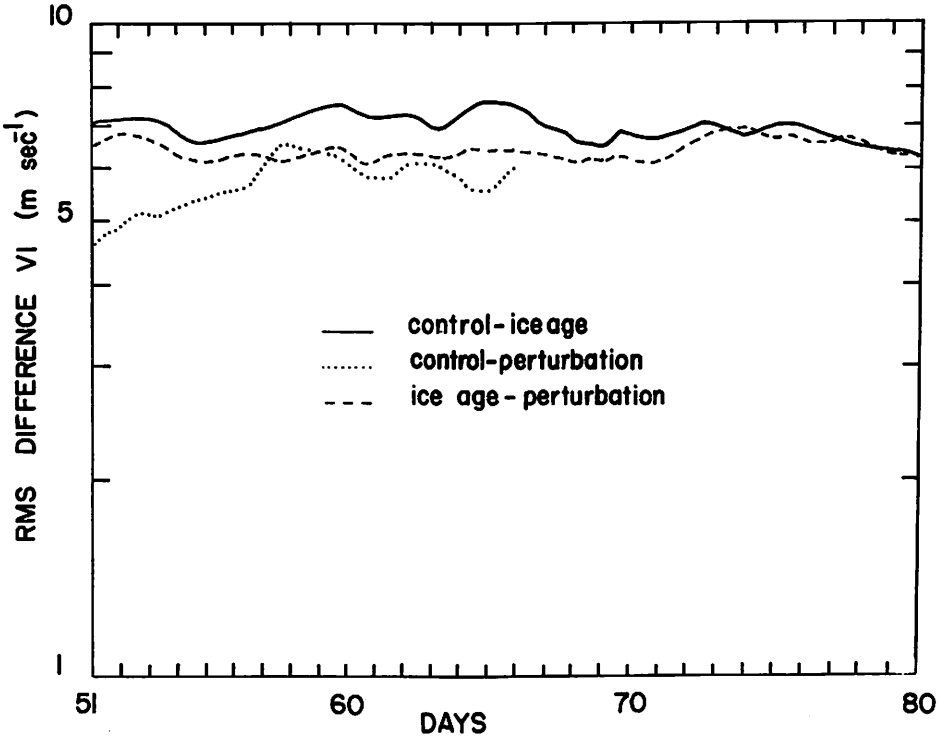

Figure 9.3. Rms differences between cases for north-south component of wind at 1.5 km. Solid line - difference between January control case (5) and January ice age case (3). Dashed line - differences between January ice age case (3) and perturbed January ice age case (4). Dotted line - differences between January control case (1) and perturbed January control case (2).

differences are about 5-6 m sec^{-1} and the ice age case (3)-perturbation (4) differences are about 6-7 m sec^{-1}. The latter rms differences become slightly greater than the control case-ice age case differences on day 74. So, while U1 and T1 rms differences between the control and ice age cases are above the noise level, V1 is rather close to the noise level (within 1 m sec^{-1}). One could therefore have more confidence in the U1, T1 results than V1 results.

In Figures 9.1, 9.2, 9.3 the plots of control (1)-perturbation (2) and ice age (3)-perturbation (4) rms differences are rather similar, there are no consistently large differences between the dashed and dotted lines. The control case (5)-ice age case (3) rms differences are in each diagram greater than the control (1)-perturbation (2) differences. Since the latter differences were only available for the variables T, U, V, it is assumed in the next section that the ice age case (3)-perturbed ice age case (4) rms differences represent the noise level of the model.

Figure 9.4 illustrates the rms differences for low cloud. The rms differences within the two pairs of cases are remarkably constant with time. The rms differences between the January control case and ice age case are just less than three-tenths while those between the ice age case-perturbed ice age case are about two-tenths or a little more. The actual separation of the dashed line

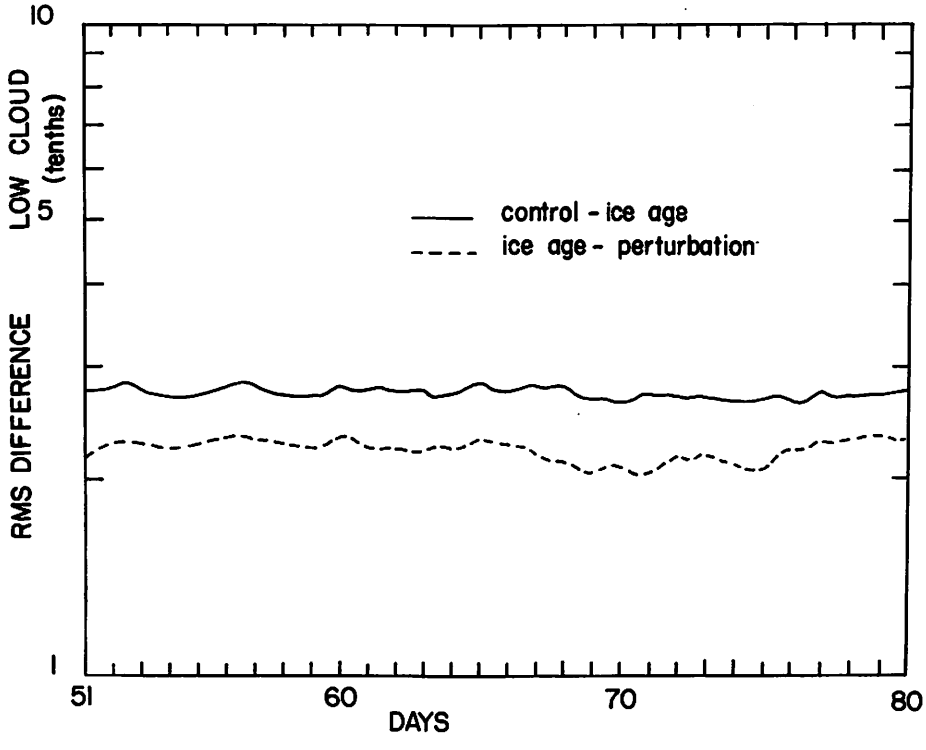

Figure 9.4. Rms differences between cases for low cloud. Solid line - differences between January control case (5) and January ice age case (3). Dashed line - difference between January ice age case (3) and perturbed January ice age case (4).

and solid line is not large (less than one-tenth) but the consistent separation suggests that the differences in low cloud between the January control case and January ice age case are greater than the noise level of the model.

In Figure 9.5 the rms differences of pressure at sea level are shown. For this variable the ice age case (3)-perturbed ice age case (4) rms differences are not much lower than those between the January control case and ice age case and actually become greater between days 62 and 66. On day 51 the rms difference between the dashed and dotted lines is almost 10 mb but elsewhere it is less than this. Figure 9.5 suggests that the control case-ice age case differences in pressure are not much greater than the noise level of the model. It must be pointed out however, that sea level pressure is very "noisy" near the poles because of the smaller number of grid points and consequent sampling problem (Washington, personal communication, 1974), and if rms differences were taken then probably only polar PSL changes would be close to the noise level of the GCM.

Figure 9.6 is very different from the preceding five figures. Rms differences are presented for precipitation and it is clear that there is a lot of noise in all cases with this variable. The January control case (5)-ice age case (3) rms differences are not greater than the noise level of the GCM. Precipitation is very

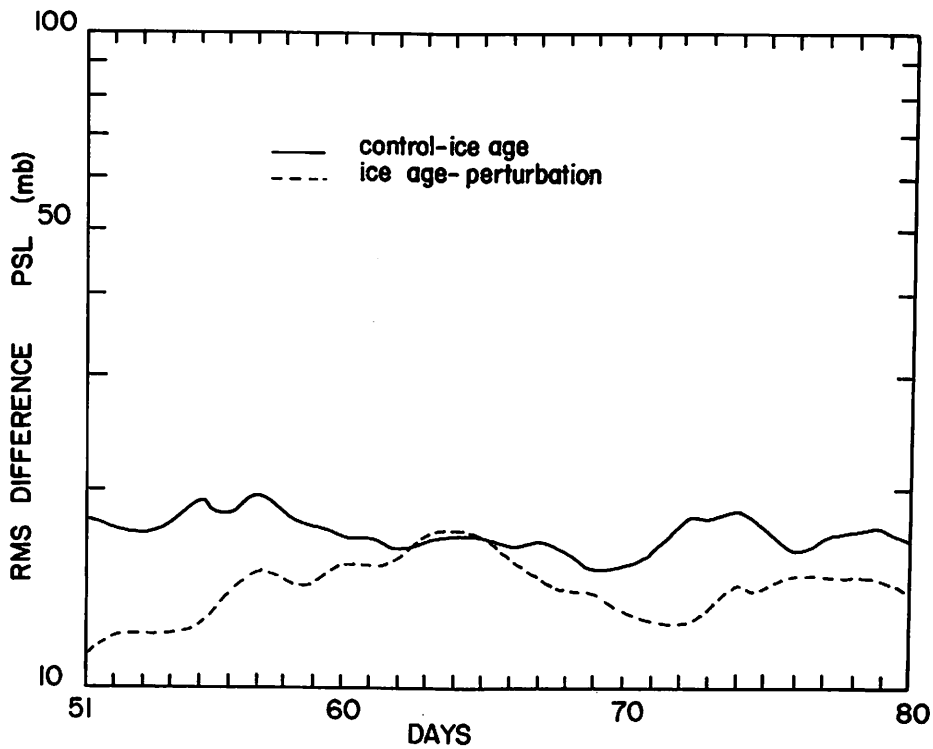

Figure 9.5. Rms differences between cases for PSL. Solid line - difference between January control case (5) and January ice age case (3). Dashed line - difference between January ice age case (3) and perturbed January ice age case (4).

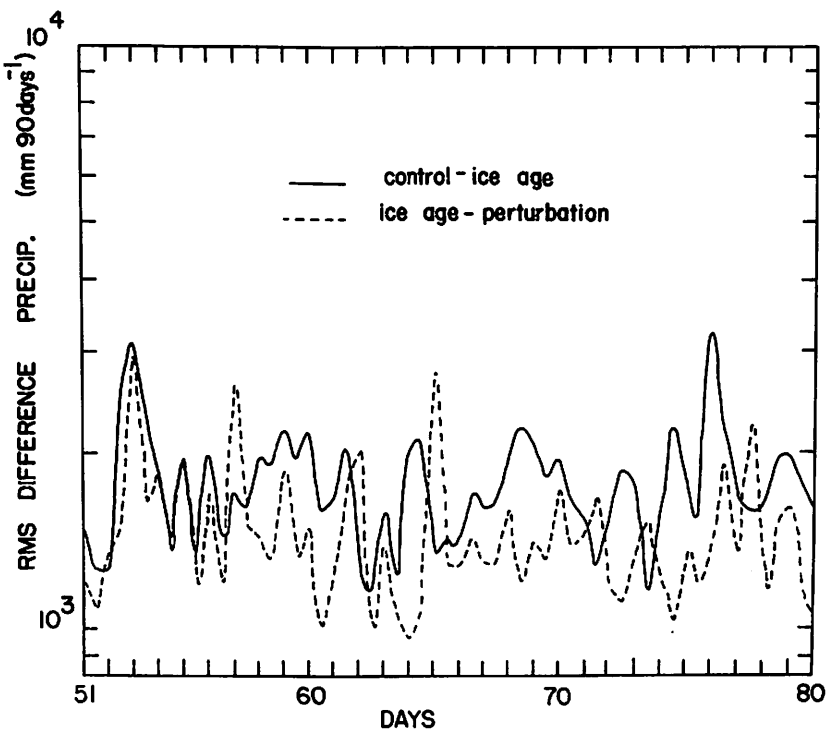

Figure 9.6. Rms differences between cases for precipitation. Solid line - difference between January control case (5) and January ice age case (3). Dashed line - difference between January ice age case (3) and perturbed January ice age case (4).

variable with time, depending on the number and location of storms, humidity and vertical velocity variations, etc.

(d) Conclusions

Rms differences between different cases have been investigated in order to examine the significance of differences between the control and ice age cases. For the variables T1, U1 and low clouds it is found that the control case-ice age case differences are above the noise level of the model. For the variables V1 and PSL the differences are only just greater than the noise level and this suggests that too much emphasis should not be placed on these variables. Precipitation is extremely "noisy" in all cases and the control case-ice age case differences are not above the noise level of the GCM.

As pointed out above, the noise level varies with latitude and with the period of time-averaging in the model, these effects are studied by Chervin and Schneider (1973). The noise level also depends on the variable under consideration, as is indicated somewhat by the six variables discussed in this chapter. Some variables such as temperature are less noisy because they are kept within bounds by the surface energy balance or some other formulation. Variables which depend upon the interaction of two or more other variables,

e.g., precipitation depends on vertical velocity and humidity, tend to be more noisy. The most significant differences between a control case and a non-random perturbation ("climate change") case will be seen in the less noisy variables such as temperature.

CHAPTER X

CONCLUSIONS

(a) Aim of the Study

Four different sets of boundary conditions have been used in the NCAR global circulation model of the atmosphere in order to investigate the response of the simulated atmospheric circulation to large changes in boundary conditions. In the January and July control cases the atmospheric circulation was simulated with the present day boundary conditions (orography, albedos and sea-surface temperatures). In the January and July ice age cases the boundary conditions represented those at the maximum of the last glacial period (about 20,000 years before present). The results of the ice age cases do not necessarily describe the atmospheric circulation at the maximum of the last glacial period, but the major and consistent differences between the present day and glacial period simulations should give at least a first idea of the direction of the changes in atmospheric circulation between the present day and the last glacial period.

This is the first time that a global model of the atmospheric circulation has been used to simulate the

circulation with glacial period boundary conditions, the results are interesting as a first estimate of the impact of large changes in orography, albedo and sea-surface temperature on the atmospheric circulation. Since the NCAR GCM includes many of the physical processes that we know are important and all the equations of motion and thermodynamics are applied together, the results should give at least as good an estimate of the glacial period maximum circulation as earlier, more empirical studies.

Basically this study is a sensitivity analysis to examine how large changes in boundary conditions affect the simulated atmospheric circulation. We should, therefore, be careful not to place too much emphasis on the differences between the control cases and observed data. On the other hand, the question of whether the ice age case results are realistic can only be answered on the basis of whether the GCM can simulate present day climate realistically in the first place.

(b) Some Interesting Results

Earlier studies have commonly concluded that the winds were stronger and that winds and storm tracks were forced south of the ice sheets during a glacial period. According to the GCM results the strength of the jet streams is not stronger at all longitudes in the ice age cases compared with the control cases. Also, the storm tracks and particularly the winds are not forced south to

skirt the ice sheets. However, in support of earlier common conclusions the study does show: air temperatures in the July ice age case more like those of winter of the present day; Icelandic low shifted southward in January ice age case; pressure distribution more meridional in January ice age case; intensified Hadley cell in tropics; transient cyclone activity greater over Atlantic in both ice age cases.

At 1.5 km in the model atmosphere the temperature gradient between equator and pole increased from the control to the ice age cases at nearly all latitudes. At 10.5 km in the model atmosphere, temperature gradients decreased in the ice age cases. Based on global averages of eddy kinetic energy we find that baroclinicity decreased in the July ice age case but slightly increased in the January ice age case.

Meridional cross sections of the east-west component of the wind and pressure and temperature distributions at about 200 mb indicate that the northern hemisphere summer monsoon is simulated in the July control case but not in the July ice age case. This feature has also been suggested on the basis of geological evidence. The absence of the monsoon, due to the elimination of land/sea heating contrasts, has important effects upon global energetics.

Recent geological and biological evidence has suggested that earlier theories of "glacial-pluvial

synchrony" should be rejected in favor of the theory of ice age aridity. In both January and July cases, the amount and vertical and latitudinal extents of water vapor in the atmosphere are less in the ice age cases than in the control cases. The ice age case meridional and vertical transports of water vapor by the mean circulation and eddies are weaker except in the tropics in January, where transports by the mean circulation are stronger than in the control case.

For both January and July ice age cases, solar radiation absorbed in the troposphere is less than that computed for the control cases. The January ice age case atmosphere has lower net heating than the control case in the northern hemisphere. In the July ice age case the atmospheric net heating is much less than that in the control case in the northern hemisphere. In the southern hemisphere the July ice age net heating is greater than that in the control case between 5°S and 35°S and not much different elsewhere. The ice age case transports of sensible heat differ considerably from those in the control cases.

In the January cases, the differences in global mean zonal and eddy kinetic energy between the control and ice age cases are not great. In the July cases, the global mean zonal kinetic energy is much greater in the ice age case than the control case, while global mean eddy kinetic energy is much less in the ice age case

than in the control case. Zonal potential energy is not very different between the four cases. Zonal internal energy is larger in the control cases than the ice age cases since atmospheric temperature is also larger in the control cases. Differences in kinetic energy in the July cases are due to the monsoon and baroclinicity differences.

Rms differences between different cases (including two "random error" experiments) have been investigated in order to discuss the significance of differences between the control and ice age cases. For the variables temperature at 3 km, east-west component of the wind at 3 km, and low cloud, it is found that the control case-ice age case differences are above the noise level of the model. For the variables north-south component of the wind and pressure at sea level, the differences between the ice age case and control case are only just above the noise level and this suggests that too much emphasis should not be put upon these variables. Precipitation is extremely "noisy" in all cases and the control case-ice age case differences are not above the noise level of the GCM.

(c) Problems Encountered in this Study and Some Suggestions for Future Work

In Chapter VIII certain model-dependent and data-dependent problems are described. These included

such topics as the treatment of physical processes at the earth's surface; cloud formulation in the model; horizontal grid resolutions; evaluation of torques on the atmosphere; and the lack of observed data, especially of precipitation and for evaluation of fluxes of heat, moisture and momentum.

The model-dependent problems are in general not too difficult and can be taken into account in the interpretation of the results. Many of them are also removable and recent versions of the NCAR GCM have added such improvements as a finer grid, soil moisture and snow cover computations. The observed data-dependent problems generally mean that the GCM control case data cannot be evaluated. In the future, satellite and increased network data should remove much of this problem.

Model- and data-dependent problems such as those described above and in Chapter VIII will be common to all studies involving the GCM. The major shortcoming of the available models with respect to studies such as the present one is that an atmospheric model is <u>not</u> a climate model, since ocean surface temperatures are specified rather than computed. Given the ocean surface temperatures, the model can compute the global circulation (within the limitations of the model). Only if an ocean model were successfully coupled with the atmospheric

model could we study the influence on climate of large changes in boundary conditions. However, not only are the observations of the oceans even poorer than those of the atmosphere but both the modelling of the general ocean circulation and the coupling of an ocean model to the atmosphere are going to be difficult. However there is the possibility that in some years from the present, a joint atmosphere-ocean model could be used for the type of sensitivity experiment described in this study. There is also the possibility that "climate models," in which many processes are parameterized so that it becomes feasible to run experiments for hundreds of years of model time (instead of the present 80 days per experiment), can be used, together with our knowledge of past boundary conditions, to investigate climatic change. Results of the present study could therefore become "observed data" for comparison with the results of less explicit climate models.

For the purposes of the present type of study, in the absence of more sophisticated types of model, there are still necessary areas of research. Firstly, there is presently a lack of compiled data on conditions at the maximum of the last glacial period. Geological and biological evidence is scattered in many journals and books and there is a need for the evidence on say winds, precipitation and temperatures at the maximum of the last

glacial period to be compiled and mapped. This information would enable the evaluation of results from "ice age cases." Likewise, more information is needed on the glacial maximum ocean circulation and ocean surface temperatures. These data would be useful both as input to models and for comparison with the results. Analysis of the results of the present study suggests that the Gulf Stream transport was weakened at the maximum of the last glacial period; more information is needed for other oceans.

Two further possibilities for future research also arise out of the present study. Firstly, the question of whether the differences between the ice age cases and control cases are a result of changes in thermal or orographic forcing can be examined. Secondly, it is clear that statistical methods must be developed so that the differences between numerical "climate change" experiments can be objectively tested for significance.

This is the first time that a global model of the atmospheric circulation has been used to investigate the influence of glacial period boundary conditions on the atmospheric circulation and although the approach will no doubt be used again with more sophisticated models and better input data, the results of this study are a first estimate of the likely direction of changes between the present day and glacial period atmospheric circulations.

BIBLIOGRAPHY

Adem, J., 1968, A parametric method for computing the mean water budget of the atmosphere. Tellus, 20, pp. 621-632.

Alyea, F. N., 1972, Numerical simulation of an ice age paleoclimate. Atmospheric Science Paper, No. 193, Dept. Atmos. Science, Colorado State University, Colorado, 120 pp.

Andrews, J. T., 1970, A geomorphological study of post-glacial uplift with particular reference to Arctic Canada. Institute of British Geographers, Special Publication No. 2, 156 pp.

Barry, R. G., 1973, The conditions favoring glacierization and deglacierization in North America from a climatological viewpoint. Arctic and Alpine Research, 5, pp. 171-184.

Barry, R. G. and Williams, Jill, 1973, Experiments with the NCAR global circulation model using glacial maximum boundary conditions: Southern Hemisphere results and interhemispheric comparison. Paper presented at INQUA congress, New Zealand, December, 1973.

Beaty, C. B., 1971, Climatic Change: some doubts. Geol. Soc. Amer. Bull., 82, pp. 1395-1398.

Bolin, B., 1950, On the influence of the earth's orography on the general character of the westerlies. Tellus, 2, pp. 185-195.

Bonatti, E., 1966, North Mediterranean climate during the last Würm glaciation. Nature, 209, pp. 984-985.

Bonatti, E. and Gartner, S., 1973, Caribbean climate during Pleistocene ice ages. EOS, 54, p. 327.

Brinkmann, W. A. R., 1973, A climatological study of strong downslope winds in the Boulder area. INSTAAR Occas. Paper No. 7, 228 pp.

Brinkmann, W. A. R. and Barry, R. G., 1972, Palaeoclimatological aspects of the synoptic climatology of Keewatin, Northwest Territories, Canada. Palaeogeog., Palaeoclimatol., Palaeoecol., 11, pp. 77-91.

Brooks, C. E. P. and Hunt, T., 1930, The zonal distribution of rainfall over the earth. Mem. Roy. Meteor. Soc., 3. No. 28, pp. 129-157.

Bryan, K. and Cady, R. C., 1934, The Pleistocene climate of Bermuda. American Jour. Sci., 27, pp. 241-264.

Büdel, J., 1959, The "periglacial"-morphologic effects of the Pleistocene climate over the entire world. International Geol. Review, 1, pp. 1-16.

Charlesworth, J. K., 1957, The Quaternary Era. Volume II. London, Edward Arnold, 1700 pp.

Charney, J. G. and Eliassen, A., 1949, A numerical model for predicting the perturbations of the middle latitude westerlies. Tellus, 1, pp. 38-54.

Chervin, R. M. and Schneider, S. H., 1973, Effect of time-averaging on the noise level of climatological statistics generated by the NCAR general circulation model (GCM). Bull. Amer. Meteor. Soc., 54, p. 743.

Coope, A. R., Morgan, A. and Osborne, P. J., 1971, Fossil Coloeptera as indicators of climatic fluctuations during the last glaciation in Britain. Palaeogeog., Palaeoclimatol., Palaeoecol., 10, pp. 87-101.

Cressman, G. P., 1960, Improved terrain effects in barotropic forecasts. Mon. Wea. Rev., 88, pp. 327-342.

Crutcher, H. L. and Meserve, J. M., 1970, Selected level heights, temperatures and dew points for the Northern Hemisphere. NAVAIR 50-1C-52. Revised, Naval Weather Service Command, Washington, D. C.

Damuth, J. E. and Fairbridge, R. W., 1970, Equatorial Atlantic deep sea arkosic sands and ice age aridity in tropical South America. Geol. Soc. Amer. Bull., 81, pp. 189-206.

Davis, P. A., 1963, An analysis of the atmospheric heat budget. J. Atmos. Sci., 20, pp. 5-22.

Davis, P. A., 1971, Analysis of the global atmospheric heat budget and the applicability of satellite data. Proc. Miami Workshop on Remote Sensing, Atlantic Oceanogr. Meteor. Labs., NOAA, pp. 85-98.

Delsol, F., Miyakoda, K., and Clarke, R. H., 1971, Parameterized processes in the surface boundary layer of an atmospheric circulation model. Quart. J. Roy. Meteor. Soc., 97, pp. 181-208.

Döös, B. R., 1969, The influence of the large scale heat sources on the dynamics of the ultra-long waves. Tellus, 21, pp. 25-39.

Dopplick, T. G., 1970, Global radiative heating of the earth's atmosphere. MIT, Dept. Meteor., Planetary circulations project, Report No. 24.

Dutton, J. A. and Johnson, D. R., 1967, The theory of available potential energy and a variation approach to atmospheric energetics. Advances in Geophys., 12, Academic Press, New York, pp. 333-436.

Elsasser, H. W., 1969, A climatology of epsilon (atmospheric dissipation). Mon. Wea. Rev., 97, pp. 415-423.

Emiliani, C., 1971, The amplitude of Pleistocene climatic cycles at low latitudes and the isotopic composition of glacial ice. In, "Late Cenozoic Glacial Ages," Ed. K. K. Turekian, pp. 183-198.

Fairbridge, R. W., 1964, African ice-age aridity. In, "Problems in Palaeoclimatology," Ed. A. E. M. Nairn, Interscience, pp. 356-359.

Fairbridge, R. W., 1970, World paleoclimatology of the Quaternary. Rev. de Geog. Phys. et de Geol. Dynam., 12, pp. 97-104.

Fairbridge, R. W., Climatology of a glacial cycle. Quaternary Research, 2, pp. 283-302.

Flint, R. F., 1971, Glacial and Quaternary geology. John Wiley & Sons, New York, 892 pp.

Flohn, V. H., 1953, Studien über die atmosphärische Zirculation in der letzten Eiszeit, Erdkunde, 7, pp. 266-275.

Flohn, V. H., 1969, Ein Geophysicalisches Eiszeit-Modell. Eiszeitalter und Gegenwart, 20, pp. 204-231.

Frenzel, B., 1968, The Pleistocene vegetation of Northern Eurasia. Science, 161, pp. 637-648.

Frenzel, B. and Troll, C., 1952, Die Vegetationszonen des nordlichen Eurasiens wahrend der letzten Eiszeit. Eiszeitalter und Gegenwart, 2, pp. 154-167.

Gabites, J. F., 1950, Seasonal variations in the atmospheric heat balance. Sc.D. thesis, Dept. of Meteor., MIT, 96 pp.

Galloway, R. W., 1965, Late Quaternary climates in Australia. J. Geol., 73, pp. 603-648.

Galloway, R. W., 1970, The full-glacial climate in the southwestern United States. Annals Amer. Assoc. Geog., 60, pp. 245-256.

Gandin, L. S., 1965, Objective analysis of meteorological fields. U. S. Dept. Commerce, 242 pp.

Grove, A. T., 1968, The last 20,000 years in the tropics. British Geomorph. Research Group Occas. Paper No. 5, pp. 51-62.

Hare, F. K., 1953, Two pictures of the recent past. Arctic, 6, pp. 58-60.

Hellerman, S., 1967, An updated estimate of the wind stress on the world ocean. Mon. Wea. Rev., 95, pp. 607-626.

Holloway, J. L. and Manabe, S., 1971, Simulation of climate by a global general circulation model. Mon. Wea. Rev., 99, pp. 335-370.

Holopainen, E. O., 1963, On the dissipation of kinetic energy in the atmosphere. Tellus, 15, pp. 26-32.

Holopainen, E. O., 1965, On the role of mean meridional circulations in the energy balance of the atmosphere. Tellus, 17, pp. 285-294.

Houghton, D. D., Kutzbach, J. E., McClintock, M. and Suchman, D., 1973, Response of a general circulation model to a sea temperature perturbation. To be published in J. Atmos. Sci.

Jeffreys, H., 1926, On the dynamics of geostrophic winds, Quart. J. Roy. Meteor. Soc., 52, pp. 85-104.

Jao, Z-K, 1972, The mountain torque, In, "The general circulation of the tropical atmosphere. Volume I," by Newell et al., pp. 151-153.

Joshi, R., 1969, The characteristics of the Pleistocene climatic events in the Indian sub-continent. A land of monsoon climate. Études sur le Quaternaire dans le monde. VIII Congrès, INQUA, Paris, 1969.

Kasahara, A. and Washington, W. M., 1967, NCAR global general circulation model of the atmosphere. Mon. Wea. Rev., 95, pp. 389-402.

Kasahara, A. and Washington, W. M., 1968, Thermal and dynamical effects of orography on the general circulation of the atmosphere. Proc. WMO/IUGG Symp. Numerical Weather Prediction, Japan Meteorological Agency, Tokyo, IV47-IV56.

Kasahara, A. and Washington, W. M., 1971, General circulation experiments with a six layer NCAR model, including orography, cloudiness and surface temperature calculations. J. Atmos. Sci., 28, pp. 657-701.

Kasahara, A., Sasamori, T., and Washington, W. M., 1973, Simulation experiments with a twelve layer stratospheric global circulation model. I. Dynamical effect of the earth's orography and thermal influence of continentality. J. Atmos. Sci., 30, pp. 1229-1251.

Katayama, A., 1967, On the radiation budget of the troposphere over the northern hemisphere. II. Hemispheric distribution. J. Meteor. Soc. Japan, 45, pp. 1-25.

Kidson, J. W., Vincent, D. G. and Newell, R. E., 1969, Observational studies of the general circulation of the tropics, long term mean values. Quart. J. Roy. Meteor. Soc., 95, pp. 258-287.

Kraus, E. B., 1960, Synoptic and dynamic aspects of climate change. Quart. J. Roy. Meteor. Soc., 86, pp. 1-15.

Kraus, E. B., 1973, Comparison between ice age and present general circulations. Nature, 245, pp. 129-133.

Krishnamurti, T. N., 1971a, Observational study of the tropical upper tropospheric motion field during the northern hemisphere summer. J. Appl. Meteor., 10, pp. 1066-1096.

Krishnamurti, T. N., 1971b, Tropical east-west circulations during the northern summer. J. Atmos. Sci., 28, pp. 1342-1347.

Krishnamurti, T. N., Daggupaty, S. M., Fein, J., Kanamitsu, M. and Lee, J. D., 1973a. Tibetan high and upper tropospheric tropical circulations during the northern summer. Bull. Amer. Meteor. Soc., 54, pp. 1234-1249.

Krishnamurti, T. N., Kanamitsu, M., Koss, W. J., and Lee, J. D., 1973b. Tropical east-west circulations during the northern winter. J. Atmos. Sci., 30, pp. 780-787.

Kung, E. C., 1963, Climatology of aerodynamic roughness parameter and energy dissipation in the planetary boundary layer of the northern hemisphere. Annual Report, Contract DA-36-039-AMC-00878, Dept. of Meteor., Univ. Wisconsin, pp. 37-96.

Kung, E. C., 1966, Kinetic energy generation and dissipation in the large scale atmospheric circulation. Mon. Wea. Rev., 94, pp. 67-82.

Kung, E. C., 1967, Diurnal and long-term variations of the kinetic energy generation and dissipation for a five-year period. Mon. Wea. Rev., 95, pp. 593-606.

Kung, E. C., 1968, On the momentum exchange between the atmosphere and earth over the northern hemisphere. Mon. Wea. Rev., 96, pp. 337-341.

Kung, E. C., 1969, Further study on the kinetic energy balance. Mon. Wea. Rev., 97, pp. 573-581.

Laevastu, T., Clarke, L. and Wolff, P. M., 1969, Oceanic part of the hydrological cycle. WMO/IHD Projects Report No. 11, Geneva, 71 pp.

Lamb, H. H., 1961, Fundamentals of climate. In, "Descriptive Palaeoclimatology," Ed., A. E. M. Nairn, Interscience, New York, pp. 8-44.

Lamb, H. H., 1971, Climates and circulation regimes developed over the northern hemisphere during and since the last Ice Age. Palaeogeog. Palaeoclimatol. Palaeoecol., 10, pp. 125-162.

Lamb, H. H., Lewis, R. P. W., and Woodroffe, A., 1966, Atmospheric circulation and the main climatic variables. Proc. International Symp. on World Climate 8000-0 BC. Roy. Meteor. Soc., London, pp. 174-217.

Lamb, H. H. and Woodroffe, A., 1970, Atmospheric circulation during the last ice age. Quaternary Research, 1, pp. 29-58.

Leith, C. E., 1973, The standard error of time-average estimates of climatic means. J. Appl. Meteor., 12, pp. 1066-1069.

Lilly, D. K., 1972, Wave momentum flux - a GARP problem. Bull. Amer. Meteor. Soc., 53, pp. 17-23.

Loewe, F., 1971, Considerations on the origin of the Quaternary ice sheet of North America, Arctic and Alpine Research, 3, pp. 331-345.

Lorenz, E. N., 1955, Available potential energy and the maintenance of the general circulation. Tellus, 7, pp. 157-167.

Lorenz, E. N., 1967, The nature and theory of the general circulation of the atmosphere. WMO, No. 218.TP. 115.

London, J., 1953, The distribution of infrared cooling for winter and summer seasons. Proc. Toronto Meteor. Conf. Roy. Meteor. Soc., pp. 60-67.

London, J., 1957, A study of the atmospheric heat balance. College of Engineering, New York Univ., Final Report, Contract AF-19-(122)-165.

MacCracken, M. D., 1970, Test of ice age theories using a zonal atmospheric model. Lawrence Radiation Laboratory, UCRL-72803, Livermore, California, 58 pp.

Malkus, J. S., Interchange of properties between sea and air. Large scale interactions. In, "The Sea," Ed. M. N. Hill, Wiley, New York, pp. 88-294.

Manabe, S. and Bryan, K., 1969, Climate calculations with a combined ocean-atmosphere model. J. Atmos. Sci., 26, pp. 786-789.

Manabe, S., Holloway, J. H. and Stone, H. N., 1970a, Tropical circulation in a time integration of a global model of the atmosphere. J. Atmos. Sci., 27, pp. 580-613.

Manabe, S. and Smagorinsky, J., 1967, Simulated climatology of a general circulation model with a hydrologic cycle. II. Analysis of the tropical atmosphere. Mon. Wea. Rev., 95, pp. 155-169.

Manabe, S., Smagorinsky, J., Holloway, J. L., Stone, H. M., 1970b, Simulated climatology of a general circulation model with a hydrologic cycle. III. Effects of increased horizontal computational resolution. Mon. Wea. Rev., 98, pp. 175-212.

Mather, J. R., 1954, The present climatic fluctuation and its bearing on a reconstruction of Pleistocene climatic conditions. Tellus, 6, pp. 287-301.

McIntyre, A., 1967, Coccoliths as paleoclimatic indicators of Pleistocene glaciations. Science, 158, pp. 1314-1317.

Miyakoda, K., Smagorinsky, J., Strickler, R. F. and Hembree, G. D., 1969, Experimental extended predictions with a nine-level hemispheric model. Mon. Wea. Rev., 97, pp. 1-76.

Möller, F., 1951, Vierteljahrskarten des Niederschlags für die ganze Erde. Petermann's Geograph. Mitt., 95, pp. 1-7.

Morrison, R. B., 1965, Quaternary geology of the Great Basin. In, "The Quaternary Geology of the United States," Ed. H. E. Wright and D. G. Frey, Princeton Univ. Press, pp. 265-286.

Mügge, R. and Müller, F., 1932, Zur Berechnung von Stralungströmen und temperaturänderungen in Atmosphären von beliebigem Aufbau. Z. Geophys., 8, pp. 53-64.

Murakami, T., 1967, Vertical transfer of energy due to stationary disturbances induced by topography and diabatic heat sources and sinks. J. Meteor. Soc. Japan., 45, pp. 205-231.

Newell, R. E., 1973, Climate and the Galapagos islands, Nature, 245, pp. 91-92.

Newell, R. E., Kidson, J. W., Vincent, D. G., and Boer, G. J., 1972, The general circulation of the tropical atmosphere. Volume I. MIT Press, Cambridge, Mass., 258 pp.

Newell, R. E., Vincent, D. G., Dopplick, T. G., Ferruzza, D., Kidson, J. W., 1970, The energy balance of the global atmosphere. In, "The global circulation of the atmosphere," Ed. G. A. Corby, London, Roy. Meteor. Soc., pp. 42-90.

Newton, C. W., 1971a, Mountain torques in the global angular momentum balance. J. Atmos. Sci., 28, pp. 623-628.

Newton, C. W., 1971b, Global angular momentum balance: Earth torques and atmospheric fluxes. J. Atmos. Sci., 28, pp. 1329-1341.

Newton, C. W., 1972, Southern hemisphere general circulation in relation to global energy and momentum balance requirements. Meteor. Monogr., 13, No. 35, pp. 215-246.

Obasi, G. O. P., 1963, Atmospheric momentum and energy calculations for the southern hemisphere during the IGY, Scientific Report, No. 6, MIT.

Oliger, J. E., Wellck, R. E., Kasahara, A. and Washington, W. M., 1970, Description of NCAR global circulation model, NCAR-TN/STR - 56. NCAR, Boulder, 94 pp.

Oort, A. H., 1964, On estimates of the atmospheric energy cycle. Mon. Wea. Rev., 92, pp. 483-493.

Oort, A. H. and Rasmusson, E. M., 1970, On the annual variation of the monthly mean meridional circulation. Mon. Wea. Rev., 98, pp. 423-442.

Oort, A. H. and Rasmusson, E. M., 1971, Atmospheric circulation statistics. NOAA Prof. Paper 5, U. S. Dept. of Commerce, 323 pp.

Palmén, E., 1951, The role of atmospheric disturbances in the general circulation, Quart. J. Roy. Meteor. Soc., 77, pp. 337-354.

Palmén, E., 1964, General circulation of the tropics. Proc. Symp. Tropical Meteor., New Zealand Meteor. Service, Wellington, pp. 3-30.

Palmén, E., 1967, Evaluation of atmospheric moisture transport for hydrological purposes. WMO/IHD Project Report No. 1, Geneva, 63 pp.

Palmén, E. and Alaka, M. A., 1952, On the budget of angular momentum in the zone between equator and 30°N. Tellus, 4, pp. 324-331.

Palmén, E. and Newton, C. W., 1969, Atmospheric circulation systems. New York, Academic Press, 603 pp.

Peixoto, J. P., 1958, Hemispheric humidity conditions during the year 1950. Scientific Report No. 3, MIT.

Peixoto, J. P., 1960, Hemispheric temperature conditions during the year 1950. Scientific Report No. 4, MIT.

Peixoto, J. P. and Crisi, A. R., 1965, Hemispheric humidity conditions during the IGY. Scientific Report No. 6, MIT.

Pittock, A. B., 1973, Global meridional interactions in stratosphere and troposphere. Quart. J. Roy. Meteor. Soc., 99, pp. 424-437.

Rasmusson, E. M., 1972, Seasonal variation of tropical humidity parameters. In, "The general circulation of the tropical atmosphere. Volume I," Newell et al.

Rasool, S. I. and Prabhakara, C., 1965, Heat budget of the southern hemisphere. In, "Problems of atmospheric circulation, Proc. of Sixth International Space Science Symp.," London, Macmillan, pp. 76-92.

Reed, R. K. and Elliot, W. P., 1973, Precipitation at ocean weather stations in the North Pacific. J. Geophys. Res., 78, pp. 7087-7091.

Reiter, E. R., 1969, Atmospheric transport processes. Part I. Energy transfers and transformations. USAEC, 253 pp.

Rex, D. F., 1950a, Blocking action in the middle troposphere and its effect upon regional climate. I. An aerological study of blocking action. Tellus, 2, pp. 196-211.

Rex, D. F., 1950b, Blocking action in the middle troposphere and its effect upon regional climate. II. The climatology of blocking action. Tellus, 2, pp. 275-301.

Riehl, H., 1962, General atmospheric circulation of the tropics. Science, 135, pp. 13-22.

Sasamori, T., London, J. and Hoyt, D. V., 1972, Radiation budget of the southern hemisphere. Meteor. Monogr., 13(35), pp. 9-24.

Schneider, S. H., 1972, Cloudiness as a global climatic feedback mechanism: the effects on the radiation balance and surface temperature of variations in cloudiness. J. Atmos. Sci., 28, pp. 1413-1422.

Schneider, S. H. and Washington, W. M., 1973, Cloudiness as a global climatic feedback mechanism. Bull. Amer. Meteor. Soc., 54, p. 742.

Sellers, W. D., 1965, Physical climatology. The University of Chicago Press, 272 pp.

Shaw, D. M. and Donn, W. L., 1971, A thermodynamic study of Arctic Paleoclimatology. Quaternary Research, 1, pp. 175-187.

Smagorinsky, J., 1953, The dynamical influence of large scale heat sources and sinks on the quasi-stationary mean motions of the atmosphere. Quart. J. Roy. Meteor. Soc., 79, pp. 342-366.

Smagorinsky, J., 1960, On the dynamical prediction of large scale condensation by numerical methods. Physics of Precipitation, Amer. Geophys. Union, Washington, D. C., pp. 71-78.

Starr, V. P., 1954, Commentaries concerning research on the general circulation. Tellus, 6, pp. 268-272.

Starr, V. P. and White, R. M., 1951, A hemispherical study of the atmospheric angular momentum balance. Quart. J. Roy. Meteor. Soc., 77, pp. 215-225.

Sutcliffe, R. C., 1956, Water balance and the general circulation of the atmosphere. Quart. J. Roy. Meteor. Soc., 82, pp. 385-395.

Telegadas, K. and London, J., 1954, A physical model of the Northern Hemisphere troposphere for winter and summer. New York University, Sci. Rept. No. 1, Contract AF 19(122)-165, 55 pp.

Tucker, G. B., 1959, Mean meridional circulations in the atmosphere. Quart. J. Roy. Meteor. Soc., 85, pp. 209-224.

Tucker, G. B., 1961, Precipitation over the North Atlantic Ocean. Quart. J. Roy. Meteor. Soc., 87, pp. 147-158.

Tucker, G. B., 1965, The equatorial tropospheric wind regime. Quart. J. Roy. Meteor. Soc., 91, pp. 140-150.

Turekian, K. K., (Ed.), 1971, Late Cenozoic glacial ages. New Haven, Yale University Press, 606 pp.

Van Mieghem, J., 1973, Atmospheric Energetics. Oxford University Press.

Van Loon, H., 1972, Cloudiness and precipitation in the Southern Hemisphere. Meteor. Monogr., 13(35), pp. 101-112.

Viete, G., 1949, Uber die allgemeine atmosphärische Zirculation während der diluvialen Vereisungsperioden. Tellus, pp. 102-

Vincent, D. G., 1969, Seasonal changes in the global atmospheric energy balance and results for restricted regions. Ph.D. Thesis, Dept. of Meteor., MIT, 174 pp.

Vonder Haar, T. H. and Oort, A. H., 1973, New estimate of annual poleward energy transport by Northern Hemisphere Oceans. J. Phys. Oceanogr., 3, pp. 169-172.

Vonder Haar, T. H. and Suomi, V. E., 1969, Satellite observations of the earth's radiation budget. Science, 163, pp. 667-669.

Vonder Haar, T. H. and Suomi, V. E., 1971, Measurements of the earth's radiation budget from satellites during a five year period. Part I. Extended time and space means. J. Atmos. Sci., 28, pp. 305-314.

Wallace, J. M., 1972, On the general circulation of the tropics. Part I. Monsoon and synoptic scale disturbances. In, "Dynamics of the tropical atmosphere." Notes from a colloquium, Summer 1972, NCAR, Boulder, Colorado, pp. 185-201.

Warshaw, M., 1973, The statistical analysis of simulated climatic change. R-1298-DOT, Rand Corporation, Santa Monica, Calif., 95 pp.

Warshaw, M. and Rapp, R. R., 1973, An experiment on the sensitivity of a global circulation model. J. Appl. Meteor., 12, pp. 43-49.

Washington, W. M., 1971, On the role of radiation in dynamical climate simulation and numerical weather prediction. Proc. Miami Workshop on Remote Sensing, Atlantic Oceanogr. Meteor. Labs., NOAA, pp. 39-67.

Washington, W. M., 1972, Numerical climatic-change experiments: the effect of man's production of thermal energy. J. Appl. Meteor., 11, pp. 768-772.

Washington, W. M. and Kasahara, A., 1970, A January simulation experiment with the two layer version of the NCAR global circulation model. Mon. Wea. Rev., 98, pp. 559-580.

Washington, W. M., 1974, Brief description of NCAR global circulation model. Report No. 14 in GARP Publications Series.

Wellck, R. E., Kasahara, A., Washington, W. M. and De Santo, G., 1971, Effect of horizontal resolution in a finite-difference model of the general circulation. Mon. Wea. Rev., 99, pp. 673-683.

White, R. M., 1949, The role of mountains in the angular momentum balance of the atmosphere. J. Meteor., 6, pp. 353-355.

Willett, H. C., 1949, Long period fluctuations of the general circulation of the atmosphere. J. Meteor., 6, pp. 34-50.

Willett, H. C., 1950, The general circulation at the last (Würm) glacial maximum. Geog. Annaler, 32, pp. 179-187.

Williams, Jill, 1973a, An analysis of the thermal and orographic influences on mid-tropospheric pressure distributions, using GCM ice age and control cases and observed data. Unpublished manuscript, INSTAAR, Univ. of Colorado.

Williams, Jill, 1973b, An investigation of zonal variations of the wind field using GCM control case data, ice age case data and observed data. Unpublished manuscript, INSTAAR, Univ. of Colorado.

Williams, Jill and Barry, R. G., 1973, Simulation of climate at the last glacial maximum in the vicinity of the Northern Continental Ice Sheets. Paper presented at 24th Alaska Science Conference, Fairbanks, 1973.

Williams, Jill, Barry, R. G. and Washington, W. M., 1973, Simulation of the climate at the last glacial maximum using the NCAR global circulation model. Occas. Paper No. 5, INSTAAR, Univ. of Colorado, 39 pp.

Williams, Jill, Barry, R. G. and Washington, W. M., 1974, Simulation of the atmospheric circulation using the NCAR global circulation model with ice age boundary conditions. To be published in J. Appl. Meteor.

Williamson, D. L., 1973, The effect of forecast error accumulation on four dimensional data assimilation. J. Atmos. Sci., 30, pp. 537-543.

Williamson, D. L. and Kasahara, A., 1971, Adaptation of meteorological variables forced by updating. J. Atmos. Sci., 28, pp. 1313-1324.

Williamson, D. L. and Washington, W. M., 1973, On the importance of precision for short range forecasting and climate simulation. J. Appl. Met., 12, pp. 1254-1258.

APPENDICES

APPENDIX A

SYMBOLS USED IN TEXT

η_m	zonal torque due to longitudinal surface pressure differences across mountains.
η_s	zonal torque due to longitudinal component of frictional force per unit area.
θ	potential temperature.
λ	longitude, positive eastward.
ρ	density of air.
σ	$z_{k+1} - z_k/\Delta z$.
$\tau_{\lambda,s}$	longitudinal component of stress in surface boundary layer.
ϕ	latitude, positive northward.
Ω	angular velocity of earth.
a	mean radius of earth.
$C(\alpha,\beta)$	energy conversion. $C(\alpha,\beta)$ is positive if there is an energy transfer from α to β.
C_D	drag coefficient.
c_p	specific heat at constant pressure.
c_v	specific heat at constant volume.
E	rate of change of water vapor per unit mass due to vertical and horizontal diffusion of water vapor.
F	heat flux.
ΔF	flux difference between two levels.
g	acceleration due to gravity.

H	height of the earth's surface above sea level.
$\overline{I}$	zonal internal energy.
k	index for identifying levels, e.g., $k = 1$ is the lowest level, $k = 7$ is top level.
$\overline{K}$	zonal kinetic energy.
K'	eddy kinetic energy.
K_{TH}	horizontal diffusivity of sensible heat.
L	latent heat of condensation of water vapor.
m	absolute angular momentum for a unit mass.
M	rate of condensation of water vapor.
p	pressure.
P	zonal potential energy.
q	specific humidity.
Q	heating rate.
Q_{dh}	heating rate due to horizontal subgrid scale eddy diffusion.
Q_{dv}	heating rate due to vertical subgrid scale eddy diffusion.
Q_{al}	heating (cooling) due to net long wave radiation.
Q_{as}	heating due to absorption of short wave radiation in the troposphere by water vapor.
Q_c	heating due to release of latent heat by condensation of water vapor.
R	gas constant.
s	subscript denotes value of variable evaluated at lower boundary level at anemometer level.

T	temperature.
T_g	temperature at ground.
T_3	temperature at 3 km.
u	zonal horizontal velocity component.
v	meridional horizontal velocity component.
$\overline{\mathbb{V}\cdot\mathbb{F}}$	frictional dissipation of total energy.
$\hat{\mathbb{V}}\cdot\mathbb{F}$	frictional dissipation of zonal kinetic energy.
$\overline{\mathbb{V}\cdot\mathbb{F}} - \hat{\mathbb{V}}\cdot\mathbb{F}$	frictional dissipation of eddy kinetic energy.
w	vertical velocity component.
z	height, positive upward.
Δz	layers = 3 km.
z_T	top of model atmosphere.

For any variable A,

zonal mean operator $\overline{A} = \frac{1}{2\pi}\int_0^{2\pi} A\, d\lambda$, $A = \overline{A} + A''$

i.e., A" is deviation from the zonal mean

$\overline{A''} = 0$

Density weighted mean, $\hat{A} = \overline{\rho A}/\overline{\rho}$, $A = \hat{A} + A'$

i.e., A' is the deviation from the density weighted mean

$\overline{\rho A'} = 0$.

APPENDIX B

FURTHER DIAGRAMS OF INTEREST

Figure A-1. Geographical distribution of vertical velocity (w) at 3 km, between 30°N and 30°S for (a) July control case and (b) July ice age case. Positive (upward) areas shaded.

Figure A-2. 30-day mean pressure at sea level for the January control case. Areas above 1.5 km are outlined by dashed lines. (From Williams et al., 1974).

Figure A-3. As in Figure A-2 except for July control case.

Figure A-4. As in Figure A-2 except for January ice age case.

Figure A-5. As in Figure A-2 except for July ice age case.

Figure A-6. Frequency of cyclone and anticyclone centers on days 51-80 of the January control case. Circles represent cyclones and crosses anticyclones. Numbers indicate additional disturbances within a cluster. (From Williams et al., 1974)

Figure A-7. As in Figure A-6 except for January ice age case.

Figure A-8. As in Figure A-6 except for July control case.

Figure A-9. As in Figure A-6 except for July ice age case.

Figure A-10. 30-day mean ground temperature (°C x 100) contour interval is 5°C.
(a) January control case, (b) January ice age case, (c) July control case, (d) July ice age case. (From Williams and Barry, 1973).

Figure A-11. Latitude-height distribution of 30-day mean zonally averaged zonal wind component (m sec^{-1}). (a) January control case at 75°W, (b) January ice age case at 75°W, (c) January control case at 30°E, (d) January ice age case at 30°E (From Williams and Barry, 1974).

Figure A-12. As in Figure A-11 except for July cases.

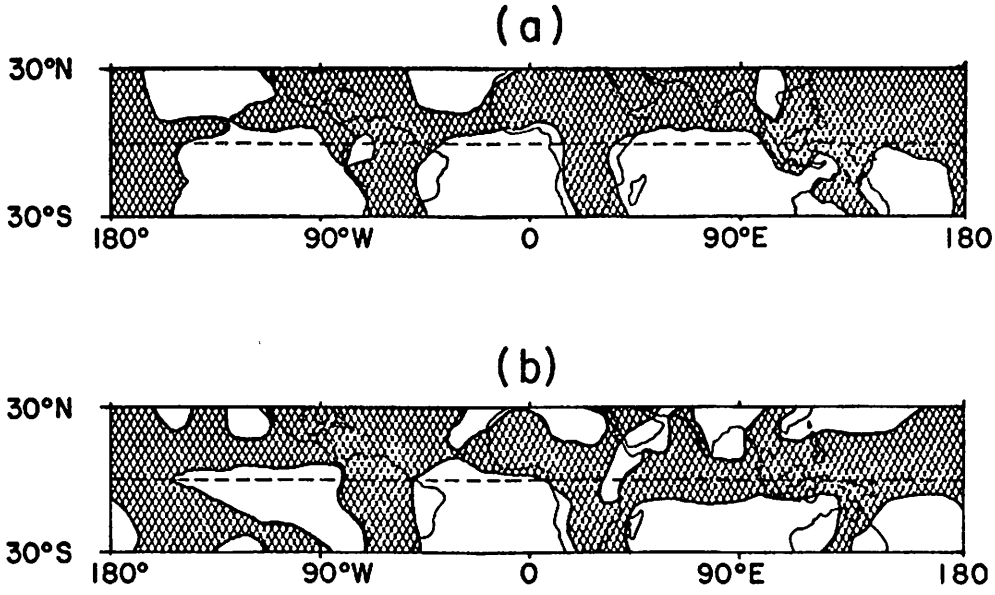

A-1

A-2

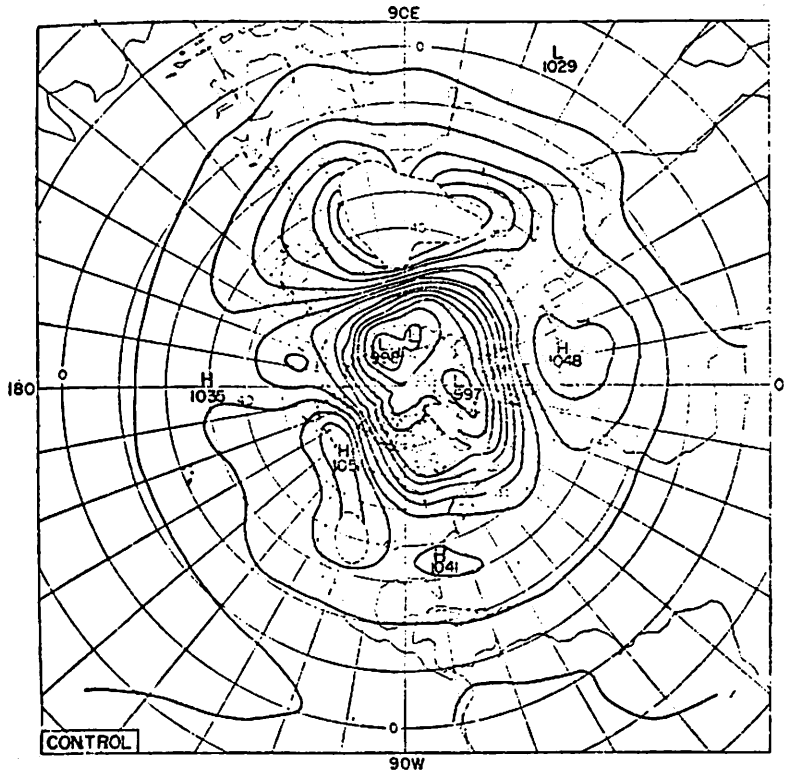
90E
0
180
0
90W
CONTROL
L
1029
H
1048
H
1035
L
997
H
1041

A-3

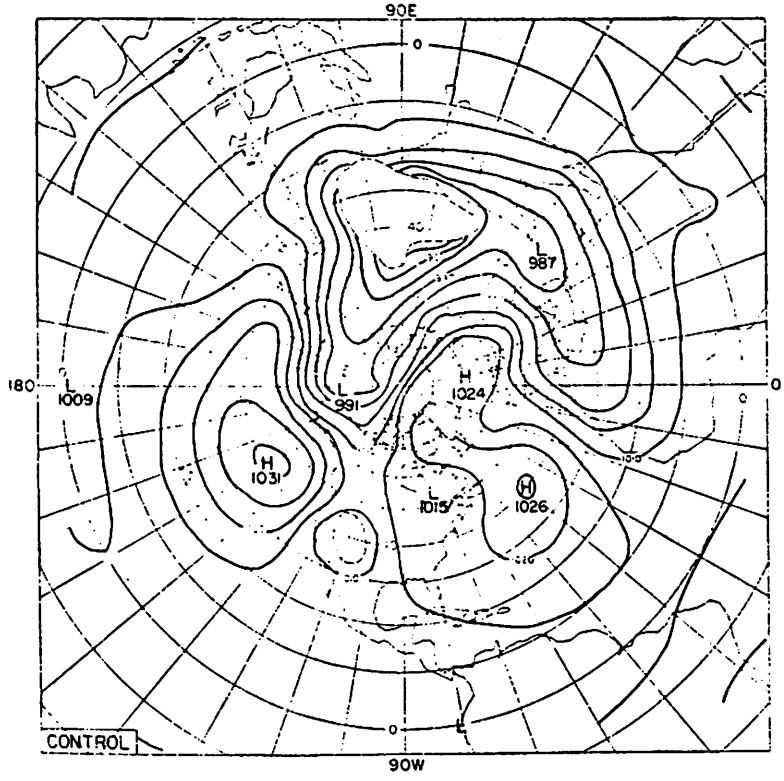
90E
0
180
0
90W
CONTROL
L
987
L
1009
L
991
H
1024
H
1031
L
1015
H
1026

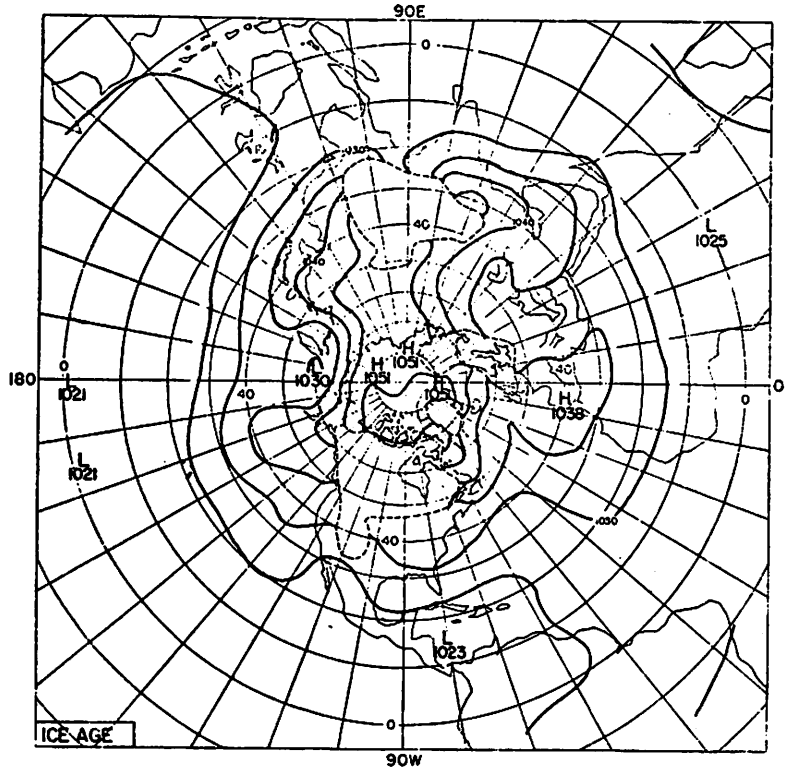
90E
0
180
0
90W
L
1025
H
1051
H
1038
L
1030
L
1021
L
1023
ICE AGE

A-4

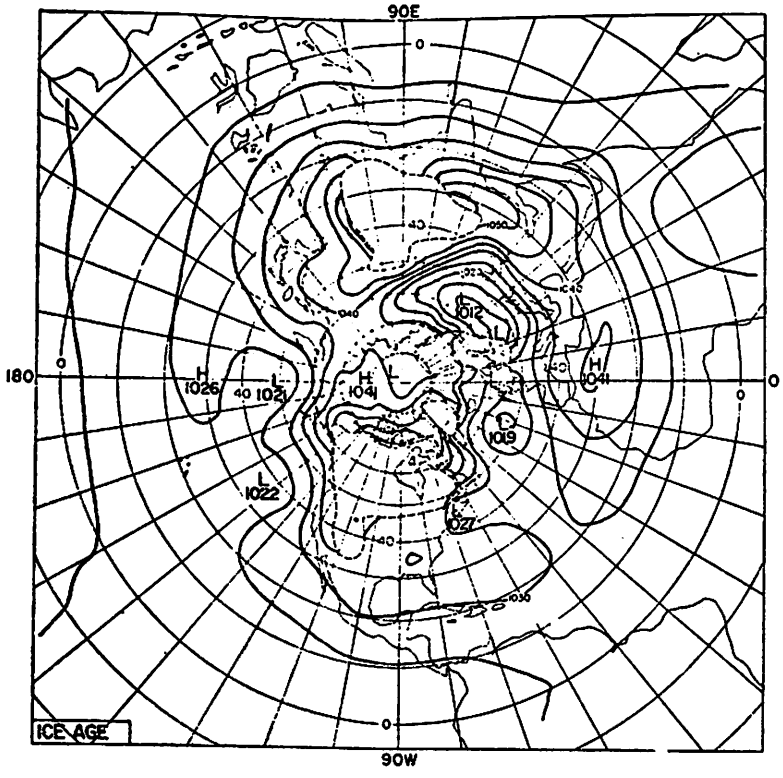
90E
0
180
0
90W
H
1026
L
1021
H
1041
H
1041
L
1022
L
1019
L
1027
ICE AGE

A-5

90N
40N
0
40S
90S
180
90W
0
90E
180

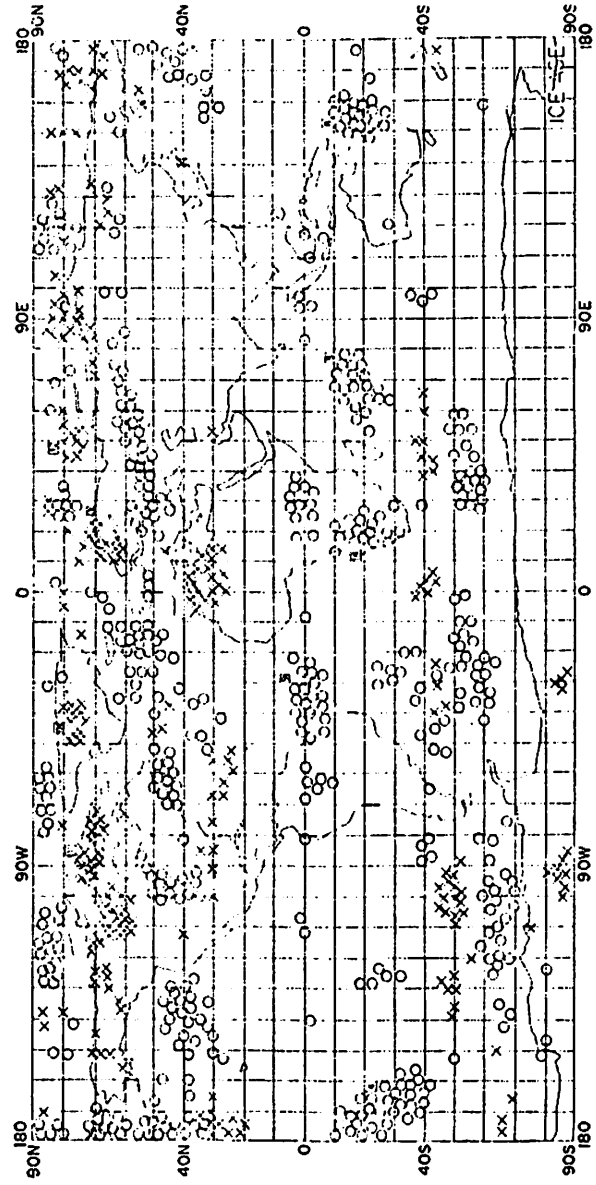
180
90N
90E
0
90W
180
90N
40N
0
40S
90S
180
ICE

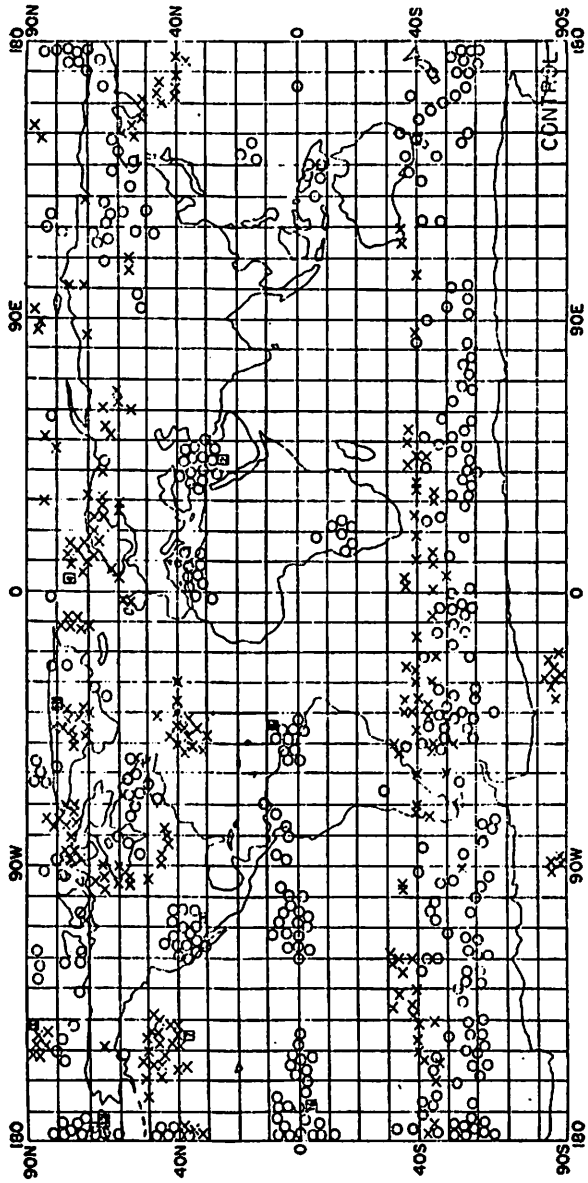
CONTROL
180
90N
40N
0
40S
90S
180
90E
0
90W
180

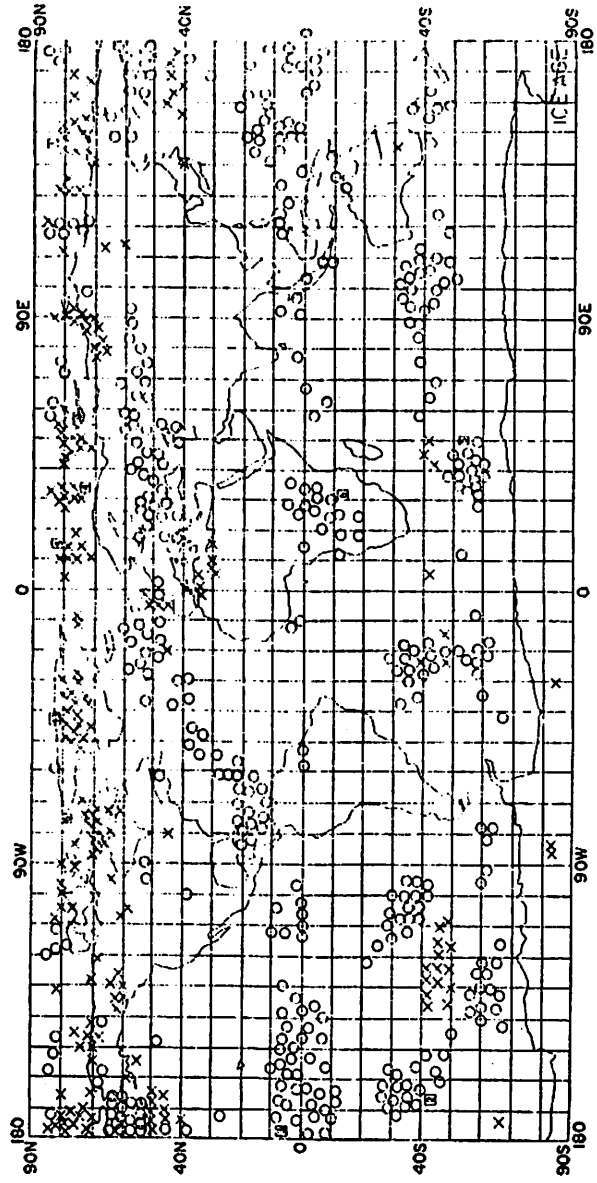
180
90N
40N
0
40S
90S
180
90E
0
90W
180
ICE EDGE

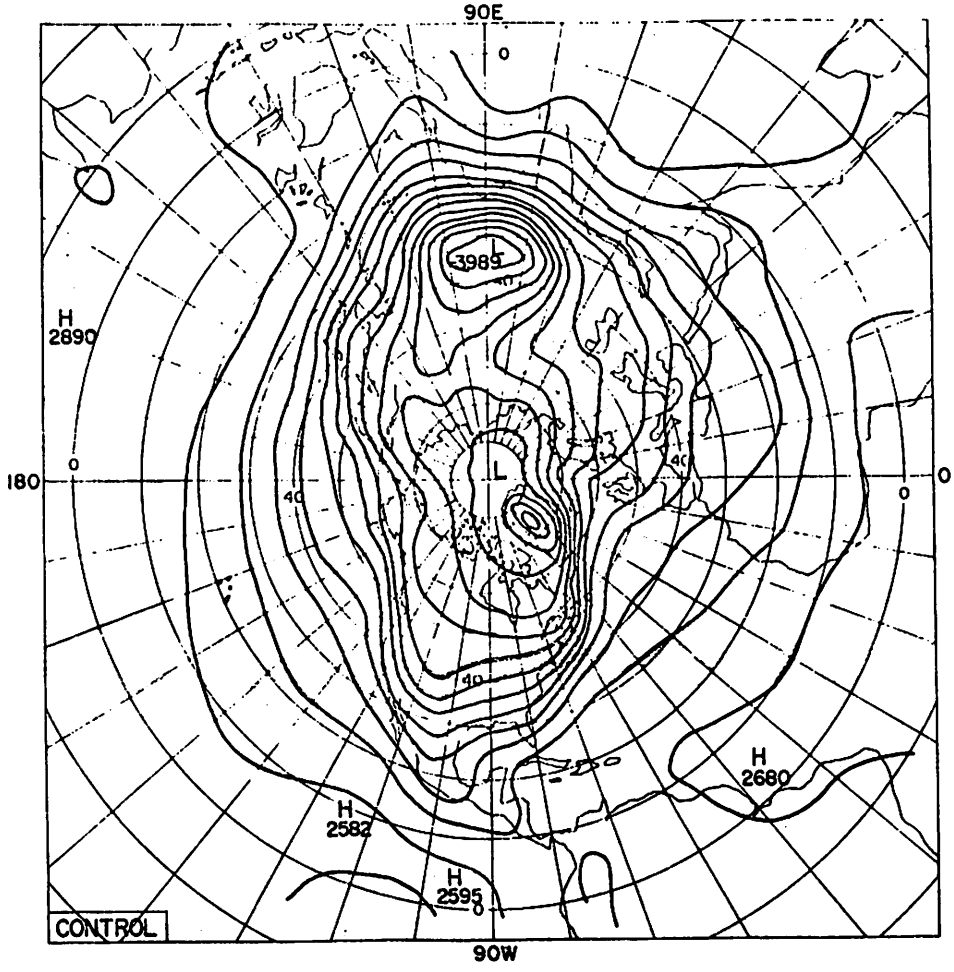
90E
0
3989
L
H
2890
180
0
40
L
40
0
0
40
H
2680
H
2582
H
2595
0
CONTROL
90W

A-10a

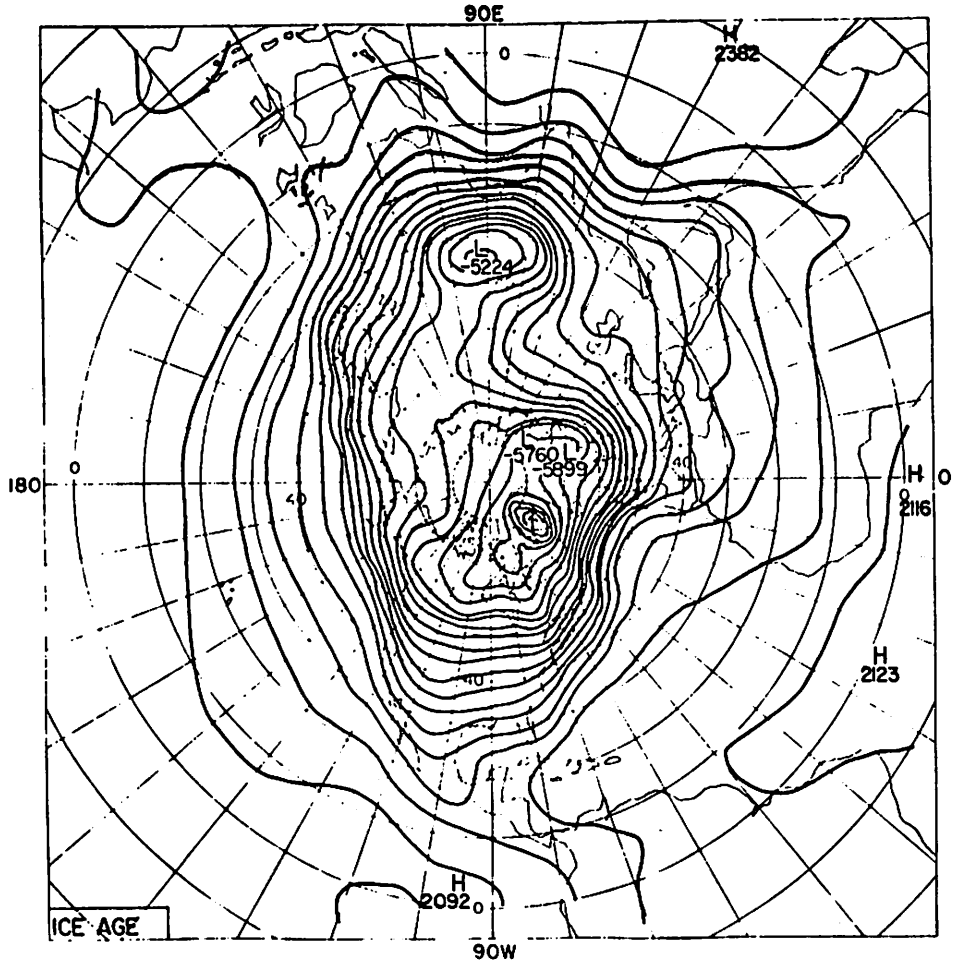
90E
0
H
2382
-5224
-5760 L
-5899
40
180
0
40
H 0
2116
H
2123
40
H
2092 0
ICE AGE
90W

A-10b

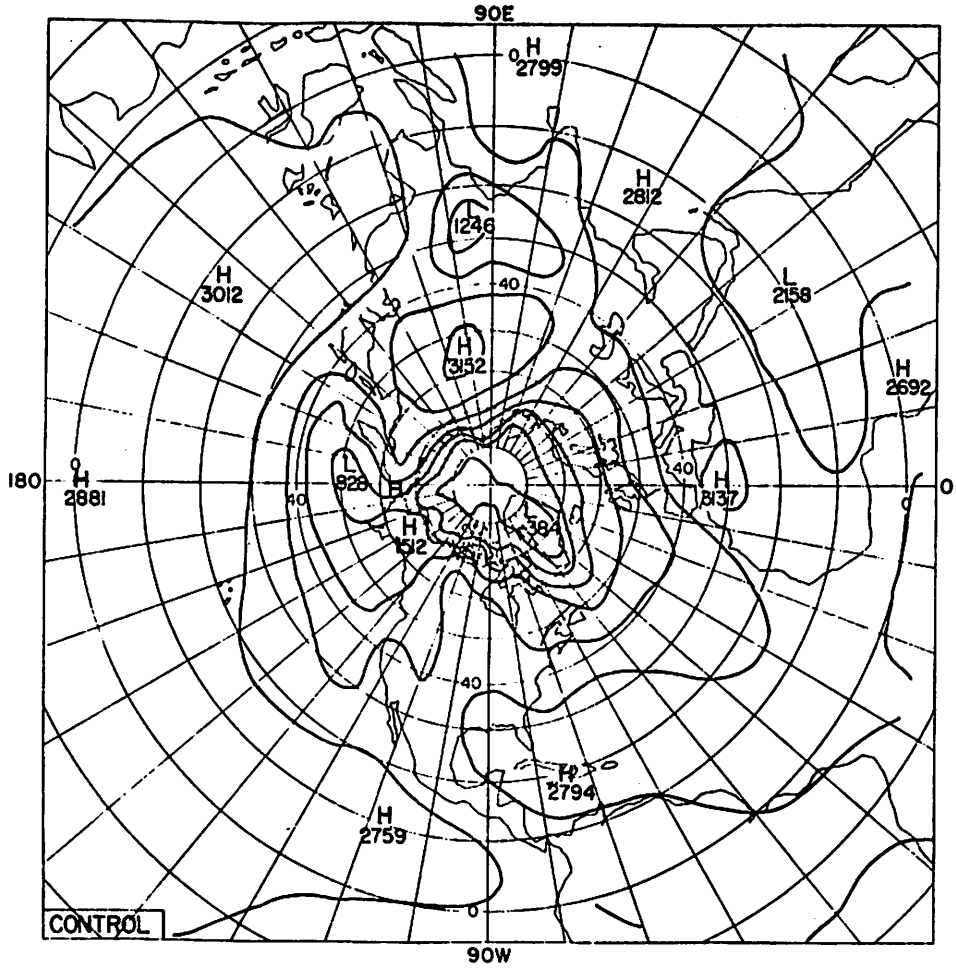
90E
H
2799
H
2812
1246
H
3012
40
L
2158
H
3152
H
2692
180
H
2881
L
829
40
H
8137
H
1512
384
40
H
2794
H
2759
0
CONTROL
90W

A-10c

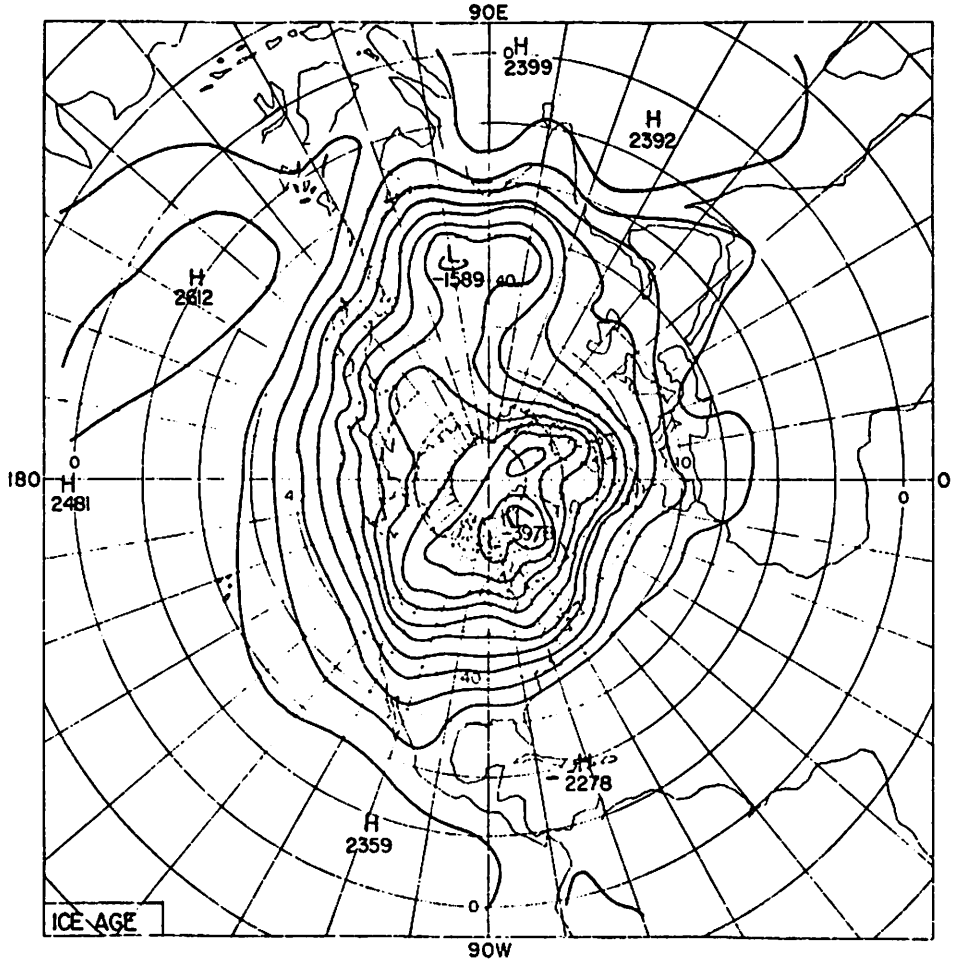
90E
H
2399
H
2392
H
2612
L
1589
180
H
2481
0
L
1971
2278
H
2359
90W
ICE AGE

A - 10d

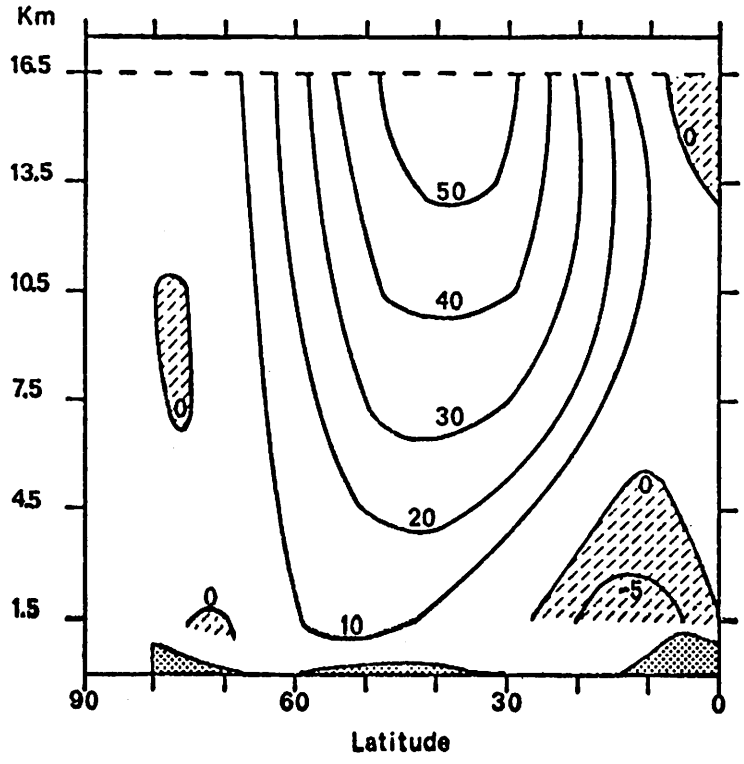
Km
16.5
13.5
10.5
7.5
4.5
1.5
50
40
30
20
10
0
-5
90
60
30
0
Latitude

A-IIa

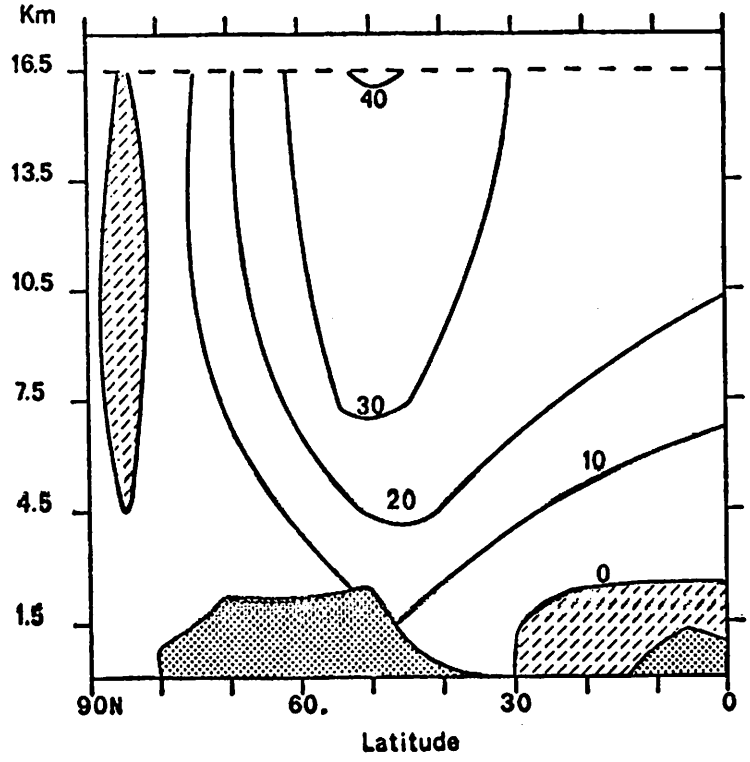
Km
16.5
13.5
10.5
7.5
4.5
1.5
40
30
20
10
0
90N
60.
30
0
Latitude

A-IIb

A-IIc

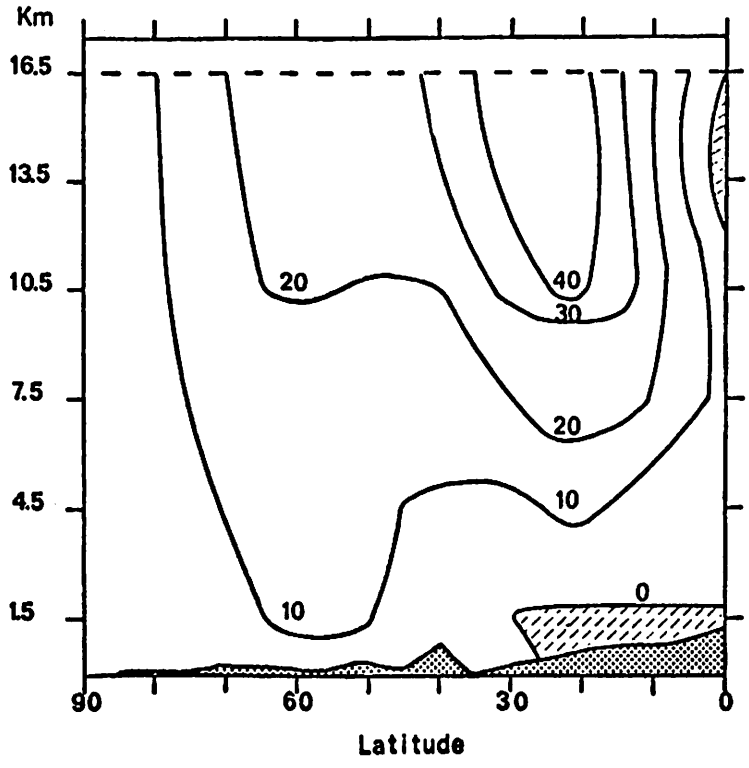
Km
16.5
13.5
10.5
7.5
4.5
1.5
20
40
30
20
10
10
0
90
60
30
0
Latitude

A-IId

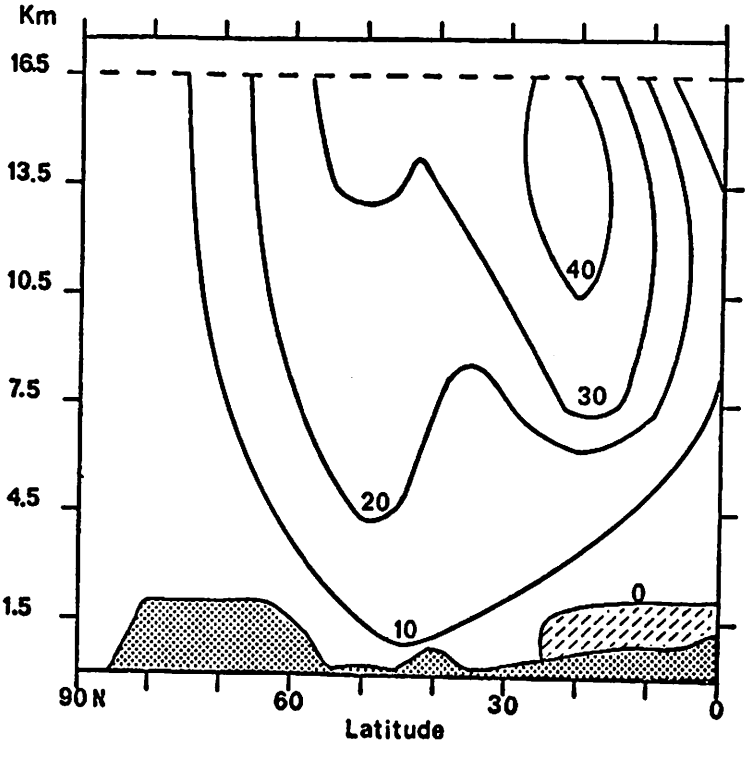
Km
16.5
13.5
10.5
7.5
4.5
1.5
40
30
20
10
0
90 N
60
30
0
Latitude

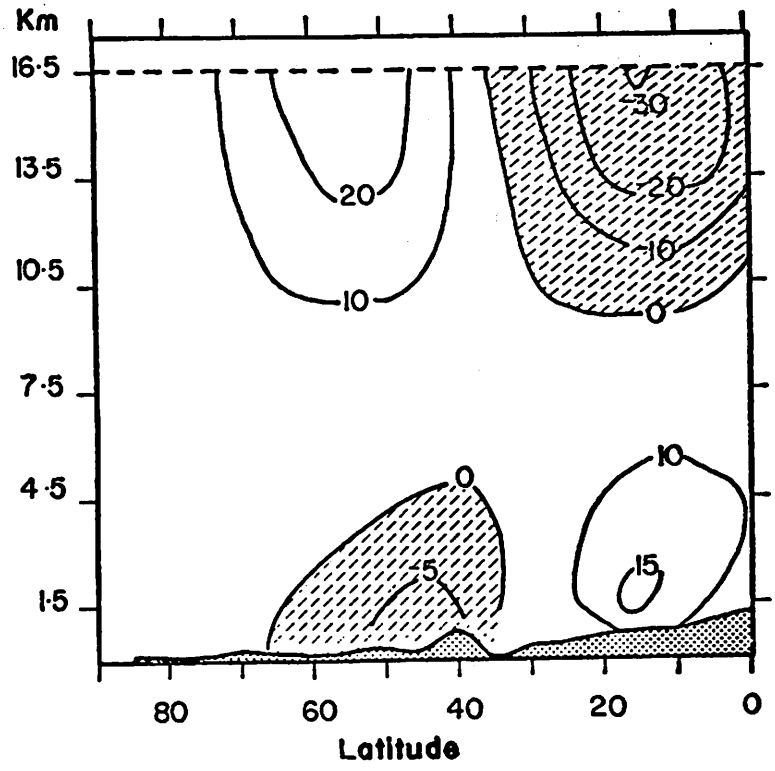
Km
16·5
13·5
10·5
7·5
4·5
1·5
-30
-20
-10
20
10
0
-5
0
10
15
80
60
40
20
0
Latitude

A-12a

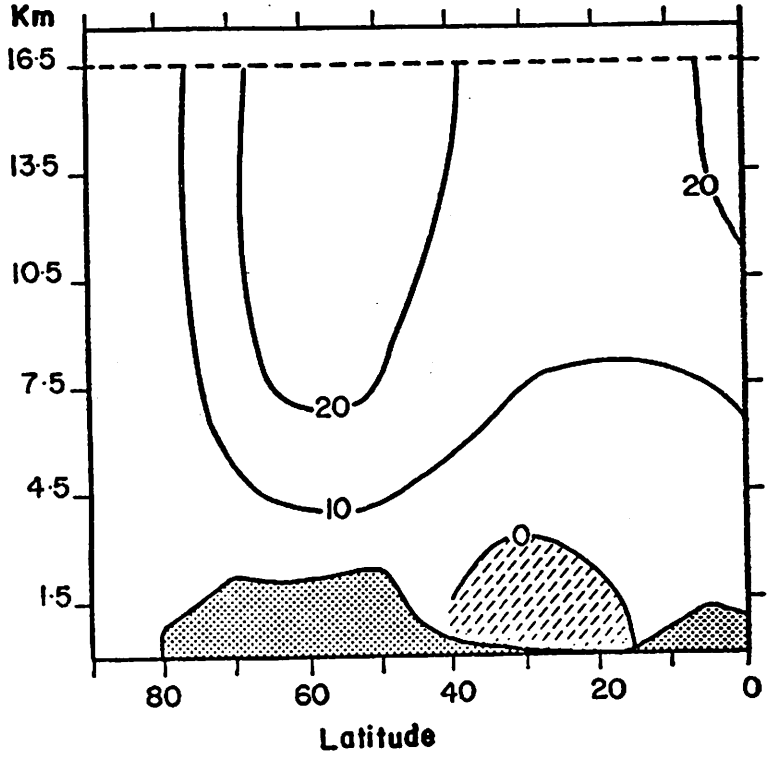
Km
16·5
13·5
10·5
7·5
4·5
1·5
20
20
10
0
80
60
40
20
0
Latitude

A-12b

APPENDIX C

CALCULATION OF THE EARTH-PLANETARY ALBEDO FOR THE FOUR CASES

Although the earth-planetary albedo is not used explicitly in the GCM calculations, it was thought that an estimate of it would be useful for climate interpretation. The values of surface albedo, cloud albedo and other factors are combined to calculate the earth-planetary albedos of the four cases.

The method used will be described briefly and was suggested to me by Dr. T. Sasamori (personal communication, 1974). Firstly, the zonally averaged values of albedo were calculated (cloud plus surface albedo):

$$T_A = c(a_c) + (100 - c)(a_s). \qquad (1)$$

T_A = total albedo

c = percent cloudiness (zonal average)

a_c = albedo of clouds

a_s = albedo of earth surface (zonal average).

Next the globally averaged value of absorption at the earth's surface was computed using:

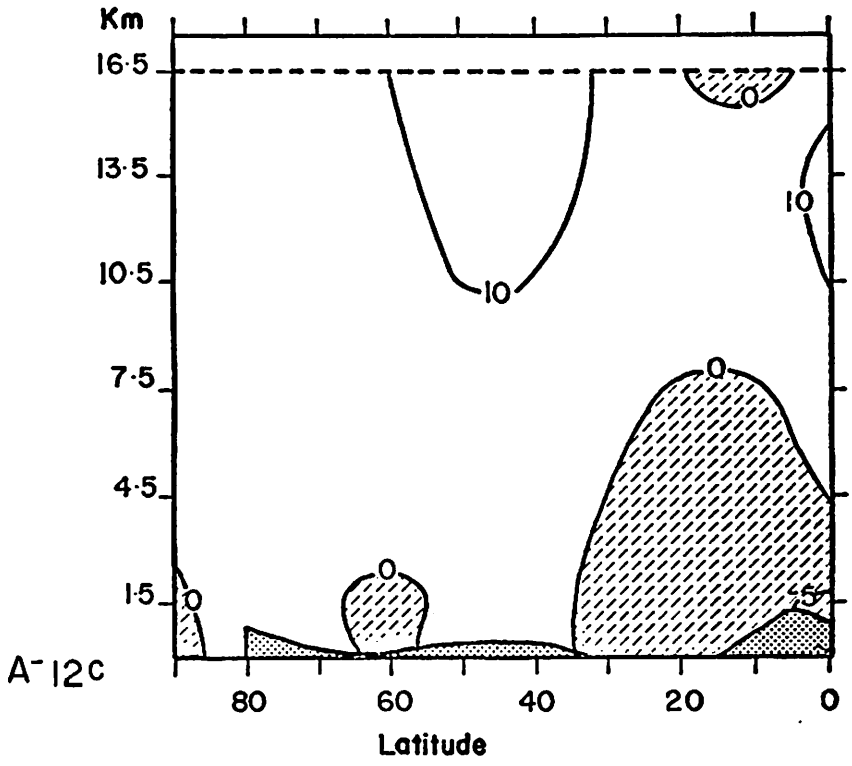
Km
16·5
13·5
10·5
7·5
4·5
1·5
0
10
0
10
0
0
5
80
60
40
20
0
Latitude

A-12c

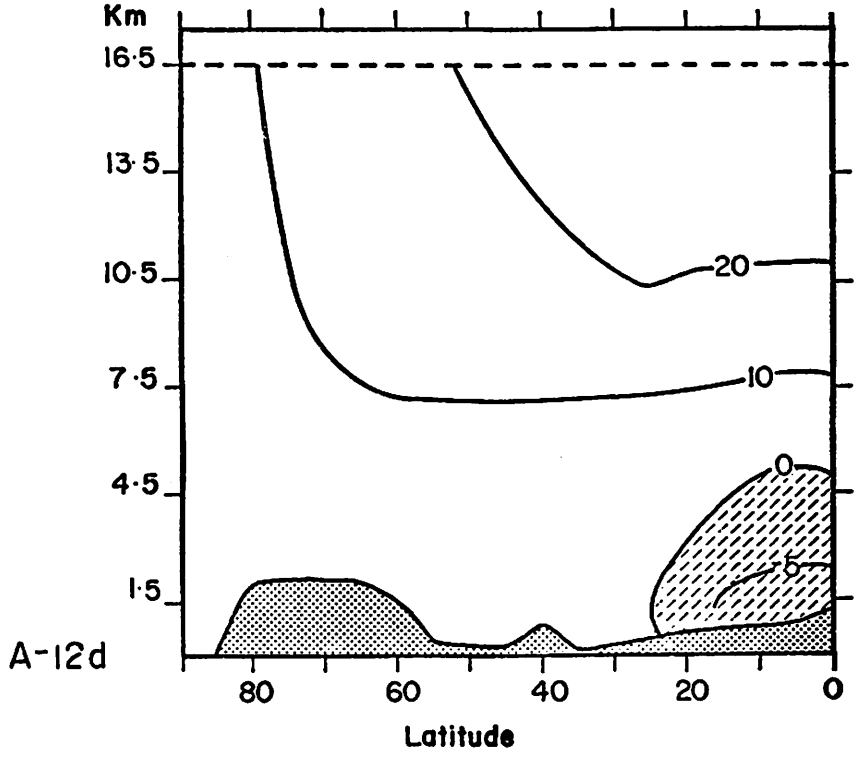
Km
16·5
13·5
10·5
7·5
4·5
1·5
20
10
0
5
80
60
40
20
0
Latitude

A-12d

$$A_{es} = \frac{\sum_{-90}^{+90} (100 - T_A)\, F(\phi) \cos \phi}{\sum_{-90}^{+90} \cos \phi} . \qquad (2)$$

A_{es} = absorption at earth's surface (global average)

$F(\phi)$ = insolation at atmospheric top (a function of latitude).

The planetary albedo, P, was calculated from the formula:

$$P = 100 - (A_{es} + A_{at}) \qquad (3)$$

where A_{at} is the globally averaged value of absorption of solar radiation in the atmosphere computed by the model.

The results for the four cases are given in the table below.

	Approx. planetary albedo w/a_c = 100%	Approx. planetary albedo w/a_c = 50%
January-		
Control Case	50%	23%
Ice Age Case	45%	
July-		
Control Case	59%	28%
Ice Age Case	61%	

In the GCM the albedo of clouds is taken as 100 per cent and it can be seen that with this assumption the earth planetary albedo is much higher than observed. (Observed values are in the range 30-35 per cent.) When the calculations are repeated using a

value of a_c = 50 percent (observed global averages of cloud albedo are in the range 50-70 percent, the lower value was assumed in order to test the sensitivity of the calculation), the earth planetary albedo of the control cases is considerably reduced. From the above results it can be concluded that the cloud albedo assumed in the model is too high. However, it should be pointed out that the planetary albedo is overestimated for other reasons too. For instance, the term A_{at} only accounts for absorption of solar radiation by water vapor. If absorption by dust, ozone and clouds were also included then A_{at} would be larger and this too would decrease the value of the planetary albedo. Sasamori et al. (1972) show that absorption by water vapor is only about half of the total absorption in the atmosphere. On this basis the planetary albedo values could be reduced by 7-8 per cent if absorption by dust, etc., were included in the GCM.